POLITECNICO DI TORINO

SCUOLA DI DOTTORATO
Doctorate in Fluid Dynamics – XV cycle

PhD Dissertation

Aerodynamic Analysis of Non-conventional Wing Configurations for Aeroelastic Applications

Luciano Demasi

Tutors
prof. Gianfranco Chiocchia
prof. Erasmo Carrera
prof. Eli Livne

Coordinator
prof. Luca Zannetti

March 2004

Summary

In this dissertation an original method of predicting the minimum induced drag conditions in a conventional or innovative lifting systems is presented. The procedure here shown is based on the lifting line theories and the small perturbation acceleration potential. Under the hypothesis of linearity and rigid wake aligned with the freestream, the optimal condition is formulated using the Euler-Lagrange integral equation under the conditions of fixed total lifting force and wing span. The Lagrange multiplier method is applied. Particular attention is paid to analyze and solve the Hadamard finite-part integrals involved in the solution process. The minimum induced drag problem is then formulated and solved numerically and analytically when possible. Classical configurations and non-planar lifting systems are extensively analyzed. In particular, the following configurations are examined:

- *Classical cantilever wing and biplane*
- *Circular annular wing*
- *Elliptical annular wing*
- *Elliptical lifting arcs*

For each system, the optimal circulation distribution and the minimum induced drag are calculated. Munk's theorems are also applied to verify the quality of the solutions. Also, comparison with the theoretical and experimental reference values is made.
In order to develop a nonlinear aeroelastic model, a structural nonlinear plate model is formulated as well. It is based on the Principal of Virtual Displacement (PVD), and the plate model adopted is the Classical Plate Lamination Theory (CLPT). The unknown displacements are written as a product between known functions and unknown coefficients (Ritz's approach). The boundary conditions and compatibility of motion between adjacent plate segments are imposed via penalty function approach. Test results obtained by the present method for a variety of plate structures show good correlation with published results and results by other computer codes. A joined wing configuration is analyzed using this procedure as well.

Preface

This dissertation should be a self-reading dissertation even for non expert readers. In this thesis several theoretical problems are analyzed. Therefore, the necessary basic concepts are introduced in the first chapters, while the "state of the art" part is discussed in chapter 4. In order to facilitate the reading, a list of the dissertation's chapters and their contents are reported here.

- **Chapter 1**
  The fundamental equations of inviscid fluids are presented. The concepts of velocity potential, acceleration potential and small perturbation potential are also introduced. Some elementary solutions of Laplace's equation are reported as well.

- **Chapter 2**
  This chapter is mainly concerned with the mathematical issues encountered in this thesis. In particular, the Gaussian quadrature formulae and the Hadamard finite-part integrals are analyzed. A quadrature formula for those hypersingular integrals is presented. A technique to solve the integral equations and the Euler-Lagrange integral equation (that minimizes the induced drag) is presented. The Lagrange multiplier method is extended for these problems. A numerical method to solve the Euler-Lagrange equation is also presented.

- **Chapter 3**
  The basic ideas of the lifting line theories are introduced in this chapter. A generic thin airfoil is studied with the velocity potential and acceleration potential. Prandtl's lifting line is presented. Weissinger's approach is reported as well. Also, the consistency of Weissinger's approach is demonstrated.

- **Chapter 4**
  This chapter is mainly concerned with the induced drag and its physical description and reduction. The "state of the art" of induced drag and its calculation/reduction is reported as well in this chapter. In particular, the different methods of calculating the induced drag are summarized. The problem of the wake modeling is also presented. Munk's Stagger Theorem and Munk's Minimum Induced Drag Theorem are described in detail. The non-planar wing systems are extensively studied. The attention is focused on the circulation distribution in such systems, and the main differences with the classical wing systems are illustrated. The concept of induced lift is also covered. Some important properties of the closed systems are described as well. The wing-grid idea is briefly reported. Finally, an Italian research project (the Prandtlplane) is discussed.

- **Chapter 5**
  This chapter introduces the procedure developed in this study. In particular, using the small perturbation acceleration potential, the well known results of the classical wing under optimal conditions are obtained. The biplane under optimal conditions is extensively analyzed. It is demonstrated that, under optimal conditions, the two wings (which have the same wing span) have the same circulation distribution. In addition, the cases of both infinite distance and infinitesimal distance between the wings are analyzed. The case with finite distance is also considered, and it is shown that the optimal distribution is, in general, not elliptical.

- **Chapter 6**
  The annular wings are studied in detail. A closed form solution is found using Weissinger's approach. Using the small perturbation acceleration potential, the expressions of induced velocity, total lifting force and induced drag for circular and elliptical annular wings are determined.

- **Chapter 7**
  The elliptical lifting arcs are analyzed using the small perturbation acceleration potential and Weissinger's approach. The equations for the lifting force and induced drag are obtained.

- **Chapter 8**
  A few numerical issues related to the solution of the integral equations are reported here. In particular, the convergence of the collocation method is demonstrated. Moreover, five numerical techniques to calculate the induced drag are presented and discussed together with some results. All tests are conducted studying an elliptical annular wing subjected to a twist

corresponding to a rigid rotation of the ellipse along the axis representing the wing span. Furthermore, a few numerical problems related to the aspect ratio are discussed.

- **Chapter 9**
  In this chapter, the circular and elliptical annular wings are analyzed under optimal conditions, and the Euler-Lagrange equation is solved analytically and numerically. The expressions of the optimal circulation, coefficient of minimum induced drag and the normalwash are determined. Munk's Minimum Induced Drag Theorem is verified in each case examined. It is also shown that the solution is not unique (general property of the closed wing systems). It is demonstrated that, in a circular annular wing, the optimal twist corresponds to a rigid rotation of the wing with respect to the axis representing the wing span. The elliptical annular wing and the biplane, both under optimal conditions, are compared. It is demonstrated that, for small aspect ratio, the elliptical annular wing and the biplane have almost the same efficiency. Additionally, a comparison with some experimental results obtained by Alenia Aeronautica (Turin, Italy) is also reported.

- **Chapter 10**
  The Euler-Lagrange equation is presented and numerically solved for the elliptical lifting arcs. Good correlation with some results available in the literature is reported. It is proved that a C-wing has almost the same induced drag as can be found in a closed system. The optimal circulation distribution along the lifting line is determined and compared with the corresponding closed system.

- **Chapter 11**
  A plate structural model is described here. The wing is divided into plate elements (wing segments) and the boundary conditions are imposed via penalty function. Moderately large displacements are considered in the model. The unknown displacement field is discretized using Ritz's approach. The nonlinear structural code is tested with some results available in the literature and with the commercial codes NASTRAN and ADINA. A nonlinear analysis of a joined wing configuration is performed and the results are compared with the displacements obtained using NASTRAN.

Acknowledgments

I greatly thank my tutors, prof. G. Chiocchia and prof. E. Carrera for their help and advice. Particular acknowledgment is given to prof. E. Livne, who gave me the opportunity to work in a different and interesting area of research. I also thank professor A. Bacciotti, who introduced and successively helped me in the variational calculus and its issues. Special acknowledgment is given to prof. G. Monegato for his continuous support and help with the numerical problems encountered during the development of this research project. I consider prof. G. Monegato as one of my tutors.
I can not forget to mention here a friend for his great support in making some difficult choices and solving problematic situations. His help was not only confined in the research field but also in important decisions making. In addition, I would like to thank Elisabetta, Wanda and, particularly, Fareeda for their comments and suggestions in improving this dissertation.

Finally, I would like to give special thanks to my family, who even during difficult moments, gave me all their support, without which this would not have been accomplished.

Table of contents

List of figures

Part I

Aerodynamic and Mathematical Tools

Chapter 1

Equations for Ideal Fluids and Aerodynamic Tools

1.1 Introduction

The fundamental equations of ideal fluids (i.e., inviscid fluids) and some important concepts are introduced in this chapter. In particular, the derivations of the *velocity potential* and *acceleration potential* are introduced. All derivations reported here are based on [1], [2] and [3].

1.2 Euler Equations

In this section the Euler equations are recalled.

- Continuity Equation:

$$\frac{\partial \rho}{\partial t} = -\nabla \cdot (\rho \boldsymbol{V}) \qquad \text{or} \qquad \frac{1}{\rho}\frac{D\rho}{Dt} = -\nabla \cdot \boldsymbol{V}, \tag{1.1}$$

  where ρ is the fluid density, $\boldsymbol{V} = V_x\boldsymbol{i} + V_y\boldsymbol{j} + V_z\boldsymbol{k}$ is the velocity vector, $\frac{\partial}{\partial t}$ is the *Euler derivative* and $\frac{D}{Dt} = \frac{\partial}{\partial t} + V_x\frac{\partial}{\partial x} + V_y\frac{\partial}{\partial y} + V_z\frac{\partial}{\partial z}$ is the *Lagrange derivative*. For constant fluid density[1]:

$$\nabla \cdot \boldsymbol{V} = 0. \tag{1.2}$$

- Equation of Motion[2]:

$$\frac{D\boldsymbol{V}}{Dt} = -\frac{1}{\rho}\nabla p, \qquad \text{or} \qquad \frac{\partial \boldsymbol{V}}{\partial t} + \nabla\left(\frac{V^2}{2}\right) = -\frac{1}{\rho}\nabla p, \tag{1.3}$$

[1] This means that $\rho = \rho_\infty$ everywhere.

[2] In aeronautical applications this equation has no other terms. But in some applications, like meteorology, other contributes have to be included.

where p is the pressure. If the fluid is incompressible (i.e., $\rho = \rho_\infty$ is a known constant), the continuity and motion equations form one system of four equations with four unknowns V_x, V_y, V_z and p. If the density is not constant, two other equations are required. These two equations are reported below.

- Energy Equation:
$$\frac{De}{Dt} = -p\frac{D}{Dt}\left(\frac{1}{\rho}\right), \tag{1.4}$$
where e is the *thermal energy for unit mass*. e is also proportional to the temperature T:
$$e = c_v T,$$
where c_v is the *specific heat for unit mass and with constant volume.*

- Constitutive Equation (for ideal gas)
$$\frac{p}{\rho} = R^\star T \tag{1.5}$$
where $R^\star$ is the gas constant. If the fluid is air, $R^\star = 287\frac{\text{J}}{\text{Kg K}}$.

1.3 Velocity Potential

In most aeronautical studies it can be assumed that the curl of the velocity is zero[3]. Therefore, it is possible to define *a scalar function Φ called velocity potential*, whose gradient is equal to the velocity:

$$\boldsymbol{V} = \nabla\Phi. \tag{1.6}$$

From the equation of motion and equation (1.6) the *equation of the velocity potential* can be derived as

$$\nabla^2\Phi - \frac{1}{c^2}\left[\frac{\partial^2\Phi}{\partial t^2} + \frac{\partial}{\partial t}\left(V^2\right) + \boldsymbol{V}\cdot\nabla\left(\frac{V^2}{2}\right)\right] = 0, \tag{1.7}$$

where $c = c(\boldsymbol{V}) = c(\Phi)$ is the *speed of sound.*
If the fluid is incompressible, the equation becomes Laplace's equation:

$$\nabla^2\Phi = 0. \tag{1.8}$$

[3]If the aeronautics bodies are well designed, the vorticity is confined in the boundary layer and in the wake (very small). Therefore, if curved shock waves are not present, the assumption of zero curl of the velocity is acceptable.

It is important to notice that equation (1.7) is *nonlinear* while equation (1.8) is *linear*. Since irrotational, incompressible flow is governed by Laplace's equation, which is linear, it can be concluded that a *complicated flow pattern for an irrotational, incompressible flow can be synthesized by superimposing a number of elementary flows which are also irrotational and incompressible.* This technique will be used in coming chapters.

1.4 Acceleration Potential

The velocity potential Φ has been defined. Similarly, the *acceleration potential* [4] can be defined. Using the equation of motion (1.3):

$$\frac{D\boldsymbol{V}}{Dt} = -\frac{1}{\rho}\nabla p. \tag{1.9}$$

If the entropy is assumed constant, the relation $\frac{p}{\rho^\gamma} = \text{const}$[4] is valid, and it is possible to prove the relation

$$\frac{1}{\rho}\nabla p = \nabla\left(\int \frac{\mathrm{d}p}{\rho}\right) = \nabla\left(\int \frac{\mathrm{d}p}{\rho} + G\left(t\right)\right). \tag{1.10}$$

The goal is to write the relation (1.9) in the form of

$$\frac{D\boldsymbol{V}}{Dt} = \nabla\Psi. \tag{1.11}$$

By combining the relations (1.11), (1.10) and (1.9), the expression of the acceleration potential Ψ can be found:

$$\Psi = -\int \frac{\mathrm{d}p}{\rho} - G\left(t\right). \tag{1.12}$$

Here, $G\left(t\right)$ is a function of time t and furnishes the value of Ψ at the start of the integration domain.

1.5 Boundary Conditions

In aeronautics it is common to have an airplane moving in an infinite field. Under the hypothesis of the viscosity $\mu = 0$ and $\rho = \text{const}$, two requirements have to be satisfied[5]:

[4] If the fluid is air, $\gamma = \frac{c_p}{c_v} = 1.4$.

[5] If these hypothesis are removed, the requirements are different.

- *Requirement 1*
  Far away from the body (toward infinity), in all directions, the flow approaches the uniform freestream conditions. Let V_∞ be aligned with the x direction in a reference coordinate system, at infinity the following relations have to be satisfied:
  $$\begin{aligned} V_x &= V_\infty \,, \\ V_y &= V_z = 0. \end{aligned} \tag{1.13}$$
  This condition is the *Boundary Condition on Velocity at Infinity* (BCVI).

- *Requirement 2*
  If the body has a solid surface then it is impossible for the flow to penetrate the surface. The *relative velocity* at the surface can be finite, but, because the flow cannot penetrate the surface, the *relative velocity* of the fluid must be *tangent* to the surface. This is the *Wall Tangency Condition*(WTC).

1.6 Thin Wings: Linear Theory

1.6.1 Boundary Conditions

Consider a thin wing, meaning that the wing has small curvature and thin thickness. Let V_∞ be aligned with the x direction. The velocity can be expressed as

$$\boldsymbol{V} = (V_\infty + v_x)\,\boldsymbol{i} + v_y\boldsymbol{j} + v_z\boldsymbol{k} \qquad v_x,v_y,v_z << V_\infty, \tag{1.14}$$

where v_x, v_y and v_z are the components of the *perturbation velocity.* Obviously, this equation satisfies the BCVI requirement.
The aim is to formulate a theory in order to calculate the *lifting force* and the *induced drag* of a wing system. It is well known from the aerodynamic theory that the thickness does not produce a lifting force. Therefore, consider the wing as a *surface without thickness.* Indicating the equation of wing surface with $z = f(x,y)$, the vector

$$\boldsymbol{n} = \frac{\partial f}{\partial x}\boldsymbol{i} + \frac{\partial f}{\partial y}\boldsymbol{j} - \frac{\partial f}{\partial z}\boldsymbol{k}, \tag{1.15}$$

is perpendicular to the wing surface. In steady conditions, the WTC can be imposed in the following manner:

$$\boldsymbol{V}\cdot\boldsymbol{n} = 0 \Rightarrow (V_\infty + v_x)\,\frac{\partial f}{\partial x} + v_y\frac{\partial f}{\partial y} - v_z = 0. \tag{1.16}$$

Suppose that the curvature is very small (*small perturbation theory*). Under this condition, the terms $v_x\frac{\partial f}{\partial x}$ and $v_y\frac{\partial f}{\partial y}$ are negligible and equation (1.16) becomes

$$V_\infty\frac{\partial f}{\partial x} - v_z = 0 \Rightarrow \frac{v_z}{V_\infty} = \frac{\partial f}{\partial x}. \tag{1.17}$$

This equation represents the WTC for thin wings.

1.6.2 Small Perturbation Velocity Potential

Under the small perturbation hypothesis, it is possible to introduce the *small perturbation velocity potential* ϕ as

$$\phi = \Phi - V_\infty x. \tag{1.18}$$

From that equation it is possible to write:

$$\begin{aligned} v_x &= \frac{\partial \phi}{\partial x} = V_x - V_\infty, \\ v_y &= \frac{\partial \phi}{\partial y} = V_y, \\ v_z &= \frac{\partial \phi}{\partial z} = V_z. \end{aligned} \tag{1.19}$$

In this case the Laplace's equation

$$\nabla^2 \phi = 0 \tag{1.20}$$

is valid.

1.6.3 Acceleration Potential and Pressure Perturbation

From its definition (see equation (1.12)), by using the isentropic relation, the acceleration potential expression can be demonstrated as

$$\Psi = \frac{\gamma}{\gamma - 1} \frac{p_\infty^{1/\gamma}}{\rho_\infty} \left[p_\infty^{(\gamma-1)/\gamma} - p^{(\gamma-1)/\gamma} \right]. \tag{1.21}$$

The quantities with the subscript ∞ are referred to the freestream far ahead of the body. Suppose it is possible to use the *linear theory* (i.e., to have very small perturbations) then the pressure can be written as

$$p = p_\infty \left(1 + \epsilon\right) \qquad (\epsilon \to 0). \tag{1.22}$$

Using equation (1.22) and the Taylor expansion truncated at the first order yields

$$p^{(\gamma-1)/\gamma} = p_\infty^{(\gamma-1)/\gamma} \left(1 + \varepsilon\right)^{(\gamma-1)/\gamma} = p_\infty^{(\gamma-1)/\gamma} \left(1 + \frac{(\gamma - 1)}{\gamma} \left(\frac{p}{p_\infty} - 1 \right) \right). \tag{1.23}$$

Substituting (1.23) into relation (1.21), the obtained result is

$$\Psi = \frac{p_\infty - p}{\rho_\infty}. \tag{1.24}$$

This expression is very important. Consider a very thin wing[6] (see figure 1.1). Using the superscript + for the upper surface and the superscript − for the lower surface, the relation between the local load $L(y)$ and the small perturbation acceleration potential can be written as[7]

$$\rho_\infty \left(\Psi^- (y) - \Psi^+ (y) \right) = \rho_\infty \triangle \Psi (y) = L (y) . \tag{1.25}$$

If the hypotheses used to obtain equation (1.25) are satisfied, and if the fluid is

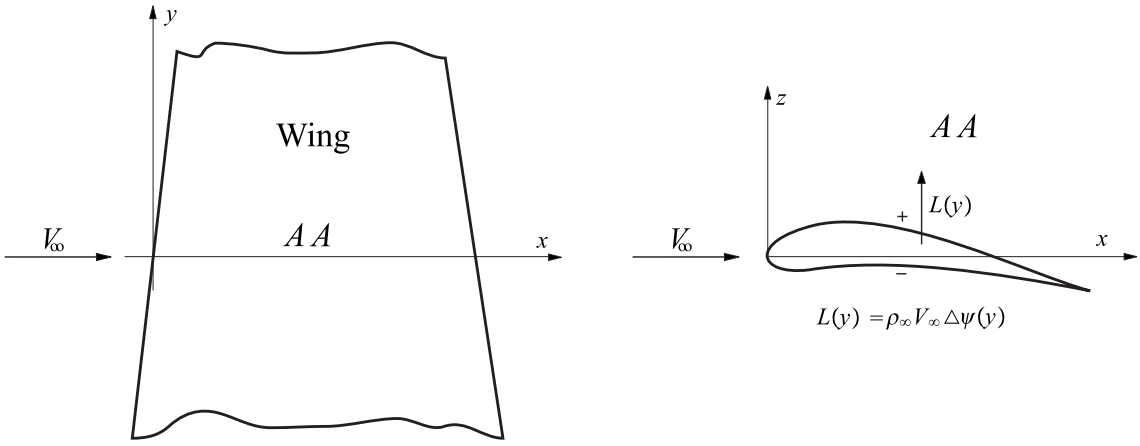

Figure 1.1. Acceleration potential and local load $\triangle p (y)$.

incompressible (i.e., $\rho = \rho_\infty$), by using the *local Kutta-Joukowski theorem*

$$L (y) = \rho_\infty V_\infty \Gamma (y) , \tag{1.26}$$

it is possible to relate the *local circulation* $\Gamma (y)$ with the quantity $\triangle \Psi (y)$ as

$$\Gamma (y) = \frac{\triangle \Psi (y)}{\rho_\infty V_\infty} . \tag{1.27}$$

This formula will be used later to switch $\Gamma (y)$ and the *dipole intensity distribution* $m (y)$.

[6] The wing must be thin in order to use the linear approach.

[7] Consider that Weissinger's approximation is valid. Only one load $L(y)$ for each y is considered. This concept will be further explained in chapter 3.

1.6.4 Acceleration Potential and Small Perturbation Velocity Potential: Relations and Concepts

For the steady case, it can be demonstrated that Laplace's equation is valid also for the acceleration potential. Therefore, the following expression is valid:

$$\nabla^2 \Psi = 0. \tag{1.28}$$

This relation is, in a formal point of view, the same equation that the small perturbation velocity potential has to fulfill. Hence, it is possible to superimpose a number of elementary solutions[8].
Why is the acceleration potential important?

- *Reason 1*
  It is directly related to the *local load* (see equation (1.25)).

- *Reason 2*
  In a simplified model for wings (like *Prandtl's lifting-line theory*), the vortices in the wake do not have to be considered if the acceleration potential is used. This is useful if the geometry of the wing is complex and the Biot Savart law is not easy to apply.

- *Reason 3*
  In the lifting line theories, the final equation *is not* an integral-differential equation but only an integral equation *if the acceleration potential is used.* This helps greatly in the numerical approach, when the circulation distribution on the wing has to be found: only the unknown distribution (and not its derivative) has to be discretized. But, if the acceleration potential is not used then an integral-differential equation has to be solved[9]. In subsequent chapters this aspect will be studied more in depth.

To correctly impose the WTC, the velocity is needed. However, the velocity is the gradient of the velocity potential. Therefore, the small perturbation velocity potential as a function of the acceleration potential has to be expressed. The wanted relation for steady flow can be demonstrated as

$$\Psi = V_\infty \frac{\partial \phi}{\partial x} \Rightarrow \phi\,(x,y,z) = \frac{1}{V_\infty} \int_{-\infty}^{x} \Psi\,(\xi,y,z)\,\mathrm{d}\xi. \tag{1.29}$$

[8] Similar operation is done when, for example, the vortices are used to analyze a wing: this is possible because they singly solve Laplace's equation and because it is linear.

[9] However, in that case, it is possible to use the integration-by-part rule and obtain an integral equation only. An example reported in chapter 3 will clarify the concept.

1.7 Some Elementary Solutions of Laplace's Equation

Laplace's equation is linear. This property will be used in subsequent chapters to study non-conventional wings.
In this section a few elementary solutions of Laplace's equation are analyzed. Only the small perturbation velocity potential expressions will be obtained, but it has to be clear that, *because of the linearity*, these expressions are valid for both the *small perturbation velocity potential* and the *acceleration potential*[10].

1.7.1 Two-Dimensional Case

The Source

Consider a two-dimensional, incompressible and steady flow. If all the streamlines are straight lines emanating from a central point O, and if the velocity changes intensity inversely with distance from point O, the flow is called a *source flow*. The velocity and the velocity potential expressions can easily be demonstrated as

$$V = V_r = \frac{Q}{2\pi r}, \tag{1.30}$$

$$\phi_s = \frac{Q}{2\pi} \ln r. \tag{1.31}$$

$Q = [\mathrm{m}^2/\mathrm{s}]$ is the intensity of the source. If the value is negative then it is called *sink*.
The source flow has the following properties:

- *Property 1*
  $\nabla \cdot \boldsymbol{V} = 0$ for all points *except* point O, where $\nabla \cdot \boldsymbol{V} \to \infty$.
- *Property 2*
  The curl of the velocity is zero on all points: $\nabla \times \boldsymbol{V} = 0$.

Figure 1.2 shows the source flow and sink flow.

The Doublet

There is a special, degenerate case of a source-sink pair that leads to a singularity called a *doublet* (see figure 1.3).

[10] Remember that under the hypothesis of linearity both the small perturbation velocity potential and the small perturbation acceleration potential satisfy Laplace's equation.

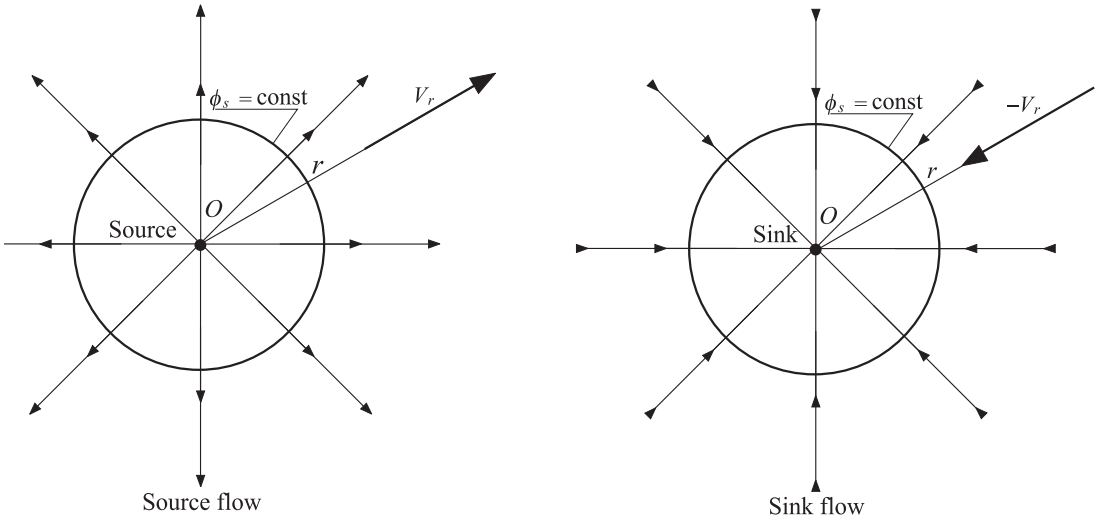

Figure 1.2. Source and sink flows.

The doublet expression is obtained by considering one source and one sink of equal strength Q separated by a distance d. With a limit process (as will be seen in the three-dimensional case), the potential of a doublet M can be demonstrated as

$$\phi_d = -\frac{M}{2\pi r}\cos(\vartheta - \alpha). \tag{1.32}$$

When $\alpha = \frac{\pi}{2}$, the previous relation becomes

$$\phi_d = -\frac{M}{2\pi}\frac{z}{x^2 + z^2}. \tag{1.33}$$

The doublet flow has the following properties:

- *Property 1*
  $\nabla \cdot \boldsymbol{V} = 0$ for all points.
- *Property 2*
  The curl of the velocity is zero on all points: $\nabla \times \boldsymbol{V} = 0$.

The Vortex

Consider a flow where the streamlines are concentric circles about a given point O. Moreover, let the velocity along any given circular streamline be constant, but let it vary from one streamline to another inversely with the distance from the common

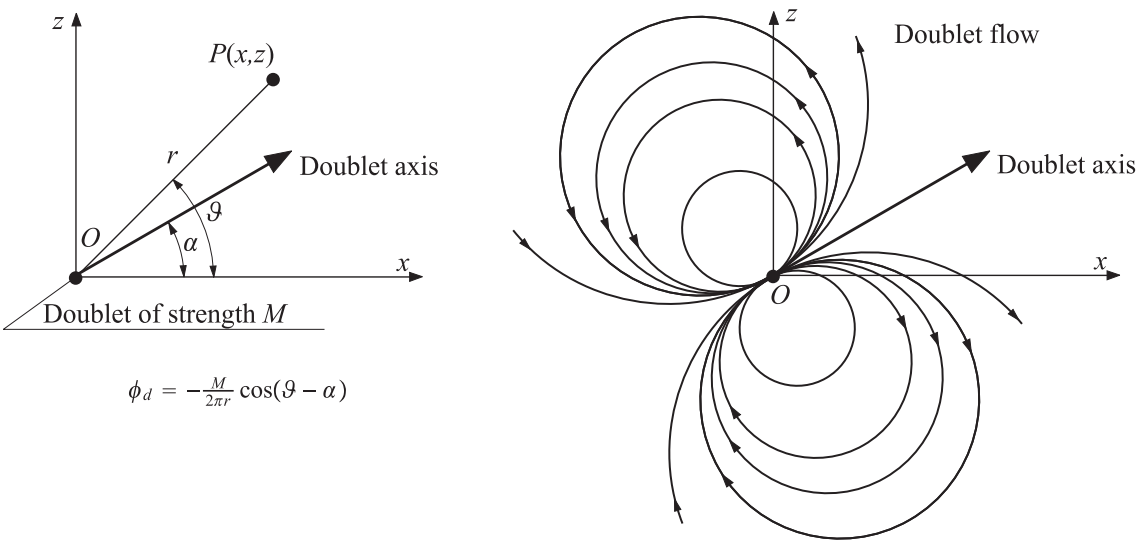

Figure 1.3. Doublet flow.

center O. Such a flow is called a *vortex flow* (see figure 1.4).
It is possible to demonstrate the following relations:

$$V_\vartheta = \frac{\Gamma}{2\pi r}, \tag{1.34}$$

$$\phi_v = \frac{\Gamma}{2\pi}\vartheta. \tag{1.35}$$

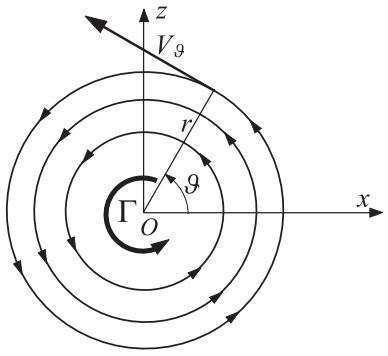

Figure 1.4. Vortex flow.

The vortex flow has the following properties:

- *Property 1*
  $\nabla \cdot \boldsymbol{V} = 0$ in every point.

- *Property 2*
  The curl of the velocity is zero on all points *except* point O, where $\nabla \times \boldsymbol{V} \to \infty$.

1.7.2 Three Dimensional Case

The Source

In a cartesian system, let the origin of the system be called O. If a *source* of intensity $Q[m^3/s]$ is positioned at that point, because of the symmetry, the potential is a constant function over a sphere which is centered at point O. Q must always be the same and independent from the sphere cosidered. For that reason and because the velocity is radial (symmetric flow), Q can be written as

$$Q = 4\pi r^2 V_r \Rightarrow V_r = \frac{Q}{4\pi r^2}. \tag{1.36}$$

The velocity V_r is also the derivative of the velocity potential. This yields

$$V_r = \frac{Q}{4\pi r^2} = \frac{\partial \phi_s}{\partial r} \Rightarrow \phi_s = -\frac{Q}{4\pi r}. \tag{1.37}$$

Therefore, the velocity potential for the source is

$$\phi_s = -\frac{Q}{4\pi\sqrt{x^2+y^2+z^2}}. \tag{1.38}$$

Obviously, even if the source is not in the origin of the system, the previous formula is still valid, but now the cartesian distance from the point $P(x,y,z)$ and the source positioned at point $P_s(x_s,y_s,z_s)$ appears in the expression of the velocity potential:

$$\phi_s = -\frac{Q}{4\pi\sqrt{(x-x_s)^2+(y-y_s)^2+(z-z_s)^2}}. \tag{1.39}$$

The Doublet

Consider two sources[11] with intensity $+Q$ and $-Q$, respectively (see figure 1.5). Because of the linearity, the small perturbation velocity potential at point $P(x,y,z)$

[11] Here the generic term "source" is used, but it is clear that when the intensity is negative it becomes a sink.

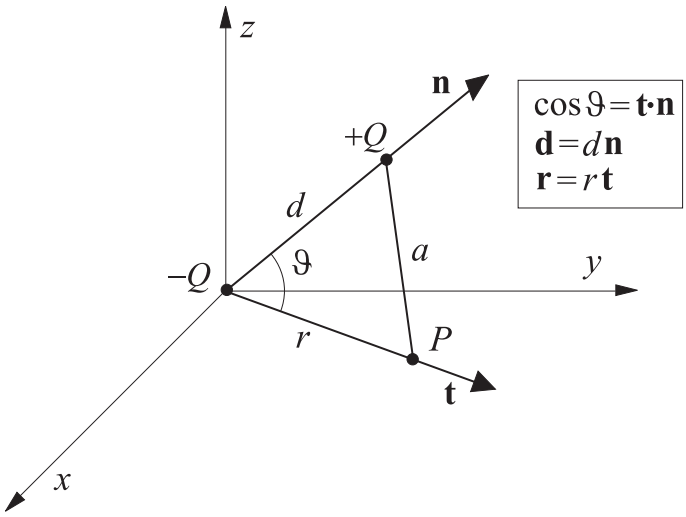

Figure 1.5. Potential of a dipole from two sources.

is the summation of two contributes[12] written as

$$\phi_d = -\frac{-Q}{4\pi r} - \frac{+Q}{4\pi a} = \frac{Q}{4\pi r}\left(1 - \frac{r}{a}\right), \tag{1.40}$$

in which equation (1.37) has been used. The unit vectors $\boldsymbol{t}$ and $\boldsymbol{n}$ are written in the following manner:

$$\begin{aligned} \boldsymbol{t} &= \tfrac{x}{r}\boldsymbol{i} + \tfrac{y}{r}\boldsymbol{j} + \tfrac{z}{r}\boldsymbol{k}, \\ \boldsymbol{n} &= n_{dx}\boldsymbol{i} + n_{dy}\boldsymbol{j} + n_{dz}\boldsymbol{k}. \end{aligned} \tag{1.41}$$

From figure 1.5, by applying the Carnot's theorem, the following relation can be written:

$$a^2 = r^2 + d^2 - 2rd\cos\vartheta = r^2 + d^2 - 2\boldsymbol{r}\cdot\boldsymbol{d}. \tag{1.42}$$

Using the relations

$$\begin{aligned} \boldsymbol{d} &= d\boldsymbol{n} = d\left(n_{dx}\boldsymbol{i} + n_{dy}\boldsymbol{j} + n_{dz}\boldsymbol{k}\right), \\ \boldsymbol{r} &= r\boldsymbol{t} = r\left(\tfrac{x}{r}\boldsymbol{i} + \tfrac{y}{r}\boldsymbol{j} + \tfrac{z}{r}\boldsymbol{k}\right), \end{aligned} \tag{1.43}$$

yields

$$a^2 = r^2 + d^2 - 2d\left(n_{dx}x + n_{dy}y + n_{dz}z\right). \tag{1.44}$$

Suppose now that d is very small. Under that condition, d^2 is negligible and the previous equation becomes

$$a^2 = r^2 - 2\epsilon \Rightarrow \frac{a^2}{r^2} = 1 - \frac{2\epsilon}{r^2} \Rightarrow \frac{r}{a} = \left(1 - \frac{2\epsilon}{r^2}\right)^{-\frac{1}{2}} \approx 1 + \frac{\epsilon}{r^2} \qquad \epsilon \to 0. \tag{1.45}$$

[12] Now the subscript d is used because the expression will lead to writing the potential of a dipole.

Using the last equation and relation (1.40), the obtained result is

$$\phi_d = -\frac{Q}{4\pi r}\frac{\epsilon}{r^2} = -\frac{Qd}{4\pi r^3}\left(n_{dx}x + n_{dy}y + n_{dz}z\right). \tag{1.46}$$

Now consider the following operations at the same time:

$$\begin{aligned} &d \to 0 \\ &Q \to \infty \\ &Qd \equiv M \quad \text{finit value, neither zero nor infinity.} \end{aligned} \tag{1.47}$$

Equation (1.46) becomes

$$\phi_d = -\frac{M}{4\pi r^3}\left(n_{dx}x + n_{dy}y + n_{dz}z\right), \tag{1.48}$$

where M is the strength of the dipole positioned in the origin of the reference cartesian coordinate system and with direction $\boldsymbol{n}$.
In a general case, the dipole is positioned at a generic point $P_d = (x_d,y_d,z_d)$. In that case, the previous equation becomes

$$\phi_d\left(x,y,z\right) = -\frac{M}{4\pi}\frac{n_{dx}\left(x-x_d\right) + n_{dy}\left(y-y_d\right) + n_{dz}\left(z-z_d\right)}{\left[\left(x-x_d\right)^2 + \left(y-y_d\right)^2 + \left(z-z_d\right)^2\right]^{\frac{3}{2}}}. \tag{1.49}$$

Observation 1 It is possible to derive the velocity potential of a dipole, with a formal derivative operation from a velocity potential of a source positioned at the same point. The derivative direction has to be the negative dipole direction $-\boldsymbol{n}$. This operation is also valid in the two dimensional case.

To prove that, consider a simple case, where the dipole M is positioned at the origin, and where its axis $\boldsymbol{n}$ is directed along $-z$. The expression of the velocity potential is

$$\phi_d\left(x,y,z\right) = -\frac{M}{4\pi}\frac{-z}{\left[x^2+y^2+z^2\right]^{\frac{3}{2}}} = \frac{M}{4\pi}\frac{z}{\left[x^2+y^2+z^2\right]^{\frac{3}{2}}}. \tag{1.50}$$

Consider now a source Q positioned at the same point. Its potential velocity is

$$\phi_s\left(x,y,z\right) = -\frac{Q}{4\pi}\frac{1}{\left[x^2+y^2+z^2\right]^{\frac{1}{2}}}. \tag{1.51}$$

It is easy to see that calculating a partial derivative $\frac{\partial}{\partial z}$ of the last relation and *formally* changing the symbol Q with M yields the relation (1.50).

Observation 2 The formal operation seen above may greatly help to write the velocity potential of a dipole in complicated geometries. However, it is a delicate process in some cases. The writer's advice is to always use the relation (1.49) to avoid possible problems.

To explain what has been said, consider the following example.
Consider a circumference and suppose that the goal is to find the velocity potential at point $P(R,\varphi)$ of a distribution m of dipoles positioned on that circumference and with orientation along the radial direction $\boldsymbol{n}$ (see figure 1.6). It is possible to start

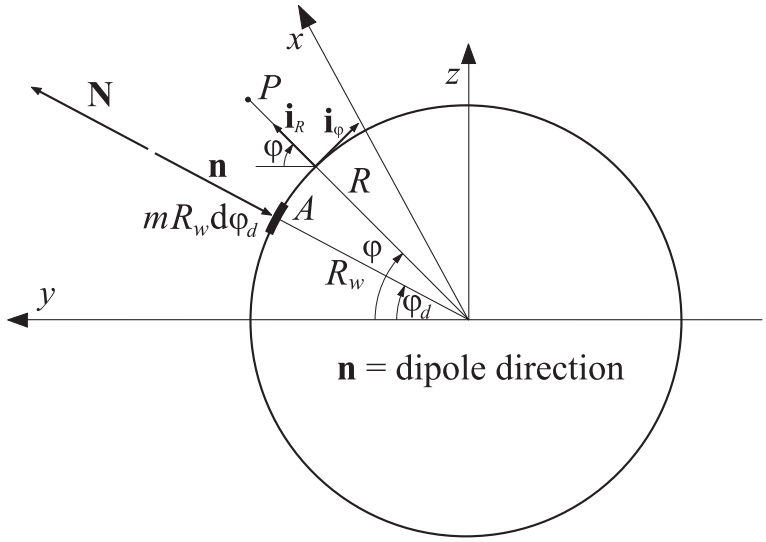

Figure 1.6. Example of potential of a dipole distribution.

from a source distribution q positioned on the circumference and use the formalism based on the derivative operation along the radial direction. Therefore, the potential of the source $Q(\varphi_d) = q(\varphi_d) R_w \mathrm{d}\varphi_d$ positioned at point A (see figure 1.6) is

$$\mathrm{d}\phi_s = -\frac{1}{4\pi}\frac{q(\varphi_d)R_w\mathrm{d}\varphi_d}{D} = -\frac{1}{4\pi}\frac{q(\varphi_d)R_w\mathrm{d}\varphi_d}{\sqrt{R_w^2X^2+R^2+R_w^2-2RR_w\cos(\varphi-\varphi_d)}} \qquad x = R_wX. \tag{1.52}$$

In the previous equation relation (1.39) was used. Now, because the dipole directions are *opposite* of the radius directions ($\boldsymbol{n} = -\boldsymbol{N}$), the potential of the m distribution is the derivative with respect to R of the previous expression (with the formal change $q \to m$) as follows:

$$\mathrm{d}\phi_d = \frac{1}{4\pi}\frac{m(\varphi_d) R_w \mathrm{d}\varphi_d (R - R_w\cos(\varphi-\varphi_d))}{(R_w^2X^2 + R^2 + R_w^2 - 2RR_w\cos(\varphi-\varphi_d))^{\frac{3}{2}}}. \tag{1.53}$$

Now, under the hypothesis of linearity, it is possible to integrate over the circumference:

$$\phi_d = \frac{1}{4\pi} \int_0^{2\pi} \frac{m(\varphi_d) R_w (R - R_w \cos(\varphi - \varphi_d))}{(R_w^2 X^2 + R^2 + R_w^2 - 2RR_w \cos(\varphi - \varphi_d))^{\frac{3}{2}}} \mathrm{d}\varphi_d. \tag{1.54}$$

But this expression *is not correct.* By using the general formula (1.49) a different result is obtained[13]:

$$\phi_d = \frac{1}{4\pi} \int_0^{2\pi} \frac{m(\varphi_d) R_w (R\cos(\varphi - \varphi_d) - R_w)}{(R_w^2 X^2 + R^2 + R_w^2 - 2RR_w \cos(\varphi - \varphi_d))^{\frac{3}{2}}} \mathrm{d}\varphi_d. \tag{1.55}$$

Only equation (1.55) is correct. Where is the error in equation (1.54)? Why is the result incorrect? The error is in the derivative operation: the directional derivative with respect to the opposite direction of the dipole *is not* $\frac{\partial}{\partial R}$ *alone*, as it has been done in the wrong derivation (equation (1.54)). Now the correct approach is shown. From equation (1.52), the *gradient in the polar coordinate system*[14] can be written as

$$\begin{aligned}
&x \text{ component}: && -\tfrac{1}{4\pi} \tfrac{R_w q(\varphi_d)\mathrm{d}\varphi_d}{(x^2+R^2+R_w^2-2RR_w\cos(-\varphi+\varphi_d))^{\frac{3}{2}}} (-x), \\
&R \text{ component}: && -\tfrac{1}{4\pi} \tfrac{R_w q(\varphi_d)\mathrm{d}\varphi_d}{(x^2+R^2+R_w^2-2RR_w\cos(-\varphi+\varphi_d))^{\frac{3}{2}}} [-R + R_w\cos(\varphi - \varphi_d)], \\
&\varphi \text{ component}: && -\tfrac{1}{4\pi} \tfrac{R_w q(\varphi_d)\mathrm{d}\varphi_d}{(x^2+R^2+R_w^2-2RR_w\cos(\varphi-\varphi_d))^{\frac{3}{2}}} \tfrac{1}{R} [-R_w R\sin(\varphi - \varphi_d)].
\end{aligned} \tag{1.56}$$

In accordance with the formal method shown in observation 1, the derivative has to be performed along the $\boldsymbol{N} = -\boldsymbol{n}$ direction because the dipole is directed along the $\boldsymbol{n}$ direction. By using the well known equation of a directional derivative along the unit vector $\boldsymbol{N}$ of a function f,

$$\frac{\partial f}{\partial v} = \nabla f \cdot \boldsymbol{N}, \tag{1.57}$$

the derivative can be written as

$$\mathrm{d}\phi_d = \frac{1}{4\pi} \frac{R_w (R\cos(\varphi - \varphi_d) - R_w) m(\varphi_d)}{(x^2 + R^2 + R_w^2 - 2RR_w \cos(\varphi - \varphi_d))^{\frac{3}{2}}} \mathrm{d}\varphi_d. \tag{1.58}$$

Here in equation (1.58), equations (1.57), (1.52), (1.56) and the fact that (see figure 1.6) $\boldsymbol{N} = -\boldsymbol{n} = \cos(\varphi - \varphi_d)\boldsymbol{i}_R - \sin(\varphi - \varphi_d)\boldsymbol{i}_\varphi$ have been used.
Now, because of the linearity, the final expression is easily written by integrating over the circumference. Thus, it can be understood that the correct equation is relation (1.55).

[13] See chapter 6.

[14] Remember the formula $\nabla f(x,R,\varphi) = \frac{\partial f(x,R,\varphi)}{\partial x}\boldsymbol{i} + \frac{\partial f(x,R,\varphi)}{\partial R}\boldsymbol{i}_R + \frac{1}{R}\frac{\partial f(x,R,\varphi)}{\partial \varphi}\boldsymbol{i}_\varphi$.

Observation 3 All the equations written in this section have been demonstrated by using the velocity potential. It has already been explained that in the linear case the acceleration potential satisfies Laplace's equation as the velocity potential. Therefore, all of these relations are also valid for the acceleration potential.

Thus, it can be written that:

$$\Psi_s = -\frac{Q}{4\pi\sqrt{(x-x_s)^2+(y-y_s)^2+(z-z_s)^2}}, \tag{1.59}$$

$$\Psi_d\,(x,y,z) = -\frac{M}{4\pi}\frac{n_{dx}\,(x-x_d)+n_{dy}\,(y-y_d)+n_{dz}\,(z-z_d)}{\left[(x-x_d)^2+(y-y_d)^2+(z-z_d)^2\right]^{\frac{3}{2}}}. \tag{1.60}$$

Obviously, the *unit of measure* of Q and M have changed. For example, $M = [\mathrm{m}^4/\mathrm{s}^2]$ instead of $M = [\mathrm{m}^4/\mathrm{s}]$ if the velocity potential is used. Similarly, now $Q = [\mathrm{m}^3/\mathrm{s}^2]$ instead of $Q = [\mathrm{m}^3/\mathrm{s}]$.

1.7.3 The Vortex Filament, the Biot-Savart Law, and Helmholtz's Theorems

The straight vortex filament extending to $\pm\infty$ has been analyzed and the expressions for the velocity and for the potential ϕ_v have been written.
Now consider a general case, where the vortex filament is *curved*. By referring to figure 1.7, it is possible to demonstrate the *Biot-Savart law*[15]:

$$\mathrm{d}\boldsymbol{V} = \frac{\Gamma}{4\pi}\frac{\mathrm{d}\boldsymbol{l}\times\boldsymbol{r}}{|\boldsymbol{r}^3|} \tag{1.61}$$

Now applying the Biot-Savart law to a straight filament of *infinite length* (see figure 1.8), the expression

$$V = \frac{\Gamma}{2\pi h} \tag{1.62}$$

can be derived. Similarly, considering a *semi-infinite* vortex filament which starts from a point A (see figure 1.9), the expression

$$V = \frac{\Gamma}{4\pi h} \tag{1.63}$$

[15]Drawing an analogy with the electromagnetic theory, in the Biot-Savart law, the magnetic field $\mathrm{d}\boldsymbol{B}$ induced at point P by a segment of the wire $\mathrm{d}\boldsymbol{l}$ with the current I moving in the direction of $\mathrm{d}\boldsymbol{l}$

$$\mathrm{d}\boldsymbol{B} = \frac{\mu I}{4\pi}\frac{\mathrm{d}\boldsymbol{l}\times\boldsymbol{r}}{|\boldsymbol{r}^3|},$$

where μ is the permeability of the medium surrounding the wire, can be recognized. Indeed, the Biot-Savart law is a general result of potential theory, and potential theory describes electromagnetic fields as well as inviscid, incompressible flows.

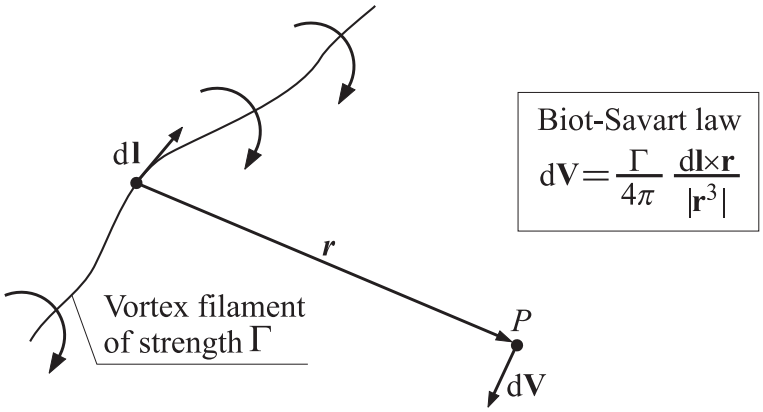

Figure 1.7. Vortex filament and Biot-Savart law.

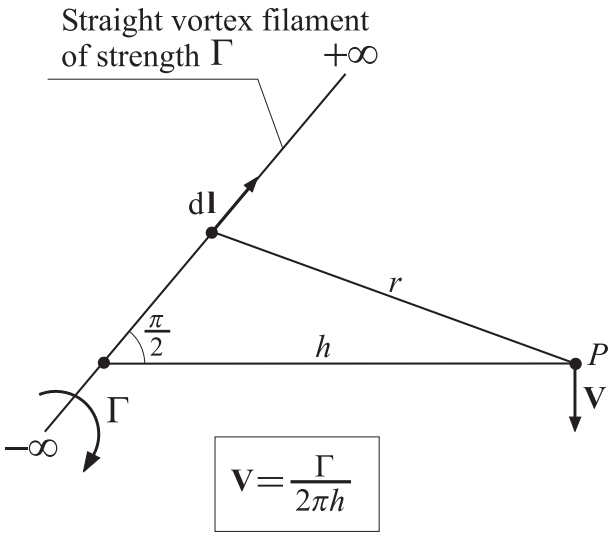

Figure 1.8. Velocity induced at point P by an infinite vortex filament.

can be obtained. Helmholtz's theorems are the following:

- *Theorem 1*
  The strength of a vortex filament is constant along its length.

- *Theorem 2*
  A vortex filament cannot end in a fluid; it must extend to the boundaries of the fluid (which can be $\pm\infty$) or form a closed path.

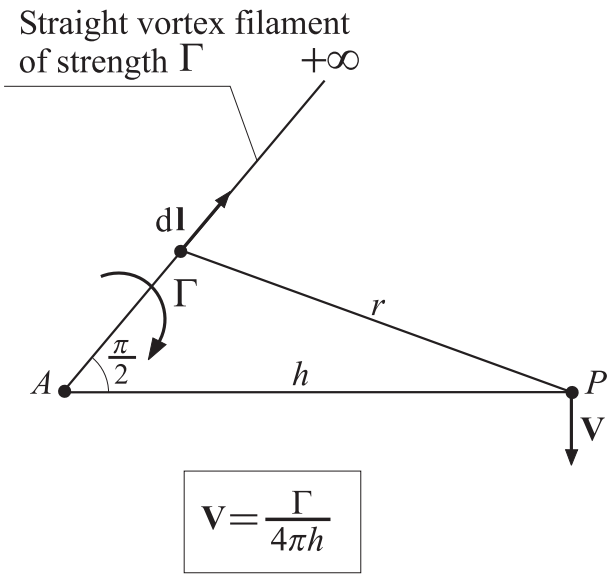

Figure 1.9. Velocity induced at point P by a semi-infinite vortex filament.

Observation 4 From these theorems, it can be understood that a vortex filament can be divided into two or more filaments, but, if the generic strength is indicated with Γ_i , the following relation must be satisfied:

$$\sum_i \Gamma_i = \Gamma. \tag{1.64}$$

The property shown in equation (1.64) will be used in the lifting-line theories (see chapter 3).

Nomenclature

ρ	fluid density
μ	fluid viscosity
p	pressure
T	temperature
t	time
$\boldsymbol{V}$	velocity vector
M	doublet strength
Q	source strength
m	doublet distribution
q	source distribution
Γ	vorticity
$BCVI$	Boundary Condition on Velocity at Infinity
WTC	Wall Tangency Condition
Φ	velocity potential
ϕ	small perturbation velocity potential
Ψ	acceleration potential or small perturbation acceleration potential
v_x	x-component perturbation velocity
v_y	y-component perturbation velocity
v_z	z-component perturbation velocity
V_x	x-component velocity
V_y	y-component velocity
V_z	z-component velocity
$\boldsymbol{i}, \boldsymbol{j}, \boldsymbol{k}$	unit vectors
e	thermal energy for unit mass
c_v, c_p	specific heat for unit mass
$R^\star$	gas costant
c	sound speed
$\frac{\partial}{\partial t}$	Euler derivative
$\frac{D}{Dt}$	Lagrange derivative

Subscripts

∞	freestream conditions
w	wing

Chapter 2

Mathematical Tools

2.1 Introduction

In this chapter a few important mathematical tools, used in the rest of the dissertation, are introduced. In particular, some properties of quadrature formulas and integral equations will be discussed. Particularly relevant and important will be the concepts of *hypersingular integrals* (see [5]).

2.2 Brief Description of the Quadrature Formulas

Most of the integral can not be solved analytically. Therefore, approximate methods have to be used. Several formulas, such as Newton-Cotes formulae and Gaussian quadrature are available. In this section, only a few of these formulae are discussed and analyzed. More details can be found in ([6]) and ([7]).

2.2.1 Gaussian Quadrature

Numerical quadrature involves estimating $\int_a^b f(x)\,\mathrm{d}x$ using a formula of the form

$$\int_a^b f(x)\,\mathrm{d}x \approx \sum_i^M c_i f(x_i). \tag{2.1}$$

A quadrature formula, whose nodes (abscissas) x_i and coefficients w_i are chosen to achieve a maximum order of accuracy, is called a *Gaussian quadrature formula.* The integrand usually involves a *weight function w.* An integral in x on an interval (a,b) must be converted into an integral in t over the interval (A,B) specified for the

weight function involved. This can be accomplished by the transformation $t = \frac{(bA-aB)}{(b-a)} + \frac{(B-A)x}{(b-a)}$. Gaussian quadrature formulae generally take the form

$$\int_A^B w(t) f(t)\, \mathrm{d}t \approx \sum_{i=1}^{M} w_i f(t_i). \tag{2.2}$$

Presented below are some of the *classical Gaussian quadrature* formulas.

- *Gauss-Legendre Quadrature*

$$\int_{-1}^{+1} f(t)\, \mathrm{d}t \approx \sum_{i=1}^{M} w_i f(t_i).$$

- *Gauss-Jacobi Quadrature*

$$\int_{-1}^{+1} (1-t)^{\alpha} (1+t)^{\beta} f(t)\, \mathrm{d}t \approx \sum_{i=1}^{M} w_i f(t_i) \qquad \alpha,\beta > -1.$$

- *Gauss-Laguerre Quadrature*

$$\int_{0}^{+\infty} \mathrm{e}^{-t} f(t)\, \mathrm{d}t \approx \sum_{i=1}^{M} w_i f(t_i).$$

- *Gauss-Hermite Quadrature*

$$\int_{-\infty}^{+\infty} \mathrm{e}^{-t^2} f(t)\, \mathrm{d}t \approx \sum_{i=1}^{M} w_i f(t_i).$$

Now consider the *Gauss-Legendre* quadrature[1]

$$\int_{-1}^{+1} f(t)\, \mathrm{d}t = \sum_{i=1}^{M} h_i f(t_i). \tag{2.3}$$

The expression for the weights[2] $h_i = w_i$ (see [6]) is

$$h_i = \frac{-2}{(M+1) P_{M+1}(t_i) P'_M(t_i)}, \tag{2.4}$$

[1] In this dissertation the *Gauss-Legendre* formula will be used often. In some cases, the adaptive quadrature is applied, and only for the Hadamard finite-part integrals a particular quadrature formula is required.

[2] In the Gauss-Legendre formula, the notation $h_i = w_i$ is used for the weights. This is required because the quadrature formula for the Hadamard finite part integrals already has the symbol w_i^I.

where the nodes t_i are the zeros of the *Legendre* polynomial $P_M(t)$. To complete this brief introduction, reported below is the recursive formula for the Legendre polynomials:

$$\begin{aligned} &P_0(t) = 1, P_1(t) = t && -1 \leq t \leq 1, \\ &(n+1) P_{n+1}(t) = (2n+1) t P_n(t) - n P_{n-1}(t) && n = 1,2... \end{aligned} \tag{2.5}$$

and the first five polynomials are:

$$\begin{aligned} P_0 &= 1, \\ P_1 &= t, \\ P_2 &= \frac{\left(3t^2-1\right)}{2}, \\ P_3 &= \frac{5}{2}t^3 - \frac{3}{2}t, \\ P_4 &= \frac{35}{8}t^4 - \frac{15}{4}t^2 + \frac{3}{8}. \end{aligned} \tag{2.6}$$

2.2.2 Adaptive Quadrature

Here, the basic concepts of adaptive quadrature method are shown. For more details see [8] and [9]. The concept is to divide the interval of integration into subintervals. If the assigned precision has not been achieved yet, the subintervals will be divided into more parts with an iterative algorithm until the integral is calculated with the desired accuracy. Figure 2.1 shows this concept. As can be seen in the figure, if the function has a very high gradient, it is very hard to calculate the integral. In such cases, even the Gaussian quadrature is not very good and an adaptive formula is required.

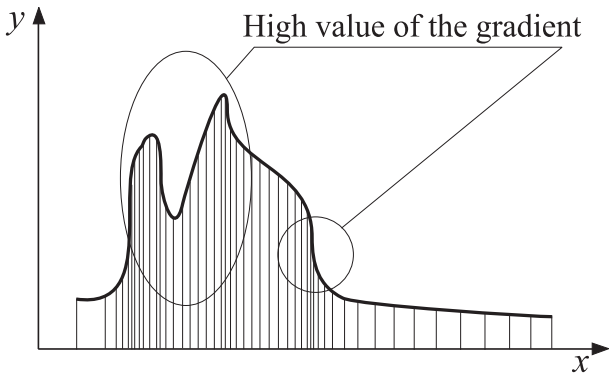

Figure 2.1. Basic concepts of the adaptive quadrature.

2.3 Integrals With Strong Singularities: Hadamard Finite-part Integrals

This section analyzes integrals with strong singularities (*hypersingular integrals*, see [5]). Such integrals exist only if they are defined in a proper sense[3], and usually they are called *finite-part integrals*. The concept of finite-part integrals was first introduced and examined by Hadamard in 1923 [10].

To introduce the concept of *finite-part integral*, consider the integral[4]

$$\int_a^b \frac{\mathrm{d}t}{t-s} \qquad a < s < b. \tag{2.7}$$

In a *standard* way, this integral is obviously not defined because, when $t \to s$, the denominator reaches zero with order 1. To correctly evaluate the integral, its definition has to be changed. Therefore, the symbol

$$⨍ \tag{2.8}$$

is introduced. Thus, equation (2.7) becomes

$$⨍_a^b \frac{\mathrm{d}t}{t-s} \qquad a < s < b. \tag{2.9}$$

To proceed, consider the following *standard non-singular*[5] integrals:

$$\begin{aligned} \int_a^{s-\epsilon} \tfrac{\mathrm{d}t}{t-s} &= \ln\epsilon - \ln(s-a), \\ \int_{s+\epsilon}^{b} \tfrac{\mathrm{d}t}{t-s} &= \ln(b-s) - \ln\epsilon. \end{aligned} \tag{2.10}$$

By using the previous expressions[6] (equation (2.10)), the following definitions can be introduced.

Definition 1

$$⨍_a^s \frac{\mathrm{d}t}{t-s} = \lim_{\epsilon\to 0}\left[\int_a^{s-\epsilon} \frac{\mathrm{d}t}{t-s} - \ln\epsilon\right] = -\ln(s-a), \tag{2.11}$$

[3] In a "classical" point of view, such integrals cannot be calculated.

[4] The case in which s coincides with one of the endpoints of the integral is not encountred in this dissertation.

[5] ϵ is a positive number.

[6] Notice that the definitions are obtained by elimination of the singular term $\ln\epsilon$ in equation (2.10). This operation is done by summing or subtracting the term $\ln\epsilon$.

$$\oint_s^b \frac{\mathrm{d}t}{t-s} = \lim_{\epsilon \to 0} \left[\int_{s+\epsilon}^b \frac{\mathrm{d}t}{t-s} + \ln \epsilon \right] = \ln (b-s)\,, \tag{2.12}$$

$$\oint_a^b \frac{\mathrm{d}t}{t-s} = \oint_a^s \frac{\mathrm{d}t}{t-s} + \oint_s^b \frac{\mathrm{d}t}{t-s} = \ln \frac{(b-s)}{(s-a)}. \tag{2.13}$$

In order to formulate definition 2, consider now an integer $p > 0$[7]. Consider also the following *standard* integrals:

$$\int_a^{s-\epsilon} \frac{\mathrm{d}t}{(t-s)^{p+1}} = \frac{1}{p} \left[\frac{1}{(a-s)^p} - \frac{1}{(-\epsilon)^p} \right], \tag{2.14}$$

$$\int_{s+\epsilon}^b \frac{\mathrm{d}t}{(t-s)^{p+1}} = \frac{1}{p} \left[-\frac{1}{(b-s)^p} + \frac{1}{\epsilon^p} \right]. \tag{2.15}$$

Eliminating the singular terms, definition 2 is obtained (see below).

Definition 2

$$\oint_a^s \frac{\mathrm{d}t}{(t-s)^{p+1}} = \lim_{\epsilon \to 0} \left[\int_a^{s-\epsilon} \frac{\mathrm{d}t}{(t-s)^{p+1}} + \frac{1}{p\,(-\epsilon)^p} \right] = \frac{1}{p\,(a-s)^p}, \tag{2.16}$$

$$\oint_s^b \frac{\mathrm{d}t}{(t-s)^{p+1}} = \lim_{\epsilon \to 0} \left[\int_{s+\epsilon}^b \frac{\mathrm{d}t}{(t-s)^{p+1}} - \frac{1}{p\epsilon^p} \right] = -\frac{1}{p\,(b-s)^p}, \tag{2.17}$$

$$\oint_a^b \frac{\mathrm{d}t}{(t-s)^{p+1}} = \oint_a^s \frac{\mathrm{d}t}{(t-s)^{p+1}} + \oint_s^b \frac{\mathrm{d}t}{(t-s)^{p+1}} = -\frac{1}{p} \left[\frac{1}{(b-s)^p} - \frac{1}{(a-s)^p} \right]. \tag{2.18}$$

From equation (2.18), it is easy to understand that

$$\oint_a^b \frac{\mathrm{d}t}{(t-s)^p} = -\frac{1}{p-1} \left[\frac{1}{(b-s)^{p-1}} - \frac{1}{(a-s)^{p-1}} \right]. \tag{2.19}$$

Because the identity

$$\frac{\mathrm{d}}{\mathrm{d}s} \left(-\frac{1}{(p-1)} \left[\frac{1}{(b-s)^{p-1}} - \frac{1}{(a-s)^{p-1}} \right] \right) = - \left[\frac{1}{(b-s)^p} - \frac{1}{(a-s)^p} \right] \tag{2.20}$$

[7] p will be an integer in this dissertation, and in some demonstrations this condition will be used. In the original work of the Prof. Monegato (see [5]), p can be a real number.

is valid, equations (2.19) and (2.18) lead to writing:

$$\frac{\mathrm{d}}{\mathrm{d}s} \oint_a^b \frac{\mathrm{d}t}{(t-s)^p} = p \oint_a^b \frac{\mathrm{d}t}{(t-s)^{p+1}}. \tag{2.21}$$

Now consider a function $f(t)$ of class C^p. Because the identity

$$f(t) = f(t) - \sum_{k=0}^{p} \frac{f^{(k)}(s)}{k!}(t-s)^k + \sum_{k=0}^{p} \frac{f^{(k)}(s)}{k!}(t-s)^k \tag{2.22}$$

is valid, the following quantity can be defined.

Definition 3

$$\oint_a^b \frac{f(t)}{(t-s)^{p+1}}\,\mathrm{d}t = \int_a^b \frac{f(t) - \sum_{k=0}^{p} \frac{f^{(k)}(s)}{k!}(t-s)^k}{(t-s)^{p+1}}\,\mathrm{d}t + \oint_a^b \frac{\sum_{k=0}^{p} \frac{f^{(k)}(s)}{k!}(t-s)^k}{(t-s)^{p+1}}\,\mathrm{d}t, \tag{2.23}$$

or equivalently

$$\oint_a^b \frac{f(t)}{(t-s)^{p+1}}\,\mathrm{d}t = \int_a^b \frac{f(t) - \sum_{k=0}^{p} \frac{f^{(k)}(s)}{k!}(t-s)^k}{(t-s)^{p+1}}\,\mathrm{d}t + \sum_{k=0}^{p} \frac{f^{(k)}(s)}{k!} \oint_a^b \frac{1}{(t-s)^{p+1-k}}\,\mathrm{d}t. \tag{2.24}$$

Observation 5 Notice that p has been assumed as an integer; thus, equation (2.24) contains the term

$$\frac{f^{(p)}(s)}{p!} \oint_a^b \frac{1}{(t-s)}\,\mathrm{d}t. \tag{2.25}$$

Because of the hypothesis $a < s < b$, the integral in the previous expression could be interpreted in the *Cauchy principal sense*[8]. By using the definitions formulated avove, the finite-part integral could be generalized as

$$\oint_a^b \frac{\mathrm{d}t}{t-s} = \lim_{\epsilon \to 0} \left[\int_a^{s-\varepsilon_1(\epsilon)} \frac{\mathrm{d}t}{t-s} + \int_{s+\varepsilon_2(\epsilon)}^b \frac{\mathrm{d}t}{t-s} \right] = \ln \frac{b-s}{s-a} + \lim_{\epsilon \to 0} \ln \frac{\varepsilon_1(\epsilon)}{\varepsilon_2(\epsilon)}. \tag{2.26}$$

Assuming that

$$\lim_{\epsilon \to 0} \ln \frac{\varepsilon_1(\epsilon)}{\varepsilon_2(\epsilon)} = \mathrm{e}^c, \tag{2.27}$$

[8] If the singularity is in an endpoint, the Cauchy integral is not defined, and the integral has to be defined as Hadamard finite-part integral.

then[9]

$$\oint\!\!\!\!\!\!-_a^b \frac{\mathrm{d}t}{t-s} = \int_a^b \frac{\mathrm{d}t}{t-s} + c. \tag{2.28}$$

Observation 6 It should be noticed that the integral in equation (2.24)

$$\int_a^b \frac{f(t) - \sum_{k=0}^{p} \frac{f^{(k)}(s)}{k!}(t-s)^k}{(t-s)^{p+1}}\,\mathrm{d}t \tag{2.29}$$

is not singular.

Observation 7 From the definitions analyzed before, it is possible to obtain the following relation[10]:

$$\frac{\mathrm{d}}{\mathrm{d}s}\oint\!\!\!\!\!\!-_a^b \frac{f(t)}{(t-s)^p}\,\mathrm{d}t = p\oint\!\!\!\!\!\!-_a^b \frac{f(t)}{(t-s)^{p+1}}\,\mathrm{d}t. \tag{2.30}$$

Using this formula, it is possible to write:

$$\oint\!\!\!\!\!\!-_a^b \frac{f(t)}{(t-s)^{p+1}}\,\mathrm{d}t = \frac{1}{p_!}\frac{\mathrm{d}^p}{\mathrm{d}s^p}\int_a^b \frac{f(t)}{(t-s)}\,\mathrm{d}t. \tag{2.31}$$

Hence, it can be said that Hadamard finite-part integrals can be seen as the derivative of an integral interpreted in the Cauchy sense.

Observation 8 From the previous definitions, it immediately follows that

$$\oint\!\!\!\!\!\!-_a^b \frac{a_1 f(t) + a_2 g(t)}{(t-s)^{p+1}}\,\mathrm{d}t = a_1\oint\!\!\!\!\!\!-_a^b \frac{f(t)}{(t-s)^{p+1}}\,\mathrm{d}t + a_2\oint\!\!\!\!\!\!-_a^b \frac{g(t)}{(t-s)^{p+1}}\,\mathrm{d}t. \tag{2.32}$$

Therefore, it can be understood that the operator $\oint\!\!\!\!\!\!-$ is a *linear operator* as the operator $\int$.

[9]Remember that the integral interpreted in the Cauchy sense is

$$\int_a^b \frac{\mathrm{d}t}{t-s} = \ln\frac{b-s}{s-a}.$$

[10] Remember that p is an integer and $a < s < b$. Only these conditions allow the use of this formula.

Observation 9 By using the expressions analyzed in this section, it is possible to show that[11]

$$\oint_a^b \frac{f(t)}{(t-s)^{p+1}}\,\mathrm{d}t = -\frac{1}{p}\left[\frac{f(b)}{(b-s)^p} - \frac{f(a)}{(a-s)^p}\right] + \frac{1}{p}\oint_a^b \frac{f'(t)}{(t-s)^p}\,\mathrm{d}t. \tag{2.33}$$

Hence, it can be said that in Hadamard finite-part integrals the integration by parts rule is still valid.

Observation 10 Consider the following Hadamard finite-part integral[12]:

$$\oint_a^b f(s) \oint_a^b \frac{f(t)}{(t-s)^2}\,\mathrm{d}t\,\mathrm{d}s. \tag{2.34}$$

The following properties are valid:

- *Property 1*
  If the function is *zero in both endpoints*, the external integral can be defined as a normal integral. Therefore,

  $$\oint_a^b f(s) \oint_a^b \frac{f(t)}{(t-s)^2}\,\mathrm{d}t\,\mathrm{d}s = \int_a^b f(s) \oint_a^b \frac{f(t)}{(t-s)^2}\,\mathrm{d}t\,\mathrm{d}s. \tag{2.35}$$

  Moreover, it is possible to change the variables of integration or switch the variables (see appendix A).

- *Property 2*
  If the function *is not* zero in both endpoints, *but the curve is a closed path*, the following equation is valid:

  $$\oint_a^b f(s) \oint_a^b \frac{f(t)}{(t-s)^2}\,\mathrm{d}t\,\mathrm{d}s = \oint_a^b f(s) \oint_a^b \frac{f(t)}{(t-s)^2}\,\mathrm{d}t\,\mathrm{d}s. \tag{2.36}$$

  Even now it is possible to change the variables of integration or switch the variables (see appendix A).

[11] Even in this case, this formula is valid because p is an integer and $a < s < b$.
[12] This is the only case that will be considered in subsequent discussions.

2.4 Summary and Examples of Hadamard Finite-part Integrals

In the previous section Hadamard finite-part integrals were introduced. Summarized below are the properties of Hadamard finite-part integrals when $a < s < b$ and p is an integer.

- *Property 1*
  They can be seen as a derivative of an integral interpreted in the Cauchy sense.
- *Property 2*
  They are linear operators.
- *Property 3*
  The integration by parts rule is valid.

As an easy example, consider the finite-part integral

$$\oint_{-1}^{+1} \frac{t^2}{(t-s)^4} \mathrm{d}t \qquad -1 < s < +1. \tag{2.37}$$

By using equation (2.31), the integral can be written as

$$\oint_{-1}^{+1} \frac{t^2}{(t-s)^4} \mathrm{d}t = \oint_{-1}^{+1} \frac{t^2}{(t-s)^{3+1}} \mathrm{d}t = \frac{1}{3!} \frac{\mathrm{d}^3}{\mathrm{d}s^3} \oint_{-1}^{+1} \frac{t^2}{(t-s)} \mathrm{d}t. \tag{2.38}$$

In order to calculate the Cauchy principal value contained in equation (2.38), the following indefinite integral is required:

$$\int \frac{t^2}{(t-s)} \mathrm{d}t = ts + \frac{1}{2}t^2 + s^2 \ln\left(|-t+s|\right). \tag{2.39}$$

The Cauchy principal value definition is:

$$\oint_{-1}^{+1} \frac{t^2}{(t-s)} \mathrm{d}t = \lim_{\epsilon \to 0} \left[\int_{-1}^{s-\epsilon} \frac{t^2}{(t-s)} \mathrm{d}t + \int_{s+\epsilon}^{+1} \frac{t^2}{(t-s)} \mathrm{d}t \right]. \tag{2.40}$$

From equation (2.39)

$$\begin{aligned} \int_{-1}^{s-\epsilon} \tfrac{t^2}{(t-s)} \mathrm{d}t &= \left[ts + \tfrac{1}{2}t^2 + s^2 \ln\left(|t-s|\right) \right]_{-1}^{s-\epsilon} = \\ &= \tfrac{3}{2}s^2 - 2s\epsilon + \tfrac{1}{2}\epsilon^2 + s^2 \ln \epsilon + s - \tfrac{1}{2} - s^2 \ln\left(s+1\right), \\ \int_{s+\epsilon}^{+1} \tfrac{t^2}{(t-s)} \mathrm{d}t &= \left[ts + \tfrac{1}{2}t^2 + s^2 \ln\left(|t-s|\right) \right]_{s+\epsilon}^{1} = \\ &= -\tfrac{3}{2}s^2 - 2s\epsilon - \tfrac{1}{2}\epsilon^2 - s^2 \ln \epsilon + s + \tfrac{1}{2} + s^2 \ln\left(1-s\right). \end{aligned} \tag{2.41}$$

Substituting these expressions into equation (2.40)

$$\oint_{-1}^{+1} \frac{t^2}{(t-s)} \mathrm{d}t = 2s + s^2 \ln \frac{(1-s)}{(1+s)}. \tag{2.42}$$

Observing that

$$\frac{\mathrm{d}^3}{\mathrm{d}s^3} \left(2s + s^2 \ln(1-s) - s^2 \ln(1+s)\right) = 4 \frac{3+s^2}{(s-1)^3 (s+1)^3}, \tag{2.43}$$

and recalling equation (2.38), the following result is obtained:

$$\oint_{-1}^{+1} \frac{t^2}{(t-s)^4} \mathrm{d}t = \frac{1}{3!} 4 \frac{3+s^2}{(s-1)^3 (s+1)^3} = \frac{2}{3} \frac{3+s^2}{(s-1)^3 (s+1)^3}. \tag{2.44}$$

Observation 11 Practically, the Hadamard finite-part integral can be calculated in a simple way. Consider the antiderivative of the function under the Hadamard integral:

$$\int \frac{t^2}{(t-s)^4} \mathrm{d}t = -\frac{1}{3} \frac{s^2}{(t-s)^3} - \frac{s}{(t-s)^2} - \frac{1}{t-s}. \tag{2.45}$$

Calculating the Hadamard finite-part integral by *ignoring that the integral in s is singular, and applying the "standard" rule for the integrals*, the result is

$$\oint_{-1}^{+1} \frac{t^2}{(t-s)^4} \mathrm{d}t = \frac{2}{3} \frac{3+s^2}{(s-1)^3 (s+1)^3}. \tag{2.46}$$

This result is *the same* as what was found in equation (2.44).
Therefore, *if the antiderivative F of the function in a Hadamard finite-part integral is known, the value of the integral will be the quantity $F(b) - F(a)$.* In a formal point of view:

$$\int \frac{f(t)}{(t-s)^{p+1}} \mathrm{d}t = F \Rightarrow \oint_{a}^{b} \frac{f(t)}{(t-s)^{p+1}} \mathrm{d}t = F(b) - F(a). \tag{2.47}$$

This property will be used often when the condition of *minimum induced drag* in the elliptical and circular annular wings is found.
It should be clear that, in general, *the antiderivative is not known.* Appropriate quadrature formula is then required.

2.5 Hadamard Finite-part Integrals: a Quadrature Formula

In this section, a quadrature formula for the Hadamard finite-part integrals is described. Only the case in which $a < s < b$ and $p = 1$ is considered. Consider the following hypersingular integral[13]:

$$\oint\!\!\!\!\!\!= \int_{-1}^{+1} \frac{f(t)}{(t-s)^2}\,\mathrm{d}t. \tag{2.48}$$

It is possible to calculate the integral by using the following formula[14]:

$$\oint\!\!\!\!\!\!= \int_{-1}^{+1} \frac{f(t)}{(t-s)^2}\,\mathrm{d}t = \sum_{i=1}^{M} w_i^I f(t_i)\,. \tag{2.49}$$

The last relation contains the following quantities:

- The *nodes* t_i. They coincide with the zeros of the *Legendre* polynomial $P_M(t)$.
- The *weights*: $w_i^I(s) = h_i \sum_{j=0}^{M-1} d_j^{-1} P_j(t_i) \left[Q_j'(s)\right]$.
- The *Gauss weights* h_i.
- The integrals of the *Legendre* polynomials: $d_j = \int_{-1}^{+1} P_j^2(t)\,\mathrm{d}t = \frac{2}{2j+1}$.
- The derivative of the integrals interpreted in the Cauchy[15] sense: $Q_j'(s) = \frac{\mathrm{d}}{\mathrm{d}s} Q_j(s) = \frac{\mathrm{d}}{\mathrm{d}s} \int\!\!\!\!\!\!- \int_{-1}^{+1} \frac{P_j(t)}{t-s}\,\mathrm{d}t$.

[13] Only the case $a = -1$ and $b = +1$ will be analyzed because, in the case examined here, p is an integer and the singularity is not in an endpoint. Therefore, it is possible to change the variables of integration in such a way as to have $a = -1$ and $b = +1$, as is usually done when calculating the standard integrals using the Gaussian quadrature rule.

[14] This is only a particular case of a general method that is possible to find in paper [5] written by prof. G. Monegato.

[15] It has been seen that the Hadamard finite-part integrals are the derivative of the Cauchy integrals. Thus, it is obvious that in the quadrature formula Cauchy integrals appear as well.

Using the definitions formulated in section 2.3, the explicit form of the quantities Q_j and their derivatives can be expressed as follows:

$$
\begin{aligned}
&Q_0(s) = \int\!\!\!\!\!\!-_{-1}^{+1} \tfrac{1}{t-s}\,\mathrm{d}t \Rightarrow \\
&Q_0(s) = \lim_{\varepsilon\to 0}\left(\int_{-1}^{s-\varepsilon} \tfrac{1}{t-s}\mathrm{d}t + \int_{s+\varepsilon}^{+1} \tfrac{1}{t-s}\mathrm{d}t\right) \Rightarrow \\
&Q_0(s) = \lim_{\varepsilon\to 0}\left(\ln|t-s|_{-1}^{s-\varepsilon} + \ln|t-s|_{s+\varepsilon}^{+1}\right) \Rightarrow \\
&Q_0(s) = \lim_{\varepsilon\to 0}\left(\ln|s-\varepsilon-s| - \ln|-1-s| + \ln|1-s| - \ln|s+\varepsilon-s|\right) \Rightarrow \\
&Q_0(s) = \lim_{\varepsilon\to 0}\left(\ln|-\varepsilon| - \ln|-1-s| + \ln|1-s| - \ln|+\varepsilon|\right) \Rightarrow \\
&Q_0(s) = -\ln|-1-s| + \ln|1-s|\,.
\end{aligned}
$$

Operating in a similar way:

$$
\begin{aligned}
&Q_1(s) = \lim_{\varepsilon\to 0}\left(\int_{-1}^{s-\varepsilon} \tfrac{t}{t-s}\,\mathrm{d}t + \int_{s+\varepsilon}^{+1} \tfrac{t}{t-s}\,\mathrm{d}t\right) \Rightarrow \\
&Q_1(s) = (1 + s\ln(|1-s|)) - (-1 + s\ln(|-1-s|))\,.
\end{aligned}
$$

Because $a = -1$, $b = +1$ and $a < s < b$, the previous equations can be rewritten as:

$$
\begin{aligned}
Q_0(s) &= -\ln(1+s) + \ln(1-s)\,, \\
Q_1(s) &= (1 + s\ln(1-s)) - (-1 + s\ln(1+s))\,.
\end{aligned}
\tag{2.50}
$$

A recursive formula is possible to use to determine the quantities $Q_j(s)$ and $Q_j'(s)$ as follows:

$$
Q_j(s) = (a_j s + b_j)\,Q_{j-1}(s) - c_j Q_{j-2}(s)\,, \tag{2.51}
$$

where

$$
a_j = \frac{2j-1}{j},\ \ b_j = 0,\ \ c_j = \frac{j-1}{j}. \tag{2.52}
$$

Substituting this relation into equation (2.51), the final expressions for the integrals interpreted in the Cauchy principal value sense can be written as

$$
\begin{aligned}
Q_j(s) &= s\tfrac{2j-1}{j}Q_{j-1}(s) - \tfrac{j-1}{j}Q_{j-2}(s) \\
Q_j'(s) &= s\tfrac{2j-1}{j}Q_{j-1}'(s) - \tfrac{j-1}{j}Q_{j-2}'(s) + \tfrac{2j-1}{j}Q_{j-1}(s)\,.
\end{aligned}
\tag{2.53}
$$

This equation leads to calculating the weights $w_i^I(s)$ and, as a result, the assigned Hadamard finite-part integral.

2.6 Integral Equations

This section contains a general analysis of the integral equations (see [6]) without demonstrations. Several types of equations will be introduced.

2.6.1 Definitions

Consider the following *integral equation*:

$$h\left(s\right)m\left(s\right)=f\left(s\right)+\Lambda\int_{a}^{b(s)}K\left(s,t\right)G\left[m\left(t\right);t\right]\,\mathrm{d}t. \tag{2.54}$$

Definitions:

- $K(s,t)$: kernel.
- $m(s)$: function to be determined.
- $h(s)$,$f(s)$: given functions.
- Λ: eigenvalue.

2.6.2 Classification of Integral Equations

The classification is:

- Linear $G[m(s);s]=m(s)$.
- Volterra $b(s)=s$.
- Fredholm $b(s)=b$.
- First kind $h(s)=0$.
- Second kind $h(s)=1$.
- Third kind $h(s)\neq 0,1$.
- Homogeneous $f(s)=0$.
- Singular $a=-\infty, b=+\infty$.

2.6.3 Classification of Kernels

- Symmetric $K(s,t) = K(t,s)$
- Separable/degenerate $K(s,t) = \sum_{i=1}^{n} a_i(s)\, b_i(t), \quad n < \infty$
- Difference $K(s,t) = K(s-t)$.
- Cauchy $K(s,t) = \frac{1}{s-t}$
- Singular $K(s,t) \to \infty$ as $t \to s$
- Hilbert-Schmidt $\int_a^b \int_a^b |K(s,t)|^2 \, \mathrm{d}s \, \mathrm{d}t < \infty$

2.6.4 Integral Equations Involving Hadamard Finite-part Integrals

A general analysis of the integral equations was presented in previous sections. In this section one particular case is analyzed: an integral equation with a symmetric[16] kernel and with an integral interpreted as Hadamard finite-part integral ($p = 1$). In subsequent chapters, a few integral equations of the following type will be derived:

$$\alpha(\varphi) = g(\varphi) \left(\int_a^b m(\varphi_d)\, K(\varphi,\varphi_d)\, \mathrm{d}\varphi_d + \hat{\int}_a^b m(\varphi_d)\, Y(\varphi,\varphi_d)\, \mathrm{d}\varphi_d \right), \tag{2.55}$$

where $K(\varphi,\varphi_d)$ and $Y(\varphi,\varphi_d)$ are the kernels of the equation, $\alpha(\varphi)$ and $g(\varphi)$ are known functions, and $m(\varphi_d)$ is the unknown function. How can this equation be solved? Because the kernel $Y(\varphi,\varphi_d)$ is singular[17], the numeric approximation must be performed carefully. One good method consists of the following steps:

- *Step 1*
  Changing of the variable of integration in such a way as to obtain the endpoints -1 and +1, respectively. In this case this is possible either because the function is zero in both endpoints or because the curve is a closed path.

- *Step 2*
  Decomposition of the function m in a series of known N functions multiplied by the unknown *constant* coefficients c_k.

[16] This hypothesis is not used here, but in this dissertation only this type of equations are used.
[17] The second integral is defined in the Hadamard finite-part sense. m is considered as a non-singular function. Therefore, the kernel $Y(\varphi,\varphi_d)$ is singular.

- *Step 3*
  Application of the *collocation method*: the integral equation has to be satisfied exactly in N points. Thus, a set of *linear algebraic* equations[18] can be written and the unknown coefficients c_k can be found.

Observation 12 In order to obtain the best results, it is important to know, with good accuracy, the coefficients of the linear system that lead to determining the unknown c_k. As can be seen in the following example, this affirmation means that the integrals ("classical" and interpreted in the Hadamard finite-part sense) have to be calculated with a sufficient precision using an efficient algorithm (for example, it is possible to use the method seen in section 2.5).

Example 1: Numerical Solution of a Simple Case

Consider the following integral equation[19]:

$$\ln\frac{(1-s)}{(1+s)} - \frac{2s}{(1-s)(1+s)} = \neq\int_{-1}^{+1} \frac{m(t)}{(t-s)^2}\,\mathrm{d}t \qquad -1 < s < +1. \tag{2.56}$$

It is easy to see that equation (2.56) is one of the types shown in equation (2.55), where:

$$\begin{aligned} &\alpha(s) = \ln\tfrac{(1-s)}{(1+s)} - \tfrac{2s}{(1-s)(1+s)},\\ &g(s) = 1,\\ &K(t,s) = 0,\\ &Y(t,s) = \tfrac{1}{(t-s)^2}. \end{aligned} \tag{2.57}$$

Now the procedure described above is applied:

- *Step 1*
  This operation has already been done (the integral in equation (2.56) has endpoints -1 and +1).

- *Step 2*
  The function m is decomposed in a series of known N functions multiplied by the unknown *constant* coefficients c_k. The *Legendre polynomials*[20] are chosen:

$$m(t) = \sum_{k=0}^{k=N-1} c_k P_k. \tag{2.58}$$

[18] These linear equations will have coefficients dependent on some integrals, as can be seen in the example below.

[19] It is supposed that the original variables have already been transformed into the new variables t and s in order to have the integrals with endpoints -1 and +1.

[20] This is not the only possible choice that can be made.

The Hadamard finite-part integral becomes:

$$\oint_{-1}^{+1} \frac{m(t)}{(t-s)^2}\,\mathrm{d}t = \oint_{-1}^{+1} \frac{\sum_{k=0}^{k=N-1} c_k P_k}{(t-s)^2}\,\mathrm{d}t = \sum_{k=0}^{k=N-1} c_k \oint_{-1}^{+1} \frac{P_k}{(t-s)^2}\,\mathrm{d}t. \tag{2.59}$$

Just to explain the method, consider a simple case where $N = 2$:

$$m(t) = c_0 P_0 + c_1 P_1, \tag{2.60}$$

$$\oint_{-1}^{+1} \frac{m(t)}{(t-s)^2}\,\mathrm{d}t = c_0 \oint_{-1}^{+1} \frac{P_0}{(t-s)^2}\,\mathrm{d}t + c_1 \oint_{-1}^{+1} \frac{P_1}{(t-s)^2}\,\mathrm{d}t. \tag{2.61}$$

Obviously, the Legendre polynomials are:

$$\begin{aligned} P_0 &= 1, \\ P_1 &= t. \end{aligned} \tag{2.62}$$

- *Step 3*
  Application of the *collocation method*: the integral equation has to be satisfied exactly in N points. A good choice is to take *the zeros of the Legendre polynomial* P_N. Let s_1 and s_2 be called the zeros of $P_2(s)$. The collocation method consists of the following N (remember that in this case $N = 2$) equations:

$$\oint_{-1}^{+1} \frac{m(t)}{(t-s_1)^2}\,\mathrm{d}t = \ln\frac{(1-s_1)}{(1+s_1)} - \frac{2s_1}{(1-s_1)(1+s_1)}, \tag{2.63}$$

$$\oint_{-1}^{+1} \frac{m(t)}{(t-s_2)^2}\,\mathrm{d}t = \ln\frac{(1-s_2)}{(1+s_2)} - \frac{2s_2}{(1-s_2)(1+s_2)}. \tag{2.64}$$

  Using equations (2.61) and (2.62):

$$c_0 \oint_{-1}^{+1} \frac{1}{(t-s_1)^2}\,\mathrm{d}t + c_1 \oint_{-1}^{+1} \frac{t}{(t-s_1)^2}\,\mathrm{d}t = \ln\frac{(1-s_1)}{(1+s_1)} - \frac{2s_1}{(1-s_1)(1+s_1)}, \tag{2.65}$$

$$c_0 \oint_{-1}^{+1} \frac{1}{(t-s_2)^2}\,\mathrm{d}t + c_1 \oint_{-1}^{+1} \frac{t}{(t-s_2)^2}\,\mathrm{d}t = \ln\frac{(1-s_2)}{(1+s_2)} - \frac{2s_2}{(1-s_2)(1+s_2)}. \tag{2.66}$$

  Observing that

$$\oint_{-1}^{+1} \frac{1}{(t-s_{1,2})^2}\,\mathrm{d}t = -\frac{2}{(1-s_{1,2})(1+s_{1,2})}, \tag{2.67}$$

$$\oint_{-1}^{+1} \frac{t}{(t-s_{1,2})^2}\,\mathrm{d}t = -\frac{2s_{1,2}}{(1-s_{1,2})(1+s_{1,2})} + \ln\frac{(1-s_{1,2})}{(1+s_{1,2})}, \tag{2.68}$$

the following *linear system* is obtained:

$$\begin{aligned} c_0\left(-\tfrac{2}{(1-s_1)(1+s_1)}\right) + c_1\left(\ln\tfrac{(1-s_1)}{(1+s_1)} - \tfrac{2s_1}{(1-s_1)(1+s_1)}\right) &= \ln\tfrac{(1-s_1)}{(1+s_1)} - \tfrac{2s_1}{(1-s_1)(1+s_1)}, \\ c_0\left(-\tfrac{2}{(1-s_2)(1+s_2)}\right) + c_1\left(\ln\tfrac{(1-s_2)}{(1+s_2)} - \tfrac{2s_2}{(1-s_2)(1+s_2)}\right) &= \ln\tfrac{(1-s_2)}{(1+s_2)} - \tfrac{2s_2}{(1-s_2)(1+s_2)}. \end{aligned} \tag{2.69}$$

The linear system has the solution:

$$\begin{aligned} c_0 &= 0, \\ c_1 &= 1. \end{aligned} \tag{2.70}$$

Therefore, the unknown function $m(t)$ is:

$$m(t) = c_0 P_0 + c_1 P_1 = t. \tag{2.71}$$

Thus, the integral equation is solved. Notice that in this example the function $m(t) = t$ *exactly* satisfies the integral equation. Usually, it is necessary to use more terms in the m expansion. Practically, $N = 20 \div 30$ is sufficient in most applications (see chapter 8 for more details).

Observation 13 In this example, the Hadamard integrals are calculated analytically, though in practical applications they are calculated numerically by using the algorithm seen in section 2.5.

Example 2: Numerical Solution of a More General Case

Consider an integral equation which has an integral of the type

$$I = \oint_{-1}^{+1} m(t)\,\frac{1}{1-\cos(\pi(t-s))}\,\mathrm{d}t \qquad -1 < s < +1. \tag{2.72}$$

Clearly, the integral has to be interpreted in the Hadamard finite-part sense, because when $t \to s$, the denominator of the integrand function is an infinitesimal function. It is easy to show that, when $t \to s$, the denominator can be written by using the Taylor expansion as

$$1-\cos(\pi(t-s)) \approx \left(\frac{1}{2}\pi^2\right)(t-s)^2 + \left(-\frac{1}{24}\pi^4\right)(t-s)^4. \tag{2.73}$$

The previous expression suggests that the original integral can be transformed into a form $\fint \frac{f(t)}{(t-s)^2}$. To achieve this result, it is sufficient to multiply and divide the function[21] $\frac{1}{1-\cos(\pi(t-s))}$ by the quantity $(t-s)^2$:

$$I = \fint_{-1}^{+1} m(t) \frac{1}{1-\cos(\pi(t-s))} \mathrm{d}t = \fint_{-1}^{+1} H(t,s) \frac{1}{(t-s)^2} \mathrm{d}t, \tag{2.74}$$

where

$$H(t,s) = m(t) \frac{(t-s)^2}{1-\cos(\pi(t-s))}. \tag{2.75}$$

Using the Legendre polynomials to expand the unknown function $m(t)$, the obtained result is:

$$m(t) = \sum_{k=0}^{N-1} c_k P_k(t) \Rightarrow H(t,s) = \frac{(t-s)^2}{1-\cos(\pi(t-s))} \sum_{k=0}^{N-1} c_k P_k(t). \tag{2.76}$$

Substituting this formula into the integral I:

$$I = \fint_{-1}^{+1} \frac{\frac{(t-s)^2}{1-\cos(\pi(t-s))} \sum_{k=0}^{N-1} c_k P_k(t)}{(t-s)^2} \mathrm{d}t = \sum_{k=0}^{N-1} c_k \fint_{-1}^{+1} \frac{\frac{(t-s)^2}{1-\cos(\pi(t-s))} P_k(t)}{(t-s)^2} \mathrm{d}t. \tag{2.77}$$

By observing equation (2.77), it can be understood that, when the collocation method is applied, the integral

$$I_l = \fint_{-1}^{+1} \frac{\frac{(t-s_l)^2}{1-\cos(\pi(t-s_l))} P_k(t)}{(t-s_l)^2} \mathrm{d}t \tag{2.78}$$

has to be calculated numerically. Clearly, s_l is the l^{th} zero of the Legendre polynomial $P_N(s)$. To calculate the previous integral, the algorithm seen in section 2.5 can be used:

$$\fint_{-1}^{+1} \frac{\frac{(t-s_l)^2}{1-\cos(\pi(t-s_l))} P_k(t)}{(t-s_l)^2} \mathrm{d}t = \sum_{i=1}^{M} w_i^I(s_l) \frac{(t_i-s_l)^2}{1-\cos(\pi(t_i-s_l))} P_k(t_i), \tag{2.79}$$

where

$$w_i^I(s_l) = h_i \sum_{j=0}^{M-1} d_j^{-1} P_j(t_i) \left[Q_j'(s_l)\right]. \tag{2.80}$$

[21] Notice that $\frac{(t-s)^2}{1-\cos(\pi(t-s))}$ is not singular because $\lim_{t\to s} \frac{(t-s)^2}{1-\cos(\pi(t-s))} = \frac{2}{\pi^2}$.

It is very important to notice that t_i are the *zeros of the Legendre polynomial* P_M, and that, in general, $M \neq N$. In this dissertation, $N = 20$ and $M = 200$ will be used very often (see chapter 8). This condition is required in order to solve the integral equation with sufficient accuracy.

Observation 14 If $t_i \approx s_l$, the function $\frac{(t_i - s_l)^2}{1-\cos(\pi(t_i - s_l))}$ is in the form $\frac{0}{0}$. To avoid numerical problems, under that condition, it is better to use the Taylor expansion as

$$\frac{(t_i - s_l)^2}{1 - \cos(\pi (t_i - s_l))} \approx \frac{2}{\pi^2} + \frac{(t_i - s_l)^2}{6} + \frac{\pi^2 (t_i - s_l)^4}{120} + \frac{\pi^4 (t_i - s_l)^6}{3024} + \frac{\pi^6 (t_i - s_l)^8}{86400}. \tag{2.81}$$

2.7 Euler-Lagrange Equation Involving Hadamard Finite-part Integrals

This is one of the most important tools used in this dissertation. The mathematical derivation is not obtained in a very rigorous way because the purpose of this section is only to help the reader better understand the next chapters.
Presented here is an original extension, proposed by the writer, of the well known Euler-Lagrange equation (see [11]) in a particular case, where the integral has to be interpreted in the Hadamard finite-part sense. Consider the following integral[22]:

$$J = C_1 \int_{-1}^{+1} m(s) \left(\oint_{-1}^{+1} m(t)\, Y(t,s)\, \mathrm{d}t \right) \mathrm{d}s, \tag{2.82}$$

where C_1 is a constant and where the kernel $Y(t,s)$ is the following symmetric function[23]:

$$Y(t,s) = Y(s,t) = \frac{1}{(t-s)^2}. \tag{2.83}$$

Suppose that the goal is to minimizes J. Consider, also, a *condition* of the following type:

$$\overline{C} = C_2 \int_{-1}^{+1} m(t)\, g(t)\, \mathrm{d}t, \tag{2.84}$$

[22] If the external integral is either a Cauchy integral or a Hadamard finite-part integral, the procedure reported below does not change.

[23] In this dissertation, only $Y(t,s) = \frac{1}{(t-s)^2}$ or a different expression referable to this will be found.

where $\overline{C}$ is an assigned constant and $g(s)$ is a *known function*. Obviously, the function m has to satisfy the boundary conditions

$$\begin{aligned} m(-1) &= m_0, \\ m(+1) &= m_1. \end{aligned} \tag{2.85}$$

In order to achieve the goal, consider now a function $\delta_1(t)$ that satisfies the condition

$$\delta_1(-1) = \delta_1(+1) = 0. \tag{2.86}$$

With this function, a solution for the problem can be found using the following relation[24]:

$$m(\cdot) = m_{\text{opt}}(\cdot) + \sigma\delta_1(\cdot) \qquad \sigma \in (-1,1). \tag{2.87}$$

Notice that in the previous equation m satisfies the boundary conditions (2.85), if

$$\begin{aligned} m_{\text{opt}}(-1) &= m_0, \\ m_{\text{opt}}(+1) &= m_1. \end{aligned} \tag{2.88}$$

Notice, also, that m_{opt} is the candidate function to minimize J. In order to apply the *Lagrange multiplier method*, condition (2.84) has to be manipulated. It can be written as

$$l(t) = C_2 \int_{-1}^{t} m(s)\, g(s)\, \mathrm{d}s \Rightarrow l'(t) - C_2 m(t)\, g(t) = 0, \tag{2.89}$$

where,

$$\begin{aligned} l(+1) &= \overline{C}, \\ l(-1) &= 0. \end{aligned} \tag{2.90}$$

As can be seen in [11], in order to apply the Lagrange multiplier method, the following steps must be taken:

- *Step 1*
  Substitution of $m(\cdot) = m_{\text{opt}}(\cdot) + \sigma\delta_1(\cdot)$ into the expression of J, and calculation of the derivative with respect to σ. The derivative has to be evaluated for $\sigma = 0$.

- *Step 2*
  Substitution of $l(\cdot) = l(\cdot)_{\text{opt}} + \sigma\delta_2(\cdot)$ and $m(\cdot) = m_{\text{opt}}(\cdot) + \sigma\delta_1(\cdot)$ into equation (2.89). Notice that $\delta_2(+1) = \delta_2(-1) = 0$, $l_{\text{opt}}(+1) = \overline{C}$ and $l_{\text{opt}}(-1) = 0$. After the substitution, the derivative with respect to σ has to be calculated and evaluated for $\sigma = 0$.

[24] The subscript "opt" indicates the optimal condition: J is minimized.

The result of the first step is:

$$J\left(m_{\text{opt}}\left(\cdot\right)+\sigma\delta_1\left(\cdot\right)\right)=C_1\int_{-1}^{+1}\left(m_{\text{opt}}\left(s\right)+\sigma\delta_1\left(s\right)\right)\left(\oint_{-1}^{+1}\left(m_{\text{opt}}\left(t\right)+\sigma\delta_1\left(t\right)\right)Y\left(t,s\right)\,\mathrm{d}t\right)\mathrm{d}s. \tag{2.91}$$

From this expression, it is easy to calculate the derivative with respect to σ:

$$\begin{aligned}\tfrac{\mathrm{d}}{\mathrm{d}\sigma}J\left(m_{\text{opt}}\left(\cdot\right)+\sigma\delta_1\left(\cdot\right)\right)=C_1\int_{-1}^{+1}\delta_1\left(s\right)\left(\oint_{-1}^{+1}\left(m_{\text{opt}}\left(t\right)+\sigma\delta_1\left(t\right)\right)Y\left(t,s\right)\,\mathrm{d}t\right)\mathrm{d}s+\\+C_1\int_{-1}^{+1}\left(m_{\text{opt}}\left(s\right)+\sigma\delta_1\left(s\right)\right)\left(\oint_{-1}^{+1}\delta_1\left(t\right)Y\left(t,s\right)\,\mathrm{d}t\right)\mathrm{d}s.\end{aligned} \tag{2.92}$$

The derivative, calculated for $\sigma=0$, is:

$$\begin{aligned}\left[\tfrac{\mathrm{d}}{\mathrm{d}\sigma}J\left(m_{\text{opt}}\left(\cdot\right)+\sigma\delta_1\left(\cdot\right)\right)\right]_{\sigma=0}=C_1\int_{-1}^{+1}\delta_1\left(s\right)\left(\oint_{-1}^{+1}m_{\text{opt}}\left(t\right)Y\left(t,s\right)\,\mathrm{d}t\right)\mathrm{d}s+\\+C_1\int_{-1}^{+1}m_{\text{opt}}\left(s\right)\left(\oint_{-1}^{+1}\delta_1\left(t\right)Y\left(t,s\right)\,\mathrm{d}t\right)\mathrm{d}s.\end{aligned} \tag{2.93}$$

The two integrals seen in equation (2.93) are equal to each other (see appendix A for the demonstration). Thus, it can be deduced that

$$\left[\frac{\mathrm{d}}{\mathrm{d}\sigma}J\left(m_{\text{opt}}\left(\cdot\right)+\sigma\delta_1\left(\cdot\right)\right)\right]_{\sigma=0}=2C_1\int_{-1}^{+1}\delta_1\left(t\right)\left(\oint_{-1}^{+1}m_{\text{opt}}\left(s\right)Y\left(t,s\right)\,\mathrm{d}s\right)\mathrm{d}t. \tag{2.94}$$

Now, calculating the derivative for the condition written in equation (2.89), it is possible to write:

$$\left[\frac{\mathrm{d}}{\mathrm{d}\sigma}\left(\left(l_{\text{opt}}\left(t\right)+\sigma\delta_2\left(t\right)\right)'-C_2\left(m\left(t\right)+\sigma\delta_1\left(t\right)\right)g\left(t\right)\right)\right]_{\sigma=0}=\delta_2'\left(t\right)-C_2\delta_1\left(t\right)g\left(t\right)=0. \tag{2.95}$$

Multiplying this expression by $\lambda\left(t\right)$, integrating by parts the term which contains the derivative of δ_2[25] and summing the result with equation (2.94), the resulting expression is:

$$2C_1\int_{-1}^{+1}\delta_1\left(t\right)\left(\oint_{-1}^{+1}m_{\text{opt}}\left(s\right)Y\left(t,s\right)\,\mathrm{d}s\right)\mathrm{d}t-\int_{-1}^{+1}\lambda'\left(t\right)\delta_2\left(t\right)\,\mathrm{d}t-C_2\int_{-1}^{+1}\lambda\left(t\right)\delta_1\left(t\right)g\left(t\right)\,\mathrm{d}t=0. \tag{2.96}$$

[25] Remember the condition for δ_2: $\delta_2\left(+1\right)=\delta_2\left(-1\right)=0$.

Observing that $\delta_1(t)$ and $\delta_2(t)$ are independent and arbitrary functions, $\delta_1 \equiv 0$ and $\delta_2 \equiv 0$ can be imposed separately. Imposing $\delta_1 \equiv 0$:

$$\delta_1 \equiv 0 \Rightarrow -\int_{-1}^{+1} \lambda'(t)\,\delta_2(t)\,\mathrm{d}t = 0. \tag{2.97}$$

Because $\delta_2(t)$ is an arbitrary function, to always satisfy the previous relation, the following condition is required:

$$\lambda'(t) = 0 \Rightarrow \lambda = \text{const.} \tag{2.98}$$

Using this result and imposing $\delta_2 \equiv 0$, from (2.96), it can be deduced that:

$$\delta_2 \equiv 0 \Rightarrow 2C_1 \int_{-1}^{+1} \delta_1(t) \left(\fint_{-1}^{+1} m_{\text{opt}}(s)\, Y(t,s)\,\mathrm{d}s \right) \mathrm{d}t - C_2\lambda \int_{-1}^{+1} \delta_1(t)\, g(t)\,\mathrm{d}t = 0. \tag{2.99}$$

The previous equation can be rewritten as

$$\int_{-1}^{+1} \delta_1(t) \left(2C_1 \fint_{-1}^{+1} m_{\text{opt}}(s)\, Y(t,s)\,\mathrm{d}s - C_2\lambda g(t) \right) \mathrm{d}t = 0. \tag{2.100}$$

Again, the function $\delta_1(t)$ is arbitrary. Therefore, in order to solve equation (2.100), the following equation has to be satisfied:

$$2C_1 \fint_{-1}^{+1} m_{\text{opt}}(s)\, Y(t,s)\,\mathrm{d}s - C_2\lambda g(t) = 0. \tag{2.101}$$

This is the Euler-Lagrange equation, which, in usual problems, is a differential equation. Here, in this particular problem, it is an integral equation.
Obviously, the condition for the function m_{opt}

$$\overline{C} = C_2 \int_{-1}^{+1} m_{\text{opt}}(t)\, g(t)\,\mathrm{d}t \tag{2.102}$$

has to be satisfied as well as the Euler-Lagrange equation.

2.7.1 Numerical Solution of the Euler-Lagrange Integral Equation

The Euler-Lagrange equation was just introduced in previous section. How can it be solved numerically to find m_{opt}? By observing the linearity of the equations, the procedure reported below can be followed.

- *Step 1*
  The value of λ is arbitrarily chosen: $\lambda = \lambda_{\text{guess}} \neq 0$.

- *Step 2*
  The Euler-Lagrange integral equation (2.101) is solved by using the collocation method and by expanding the function, for example, with Legendre polynomials. Let m_{guess} be called the solution.

- *Step 3*
  m_{guess} is substituted into equation (2.102)

$$\overline{C}_{\text{guess}} = C_2 \int_{-1}^{+1} m_{\text{guess}}(t)\, g(t)\, \mathrm{d}t. \tag{2.103}$$

- *Step 4*
  Because of *the linearity of the Euler-Lagrange equation*, it can be concluded that:

$$m_{\text{opt}} = m_{\text{guess}} \frac{\overline{C}}{\overline{C}_{\text{guess}}}. \tag{2.104}$$

In subsequent chapters, this method will be applied often[26].

[26] In some cases, an analytical solution is possible. See chapter 9.

Nomenclature

P_j, P_n, P_M	Legendre polynomial
h_i	Gauss weights used in the Gauss-Legendre quadrature
w_i	Gauss weights used in the generic Gauss quadrature
t_i	nodes used in the quadrature formulae
$⨎$	Hadamard finite-part integral
$⨍$	integral defined in the Cauchy principal value sense
w_i^I	weights used in the quadrature of hypersingular integrals
F	antiderivative of f
Q_j	$⨍_{-1}^{+1} \frac{P_j(t)}{t-s}\,\mathrm{d}t$
d_j	$\int_{-1}^{+1} P_j^2\,\mathrm{d}t$
K	regular kernel
Y	singular kernel
J	functional
m	unknown function
m_{opt}	solution of the Euler-Lagrange equation
$\delta_1(t), \delta_2(t)$	arbitrary functions
σ	parameter with the property $\sigma \in (-1, +1)$
λ	Lagrange multiplier
g, α	known functions
$C_1, C_2, \overline{C}$	constant parameters
$l\,(t)$	$C_2 \, ⨎_{-1}^{t} m\,(s)\, g\,(s)\,\mathrm{d}s$
s_l	l^{th} zero of $P_N(s)$

Subscripts

guess	related to the numerical solution of the Euler-Lagrange equation
opt	related to the solution of the Euler-Lagrange equation

Chapter 3

Basic Concepts of Lifting-line Theories

3.1 Introduction

This chapter introduces some classical theories of airfoils and wings under the hypotheses of ideal incompressible fluid and small perturbations (linear theory). The fundamental concepts of Weissinger's assumption and Prandtl's classical lifting-line theory are treated as well.

3.2 Classical Thin Airfoil Theory

It is not of interest to determine the velocity field around the airfoil. The only interest is to calculate the *lifting force*[1], thus, only the *camber line*[2] with vortices is considered. The concept of vortex sheet is more than a mathematical method to study the problem; it also has physical significance. In reality, there is a thin layer on the surface, due to the friction between the surface and the airflow (called boundary layer), which is a highly viscous region in which the velocity gradient is large. Because of this gradient, a vorticity is produced. *The idea to use the vortices is one method to take into account the viscosity effects in the inviscid fluid* (see [1]). Since the airfoil is thin, it can be assumed that the vortices are all positioned along the x axis (the axes are chosen as shown in figure 3.2). The small perturbation velocity potential at a point $P\,(x,z)$ is:

$$\mathrm{d}\phi\,(x,z) = -\frac{\mathrm{d}\Gamma}{2\pi}\vartheta = -\frac{\mathrm{d}\Gamma}{2\pi}\arctan\frac{z}{x-\xi} = -\frac{\gamma\,(\xi)}{2\pi}\arctan\frac{z}{x-\xi}\,\mathrm{d}\xi. \tag{3.1}$$

[1] Under the assumption made before, the drag is zero. See [1] and [2] for details.

[2] In [1], [2] and [3] it is demonstrated that the thickness does not effect the lifting force.

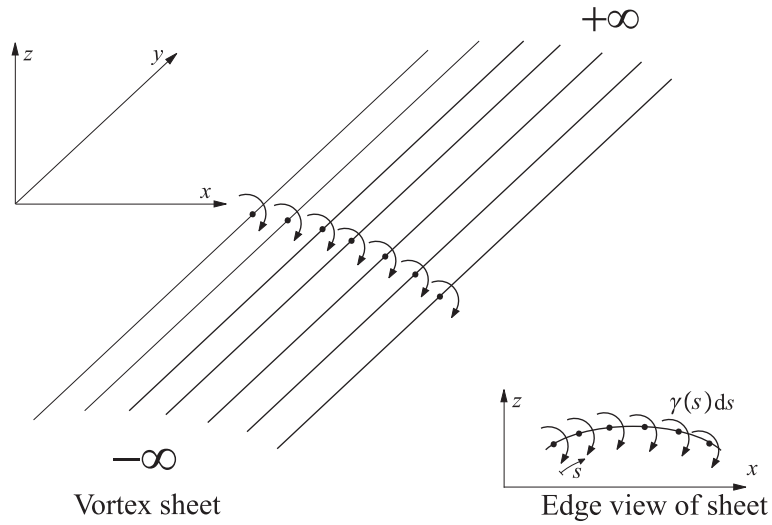

Figure 3.1. Vortex sheet.

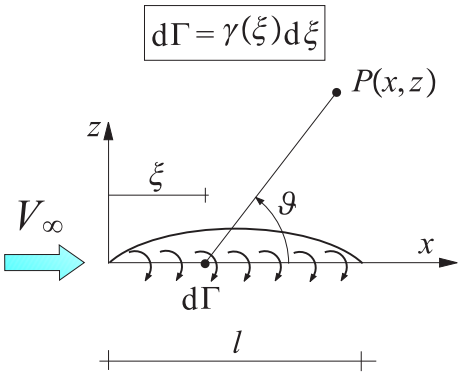

Figure 3.2. Thin airfoil and vortices along x.

Because of the linearity, the total small perturbation velocity potential is:

$$\phi\,(x,z) = -\frac{1}{2\pi}\int_0^l \gamma\,(\xi)\arctan\frac{z}{x-\xi}\,\mathrm{d}\xi. \tag{3.2}$$

It is easy to show that the potential is not a continuous function. In particular, in the wake[3], for $x > l$:

$$\begin{aligned} &\lim_{z\to 0^+} \phi\left(x > l, z \to 0^+\right) = 0, \\ &\lim_{z\to 0^-} \phi\left(x > l, z \to 0^-\right) = -\frac{1}{2\pi}\int_0^l \gamma\left(\xi\right) 2\pi \,\mathrm{d}\xi = -\Gamma. \end{aligned} \tag{3.3}$$

From these equations:

$$\Delta\phi\left(x > l, 0\right) = \phi\left(x > l, z \to 0^+\right) - \phi\left(x > l, z \to 0^-\right) = \Gamma. \tag{3.4}$$

It can be concluded that the discontinuity of the potential is equal to the circulation Γ. From the potential, it is possible to obtain the following velocities:

$$\begin{aligned} v_x\left(x,z\right) &= \frac{\partial\phi}{\partial x} = \frac{1}{2\pi}\int_0^l \gamma\left(\xi\right) \frac{z}{(x-\xi)^2+z^2}\,\mathrm{d}\xi, \\ v_z\left(x,z\right) &= \frac{\partial\phi}{\partial z} = -\frac{1}{2\pi}\int_0^l \gamma\left(\xi\right) \frac{x-\xi}{(x-\xi)^2+z^2}\,\mathrm{d}\xi. \end{aligned} \tag{3.5}$$

It is possible to demonstrate (see [3]):

$$v_x\left(x,0\right) = \pm\frac{\gamma\left(x\right)}{2}, \qquad v_z\left(x,z\right) = -\frac{1}{2\pi}\int_0^l \frac{\gamma\left(\xi\right)}{x-\xi}\,\mathrm{d}\xi. \tag{3.6}$$

The integral equation in the unknown $\gamma\left(\xi\right)$ is written by the imposition of the WTC. Let the equation of the *camber line* be called $f(x)$. The WTC is now:

$$v_z\left(x,z\right) = -\frac{1}{2\pi}\int_0^l \frac{\gamma\left(\xi\right)}{x-\xi}\,\mathrm{d}\xi = V_\infty \frac{\mathrm{d}f}{\mathrm{d}x}. \tag{3.7}$$

It is well known that the solution of equation (3.7) is not unique. To avoid this problem, the *Kutta* condition ($V_1 = V_2$, as shown in figure 3.3) is used. This condition is equivalent to[4]

$$\gamma(l) = 0. \tag{3.8}$$

Now consider a flat plate (see figure 3.4). The integral equation (3.7) becomes:

$$-\frac{1}{2\pi}\int_0^l \frac{\gamma\left(\xi\right)}{x-\xi}\,\mathrm{d}\xi = V_\infty \frac{\mathrm{d}f}{\mathrm{d}x} = -V_\infty\alpha \Rightarrow \alpha = \frac{1}{2\pi V_\infty}\int_0^l \frac{\gamma\left(\xi\right)}{x-\xi}\,\mathrm{d}\xi. \tag{3.9}$$

[3] It is correct to say that the position of the wake is known and coincident with the x axis only under the small perturbations hypothesis. See chapter 4 for more details.

[4] Notice that $\gamma(l) = 0$ is also equivalent to $\Delta p(l) = \rho_\infty V_\infty \gamma(l) = 0$.

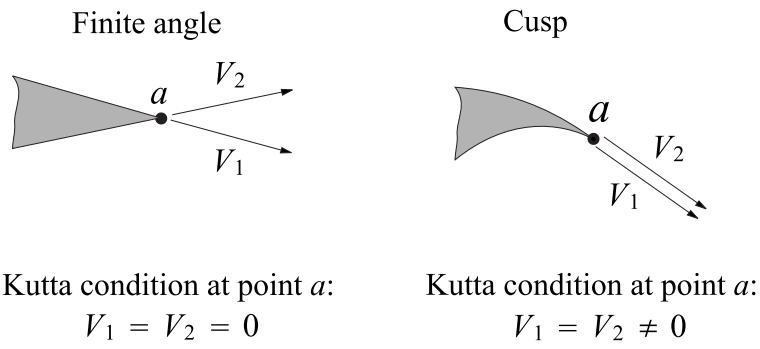

Figure 3.3. Kutta condition.

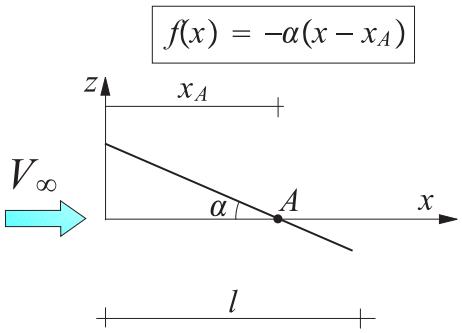

Figure 3.4. Flat plate with incidence α.

It is possible to demonstrate that the solution is:

$$\gamma(x) = 2V_\infty \alpha \sqrt{\frac{l-x}{x}}. \tag{3.10}$$

From this relation, the total circulation Γ is:

$$\Gamma = \int_0^l \gamma(\xi)\, \mathrm{d}\xi = 2V_\infty \alpha \int_0^l \sqrt{\frac{l-\xi}{\xi}}\, \mathrm{d}\xi = 2V_\infty \alpha \frac{l\pi}{2} = V_\infty \alpha l \pi. \tag{3.11}$$

Observation 15 Is it possible, for a flat plate, to concentrate all vortices at a point x_Γ *such that the total circulation* Γ *is the same?* It is possible. Obviously, the following condition has to be satisfied:

$$x_\Gamma \int_0^l \gamma(x)\, \mathrm{d}x = \int_0^l \gamma(x)\, x\, \mathrm{d}x. \tag{3.12}$$

Using equation (3.10), and observing that

$$\int_0^l \sqrt{\frac{l-x}{x}}\,\mathrm{d}x = \frac{l\pi}{2}, \tag{3.13}$$

$$\int_0^l \sqrt{\frac{l-x}{x}}x\,\mathrm{d}x = \frac{l^2\pi}{8}, \tag{3.14}$$

the obtained result is

$$x_\Gamma \frac{l\pi}{2} = \frac{l^2\pi}{8} \Rightarrow x_\Gamma = \frac{l}{4}. \tag{3.15}$$

Observation 16 By using the concentrated vortex, *what is the point where the WTC is exactly satisfied?* In other words, if the concentrated vortex $\Gamma = V_\infty \alpha l \pi$ is positioned at x_Γ, for what point is $v_z = -V_\infty \alpha$? The answer is simple. The induced velocity by the vortex Γ is:

$$v_z(x) = -\frac{\Gamma}{2\pi(x - x_\Gamma)}. \tag{3.16}$$

By imposing $v_z(x_{WTC}) = -V_\infty \alpha$:

$$-\frac{\Gamma}{2\pi(x_{WTC} - x_\Gamma)} = -V_\infty \alpha \Rightarrow x_{WTC} = \frac{3l}{4}. \tag{3.17}$$

3.3 An Alternative Thin Airfoil Theory Using the Small Perturbation Acceleration Potential

From [3], it is possible to see an alternative formulation which is based on the small perturbation acceleration potential rather than the small perturbation velocity potential. Consider the same airfoil studied in the previous section and a distribution $m_a(x)$ of doublets[5] on the x axis. Suppose that all axes are parallel and directed along z. The small perturbation acceleration potential of the doublet distribution is:

$$\Psi(x,z) = -\frac{1}{2\pi}\int_0^l m_a(\xi)\frac{z}{(x-\xi)^2 + z^2}\,\mathrm{d}\xi. \tag{3.18}$$

[5]The subscript a means "airfoil", to distinguish m_a from m, which is the doublet distribution on a wing ($m = \int_0^l m_a(\xi)\,\mathrm{d}\xi$).

This equation is formally the same as the first expression in equation (3.5) from which $v_x\left(x,0\right)=\pm\frac{\gamma(x)}{2}$ was found, and, in a similar way, the following result can be obtained:

$$\Psi\left(x,0\right)=\mp\frac{m_a\left(x\right)}{2}. \tag{3.19}$$

Under the hypothesis of small perturbations, the relation

$$\Delta p=-\rho_\infty\Delta\Psi \tag{3.20}$$

is valid, hence, it can be inferred that

$$\Delta p\left(x\right)=-\rho_\infty\left[\Psi\left(x,0^-\right)-\Psi\left(x,0^+\right)\right]=-\rho_\infty m_a\left(x\right). \tag{3.21}$$

In order to impose the WTC, the velocity is needed. Therefore, it is useful to write the small perturbation velocity potential from the small perturbation acceleration potential. Recalling

$$\phi\left(x,z\right)=\frac{1}{V_\infty}\int_{-\infty}^{x}\Psi\left(\tau,z\right)\,\mathrm{d}\tau, \tag{3.22}$$

and using equation (3.18), the small perturbation velocity potential is:

$$\phi\left(x,z\right)=-\frac{1}{2\pi V_\infty}\int_0^l m_a\left(\xi\right)\int_{-\infty}^{x}\frac{z}{\left(\tau-\xi\right)^2+z^2}\,\mathrm{d}\tau\,\mathrm{d}\xi \tag{3.23}$$

By calculating the integral[6] and the velocity $v_z=\frac{\partial\phi}{\partial z}$, the WTC can be imposed. By solving the integral equation, $m_a(x)$ can be found. When $m_a(x)$ is determined, $\Delta p\left(x\right)$ can be calculated.

[6] Observe that $\int\frac{z}{(\tau-\xi)^2+z^2}\,\mathrm{d}\tau=\arctan\frac{\tau-\xi}{z}$; therefore,

$$\int_{-\infty}^{x}\frac{z}{\left(\tau-\xi\right)^2+z^2}\,\mathrm{d}\tau=\arctan\frac{x-\xi}{z}-\lim_{\tau\to-\infty}\arctan\frac{\tau-\xi}{z}.$$

Now, observing that $\lim_{\tau\to-\infty}\arctan\frac{\tau-\xi}{z}=\text{const}$, the following relation can be written:

$$\int_{-\infty}^{x}\frac{z}{\left(\tau-\xi\right)^2+z^2}\,\mathrm{d}\tau=\arctan\frac{x-\xi}{z}-\text{const}.$$

Thus, it is deduced that

$$\phi\left(x,z\right)=-\frac{1}{2\pi V_\infty}\int_0^l m_a\left(\xi\right)\left(\arctan\frac{x-\xi}{z}-\text{const}\right)\,\mathrm{d}\xi.$$

(Continued on page 51)

Observation 17 By using the doublet distribution, it is possible to concentrate the doublets at a point x_m, as it was proved for the vortices in section 3.2. Repeating the same procedures, the following expressions can be demonstrated:

$$m_a(x) = -2V_\infty^2 \alpha \sqrt{\frac{l-x}{x}}, \tag{3.24}$$

$$m = \int_0^l m_a(\xi)\, \mathrm{d}\xi = -2V_\infty^2 \alpha \int_0^l \sqrt{\frac{l-\xi}{\xi}}\, \mathrm{d}\xi = -V_\infty^2 \alpha l \pi. \tag{3.25}$$

It is also possible to demonstrate the following relations:

$$x_\Gamma = x_m = \frac{l}{4}, \qquad x_{WTC} = \frac{3l}{4}. \tag{3.26}$$

3.4 Prandtl's Classical Lifting-line Theory

Now Prandtl's approach to predict the aerodynamic properties of a finite wing will be analyzed. In Prandtl's scheme, the wing is studied by using the scheme shown in figure (3.5). The velocity $\mathrm{d}u_n$ at a distance y induced by a vortex $\gamma(y_d)\,\mathrm{d}y_d$ is needed. Using the Biot and Savart law (see figure 3.5)[7]:

$$\mathrm{d}u_n(y) = -\frac{\gamma(y_d)\,\mathrm{d}y_d}{4\pi(y_d - y)} \Rightarrow u_n(y) = \fint_{-b_w}^{+b_w} \frac{\frac{d\Gamma(y_d)}{\mathrm{d}y_d}}{4\pi(y_d - y)}\, \mathrm{d}y_d. \tag{3.27}$$

Each airfoil is considered independently. Therefore, applying the Kutta-Joukowski theorem:

$$\mathrm{d}L = \rho_\infty V_\infty \Gamma(y)\,\mathrm{d}y = \frac{1}{2}\rho_\infty V_\infty^2 l(y)\, 2\pi \left[\alpha(y) - \alpha_i(y) - \alpha_{L=0}(y)\right] \mathrm{d}y. \tag{3.28}$$

(Continued from page 50, footnote 6)

This expression is the same as the expression (3.2) if it is observed that $\arctan\frac{x-\xi}{z} = \frac{\pi}{2} - \arctan\frac{z}{x-\xi}$ and if the following relation is used:

$$\gamma(\xi) = -\frac{m_a(\xi)}{V_\infty}.$$

[7]The induced velocity $u_n(y)$ is assumed positive if it is directed along z.

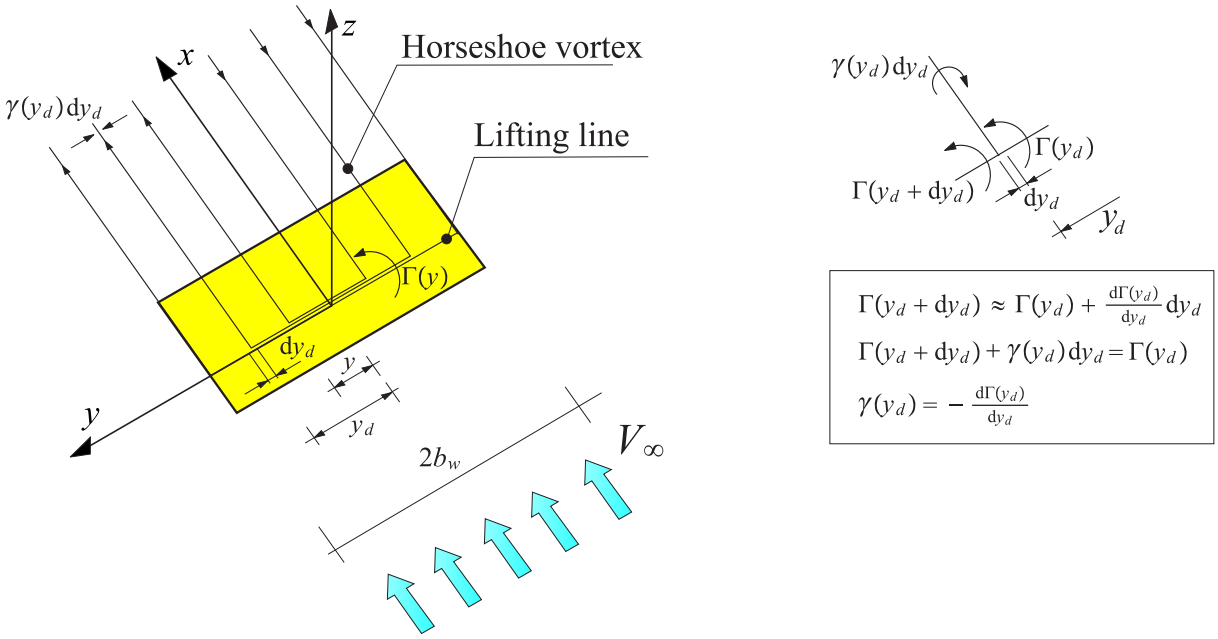

Figure 3.5. Prandtl's scheme.

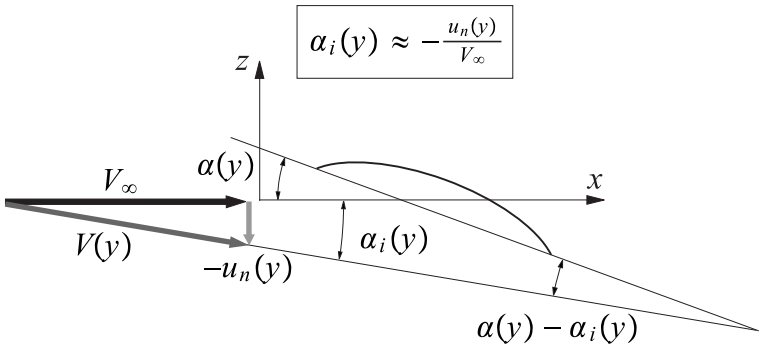

Figure 3.6. Induced angle of attack.

Using equation (3.27) and the expression of the induced angle of attack ($\alpha_i(y) = -\frac{u_n(y)}{V_\infty}$):

$$\rho_\infty V_\infty \Gamma(y) = \frac{1}{2}\rho_\infty V_\infty^2 l(y)\, 2\pi \left[\alpha(y) + \frac{\fint_{-b_w}^{+b_w} \frac{\frac{d\Gamma(y_d)}{dy_d}}{4\pi(y_d - y)}\, dy_d}{V_\infty} - \alpha_{L=0}(y) \right]. \tag{3.29}$$

Simplifying, the *fundamental equation of Prandtl's lifting-line theory* is obtained:

$$\frac{\Gamma(y)}{V_\infty l(y)\pi} = \alpha(y) - \alpha_{L=0} + \frac{1}{4\pi V_\infty} \oint_{-b_w}^{+b_w} \frac{\frac{\mathrm{d}\Gamma(y_d)}{\mathrm{d}y_d}}{(y_d - y)} \mathrm{d}y_d. \tag{3.30}$$

The solution of this equation, Γ, leads to calculating the lift and, as will be better seen later, *the induced drag.*

Observation 18 In Prandtl's lifting-line theory, the lifting-line is positioned in a non-imposed abscissa.

Observation 19 Consider Prandtl's fundamental equation. In that formula, the only unknown is the circulation $\Gamma(y)$, which appears also in the derivative form. It is possible to modify the equation *in such a way as to have only the unknown* $\Gamma(y)$ *and not its derivative.* To achieve that, observe that the circulation Γ must be zero at the tips. This is because there is a pressure equalization from the bottom to the top of the wing (precisely, at $y = \pm b_w$), and, hence, no lift is created at these points. By using these conditions, it is possible to integrate by parts the Cauchy integral:

$$\oint_{-b_w}^{+b_w} \frac{\frac{\mathrm{d}\Gamma(y_d)}{\mathrm{d}y_d}}{(y_d - y)} \mathrm{d}y_d = \left[\frac{\Gamma(y_d)}{(y_d - y)}\right]_{-b_w}^{+b_w} + \oint_{-b_w}^{+b_w} \frac{\Gamma(y_d)}{(y_d - y)^2} \mathrm{d}y_d = \oint_{-b_w}^{+b_w} \frac{\Gamma(y_d)}{(y_d - y)^2} \mathrm{d}y_d. \tag{3.31}$$

Using this relation, Prandtl's fundamental equation becomes:

$$\frac{\Gamma(y)}{V_\infty l(y)\pi} = \alpha(y) - \alpha_{L=0} + \frac{1}{4\pi V_\infty} \oint_{-b_w}^{+b_w} \frac{\Gamma(y_d)}{(y_d - y)^2} \mathrm{d}y_d. \tag{3.32}$$

This equation is much easier to solve numerically.

3.5 Weissinger's Lifting-line Theory

The airfoil theory has shown that, for a flat plate, the WTC is exactly satisfied in x_{WTC} when the vortex is positioned at x_Γ.
Weissinger's approach (see [12] and [13]) is based on this concept: the vortices are concentrated in a single vortex Γ (like in Prandtl's theory). Unlike Prandtl's theory, the vortex is now positioned at $x_\Gamma(y)$. The WTC condition is then imposed on $x_{WTC}(y)$.
In order to show Weissinger's approach, the integral equation is obtained by using the small acceleration potential and a flat plate[8]. Consider a wing without a sweep angle

[8] In a flat plate, $\alpha_{L=0} = 0$.

and with the property $l(y) = \text{const}$. It is possible to translate the coordinate system to have $x_\Gamma = x_m = 0$[9]. Obviously, in that coordinate system, $x_{WTC} = \text{const} = \frac{l}{2}$. To achieve the goal of writing the integral equation using Weissinger's method, the following steps must be taken:

- *Step 1*
  Writing the expression of the small perturbation acceleration potential of the doublet distribution along the line $x_m = 0$. The axes of the doublets directed along $+z$ can be chosen[10].

- *Step 2*
  Writing the expression of the small perturbation velocity potential from the small perturbation acceleration potential by integration.

- *Step 3*
  Imposition of the WTC on x_{WTC}. The resulting equation will be Weissinger's integral equation.

The above operations will be performed in the following subsections.

3.5.1 Writing of the Small Perturbation Acceleration Potential

Consider a doublet $M(y_d) = m(y_d)\,\mathrm{d}y_d$ positioned at a point $P_d(0,y_d,0)$. The small perturbation acceleration potential at a generic point $P(x,y,z)$ is:

$$\mathrm{d}\Psi\,(x,y,z) = -\frac{m\,(y_d)\,\mathrm{d}y_d}{4\pi}\frac{z}{\left[x^2+(y-y_d)^2+z^2\right]^{\frac{3}{2}}}. \tag{3.33}$$

Now, because of the linearity, the potential of all doublets can be written by integrating the previous equation:

$$\Psi\,(x,y,z) = -\frac{1}{4\pi}\int_{-b_w}^{+b_w} m\,(y_d)\,\frac{z}{\left[x^2+(y-y_d)^2+z^2\right]^{\frac{3}{2}}}\,\mathrm{d}y_d. \tag{3.34}$$

[9] Unlike the general case, because of the made assumptions, x_m is not a function of y.
[10] It is possible to make the opposite choice. The method is formally the same.

3.5.2 Writing of the Small Perturbation Velocity Potential

As was seen in chapter 1, this operation is easily done by using the formula

$$\phi\left(x,y,z\right)=\frac{1}{V_{\infty}}\int\limits_{-\infty}^{x}\Psi\left(\tau,y,z\right)\,\mathrm{d}\tau. \tag{3.35}$$

Substituting in the expression of Ψ:

$$\phi\left(x,y,z\right)=-\frac{1}{4\pi V_{\infty}}\int\limits_{-b_w}^{+b_w}\int\limits_{-\infty}^{x}m\left(y_d\right)\frac{z}{\left[\tau^2+\left(y-y_d\right)^2+z^2\right]^{\frac{3}{2}}}\,\mathrm{d}\tau\,\mathrm{d}y_d. \tag{3.36}$$

And, calculating the integral, the small perturbation velocity potential expression becomes:

$$\phi\left(x,y,z\right)=-\frac{1}{4\pi V_{\infty}}\int\limits_{-b_w}^{+b_w}m\left(y_d\right)\frac{z}{\left(y-y_d\right)^2+z^2}\left(\frac{x}{\sqrt{\left(x^2+\left(y-y_d\right)^2+z^2\right)}}+1\right)\mathrm{d}y_d. \tag{3.37}$$

3.5.3 Imposing of WTC and Writing of Weissinger's Integral Equation

In this particular case, the WTC is easily expressed as

$$\alpha\left(y\right)=\alpha_i\left(y\right)\Rightarrow\alpha\left(y\right)=-\frac{u_n}{V_{\infty}}=-\frac{1}{V_{\infty}}\left[\frac{\partial\phi\left(x,y,z\right)}{\partial z}\right]_{\substack{z=0\\x=\frac{l}{2}}}. \tag{3.38}$$

The derivative of the small perturbation velocity potential calculated at $z=0$ and $x=\frac{l}{2}$ is:

$$u_n\left(y\right)=\left[\frac{\partial\phi\left(x,y,z\right)}{\partial z}\right]_{\substack{z=0\\x=\frac{l}{2}}}=-\frac{1}{4\pi V_{\infty}}\,\text{⨍}\!\!\!\!\!\!-\int\limits_{-b_w}^{+b_w}\frac{m\left(y_d\right)}{\left(y-y_d\right)^2}\left(\frac{\left(\frac{l}{2}\right)}{\sqrt{\left(\frac{l}{2}\right)^2+\left(y-y_d\right)^2}}+1\right)\mathrm{d}y_d. \tag{3.39}$$

In order to use the quadrature formula for the Hadamard finite-part integral, it is convenient to isolate the singularity. To achieve that, notice the identity

$$\frac{1}{\left(y-y_d\right)^2}\left(\frac{\left(\frac{l}{2}\right)}{\sqrt{\left(\frac{l}{2}\right)^2+\left(y-y_d\right)^2}}+1\right)=\frac{-1}{\left(\left(\frac{l}{2}\right)+\sqrt{\left(\frac{l}{2}\right)^2+\left(y-y_d\right)^2}\right)\sqrt{\left(\frac{l}{2}\right)^2+\left(y-y_d\right)^2}}+\frac{2}{\left(y-y_d\right)^2}. \tag{3.40}$$

Substituting into the equation that represents u_n(y) and using equation (3.38), the final expression of Weissinger's integral equation is obtained:

$$\alpha(y) = \frac{1}{2\pi V_\infty^2} \oint_{-b_w}^{+b_w} \frac{m(y_d)}{(y-y_d)^2}\,\mathrm{d}y_d - \frac{1}{4\pi V_\infty^2} \int_{-b_w}^{+b_w} \frac{m(y_d)}{\left(\frac{l}{2}+\sqrt{\left(\left(\frac{l}{2}\right)^2+(y-y_d)^2\right)}\right)\sqrt{\left(\left(\frac{l}{2}\right)^2+(y-y_d)^2\right)}}\,\mathrm{d}y_d. \tag{3.41}$$

Observation 20 What is the difference between Weissinger's integral equation and Prandtl's integral equation? To answer this question, consider Prandtl's equation written for the same case:

$$\frac{\Gamma(y)}{V_\infty l(y)\pi} = \alpha(y) + \frac{1}{4\pi V_\infty} \oint_{-b_w}^{+b_w} \frac{\Gamma(y_d)}{(y_d-y)^2}\,\mathrm{d}y_d. \tag{3.42}$$

Observing that

$$-\rho_\infty m(y_d) = \rho V_\infty \Gamma(y_d) \Rightarrow \Gamma(y_d) = -\frac{m(y_d)}{V_\infty}, \tag{3.43}$$

it is deduced that the corresponding Prandtl's equation is:

$$\alpha(y) = -\frac{m(y)}{V_\infty^2 l\pi} + \frac{1}{4\pi V_\infty^2} \oint_{-b_w}^{+b_w} \frac{m(y_d)}{(y_d-y)^2}\,\mathrm{d}y_d. \tag{3.44}$$

Comparing this formula with Weissinger's equation (3.41), it is clear that Weissinger's equation is much more accurate. That is for two reasons:

- *Reason 1*
  Weissinger's equation contains a term dependent on l.
- *Reason 2*
  The imposition of the WTC in $x_\Gamma = x_m$ has a physical meaning, as seen in the airfoil theory.

3.5.4 An Alternative Demonstration of Kutta-Joukowski Theorem: Consistency of Weissinger's Scheme

In this section, the writer proposes an alternative demonstration for a particular case of the Kutta-Joukowski theorem. This is not a very general demonstration, but it shows some interesting aspects of Weissinger's scheme. Consider an infinite wing (see figure 3.7). Assume l = const and α = const. The y axis is coincident with

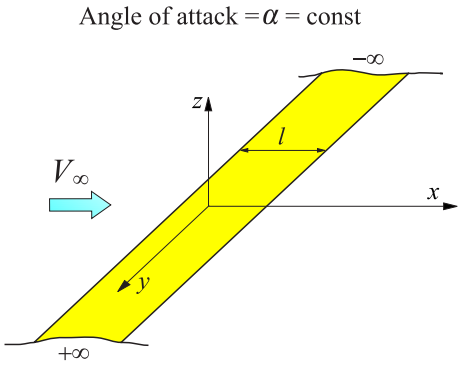

Figure 3.7. A two-dimensional wing.

the position of x_Γ. The doublet[11] distribution $m(y)$ must be constant for symmetry reason. Because of that, the small perturbation acceleration potential is:

$$\psi\left(x,y,z\right) = -\frac{m}{4\pi}\int\limits_{-\infty}^{+\infty}\frac{z}{\left[x^2+\left(y-y_d\right)^2+z^2\right]^{\frac{3}{2}}}\,\mathrm{d}y_d = -m\frac{z}{2\pi\left(x^2+z^2\right)}. \tag{3.45}$$

The small perturbation velocity potential is[12]:

$$\begin{aligned}\phi\left(x,y,z\right) &= \tfrac{1}{V_\infty}\int\limits_{-\infty}^{x}\psi\left(\tau,y,z\right)\,\mathrm{d}\tau = -\tfrac{1}{2V_\infty}\tfrac{m}{\pi}\left[\arctan\tfrac{\tau}{z}\right]_{-\infty}^{x} = \\ &= -\tfrac{1}{2V_\infty}\tfrac{m}{\pi}\arctan\tfrac{x}{z} + \tfrac{1}{2V_\infty}\tfrac{m}{\pi}\cdot\text{const}.\end{aligned} \tag{3.46}$$

The integral equation is now:

$$\alpha = -\tfrac{1}{V_\infty}\left[\left(\tfrac{\partial\phi(x,y,z)}{\partial z}\right)\right]_{\substack{x=\frac{l}{2}\\ z=0}} = -\tfrac{1}{V_\infty}\left[\tfrac{1}{2V_\infty}\tfrac{m}{\pi}\tfrac{x}{x^2+z^2}\right]_{\substack{x=\frac{l}{2}\\ z=0}} = -\tfrac{1}{V_\infty^2}\tfrac{m}{\pi}\tfrac{1}{l}. \tag{3.47}$$

Thus, it has been demonstrated that

$$m = -l\pi V_\infty^2\alpha. \tag{3.48}$$

In the airfoil theory, it has also been shown that

$$\Gamma = V_\infty\alpha l\pi. \tag{3.49}$$

[11] It is assumed that all doublets have axes directed along $+z$.

[12] If it is supposed that $z > 0$, the constant is $+\frac{\pi}{2}$. If it is supposed that $z < 0$, the constant is $-\frac{\pi}{2}$. Notice that in this demonstration the constant value is not important, because the expression of the potential will be derived to obtain the velocity.

Substituting:

$$m = -l\pi V_\infty^2 \alpha = -V_\infty \Gamma. \tag{3.50}$$

Remembering that the lift for unit of length is $L = -\rho m$, the obtained results is:

$$L = \rho_\infty V_\infty \Gamma. \tag{3.51}$$

Therefore, the Kutta-Joukowski theorem has been obtained. This shows that Weissinger's scheme is consistent.

Nomenclature

$\fint$	Hadamard finite-part integral
$\int$	integral defined in the Cauchy principal value sense
ρ	fluid density
Δp	pressure jump
m	doublet distribution
Γ	circulation
γ	distributed vorticity, distributed trailing vorticity
WTC	Wall Tangency Condition
ϕ	small perturbation velocity potential
Ψ	small perturbation acceleration potential
$\Delta\Psi$	small perturbation acceleration potential jump
v_x	x-component perturbation velocity
v_y	y-component perturbation velocity
v_z	z-component perturbation velocity
l	chord
f	equation of the chamber line
α	angle of attack
α_i	induced angle of attack
$\alpha_{L=0}$	angle of attack corresponding to the condition of zero lift
u_n	normalwash
$2b_w$	wing span

Subscripts

∞	freestream conditions
a	airfoil
Γ	position where the vortex is concentrated
m	position where the doublet is concentrated
WTC	position where WTC is imposed

Chapter 4

Induced Drag

4.1 Introduction

This chapter introduces the fundamental concept of *induced drag.*
The induced drag is an important issue in the aeronautic field. At present, airlines pay hundreds of millions of dollars in fuel costs annually, and the environmental impact of aircraft is closely tied to the amount of fuel consumed, therefore, the accurate estimation and reduction of this drag is of great interest.
It is well known (see [14]) that the induced drag is 80%-90% of the entire drag at takeoff[1]. The takeoff phase is a small portion of the entire aircraft mission, but the design constraints of the engines are critical constraints in the aircraft design. Hence, the induced drag reduction is very important to optimize the entire design of an airplane. Moreover, the induced drag is directly tied to takeoff noise, and a reduction of its amount is very desirable.

4.2 Physical description of the Induced Drag

In an ideal fluid (i.e., a fluid without viscosity), an airfoil has no drag[2] (see [1], [2]). Physically, the result of zero drag makes no sense. It is known that any aerodynamic body immersed in a real flow will experience a drag. Why is this possible? It is possible because the viscous effects, which generate frictional shear stress at the body surface (skin friction drag) and which cause the flow to separate from the surface on the back of the body (form drag), thus creating a wake downstream, are not taken into account.
Now consider a *finite wing.* It is well known that even if the fluid is inviscid the drag

[1] The induced drag constitutes approximately 40% of the total drag of typical transport aircraft at cruise conditions (see [14]).
[2] This is the well known D'Alambert's paradox.

is not zero. How is it possible? To explain this concept, consider the mechanism that creates the lift. In a wing the lift is generated by the net imbalance of the pressure distribution around the airfoil. This pressure distribution creates also a flow around the tips (see figure 4.1). It is not difficult to understand that trailing vortices are created. This is the difference with the two-dimensional case: in the three-dimensional case there is the wake and it *induces* a vertical velocity[3] called *downwash.* That is why each airfoil of the wing is now subjected to the velocity V_∞ and to the downwash velocity (see figure 56). As a consequence, the relative velocity is no longer V_∞, and the effective angle of attack is $\alpha_{\text{eff}} = \alpha - \alpha_{L=0} - \alpha_i$. The component $\mathrm{d}D_i$ of the aerodynamic force $\mathrm{d}F$ is the *induced drag.* For a very good overview of the theory related to induced drag, see [14]-[17].

Observation 21 As seen in chapter 3, the *induced velocity depends on the gradients of the circulation.* This is the mathematical explanation of the physical generation of the induced drag (see figure 4.1): at the tips the circulation must be zero[4] and, therefore, the gradient of the circulation is large. Consequently, the induced drag is generated.
Based on this fact, the induced drag can be reduced by reducing such high gradients (C-wings, winglets, non-planar wings, closed wing systems, wing-grid concepts; see for more details [14]).

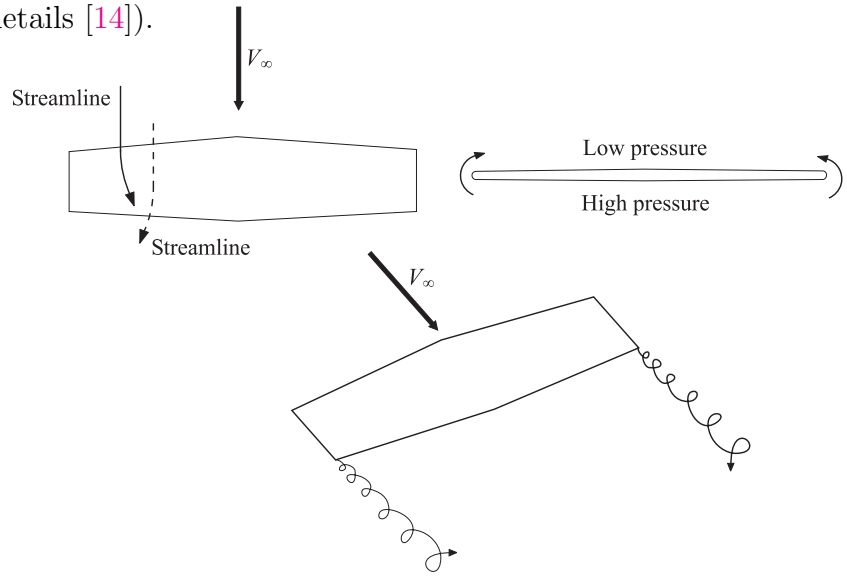

Figure 4.1. Aerodynamic of a finite wing.

[3] A classical cantilever wing is implicitly considered. In general, the induced velocity is not vertical.

[4] The circulation is related to the jump of pressure, and at the tips it has to be zero. Thus, the circulation has to be zero as well.

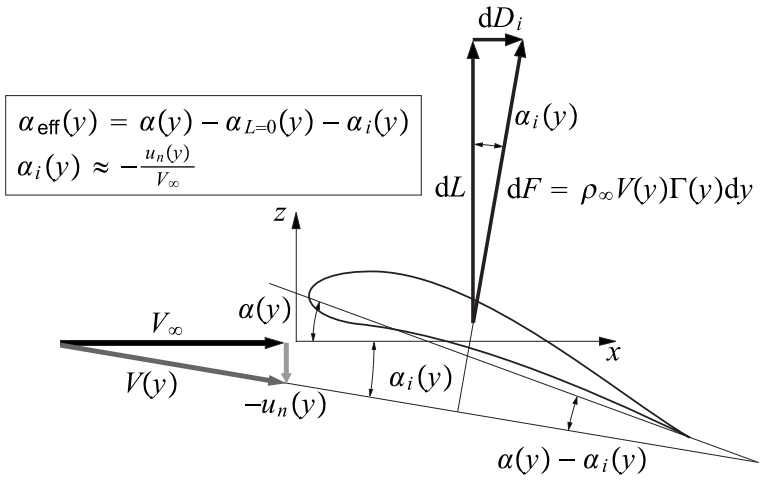

Figure 4.2. Induced drag and induced angle of attack.

4.2.1 Wake Description

It has been shown that the wake has an important role in the induced velocity and, therefore, in the induced drag. As described in [18]-[22], two different approaches can be used (see figure 4.3).

- *Approach 1*
  Wake aligned with freestream.
- *Approach 2*
  Wake not aligned with freestream.

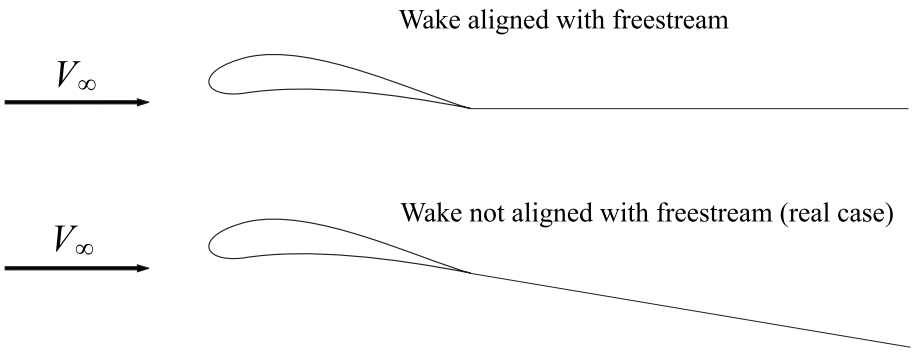

Figure 4.3. Wake models in a wing.

Clearly, in the real case, the wake is not aligned with freestream. This last case is much more complicated (see [18]) because the final position of the wake is not known and has to be determined (see [21]). Therefore, the problem becomes *nonlinear* even if the flow governing equations are *linear*.
The wake modelization is well described in the Ph.D. dissertation of Smith [20] and in [21]. Summarizing, Smith takes a control volume around the wing. From

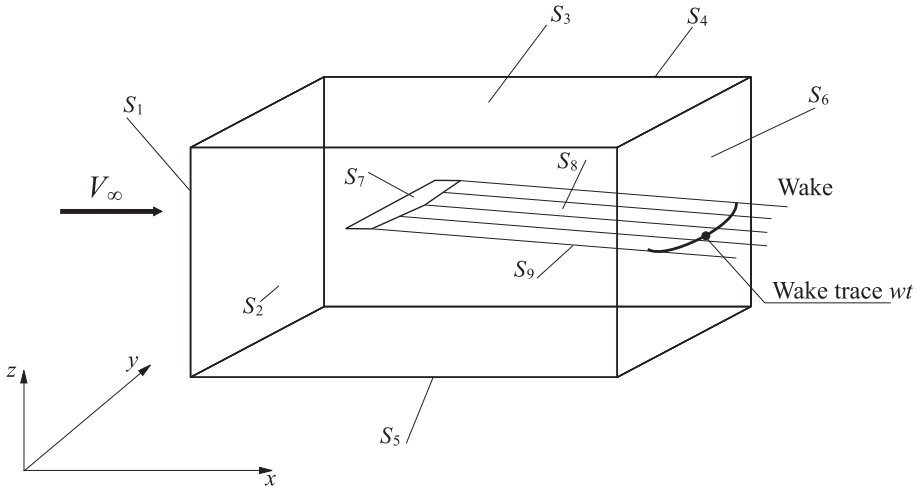

Figure 4.4. Control volume (from [20]).

momentum conservation, he derives, in a steady flow, the following induced drag expression (referred to the surface S_6, see figure 4.4):

$$D_i = -\int_{S_6} (p - p_\infty)\, \mathrm{d}s - \int_{S_6} \rho v_x \left(V_\infty + v_x\right) \mathrm{d}s. \tag{4.1}$$

Smith also uses the small perturbations second-order accurate Bernoulli's equation (isentropic flow):

$$p - p_\infty = -\frac{1}{2}\rho_\infty \left(2v_x V_\infty + \left(1 - M_\infty^2\right) v_x^2 + v_y^2 + v_z^2\right), \tag{4.2}$$

and a similar expression for the density $\rho' = \rho - \rho_\infty$:

$$\rho' = -\frac{1}{2}\rho_\infty \frac{M_\infty^2}{V_\infty^2} \left(2v_x V_\infty + \left(1 - (2-\gamma) M_\infty^2\right) v_x^2 + v_y^2 + v_z^2\right). \tag{4.3}$$

Using these relations, he obtains:

$$D_i = \tfrac{1}{2}\rho_\infty \int_{S_6} \left[\left(v_x^2 + v_y^2 + v_z^2\right) + \left(M_\infty^2 - 2\right) v_x^2 + \tfrac{M_\infty^2 v_x}{V_\infty} \left((\gamma - 2) M_\infty^2 v_x^2 + v_y^2 + v_z^2\right)\right] \mathrm{d}s. \tag{4.4}$$

This expression is valid for both wake models (either aligned with the local flow or aligned with the freestream). Introducing the small perturbation velocity potential ϕ and using the Laplace's equation and Gauss' theorem, Smith obtains the induced drag expression:

$$\begin{aligned} D_i = \tfrac{1}{2}\rho_\infty \int\limits_{wt} \Delta\phi \left(\tfrac{\partial\phi}{\partial n}\right) \mathrm{d}l + \tfrac{1}{2}\rho_\infty \int\limits_{S_6} \Big(\phi \tfrac{\partial v_x}{\partial x} + \left(M_\infty^2 - 1\right) v_x^2 + \\ + \tfrac{M_\infty^2 v_x}{V_\infty} \left(\left(\gamma - 2\right) M_\infty^2 v_x^2 + v_y^2 + v_z^2 \right) \Big) \mathrm{d}s. \end{aligned} \tag{4.5}$$

In the last expression, the following properties are satisfied:

- *Property 1*
  In the line integral along the wake trace from tip to tip, the potential jump $\Delta\phi$, from the upper side to the lower side of the wake, is present.

- *Property 2*
  The velocity potential is discontinuous across the wake, but the normal velocity $\frac{\partial\phi}{\partial n}$ is continuous.

- *Property 3*
  The induced drag expression also contains the v_x perturbation and its streamwise gradient $\frac{\partial v_x}{\partial x}$.

When the rear surface (S_6 in figure 4.4) of the control volume is moved far downstream of the lifting system, the v_x perturbation produced by the bound vorticity becomes diminishingly small, leaving only the perturbations produced by the trailing wake[5].
Now it is possible to see the effect of the wake model. If the wake is considered to be rigid and aligned with the freestream, no v_x component can be produced, and equation (4.5) leads to the well known expression for the induced drag:

$$D_i = \frac{1}{2}\rho_\infty \int\limits_{wt} \Delta\phi \left(\frac{\partial\phi}{\partial n}\right) \mathrm{d}l. \tag{4.6}$$

If the wake is modeled like depicted in figure 4.5, a v_x component is produced and the correct expression for the induced drag is equation (4.5). The quantity v_z' in figure 4.5 is the induced velocity on the wake.

[5]When the surface S_6 is moved far from the lifting system, it is traditionally referred to as the Trefftz plane (see [23] and [24]).

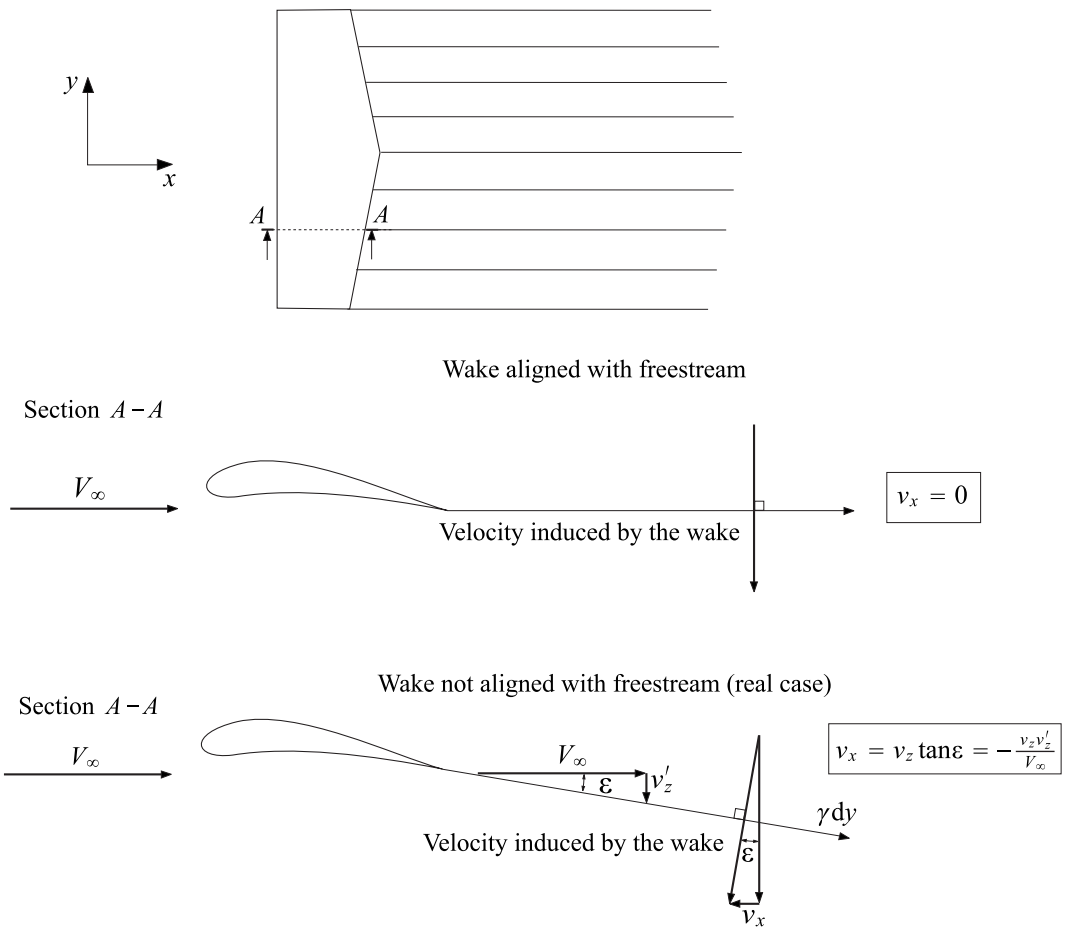

Figure 4.5. v_x perturbation in the wake.

4.3 Induced Drag Calculation

There are several methods available in the literature to calculate the induced drag. A very good overview of these procedures is given in [14], [18] and [21]. As reported in [18], to calculate the induced drag generated by a lifting surface, it is required that all, or at least a portion, of the velocity field has to be determined in the vicinity of the wing. Linear potential flow methods generally solve for the velocity over only a small part of the flow field *and save a tremendous amount of computational time.* In the present thesis, this approach will be used, introducing *a new and original technique to calculate the minimum induced drag in planar and non-planar wing systems.*
Some methods used to calculate the induced drag are briefly described here.

- *Method 1*
  Lifting-line theories

- *Method 2*
  Vortex lattice methods

- *Method 3*
  Linear panel methods

4.3.1 Lifting-line Theories

As was seen in chapter 3, the lifting-line theory analyzes the flow field as a potential field with the wing modeled as a singularity in the form of a line vortex strength located at the wing in an undefined or defined position ([1], [2], [13], [18] and [25]). Helmholtz's theorem requires that the spanwise change in vorticity of the lifting line be shed into a sheet of distributed trailing vorticity. Typically, the trailing vorticity is assumed to be aligned with the free-stream velocity and extended downstream to infinity. As seen in chapter 3, the strength of the trailing vortex sheet at any point is equal to the spanwise change in vortex strength at the corresponding point on the lifting line. *The sheet of trailing vorticity is assumed to be rigid and does not deform under its own induced velocity.* Referring to figure 56, the velocity u_n that the trailing vortex sheet induces on the lifting line is used to calculate the induced drag of the wing. Here, it should be noticed that *the lifting-line model ignores the effect of the chordwise distribution of vorticity on the downwash distribution, since it collapses all of the vorticity generated at a given spanwise location to a single point.* Also, the effect that the deforming wake might have on a wing performance is neglected. An interesting lifting-line theory has been formulated by Eppler [26]. Eppler used the lifting line located at the trailing edge of the planform. The advantage of the method is that it has the simplicity of Prandtl's lifting-line model, but it includes some planform effects in the form of the trailing-edge shape.

4.3.2 Vortex-lattice Methods

The vortex-lattice methods are very useful: it is possible to capture the effect of the chordwise loading on the overall wing aerodynamics. It is based (see [1], [3], [18] and [27]-[38]) on the concept used in the lifting-line theories. The difference is that, now, the vorticity along the wing is a function of x and y (lifting surface). From a numerical point of view, the vortex-lattice method uses an array of horseshoe vortices with spanwise segments bound to the wing and streamwise segments trailing downstream from the trailing edge parallel to the free-stream velocity. The strength of each vortex is determined by satisfying the condition that the flow has to be

tangent to the wing (considered as a surface without thickness) at a number of *control points* equal to the number of vortices used. This constraint defines a system of simultaneous linear equations which are solved for the vortex strength. The strength of the streamwise trailing vortex filaments are taken as the sum of the strength of the horseshoe vortices distributed over the chord at a given spanwise position. This method is shown in figure 4.6. Induced drag is normally calculated

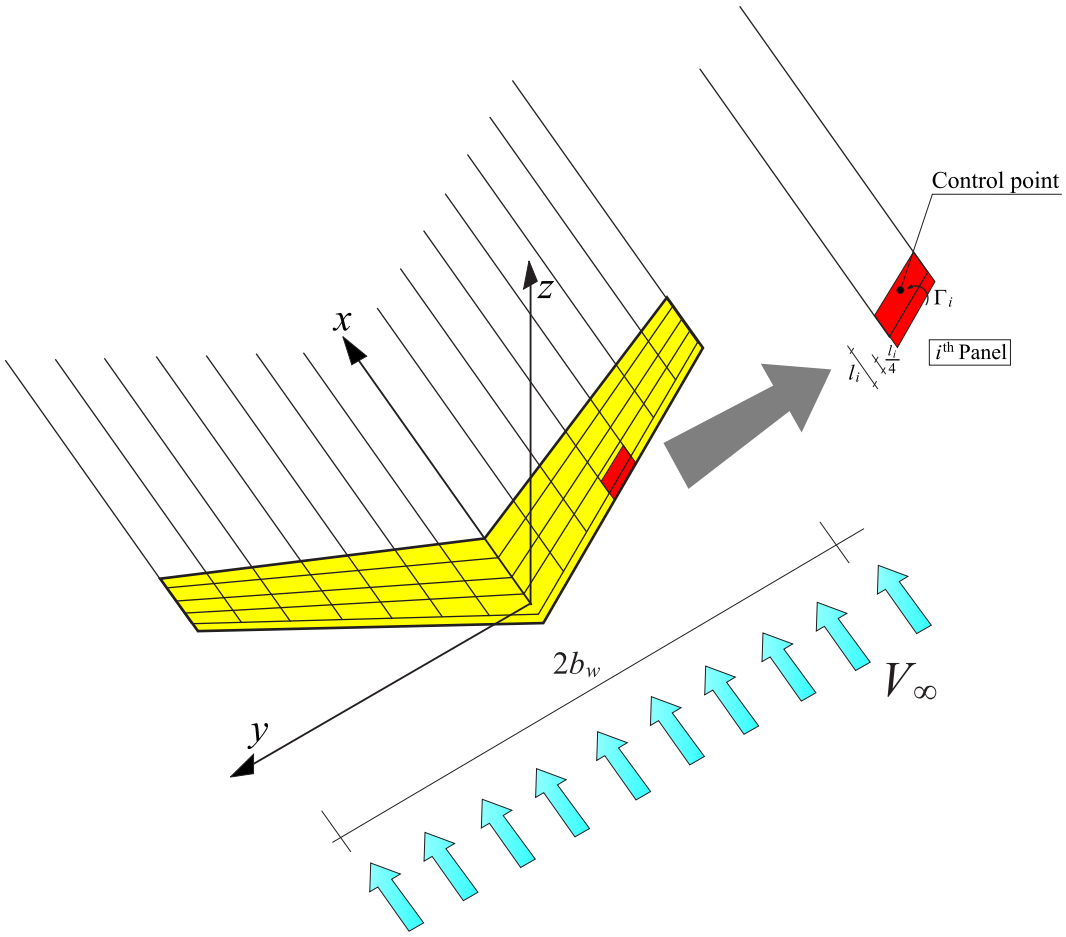

Figure 4.6. Vortex-lattice system in a finite wing.

in the vortex-lattice method by applying the Kutta-Joukowski law on the spanwise bound vortex segments under the influence of the local downwash. As is said in [18], if the bound vortex segments are aligned perpendicular to the free-stream velocity or aligned in some other direction depending on the wing planform shape, the solution can be significantly different.

4.3.3 Linear Panel Methods

Panel methods (see [39] and [40], for example) discretize wing's upper and lower surfaces into source, doublet, or vortex panels which induce a perturbation (see previous chapters) on the uniform velocity field. The advantage of these methods is that the wing thickness is taken into account. The strength of each panel is determined by satisfying the flow tangency condition at a number of control points equal to the number of panels used. A linear system of equations has to be solved in order to find the unknowns. The shape of the freely deforming wake can also be computed by discretizing the wake into panels and calculating the flow velocity at each panel. If the wake is not oriented with the local velocity vector then the panels in the wake are reoriented. An iterative process has to be conducted until the convergence is reached. In the panel methods, the induced drag can be calculated by taking the streamwise component of the product of surface pressure and panel area and summing over all of the wing panels. The problem with this approach is that the error in the calculated pressure distribution affects the induced drag calculation. More details can be found in [2] and [18].

4.4 Munk's Induced Drag Theorems

One of the most important contributes to the induced drag calculation and minimization was given by Munk in one of his papers, [41]. In this section, Munk's two famous theorems will be analyzed.

4.4.1 Munk's Stagger Theorem

The total induced drag of any three-dimensional system of lifting elements is independent of the positions of the various elements in the direction of the freestream velocity V_∞.

This theorem is valid under the hypothesis of small perturbations, incompressible fluid and rigid wake aligned with the freestream velocity. This theorem is very useful. If all the lifting elements of a system are translated, parallel to V_∞, into a single plane normal to V_∞, while the initial circulation is maintained constant, the induced drag of the resulting two-dimensional system will be exactly the same as that of the three-dimensional system. In figure 4.7, this theorem is explained with an example. In particular, it is shown that the swept wing has the same induced drag as the wing with straight lifting line (contained in a plane perpendicular to V_∞).

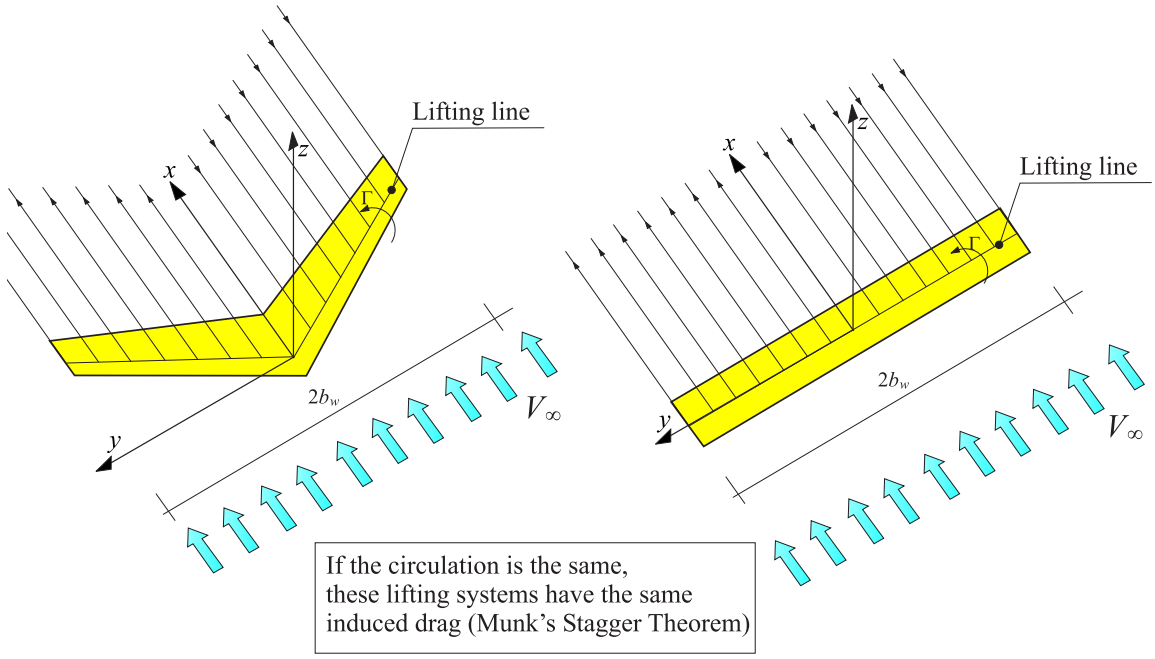

Figure 4.7. Munk's Stagger Theorem.

4.4.2 Munk's Minimum Induced Drag Theorem

When all the elements of a lifting system have been translated into a single plane (Munk's Stagger Theorem), the induced drag will be minimum when the component of the induced velocity normal to the lifting element at each point is proportional to the cosine of the angle of inclination of the lifting element at that point.

This is Munk's most important theorem. Incredibly, it is often ignored in the literature. For that reason, the contents of this theorem are analyzed in detail. In order to demonstrate the theorem[6], consider the lifting line representing a non-planar wing, as depicted in figure 4.8. *Suppose that the distribution of circulation is optimal, and, therefore, the induced drag is the minimum.* Now consider an arbitrary variation in the circulation distribution represented by $\delta\Gamma_1$ and $\delta\Gamma_2$. The local aerodynamic load will be represented by $\rho_\infty V_\infty \delta\Gamma_1$ and $\rho_\infty V_\infty \delta\Gamma_2$, respectively. As a result, the variation of the lifting contribute (see figure 4.8) is

$$\delta L = \rho_\infty V_\infty \delta\Gamma_1 \cos\vartheta_1 + \rho_\infty V_\infty \delta\Gamma_2 \cos\vartheta_2. \tag{4.7}$$

[6]The demonstration reported here is not the original demonstration used by Munk.

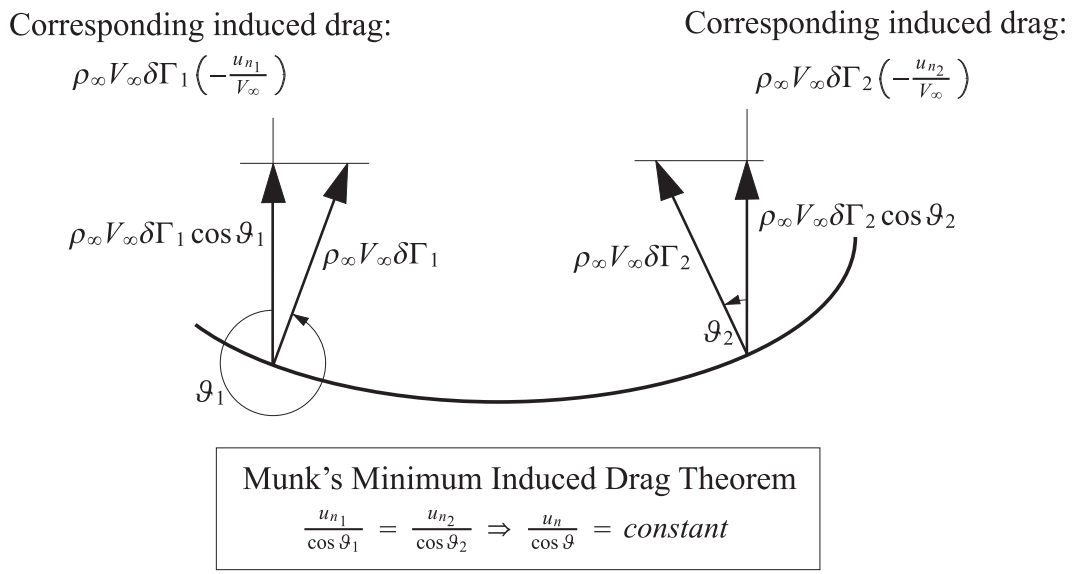

Figure 4.8. Munk's Minimum Induced Drag Theorem in a non-planar wing.

Variations of circulation that do not change the lift are considered. Consequently, δL has to be zero:

$$\delta L = \rho_\infty V_\infty \delta\Gamma_1 \cos\vartheta_1 + \rho_\infty V_\infty \delta\Gamma_2 \cos\vartheta_2 = 0. \tag{4.8}$$

Now, *because the initial condition is optimal*, the variation of induced drag has to be zero too:

$$\delta D_i = \rho_\infty V_\infty \delta\Gamma_1 \left(-\frac{u_{n_1}}{V_\infty}\right) + \rho_\infty V_\infty \delta\Gamma_2 \left(-\frac{u_{n_2}}{V_\infty}\right) = 0. \tag{4.9}$$

Thus:

$$\begin{cases} \delta L = 0 \Rightarrow \delta\Gamma_1 \cos\vartheta_1 + \delta\Gamma_2 \cos\vartheta_2 = 0, \\ \delta D_i = 0 \Rightarrow \delta\Gamma_1 u_{n_1} + \delta\Gamma_2 u_{n_2} = 0. \end{cases} \tag{4.10}$$

Clearly, if $u_{n_1} = k\cos\vartheta_1$ and $u_{n_2} = k\cos\vartheta_2$ (k is a constant), the previous system is satisfied. This last statement demonstrates Munk's Minimum Induced Drag Theorem[7].

Observation 22 Using Munk's Minimum Induced Drag Theorem, interesting properties can be observed in conventional and non-conventional wing configurations. For

[7]Notice that if other conditions are imposed (like the structural weight) this theorem is no longer valid (see [42], [43] and [44], for example).

example, in a classical cantilever wing $\cos\vartheta = 1$ everywhere. Therefore, the induced velocity must be constant along the longitudinal direction under optimal conditions. It is also well known that when the circulation distribution is elliptical the induced velocity is constant. Hence, the elliptical distribution is the optimal one. Another example is the box wing (see Figure 4.9): in the vertical parts $\vartheta = \pi/2$. For that reason, u_n has to be zero in order to have the minimum induced drag[8].

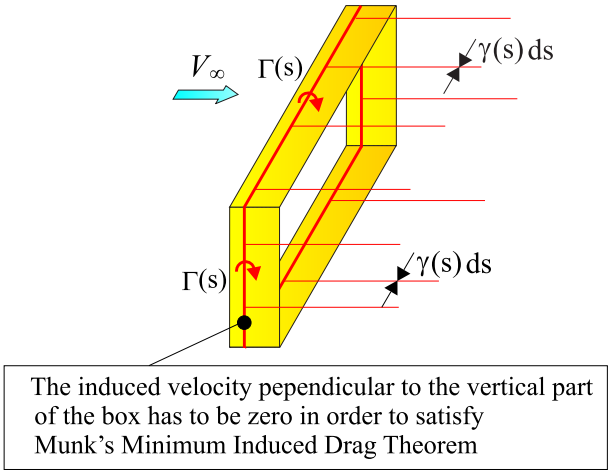

Figure 4.9. Munk's Minimum Induced Drag Theorem in a box wing.

More details about this theorem and its applications can be found in [15] and [18].

4.5 Induced Drag Reduction: Non-planar Wing Systems

As was said in the introduction, a reduction of the induced drag is of great interest in the aircraft design. *The non-planar wing system can influence a larger mass of air than a classical wing with the same wing span and it can impart, to this air mass, a lower average velocity change and, therefore, it has less drag.* Biplane, multiplanes, winglets, C-wings and closed wing systems are examples of non-planar wing systems. Prandtl in [46] studied the multiplanes, and he outlined the following conclusions:

- *Prandtl's Conclusion 1*
  The biplane has less induced drag than a monoplane.

[8]The distribution over the horizontal parts is not discussed here. Details can be found in [45].

- *Prandtl's Conclusion 2*
  The triplane has less induced drag than a biplane and so forth.

- *Prandtl's Conclusion 3*
  The wing system with minimum induced drag is the box wing system (see figure 4.9 and, for more details, [45]). It was called *best wing system* by Prandtl.

It is evident that nonplanar wings have a better performance than classical wings with the same wing span and total lift. Several authors have studied non-planar wings. The most important contributes have been made by Kroo ([14]) and Cone ([15]). They studied several non-planar wing configurations and showed the high efficiency of those systems. An interesting example of non-planar wing is the wing-grid tip device (for more details see [47]-[51]). In figure 4.10 and 4.11 a few examples of the wing-grid concept are reported.

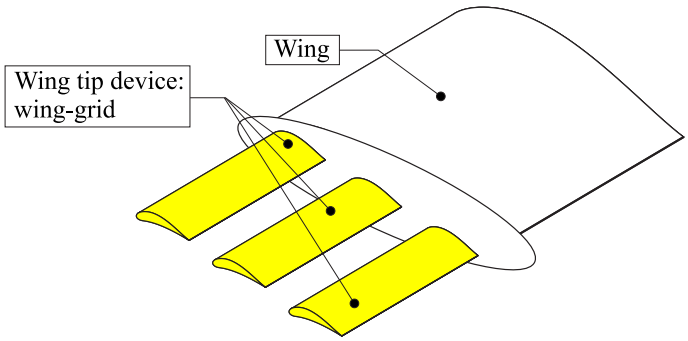

Figure 4.10. Wing-grid concept.

4.5.1 Non-planar Wing Systems: The Induced Lift

Induced lift is an important concept in non-planar wings, but it is often not considered in the theoretical approaches. Consider a non-planar wing system (see figure 4.12). As well explained in [15], the generic vortex positioned at point A induces a velocity $\mathrm{d}u_T$ at point B. As result of this induced velocity, an induced lift $\mathrm{d}L_i$ is produced at point B. The concept of induced lift is interesting when two different wings with the same induced drag and total lift are considered. In some cases the induced lift is positive and in other cases it is negative. As reported in [15], for a lifting segment represented using an arc,
the induced lift is positive when the local aerodynamic force F acts towards the local center of curvature of the arc and negative when this force is directed outward from the center of curvature (see figure (4.13)).

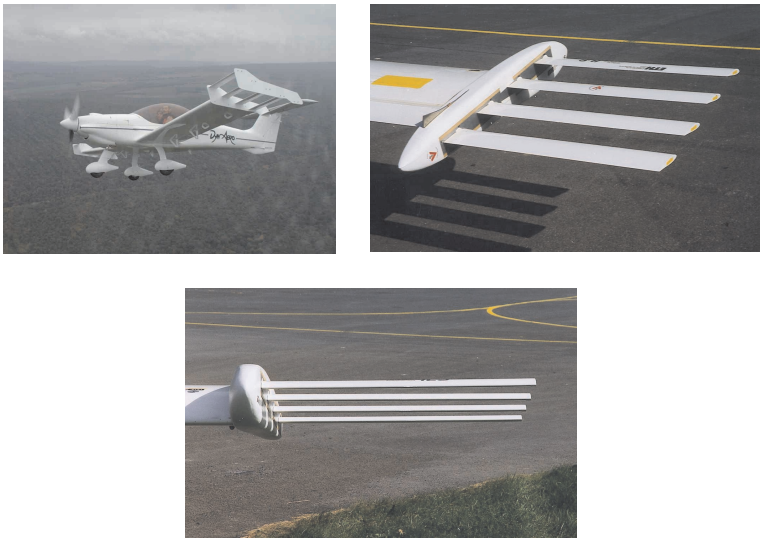

Figure 4.11. Wing-grid examples (figures from [47]).

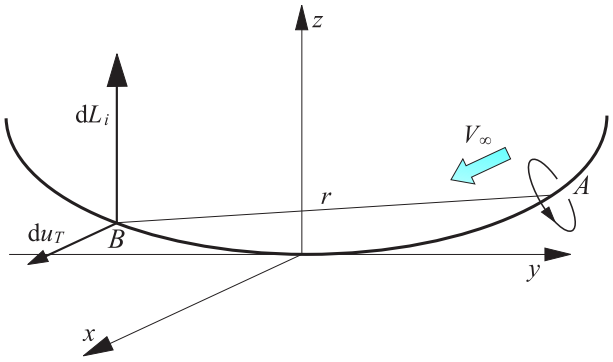

Figure 4.12. Induced lift in a non-planar wing.

Under the assumption of small velocities, u_T can be neglected in comparison with V_∞. Therefore, *In this dissertation, the induced lift effects are not considered.*

4.5.2 Non-planar Wing Systems: Closed Wing Systems

A simple closed wing system is shown in figure 4.9. A possible practical closed wing system could be a *joined wing configuration* as shown in figure 4.14. Why is a closed system useful? There are several interesting properties that involve different fields (aerodynamic, structures, flight mechanics, aeroelasticity and so forth) that should be analyzed in order to answer this question. Here, only the aerodynamic point of

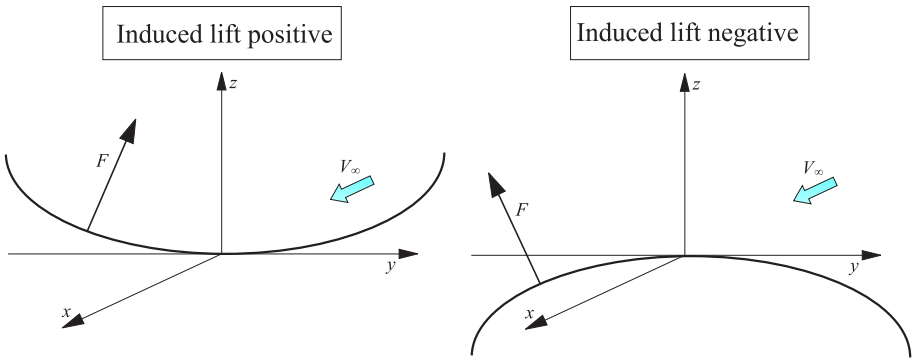

Figure 4.13. Induced lift. Relation with the local aerodynamic force.

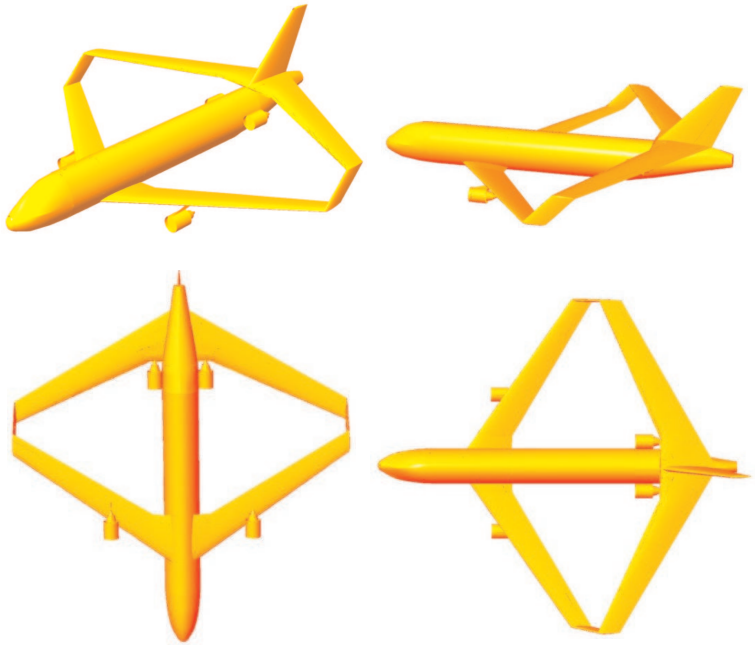

Figure 4.14. Closed wing system example: a joined wing configuration

view of the problem is analyzed. For more details see [52] and [53].
The main aerodynamic characteristics of a closed wing system are the following:

- *Characteristic 1*
  The optimal induced drag is smaller in such wings than in a classical cantilever wing with the same wing span and total lift. This property, for the annular wings, will be demonstrated in chapter 9. Interesting considerations can be found in [14] and [15].

- *Characteristic 2*
  It is possible to add a *constant circulation vortex* to the system *without changing the wake*. Such a constant strength vortex distribution *does not add any lift and the induced drag does not change*. It may be used to manipulate the section lift coefficients in a desirable way. This property, often not considered in the theoretical derivations, will be used in chapter 9.

These characteristics will be extensively analyzed later. Here they are analyzed in an intuitive way using graphical examples.
Consider the first property mentioned above. Why is the induced drag in a closed wing system smaller? In order to answer the question, consider figure 4.15. As it is

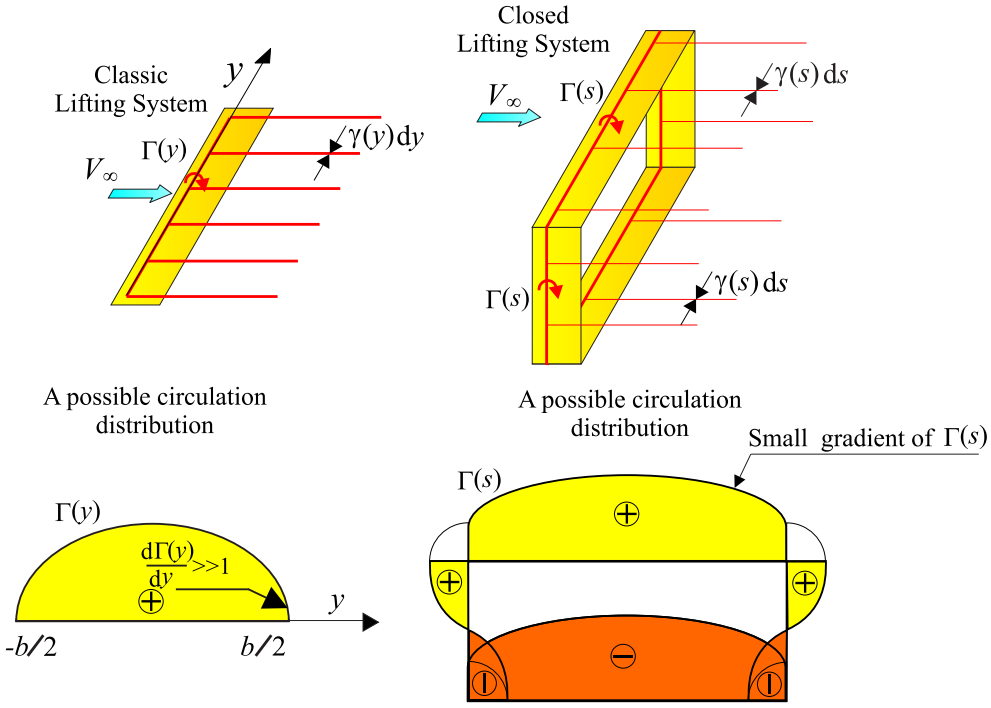

Figure 4.15. Circulation distribution in a classical and closed wing systems.

easy to see, the circulation gradients are higher in the classical wing systems where the circulation must be zero at the tips. In a closed wing system, there is not a particular point where the circulation has to be zero, thus, the wing can be designed to have a circulation distribution which has less induced drag (with the same lift). It will be demonstrated that in an elliptical annular wing, the induced drag is smaller than in a classical wing, even under optimal conditions for both wings[9].

[9]This is true if the wing span and the total lift are the same.

Now consider the second property. Because the induced drag is related to the circulation gradients, it is clear that if a constant circulation is added, no lift or induced drag are added (that property will be demonstrated for the elliptical annular wing in chapter 9). This is very useful, since the circulation distribution (therefore the lift distribution) can be modified as desired or needed *without induced drag penalty and without changing the total lift.* For a box wing system, the property is illustrated[10] in figure 4.16.

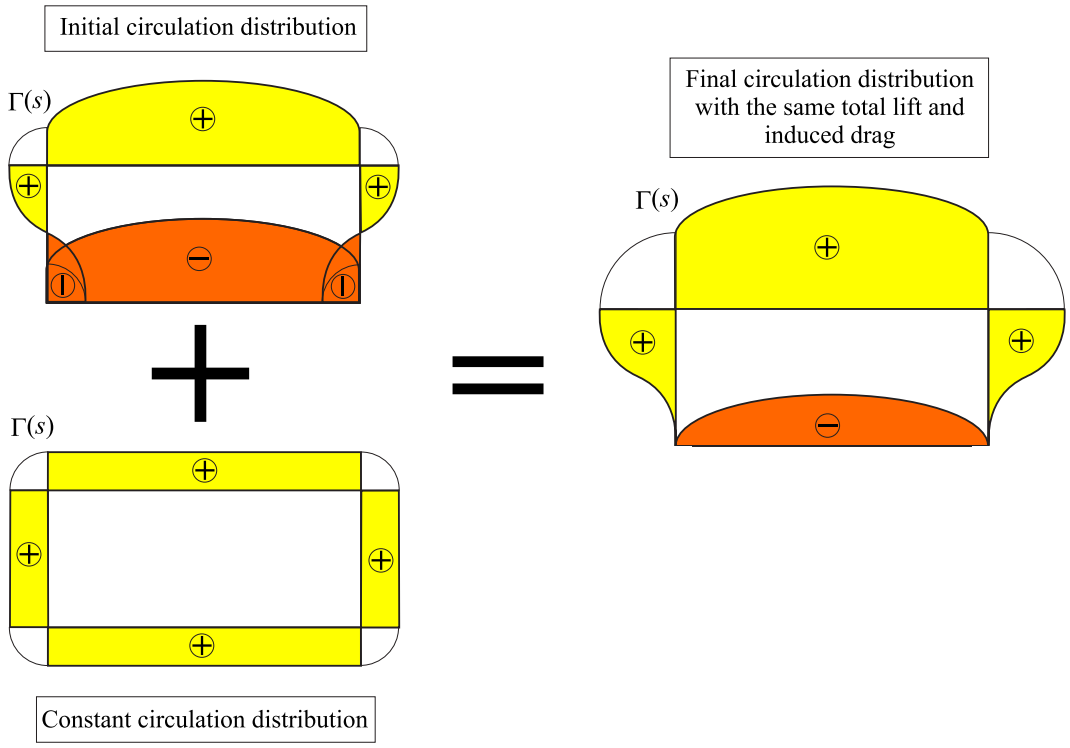

Figure 4.16. A property in a closed wing system.

Using the previous property, it is easy to show ([14] and [54]-[55]) that a C-wing has an optimal induced drag similar to the "best wing system" (see also chapter 10). It is possible to add a constant circulation distribution[11] in such a way as to reduce the load in the upper wing and increase the aerodynamic load in the lower wing *without changing the total load and induced drag* . As can be seen in figure 4.17, after this ideal operation the upper wing is almost with no load which explains, in a

[10]The initial circulation distribution corresponds to the optimal distribution (Prandtl's best wing system), see [45] for more details.

[11]Notice that, in figure 4.17, the optimal circulation distribution in the box wing system is still considered.

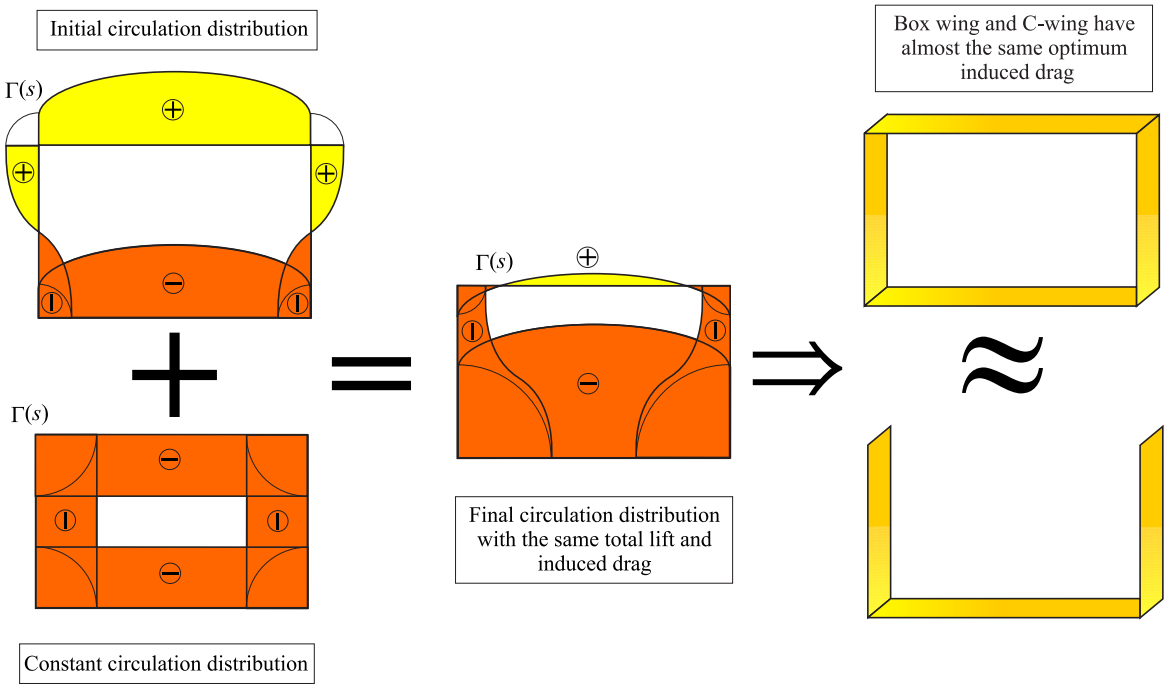

Figure 4.17. Box wing and C wing. An intuitive comparison.

qualitative way, the similar efficiency between the box wing and the C-wing found by Kroo.

Closed Wing Systems. An Italian Research Project: the Prandtlplane

Following Prandtl's idea of the best wing system, many scientists studied new configurations (see, for example, [52]). One of these, the Prandtlplane, is a joined wing configuration which consists of two swept wings (with opposite swept angle) and is closed by two vertical additional surfaces. A comprehensive study of a similar configuration was first performed by Lange [56]. The aeroelastic phenomena was found to be a weak point of the considered analyses. Extensive use of composite materials along with aeroelastic tailoring could be conveniently employed to this purpose. For this reason, the configuration is nowadays very interesting. It could increase the payload considerably and reduce the induced drag. In Italy, five universities (Università di Pisa, Politecnico di Torino, Politecnico di Milano, Università La Sapienza and Università Roma 3) and the aerospace company Alenia Aeronautica have been working on this project. Several papers can be found in literature (see, for example, [57]-[68]) covering aerodynamic, flight mechanics and structures of the Prandtlplane. Particularly interesting are the wind tunnel tests

conducted in Alenia Aeronautica company and Politecnico di Torino. The wind tunnel models are reported in figures 4.19 and 4.20. The logo of the italian research is shown in figure 4.18[12].

Figure 4.18. Italian research project on Prandtlplane. Logo.

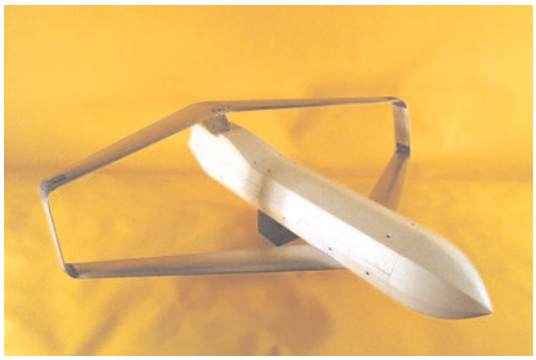

Figure 4.19. Alenia's Prandtlplane model (figure from [68]).

[12]The logo has been designed by the writer.

Figure 4.20. Politecnico di Torino's Prandtlplane model.

Nomenclature

α	angle of attack
α_i	induced angle of attack
$\alpha_{L=0}$	angle of attack corresponding to the condition of zero lift
ρ	fluid density
ρ'	perturbation density
v_x	x-component perturbation velocity
v_y	y-component perturbation velocity
v_z	z-component perturbation velocity
v'_z	induced velocity on the wake
M_∞	Mach number (freestream conditions)
ϕ	small perturbation velocity potential
$\Delta\phi$	small perturbation velocity potential jump
wt	wake trace
Γ	circulation
$\delta\Gamma$	arbitrary variation of Γ
γ	ratio of specific heats, distributed trailing vorticity
u_n	normalwash
$2b_w$	wing span
ϑ	angle of inclination of the lifting element
L	lift
L_i	induced lift
D_i	induced drag
δL	arbitrary variation of lift
δD_i	arbitrary variation of induced drag
F	aerodynamic force
u_T	induced velocity in the direction of V_∞

Subscripts

∞	freestream conditions

Part II

Non-planar Lifting Systems

Chapter 5

Validation of the Present Optimization Method: Cantilever Wing and Biplane

5.1 Introduction

This chapter demonstrates the well known result concerning a classical wing: the elliptical circulation distribution is the optimal distribution, and the induced velocity is constant along the wing span (Munk's Minimum Induced Drag Theorem).
This operation is done using the methods exposed in previous chapters: lifting-line theory (Weissinger's lifting-line model) for the aerodynamic part and Hadamard finite-part integral equation for the mathematical aspect of the problem. The optimum is found using the Euler-Lagrange integral equation obtained using the Lagrange multiplier method.
The same procedure *proposed by the writer* is applied in another classical (but non-planar) wing: the biplane. It is an interesting case often not well considered. Commonly, it is believed that, in a biplane, the optimal circulation distribution is an ellipse. As will be shown, this is true only in two particular cases: wings indefinitely distant from each other and wings indefinitely close together.

5.2 Classical Cantilever Wing. Minimum Induced Drag

In this section, the classical cantilever wing will be studied. Its study is the easiest and clearly shows the minimizing procedure used in this dissertation.

5.2.1 Geometrical Derivation of the Induced Velocity and Induced Drag

Considering figures 5.1 and 5.2[1], it can be understood that the induced velocity (positive when oriented along the z axis) is

$$u_n(y) = \frac{1}{4\pi} \fint_{-b_w}^{+b_w} \frac{-\frac{\mathrm{d}\Gamma(y_d)}{\mathrm{d}y_d}}{(y - y_d)} \mathrm{d}y_d. \tag{5.1}$$

Integrating by parts and observing that $\Gamma(+b_w) = \Gamma(-b_w) = 0$:

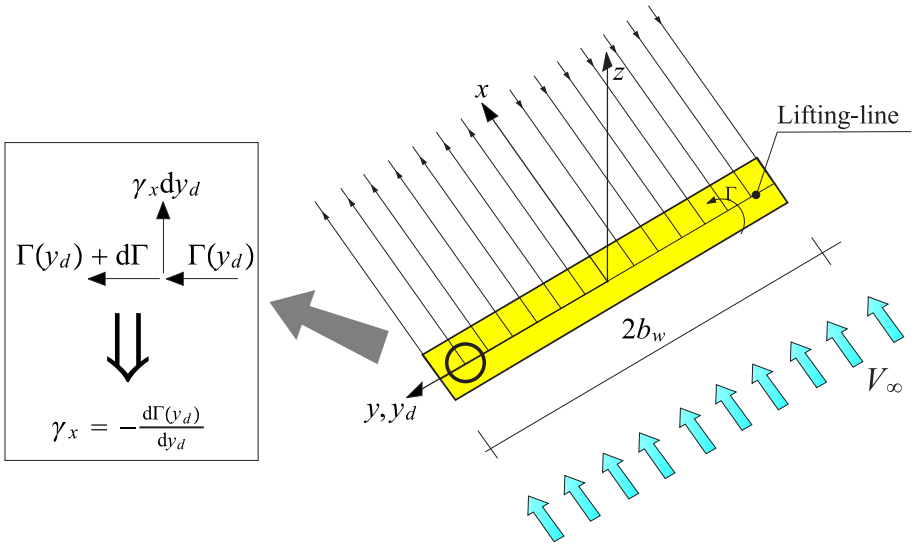

Figure 5.1. Lifting-line model in a classical wing.

$$u_n(y) = \frac{1}{4\pi} \fint_{-b_w}^{+b_w} \frac{\Gamma(y_d)}{(y - y_d)^2} \mathrm{d}y_d. \tag{5.2}$$

The consequent induced incidence is $\alpha_i(y) = -\frac{u_n(y)}{V_\infty}$, and the *induced drag*[2] is

$$D_i = \int_{-b_w}^{+b_w} \rho_\infty V_\infty \left(-\frac{1}{4\pi V_\infty} \Gamma(y) \fint_{-b_w}^{+b_w} \frac{\Gamma(y_d)}{(y - y_d)^2} \mathrm{d}y_d \right) \mathrm{d}y. \tag{5.3}$$

[1]The distributed trailing vorticity is indicated by γ_x instead of γ to clarify that the velocity V_∞ is directed along x.

[2]The external integral *is not defined as Hadamard finite-part integral* because the circulation Γ is zero at both endpoints (the tips).

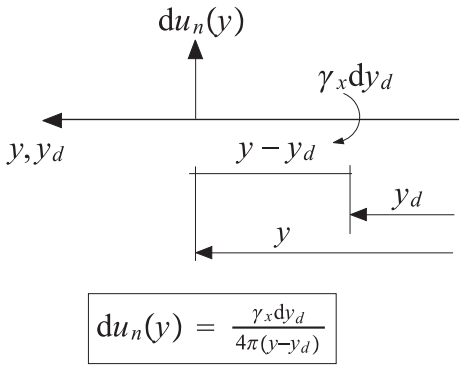

Figure 5.2. Induced velocity by the vortex $\gamma_x \, \mathrm{d}y_d$.

With a few simple algebraic manipulations, the expressions of the lift and induced drag coefficients are obtained:

$$\begin{aligned} C_{D_i} &= -\frac{1}{4\pi V_\infty^2 b_w l} \int_{-b_w}^{+b_w} \Gamma(y) \, \fint_{-b_w}^{+b_w} \frac{\Gamma(y_d)}{(y-y_d)^2} \, \mathrm{d}y_d \, \mathrm{d}y, \\ C_L &= \frac{1}{V_\infty b_w l} \int_{-b_w}^{+b_w} \Gamma(y) \, \mathrm{d}y. \end{aligned} \tag{5.4}$$

The previous expression can easily be rewritten using the small perturbation acceleration potential and a doublet distribution along the lifting line[3] (with the positive direction along $-z$):

$$\begin{aligned} C_{D_i} &= -\frac{1}{4\pi V_\infty^4 b_w l} \int_{-b_w}^{+b_w} m(y) \, \fint_{-b_w}^{+b_w} \frac{m(y_d)}{(y-y_d)^2} \, \mathrm{d}y_d \, \mathrm{d}y, \\ C_L &= \frac{1}{V_\infty^2 b_w l} \int_{-b_w}^{+b_w} m(y) \, \mathrm{d}y. \end{aligned} \tag{5.5}$$

5.2.2 Euler-Lagrange Equation

The goal is to find the minimum C_{D_i} under fixed C_L. As have been seen in chapter 2, the Euler-Lagrange equation[4] is:

$$2C_1 \fint_{-b_w}^{+b_w} m_{\text{opt}}(y) \, Y(y_d,y) \, \mathrm{d}s - C_2 \lambda g(y_d) = 0. \tag{5.6}$$

[3] Remember that $\rho_\infty V_\infty \Gamma(y) = \rho_\infty m(y)$.

[4] It should be observed that in this case $Y(y_d,y) = \frac{1}{(y-y_d)^2}$, $g(y_d) = 1$, $C_1 = -\frac{1}{4\pi V_\infty^4 b_w l}$ and $C_2 = \frac{1}{V_\infty^2 b_w l}$, where $Y(y_d,y)$, $g(y_d)$, C_1 and C_2 are defined in chapter 2.

In explicit form:

$$-\frac{1}{2\pi V_\infty^2}\,\fint_{-b_w}^{+b_w} m_{\text{opt}}(y)\,\frac{1}{(y-y_d)^2}\,\mathrm{d}y-\lambda=0, \tag{5.7}$$

with the condition

$$\overline{C}_L=\frac{1}{V_\infty^2 b_w l}\int_{-b_w}^{+b_w} m_{\text{opt}}(y)\,\mathrm{d}y. \tag{5.8}$$

Now, the fact that the optimum distribution is an ellipse, will be verified. Thus, consider a solution in the form

$$m_{\text{opt}}(y)=\overline{m}\sqrt{1-\frac{y^2}{b_w^2}}. \tag{5.9}$$

Substituting this expression into (5.7) and (5.8):

$$\begin{cases} \dfrac{\overline{m}}{2\pi V_\infty^2}\,\fint_{-b_w}^{+b_w}\dfrac{\sqrt{1-\frac{y^2}{b_w^2}}}{(y-y_d)^2}\,\mathrm{d}y+\lambda=0, \\ \overline{C}_L=\dfrac{\overline{m}}{V_\infty^2 b_w l}\displaystyle\int_{-b_w}^{+b_w}\sqrt{1-\frac{y^2}{b_w^2}}\,\mathrm{d}y. \end{cases} \tag{5.10}$$

With the substitution $y=b_w\sin\Theta$ and $y_d=b_w\sin\Theta_d$, the system becomes:

$$\begin{cases} \dfrac{\overline{m}}{2\pi V_\infty^2 b_w}\,\fint_{-\frac{\pi}{2}}^{+\frac{\pi}{2}}\dfrac{\cos^2\Theta}{(\sin\Theta-\sin\Theta_d)^2}\,\mathrm{d}\Theta+\lambda=0, \\ \overline{C}_L=\dfrac{\overline{m}}{V_\infty^2 l}\displaystyle\int_{-\frac{\pi}{2}}^{+\frac{\pi}{2}}\cos^2\Theta\,\mathrm{d}\Theta=\frac{\overline{m}\pi}{2V_\infty^2 l}. \end{cases} \tag{5.11}$$

With a few algebraic operations[5] the result is:

$$\begin{aligned} \overline{m}&=\frac{2V_\infty^2 l}{\pi}\overline{C}_L, \\ \lambda&=\frac{\overline{C}_L l}{\pi b_w}. \end{aligned} \tag{5.12}$$

[5] Setting $u=\tan\frac{\Theta}{2}$, $v=\tan\frac{\Theta_d}{2}$:

$$u=\tan\tfrac{\Theta}{2},\quad v=\tan\tfrac{\Theta_d}{2},\quad \cos\Theta=\tfrac{1-u^2}{1+u^2},$$
$$\sin\Theta=\tfrac{2u}{1+u^2},\quad \sin\Theta_d=\tfrac{2v}{1+v^2},\quad \mathrm{d}\Theta=\tfrac{2}{u^2+1}\,\mathrm{d}u.$$

The Euler-Lagrange equation becomes

$$\frac{\overline{m}}{2\pi V_\infty^2 b_w}\,\fint_{-1}^{+1}\frac{2}{u^2+1}\,\frac{\left(\frac{1-u^2}{1+u^2}\right)^2}{\left(\frac{2u}{1+u^2}-\frac{2v}{1+v^2}\right)^2}\,\mathrm{d}u+\lambda=0.$$

The system is satisfied, and, thus, the distribution $m_{\text{opt}}(y) = \overline{m}\sqrt{1-\frac{y^2}{b_w^2}} = \frac{2V_\infty^2 l}{\pi}\overline{C}_L\sqrt{1-\frac{y^2}{b_w^2}}$ is the optimal distribution. This can be verified by observing that u_n is constant for that distribution, satisfying Munk's Minimum Induced Drag Theorem. In completeness, the minimum induced drag coefficient is:

$$\left[(C_{D_i})_{\text{opt}}\right]_{\text{ref}} = \frac{l\overline{C}_L^2}{2b_w\pi}. \tag{5.13}$$

The subscript "ref" indicates "reference" and has been placed with C_{D_i} because the classical wing will be used as a reference case and all wings will be compared with the classical cantilever wing.

5.3 Classical Biplane Wing System. Minimum Induced Drag

In some publications, it is said that the minimum induced drag in a biplane is obtained when the distribution of each wing is elliptical and when the wings have the same load distribution. This statement is *false.* The misunderstanding is from article [46], where Prandtl assumed the elliptical distribution for each wing in a biplane and obtained that, under this condition, the best biplane had wings with the same wing span. *But Prandtl never said that the elliptical distribution is the optimal distribution for a biplane.* This chapter will demonstrate that the elliptical circulation distribution is the optimum *only* if the distance between the two wings is either near zero or infinity.

Consider a biplane (see figure 5.3[6]) with wing span $2b_w$ and distance between the

(Continued on page 86)
(Continued from page 85, footnote 5)

Now, observing that

$$\int \frac{2}{u^2+1}\frac{\left(\frac{1-u^2}{1+u^2}\right)^2}{\left(\frac{2u}{1+u^2}-\frac{2v}{1+v^2}\right)^2}\,\mathrm{d}u = 2\left[\frac{(1+v^2)(2v-u-v^2u)}{4v(v-u-v^2u+vu^2)} - \arctan u + \frac{v\ln|-v+u|}{-1+v^2} - \frac{v\ln|-1+vu|}{-1+v^2}\right],$$

and remembering the Hadamard finite-part integral definition, the Euler-Lagrange equation becomes:

$$-\frac{\overline{m}}{2\pi V_\infty^2 b_w}\pi + \lambda = 0 \Rightarrow \lambda = \frac{\overline{C}_L l}{\pi b_w}.$$

[6]Even if the wings have sweep angles, the biplane depicted in the figure is useful because Munk's Stagger Theorem can be applied (see chapter 4).

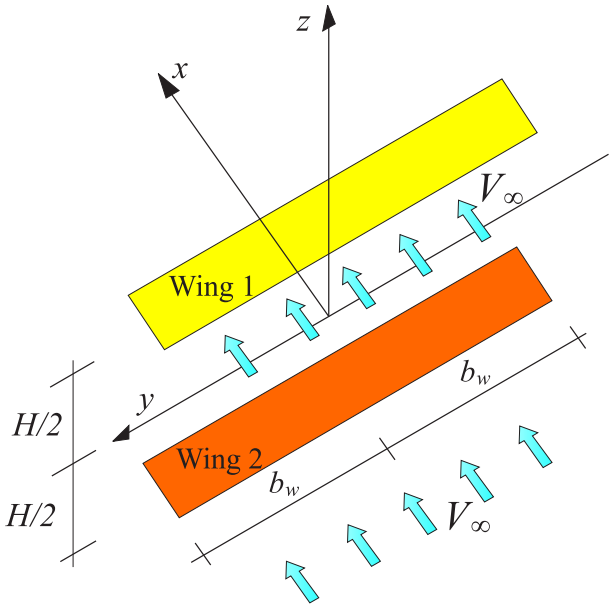

Figure 5.3. Biplane. Geometry and notations.

wings H. Clearly, the upper wing (here called wing 1) is positioned at $z = +\frac{H}{2}$, while the lower wing (here called wing 2) is positioned at $z = -\frac{H}{2}$ in the reference system shown in figure 5.3.

5.3.1 Writing of the Integral Equations

As seen in chapter 3 and 4, the lifting-line theory can be used to describe the wings. If the small perturbation acceleration potential is used, the writing of the integral equations[7] can be accomplished using the procedures shown in the following steps:

- *Step 1*
  Writing of the *small perturbation acceleration potential* of the dipole distribution over the wings.

- *Step 2*
  Writing of the *small perturbation velocity potential* by integration of the small perturbation acceleration potential.

- *Step 3*
  Imposition of the WTC using Weissinger's approach.

[7] As will be seen, in this case there are two integral equations containing the unknown dipole distributions on the wings 1 and 2.

Small Perturbation Acceleration Potential

In order to start this procedure, the distance between a generic point in space with coordinates x, y, z and a point on *wing 1* with coordinates x_{d1}, y_{d1}, z_{d1}, in which a generic doublet is positioned[8], has to be calculated. It is easy to obtain

$$D_1 = \sqrt{(x - x_{d1})^2 + (y - y_{d1})^2 + (z - z_{d1})^2}. \tag{5.14}$$

The reference coordinate system is chosen in such a way as to have the lifting lines contained in the $y - z$ plane, so $x_{d1} = 0$. Moreover, $z_{d1} = \frac{H}{2}$. Using these relations:

$$D_1 = \sqrt{x^2 + (y - y_{d1})^2 + \left(z - \frac{H}{2}\right)^2}. \tag{5.15}$$

Similarly for the wing 2:

$$D_2 = \sqrt{x^2 + (y - y_{d2})^2 + \left(z + \frac{H}{2}\right)^2}. \tag{5.16}$$

Next consider wing 1. The generic expression for the small perturbation acceleration potential is

$$\mathrm{d}\Psi_1(x,y,z) = -\frac{m_1(y_{d1})\,\mathrm{d}y_{d1}}{4\pi} \frac{n_{d1x}(x - x_{d1}) + n_{d1y}(y - y_{d1}) + n_{d1z}(z - z_{d1})}{\left[(x - x_{d1})^2 + (y - y_{d1})^2 + (z - z_{d1})^2\right]^{\frac{3}{2}}}. \tag{5.17}$$

Now, choosing the doublet axis to be directed along $+z$, it can be deduced that $n_{d1x} = n_{d1y} = 0$ and $n_{d1z} = 1$. Substituting into the previous equation and remembering that $z_{d1} = +\frac{H}{2}$:

$$\mathrm{d}\Psi_1(x,y,z) = -\frac{m_1(y_{d1})\,\mathrm{d}y_{d1}}{4\pi} \frac{\left(z - \frac{H}{2}\right)}{\left[x^2 + (y - y_{d1})^2 + \left(z - \frac{H}{2}\right)^2\right]^{\frac{3}{2}}}. \tag{5.18}$$

Now, because of the linearity, it is possible to integrate over wing 1:

$$\Psi_1(x,y,z) = \int_{-b_w}^{+b_w} -\frac{m_1(y_{d1})}{4\pi} \frac{\left(z - \frac{H}{2}\right)}{\left[x^2 + (y - y_{d1})^2 + \left(z - \frac{H}{2}\right)^2\right]^{\frac{3}{2}}}\,\mathrm{d}y_{d1}. \tag{5.19}$$

The same operations can be repeated for wing 2:

$$\Psi_2(x,y,z) = \int_{-b_w}^{+b_w} -\frac{m_2(y_{d2})}{4\pi} \frac{\left(z + \frac{H}{2}\right)}{\left[x^2 + (y - y_{d2})^2 + \left(z + \frac{H}{2}\right)^2\right]^{\frac{3}{2}}}\,\mathrm{d}y_{d2}. \tag{5.20}$$

[8]The subscript "1" indicates that wing 1 is being considered.

It is possible to think that the integration process is done in such a way as to have $y_{d1} = y_{d2}$. Calling y_d the common value, the previous expressions become:

$$\Psi_1(x,y,z) = \int_{-b_w}^{+b_w} -\frac{m_1(y_d)}{4\pi} \frac{\left(z - \frac{H}{2}\right)}{\left[x^2 + (y-y_d)^2 + \left(z - \frac{H}{2}\right)^2\right]^{\frac{3}{2}}} \mathrm{d}y_d, \tag{5.21}$$

$$\Psi_2(x,y,z) = \int_{-b_w}^{+b_w} -\frac{m_2(y_d)}{4\pi} \frac{\left(z + \frac{H}{2}\right)}{\left[x^2 + (y-y_d)^2 + \left(z + \frac{H}{2}\right)^2\right]^{\frac{3}{2}}} \mathrm{d}y_d. \tag{5.22}$$

Small Perturbation Velocity Potential

The small perturbation velocity potential has the expression

$$\phi(x,y,z) = \frac{1}{V_\infty} \int_{-\infty}^{x} \Psi_1(\tau,y,z)\,\mathrm{d}\tau + \frac{1}{V_\infty} \int_{-\infty}^{x} \Psi_2(\tau,y,z)\,\mathrm{d}\tau = \phi_1 + \phi_2, \tag{5.23}$$

where ϕ_1 and ϕ_2 are the contributes of the wings 1 and 2, respectively. Therefore, the following can be written:

$$\begin{aligned} \phi_1(x,y,z) &= \tfrac{1}{V_\infty} \int_{-\infty}^{x} \Psi_1(\tau,y,z)\,\mathrm{d}\tau = \\ &= -\tfrac{1}{4\pi V_\infty} \int_{-b_w}^{+b_w} m_1(y_d)\left(z - \tfrac{H}{2}\right) \int_{-\infty}^{x} \frac{1}{\left[\tau^2 + (y-y_d)^2 + \left(z - \frac{H}{2}\right)^2\right]^{\frac{3}{2}}} \mathrm{d}\tau \mathrm{d}y_d, \end{aligned} \tag{5.24}$$

$$\begin{aligned} \phi_2(x,y,z) &= \tfrac{1}{V_\infty} \int_{-\infty}^{x} \Psi_2(\tau,y,z)\,\mathrm{d}\tau = \\ &= -\tfrac{1}{4\pi V_\infty} \int_{-b_w}^{+b_w} m_2(y_d)\left(z + \tfrac{H}{2}\right) \int_{-\infty}^{x} \frac{1}{\left[\tau^2 + (y-y_d)^2 + \left(z + \frac{H}{2}\right)^2\right]^{\frac{3}{2}}} \mathrm{d}\tau \mathrm{d}y_d. \end{aligned} \tag{5.25}$$

Observing that

$$\int_{-\infty}^{x} \frac{f}{\left(\sqrt{\tau^2 + g}\right)^3} \mathrm{d}\tau = f \frac{x + \sqrt{(x^2+g)}}{g\sqrt{(x^2+g)}} = \frac{f}{g}\left(\frac{x}{\sqrt{(x^2+g)}} + 1\right), \tag{5.26}$$

the previous expressions become:

$$\phi_1(x,y,z) = -\tfrac{1}{4\pi V_\infty} \int_{-b_w}^{+b_w} \frac{m_1(y_d)\left(z - \frac{H}{2}\right)}{(y-y_d)^2 + \left(z - \frac{H}{2}\right)^2} \left(\frac{x}{\sqrt{\left(x^2 + (y-y_d)^2 + \left(z - \frac{H}{2}\right)^2\right)}} + 1\right) \mathrm{d}y_d, \tag{5.27}$$

$$\phi_2\left(x,y,z\right) = -\frac{1}{4\pi V_\infty}\int_{-b_w}^{+b_w}\frac{m_2(y_d)\left(z+\frac{H}{2}\right)}{(y-y_d)^2+\left(z+\frac{H}{2}\right)^2}\left(\frac{x}{\sqrt{\left(x^2+(y-y_d)^2+\left(z+\frac{H}{2}\right)^2\right)}}+1\right)\mathrm{d}y_d. \tag{5.28}$$

WTC Imposition Using Weissinger's Approach

The WTC have to be imposed on both wings. Thus:

$$\begin{aligned} -\alpha_1\left(y,z_1\right) &= \frac{1}{V_\infty}\left(\frac{\partial\phi(x,y,z)}{\partial z}\right) \quad z=z_1 \\ & \qquad\qquad\qquad\qquad\quad x=x_0 \\ -\alpha_2\left(y,z_2\right) &= \frac{1}{V_\infty}\left(\frac{\partial\phi(x,y,z)}{\partial z}\right) \quad z=z_2 \\ & \qquad\qquad\qquad\qquad\quad x=x_0 \end{aligned} \tag{5.29}$$

where $x_0 = \frac{l}{2}$. Calculating the derivative of the small perturbation velocity potential ϕ_1:

$$\begin{aligned} \frac{\partial\phi_1}{\partial z} = &-\frac{1}{4\pi V_\infty}\int_{-b_w}^{+b_w} m_1\left(y_d\right)\frac{(y-y_d)^2-\left(z-\frac{H}{2}\right)^2}{\left((y-y_d)^2+\left(z-\frac{H}{2}\right)^2\right)^2}\left(\frac{x}{\sqrt{\left(x^2+(y-y_d)^2+\left(z-\frac{H}{2}\right)^2\right)}}+1\right)\mathrm{d}y_d + \\ &+\frac{1}{4\pi V_\infty}\int_{-b_w}^{+b_w} m_1\left(y_d\right)\frac{x\left(z-\frac{H}{2}\right)^2}{\left((y-y_d)^2+\left(z-\frac{H}{2}\right)^2\right)\left(x^2+(y-y_d)^2+\left(z-\frac{H}{2}\right)^2\right)^{\frac{3}{2}}}\mathrm{d}y_d. \end{aligned} \tag{5.30}$$

And, similarly, for ϕ_2:

$$\begin{aligned} \frac{\partial\phi_2}{\partial z} = &-\frac{1}{4\pi V_\infty}\int_{-b_w}^{+b_w} m_2\left(y_d\right)\frac{(y-y_d)^2-\left(z+\frac{H}{2}\right)^2}{\left((y-y_d)^2+\left(z+\frac{H}{2}\right)^2\right)^2}\left(\frac{x}{\sqrt{\left(x^2+(y-y_d)^2+\left(z+\frac{H}{2}\right)^2\right)}}+1\right)\mathrm{d}y_d + \\ &+\frac{1}{4\pi V_\infty}\int_{-b_w}^{+b_w} m_2\left(y_d\right)\frac{x\left(z+\frac{H}{2}\right)^2}{\left((y-y_d)^2+\left(z+\frac{H}{2}\right)^2\right)\left(x^2+(y-y_d)^2+\left(z+\frac{H}{2}\right)^2\right)^{\frac{3}{2}}}\mathrm{d}y_d. \end{aligned} \tag{5.31}$$

Calculating the derivatives on the wings[9] at $x = x_0$ and *isolating the singular term*[10]:

$$\begin{aligned}
\left[\frac{\partial \phi_1}{\partial z}\right]_{\substack{z=z_1\\x=x_0}} &= -\frac{1}{4\pi V_\infty} \int_{-b_w}^{+b_w} \frac{-m_1(y_d)}{\left(x_0+\sqrt{\left(x_0^2+(y-y_d)^2\right)}\right)\sqrt{\left(x_0^2+(y-y_d)^2\right)}}\,\mathrm{d}y_d + \\
&\quad -\frac{1}{4\pi V_\infty} \oint_{-b_w}^{+b_w} \frac{2m_1(y_d)}{(y-y_d)^2}\,\mathrm{d}y_d, \\
\left[\frac{\partial \phi_2}{\partial z}\right]_{\substack{z=z_1\\x=x_0}} &= -\frac{1}{4\pi V_\infty} \int_{-b_w}^{+b_w} m_2\left(y_d\right) \frac{(y-y_d)^2-H^2}{\left((y-y_d)^2+H^2\right)^2}\left(\frac{x_0}{\sqrt{\left(x_0^2+(y-y_d)^2+H^2\right)}}+1\right)\mathrm{d}y_d + \\
&\quad +\frac{1}{4\pi V_\infty} \int_{-b_w}^{+b_w} m_2\left(y_d\right) \frac{x_0 H^2}{\left((y-y_d)^2+H^2\right)\left(x_0^2+(y-y_d)^2+H^2\right)^{\frac{3}{2}}}\,\mathrm{d}y_d, \\
\left[\frac{\partial \phi_2}{\partial z}\right]_{\substack{z=z_2\\x=x_0}} &= -\frac{1}{4\pi V_\infty} \int_{-b_w}^{+b_w} \frac{-m_2(y_d)}{\left(x_0+\sqrt{\left(x_0^2+(y-y_d)^2\right)}\right)\sqrt{\left(x_0^2+(y-y_d)^2\right)}}\,\mathrm{d}y_d + \\
&\quad -\frac{1}{4\pi V_\infty} \oint_{-b_w}^{+b_w} \frac{2m_2(y_d)}{(y-y_d)^2}\,\mathrm{d}y_d \\
\left[\frac{\partial \phi_1}{\partial z}\right]_{\substack{z=z_2\\x=x_0}} &= -\frac{1}{4\pi V_\infty} \int_{-b_w}^{+b_w} m_1\left(y_d\right) \frac{(y-y_d)^2-H^2}{\left((y-y_d)^2+H^2\right)^2}\left(\frac{x_0}{\sqrt{\left(x_0^2+(y-y_d)^2+H^2\right)}}+1\right)\mathrm{d}y_d + \\
&\quad +\frac{1}{4\pi V_\infty} \int_{-b_w}^{+b_w} m_1\left(y_d\right) \frac{x_0 H^2}{\left((y-y_d)^2+H^2\right)\left(x_0^2+(y-y_d)^2+H^2\right)^{\frac{3}{2}}}\,\mathrm{d}y_d.
\end{aligned} \tag{5.32}$$

Substituting these quantities into equation (5.29), the integral equations containing the unknown m_1 and m_2 representing the doublet distributions on wings 1 and 2 are obtained. It should be noticed that there is no condition that imposes $m_1 = m_2$, since the wings can have different aerodynamic properties (for example, the twist); hence, in general, $m_1 \neq m_2$. It is important to see that the integral equations (5.29)

[9] That means $z = +\frac{H}{2}$ over the wing 1, and $z = -\frac{H}{2}$ over the wing 2.

[10] To do that, the following identity is used:

$$\frac{1}{(y-y_d)^2}\left(\frac{x_0}{\sqrt{\left(x_0^2+(y-y_d)^2\right)}}+1\right) = \frac{-1}{\left(x_0+\sqrt{\left(x_0^2+(y-y_d)^2\right)}\right)\sqrt{\left(x_0^2+(y-y_d)^2\right)}}+\frac{2}{(y-y_d)^2}.$$

can be used to solve the *direct problem*: what are the unknown doublet distributions m_1 and m_2 over the wings 1 and 2 under the velocity V_∞ and with the twist laws $\alpha(y,z_1)$ and $\alpha(y,z_2)$? Applying the numerical methods explained in chapter 2, it is possible to solve the integral equations and find m_1 and m_2. The direct problem will not be solved here.

5.3.2 Normalwash

The expression of the induced drag has been seen. The *normalwash* u_n is involved in its formula. Now the expression of the induced velocity over the wings will be determined. From the definition of small perturbation velocity potential, for the wing 1, the induced velocity has the expression

$$u_{n1} = \left[\frac{\partial \phi_1}{\partial z}\right]_{\substack{z=z_1 \\ x=0}} + \left[\frac{\partial \phi_2}{\partial z}\right]_{\substack{z=z_1 \\ x=0}} . \tag{5.33}$$

Using the previous expressions, the normalwash for the wing 1 is determined:

$$u_{n1}(y) = -\frac{1}{4\pi V_\infty} \oint_{-b_w}^{+b_w} \frac{m_1(y_d)}{(y-y_d)^2}\,\mathrm{d}y_d - \frac{1}{4\pi V_\infty} \int_{-b_w}^{+b_w} m_2(y_d)\,\frac{(y-y_d)^2 - H^2}{\left((y-y_d)^2 + H^2\right)^2}\,\mathrm{d}y_{d1}. \tag{5.34}$$

Similarly for the wing 2:

$$u_{n2}(y) = -\frac{1}{4\pi V_\infty} \oint_{-b_w}^{+b_w} \frac{m_2(y_d)}{(y-y_d)^2}\,\mathrm{d}y_d - \frac{1}{4\pi V_\infty} \int_{-b_w}^{+b_w} m_1(y_d)\,\frac{(y-y_d)^2 - H^2}{\left((y-y_d)^2 + H^2\right)^2}\,\mathrm{d}y_d. \tag{5.35}$$

Observation 23 The normalwash can also be determined geometrically. Obviously, the final expressions must be the same as the expressions found in (5.34) and (5.35). Supposing that the circulation distributions on the wings are known, and using the Biot-Savart law, the normalwash is computed geometrically in appendix B.

5.3.3 Induced Drag

Consider the upper wing. The doublets have axes directed along $+z$. Hence, the aerodynamic force is

$$F_1(y_d) = -\rho_\infty m_1(y_d)\,. \tag{5.36}$$

The induced incidence on the wing 1 is

$$\alpha_{i1}\left(y_d\right) = -\frac{\left[u_{n1}\left(y_d\right)\right]_{x=0}}{V_\infty}, \tag{5.37}$$

while the induced drag on the same wing is

$$D_{i1}\left(y_d\right) = \int_{-b_w}^{+b_w} F\left(y_d\right) \tan\left(\alpha_{1i}\left(y_d\right)\right) \mathrm{d}y_d \simeq \int_{-b_w}^{+b_w} F_1\left(y_d\right) \alpha_{1i}\left(y_d\right) \mathrm{d}y_d. \tag{5.38}$$

Using the previous expressions:

$$D_{i1} = -\frac{\rho_\infty}{4\pi V_\infty^2} \int_{-b_w}^{+b_w} m_1\left(y_d\right) \left(\fint_{-b_w}^{+b_w} \frac{m_1\left(y\right)}{\left(y-y_d\right)^2} \mathrm{d}y + \int_{-b_w}^{+b_w} m_2\left(y\right) \frac{\left(y-y_d\right)^2 - H^2}{\left(\left(y-y_d\right)^2 + H^2\right)^2} \mathrm{d}y \right) \mathrm{d}y_d. \tag{5.39}$$

Repeating the same procedure for the wing 2:

$$D_{i2} = -\frac{\rho_\infty}{4\pi V_\infty^2} \int_{-b_w}^{+b_w} m_2\left(y_d\right) \left(\fint_{-b_w}^{+b_w} \frac{m_2\left(y\right)}{\left(y-y_d\right)^2} \mathrm{d}y + \int_{-b_w}^{+b_w} m_1\left(y\right) \frac{\left(y-y_d\right)^2 - H^2}{\left(\left(y-y_d\right)^2 + H^2\right)^2} \mathrm{d}y \right) \mathrm{d}y_d. \tag{5.40}$$

Obviously, the total induced drag is the summation of the contributes of the wings 1 and 2; thus,

$$\begin{aligned} D_i = &-\tfrac{\rho_\infty}{4\pi V_\infty^2} \int_{-b_w}^{+b_w} \fint_{-b_w}^{+b_w} \left(\tfrac{m_1(y_d) m_1(y)}{\left(y-y_d\right)^2} + \tfrac{\left[m_1(y_d) m_2(y) + m_1(y) m_2(y_d)\right]\left(\left(y-y_d\right)^2 - H^2\right)}{\left(\left(y-y_d\right)^2 + H^2\right)^2} \right) \mathrm{d}y \, \mathrm{d}y_d \\ &-\tfrac{\rho}{4\pi V_\infty^2} \int_{-b_w}^{+b_w} \fint_{-b_w}^{+b_w} \left(\tfrac{m_2(y) m_2(y_d)}{\left(y-y_d\right)^2} \mathrm{d}y \right) \mathrm{d}y_d. \end{aligned} \tag{5.41}$$

5.3.4 Total Lifting Force

It is very simple to calculate the total lifting force. Recalling the expressions of the aerodynamic forces, the expression for total lifting force can be written as

$$\begin{aligned} L = L_1 + L_2 &= \int_{-b_w}^{+b_w} F_1\left(y_d\right) \, \mathrm{d}y_d + \int_{-b_w}^{+b_w} F_2\left(y_d\right) \, \mathrm{d}y_d = \\ &= -\rho_\infty \int_{-b_w}^{+b_w} m_1\left(y_d\right) \, \mathrm{d}y_d - \rho_\infty \int_{-b_w}^{+b_w} m_2\left(y_d\right) \, \mathrm{d}y_d. \end{aligned} \tag{5.42}$$

5.3.5 Derivation of the Euler-Lagrange Equations

The purpose is *to minimize the induced drag under the condition of fixed total lifting force and wing span.* To achieve this goal, the methods explained in chapter 2 have to be used. The functional is reported in (5.41). Setting:

$$\begin{aligned} m_1(\cdot) &= (m_1)_{\text{opt}}(\cdot) + \sigma\delta_1(\cdot) \qquad \sigma \in (-1,1), \\ m_2(\cdot) &= (m_2)_{\text{opt}}(\cdot) + \sigma\delta_2(\cdot) \qquad \sigma \in (-1,1), \end{aligned} \tag{5.43}$$

the functional becomes

$$\begin{aligned} &J\left((m_1)_{\text{opt}}(\cdot) + \sigma\delta_1(\cdot), (m_2)_{\text{opt}}(\cdot) + \sigma\delta_2(\cdot)\right) = \\ &= -\frac{\rho_\infty}{4\pi V_\infty^2} \int_{-b_w}^{+b_w} \!\!\!\!\!\!\diagup\!\!\!\!\!\!\int_{-b_w}^{+b_w} \frac{[A_1(y_d)][A_1(y)]}{(y-y_d)^2}\,\mathrm{d}y\,\mathrm{d}y_d + \\ &\quad -\frac{\rho_\infty}{4\pi V_\infty^2} \int_{-b_w}^{+b_w} \int_{-b_w}^{+b_w} \frac{[A_1(y_d)][A_2(y)]+[A_1(y)][A_2(y_d)]}{\left((y-y_d)^2+H^2\right)^2}\left((y-y_d)^2 - H^2\right)\mathrm{d}y\,\mathrm{d}y_d + \\ &\quad -\frac{\rho_\infty}{4\pi V_\infty^2} \int_{-b_w}^{+b_w} \!\!\!\!\!\!\diagup\!\!\!\!\!\!\int_{-b_w}^{+b_w} \frac{[A_2(y_d)][A_2(y)]}{(y-y_d)^2}\,\mathrm{d}y\,\mathrm{d}y_d, \end{aligned} \tag{5.44}$$

where

$$\begin{aligned} A_1(y_d) &= (m_1)_{\text{opt}}(y_d) + \sigma\delta_1(y_d), \\ A_1(y) &= (m_1)_{\text{opt}}(y) + \sigma\delta_1(y), \\ A_2(y_d) &= (m_2)_{\text{opt}}(y_d) + \sigma\delta_2(y_d), \\ A_2(y) &= (m_2)_{\text{opt}}(y) + \sigma\delta_2(y). \end{aligned} \tag{5.45}$$

Following the procedure used in chapter 2 (see appendix C for details), the Euler-Lagrange integral equations are obtained:

$$\boxed{-\frac{\rho_\infty}{2\pi V_\infty^2} \int_{-b_w}^{+b_w} \!\!\!\!\!\!\diagup\!\!\!\!\!\!\int \frac{(m_1)_{\text{opt}}(y)}{(y-y_d)^2}\,\mathrm{d}y - \frac{\rho_\infty}{2\pi V_\infty^2} \int_{-b_w}^{+b_w} \frac{(m_2)_{\text{opt}}(y)\left((y-y_d)^2-H^2\right)}{\left((y-y_d)^2+H^2\right)^2}\,\mathrm{d}y + \rho_\infty\lambda = 0.} \tag{5.46}$$

$$\boxed{-\frac{\rho_\infty}{2\pi V_\infty^2} \int_{-b_w}^{+b_w} \!\!\!\!\!\!\diagup\!\!\!\!\!\!\int \frac{(m_2)_{\text{opt}}(y)}{(y-y_d)^2}\,\mathrm{d}y - \frac{\rho_\infty}{2\pi V_\infty^2} \int_{-b_w}^{+b_w} \frac{(m_1)_{\text{opt}}(y)\left((y-y_d)^2-H^2\right)}{\left((y-y_d)^2+H^2\right)^2}\,\mathrm{d}y + \rho_\infty\lambda = 0.} \tag{5.47}$$

It can be observed that:

- One equation is identical to the other if the subscripts 1 and 2 are switched. This implies that, *under optimal conditions, the distributions on the wings must be the same*: $(m_1)_{\text{opt}} = (m_2)_{\text{opt}}$. This result makes perfect sense, since, in a physical point of view, there is no reasonable motivation to suppose $(m_1)_{\text{opt}} \neq (m_2)_{\text{opt}}$.

- *The induced velocity over the wings must be constant* [11].
- Munk's Minimum Induced Drag Theorem is satisfied, and it can be observed that $\vartheta = 0 = \text{const}_1$ and $u_n = \text{const}_2$ in both wings.

It has been demonstrated that the doublet (or circulation) distributions over the wings are the same. Hence, the equations can be summarized as[12]:

$$(D_i)_{\text{opt}} = -\frac{\rho_\infty}{2\pi V_\infty^2} \int_{-b_w}^{+b_w} (m)_{\text{opt}}(y_d) \left(\oint_{-b_w}^{+b_w} \frac{(m)_{\text{opt}}(y)}{(y-y_d)^2}\,\mathrm{d}y + \int_{-b_w}^{+b_w} \frac{(m)_{\text{opt}}(y)\left((y-y_d)^2-H^2\right)}{\left((y-y_d)^2+H^2\right)^2}\,\mathrm{d}y \right) \mathrm{d}y_d, \tag{5.48}$$

$$\overline{L} = -2\rho_\infty \int_{-b_w}^{+b_w} (m)_{\text{opt}}(y)\,\mathrm{d}y, \tag{5.49}$$

$$-\frac{\rho_\infty}{2\pi V_\infty^2} \oint_{-b_w}^{+b_w} \frac{(m)_{\text{opt}}(y)}{(y-y_d)^2}\,\mathrm{d}y - \frac{\rho_\infty}{2\pi V_\infty^2} \int_{-b_w}^{+b_w} \frac{(m)_{\text{opt}}(y)\left((y-y_d)^2-H^2\right)}{\left((y-y_d)^2+H^2\right)^2}\,\mathrm{d}y + \rho_\infty \lambda = 0, \tag{5.50}$$

where the last expression is the Euler-Lagrange equation. Notice that it no longer contains two equations.

5.3.6 Optimal Doublet Distribution: $H \to 0$ Case

When $H \to 0$, the equations become:

$$(D_i)_{\text{opt}} = -\frac{\rho_\infty}{\pi V_\infty^2} \int_{-b_w}^{+b_w} (m)_{\text{opt}}(y_d) \left(\oint_{-b_w}^{+b_w} \frac{(m)_{\text{opt}}(y)}{(y-y_d)^2}\,\mathrm{d}y \right) \mathrm{d}y_d, \tag{5.51}$$

$$\overline{L} = -2\rho_\infty \int_{-b_w}^{+b_w} (m)_{\text{opt}}(y)\,\mathrm{d}y, \tag{5.52}$$

$$-\frac{\rho_\infty}{\pi V_\infty^2} \oint_{-b_w}^{+b_w} \frac{(m)_{\text{opt}}(y)}{(y-y_d)^2}\,\mathrm{d}y + \rho_\infty \lambda = 0. \tag{5.53}$$

It will be demonstrated now that *under this particular condition ($H \to 0$ case) the optimal distribution is elliptical and the induced drag is the same as an optimally*

[11] See the expressions of u_{n1} and u_{n2} and compare with equations (5.46) and (5.47).

[12] It has already been demonstrated that, under optimal condition, the distribution over the wing 1 is equal to the distribution over the wing 2. Therefore, the optimal doublet distribution along wing 1 *or* wing 2 is indifferently indicated by $(m)_{\text{opt}}$.

loaded classical wing with the same total lift and wing span. Consider an elliptical doublet distribution:

$$\frac{(m)_{\text{opt}}(y)}{\overline{m}} = \sqrt{1 - \frac{y^2}{b_w^2}}. \tag{5.54}$$

Using the same procedure seen in the classical cantilever wing and operating the same techniques to solve the integrals, yields:

$$\overline{m} = -\frac{\overline{L}}{\rho_\infty \pi b_w}, \tag{5.55}$$

$$(D_i)_{opt} = \frac{\rho_\infty}{\pi V_\infty^2}\left(\frac{\overline{L}}{\rho_\infty \pi b_w}\right)^2 \frac{\pi^2}{2} = \frac{\overline{L}^2}{2\pi\rho_\infty b_w^2 V_\infty^2}. \tag{5.56}$$

Thus, the same induced drag as an optimally loaded cantilever wing has been found.

5.3.7 Optimal Doublet Distribution: $H \to \infty$ Case

When $H \to \infty$, the equations become:

$$(D_i)_{\text{opt}} = -\frac{\rho_\infty}{2\pi V_\infty^2} \int_{-b_w}^{+b_w} (m)_{\text{opt}}(y_d) \left(\oint_{-b_w}^{+b_w} \frac{(m)_{\text{opt}}(y)}{(y-y_d)^2}\, \mathrm{d}y \right) \mathrm{d}y_d, \tag{5.57}$$

$$\overline{L} = -2\rho_\infty \int_{-b_w}^{+b_w} (m)_{\text{opt}}(y)\, \mathrm{d}y, \tag{5.58}$$

$$-\frac{\rho_\infty}{2\pi V_\infty^2} \oint_{-b_w}^{+b_w} \frac{(m)_{\text{opt}}(y)}{(y-y_d)^2}\, \mathrm{d}y + \rho_\infty \lambda = 0. \tag{5.59}$$

It will be demonstrated now that *under this particular condition ($H \to \infty$ case) the optimal distribution is elliptical and the induced drag is $\frac{1}{2}$ of an optimally loaded classical wing with the same total lift and wing span.* Consider an elliptical doublet distribution:

$$\frac{(m)_{\text{opt}}(y)}{\overline{m}} = \sqrt{1 - \frac{y^2}{b_w^2}}. \tag{5.60}$$

Using the same procedure seen in the classical cantilever wing and operating the same techniques to calculate the integrals, produces the following results:

$$\overline{m} = -\frac{\overline{L}}{\rho_\infty \pi b_w}, \tag{5.61}$$

$$(D_i)_{opt} = \frac{\overline{L}^2}{4\pi\rho_\infty b_w^2 V_\infty^2}. \tag{5.62}$$

Thus, $\frac{1}{2}$ the induced drag of an optimally loaded cantilever wing has been found.

Observation 24 This result can be understood in a different way. Consider a biplane with an elliptical doublet distribution *in both wings*. Suppose that the wings have the same total load ($L_1 = L_2 = \frac{L}{2}$) and that their distance from each other is infinite. Now, because the distance between the wings is infinite, the wings can be considered as *two identical and independent classical wings*. Therefore, the induced drag can be considered only as a sum of two contributions without interaction:

$$D_i = D_{i1} + D_{i2}. \tag{5.63}$$

But in a classical wing it is known that the induced drag is proportional to the square of the lift[13]:

$$\begin{aligned} D_{i1} &= kL_1^2 = k\left(\tfrac{L}{2}\right)^2, \\ D_{i2} &= kL_2^2 = k\left(\tfrac{L}{2}\right)^2. \end{aligned} \tag{5.64}$$

Thus,

$$D_i = D_{i1} + D_{i2} = 2k\left(\frac{L}{2}\right)^2 = k\frac{L^2}{2}. \tag{5.65}$$

A classical wing with the same load has the induced drag

$$D_i = kL^2. \tag{5.66}$$

Comparing the last two expressions, it is clear that the induced drag in a biplane, with $H \to \infty$ and under optimal conditions, is $\frac{1}{2}$ of the induced drag in an optimally loaded classical wing with the same wing span.

5.3.8 Optimal Doublet Distribution: $H \neq 0,\infty$ Case

Is the optimal distribution elliptical? In order to answer the question, it is useful to change the variables and manipulate the Euler-Lagrange equation. Setting $s = \frac{y}{b_w} \Rightarrow y = sb_w$, $t = \frac{y_d}{b_w} \Rightarrow y_d = tb_w$ and $h = \frac{H}{b_w}$, the Euler-Lagrange equation becomes:

$$\frac{1}{2\pi b_w V_\infty^2}\int_{-1}^{+1}\frac{(m)_{\text{opt}}(s)\left((t-s)^2-h^2\right)}{\left((t-s)^2+h^2\right)^2}\,\mathrm{d}s + \frac{1}{2\pi b_w V_\infty^2}\fint_{-1}^{+1}\frac{(m)_{\text{opt}}(s)}{(t-s)^2}\,\mathrm{d}s - \lambda = 0. \tag{5.67}$$

Suppose that the optimal distribution is elliptical. Then, the distribution $(m)_{\text{opt}}$ *should be*:

$$(m)_{\text{opt}}(s) = \overline{m}\sqrt{1-s^2}. \tag{5.68}$$

[13]The constant k must be the same because the wings are exactly identical and the lift distribution is the same.

Substituting this expression into equation (5.67), equation (5.67) has to be satisfied. Now consider the Lagrange multiplier: it is constant. The Hadamard finite-part integral is constant as well, because the distribution is elliptical[14]. It is evident that equation (5.67) can be satisfied under elliptical distribution *only* if

$$\int_{-1}^{+1} \frac{(m)_{\text{opt}}(s)\left((t-s)^2-h^2\right)}{\left((t-s)^2+h^2\right)^2}\,\mathrm{d}s = \int_{-1}^{+1} \frac{\overline{m}\sqrt{1-s^2}\left((t-s)^2-h^2\right)}{\left((t-s)^2+h^2\right)^2}\,\mathrm{d}s = \text{constant}. \tag{5.69}$$

In other words, for a fixed value of the parameter h, the integral *must not be dependent on the value of the variable* t. For example, consider $h = \overline{m} = 1$. It is easy to see that the integral *is not constant* with t. For example, using $t = 0.2$ or $t = -0.5$, yields different values[15]:

$$\begin{aligned} &\int_{-1}^{+1} \frac{\sqrt{1-s^2}\left((0.2-s)^2-1\right)}{\left((0.2-s)^2+1\right)^2}\,\mathrm{d}s = -0.8869751615 \\ &\int_{-1}^{+1} \frac{\sqrt{1-s^2}\left((-0.5-s)^2-1\right)}{\left((-0.5-s)^2+1\right)^2}\,\mathrm{d}s = -0.7188925775 \neq -0.8869751615. \end{aligned} \tag{5.70}$$

Thus, it has been demonstrated that, *under optimal condition, the doublet distribution is not elliptical if the distance* H *between the wings is finite (not zero).* This will be further demonstrated in the next section.

5.3.9 Numerical Evaluations

In previous sections the optimization problem in a theoretical point of view was analyzed. Here, a few numerical solutions to the optimization problem are analyzed. The Euler-Lagrange equation is solved using the collocation method and guessing the initial value of the Lagrange multiplier λ (see chapter 2).
Consider a biplane with the following parameters[16]: $C_L = 1.0$, $\frac{b_w}{l} = 12$. The effect of the parameter $\frac{H}{l}$ is now discussed. The following cases are analyzed:

- *Case 1*
  $H \to 0$ case. It is studied considering $Hl = 10^{-4}$
- *Case 2*
  $H \to \infty$ case. It is studied considering $Hl = 10^{+4}$

[14] In a classical wing under optimal conditions, the Hadamard finite-part integral is constant, as it has been seen. For a biplane with elliptical distribution, the Hadamard finite-part integral has the same formal expression as the classical wing case; therefore, it has to be constant as well.
[15] The integrals have been calculated using MAPLE.
[16] The reference surface for the non-dimensional coefficients of lift and induced drag is $4b_w l$.

- *Case 3*
  $H \neq 0,\infty$ case. It is studied considering $Hl = 6$

The optimal non-dimensional doublet distribution along a wing[17] is plotted against the elliptical distribution[18] in all three cases (see figures 5.4, 5.5 and 5.6). In the numerical solution of the Euler-Lagrange equation, 20 collocation points are used. It

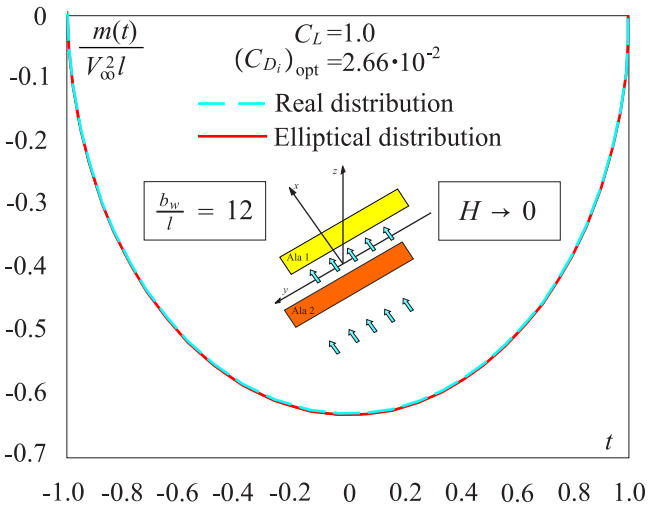

Figure 5.4. Optimal doublet distribution when $H \to 0$. Comparison with the elliptical distribution.

is clear that the previous theoretical considerations are correct: *in the general case, the optimal doublet (or circulation) distribution along a wing in a biplane is not elliptical. The optimal distribution is elliptical only when the distance between the wings is near zero or infinity.* Comparison of figures 5.4, 5.5 and 5.6, shows that the least induced drag in a biplane occurs when the wings are indefinitely distant and, in that case, its value is 1/2 the induced drag of an optimally loaded classical wing with the same wing span and total lift. The behavior of the induced drag is more clear when figures 5.7 and 5.8 are analyzed. In particular, the optimal induced drag starts from the same value as the classical wing and it decreases as H increases[19]. From figure 5.8[20], it is clear that, when $H/b_w = 0.4$, the induced drag coefficient is

[17]Remember that, in the biplane, the optimal distribution is the same over the two wings. Therefore, it is not important to specify the wing in which the distribution is considered.

[18]Notice that if the total lift is fixed and the distribution is elliptical, the amplitude of the load (the semi-axis of the ellipse) does not change if the parameter H is changed. For that reason, in all three figures 5.4, 5.5 and 5.6, the elliptical distribution is always the same even if the distance H changes.

[19]This is a general result for non-planar wings.

[20]For that analysis, $b_w = 10$, $l = 1$ and $C_L = 1.0$ have been considered.

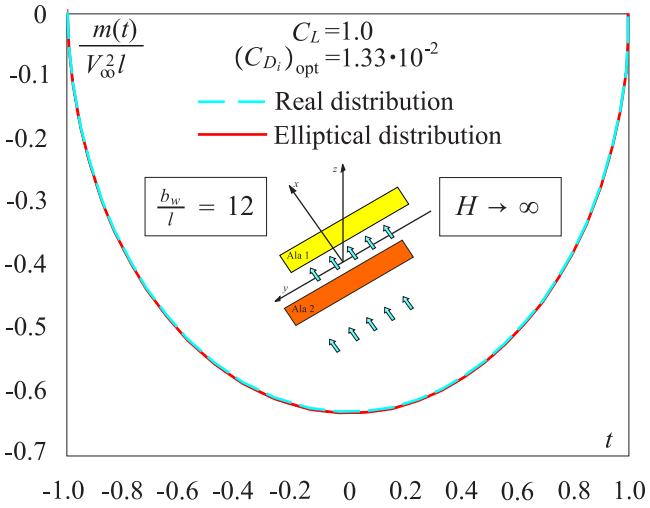

Figure 5.5. Optimal doublet distribution when $H \to \infty$. Comparison with the elliptical distribution.

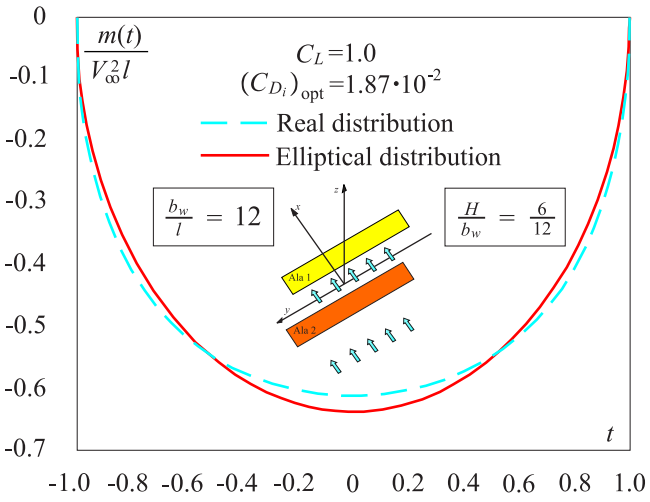

Figure 5.6. Optimal doublet distribution when $H \neq 0,\infty$. Comparison with the elliptical distribution.

1.36 times smaller than the value obtained for $H/b_w = 0.0$ (this is the same as the optimally loaded classical wing with the same wing span and total lift). This result has been found also by Kroo [14].

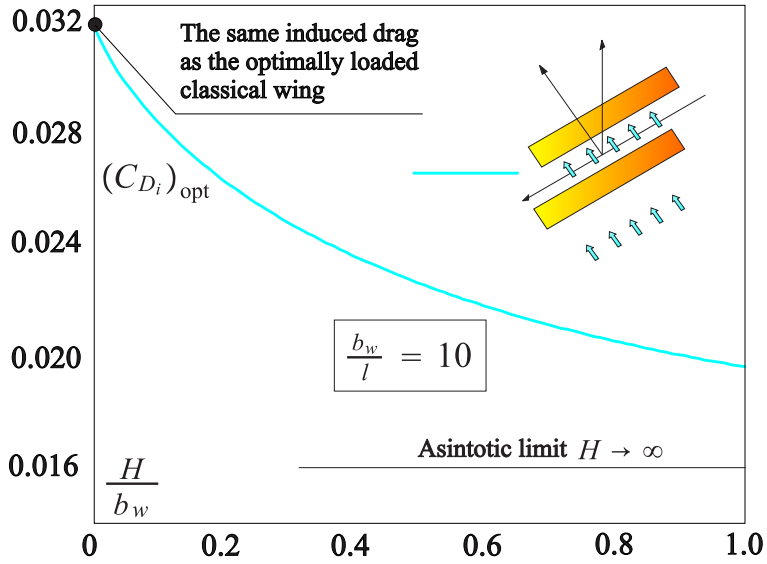

Figure 5.7. Optimal induced drag coefficient versus H/b_w.

H/b_w	100 $(C_{D_i})_{\text{opt}}$	H/b_w	100 $(C_{D_i})_{\text{opt}}$
0.00	3.18	0.50	2.25
0.01	3.11	0.55	2.21
0.05	2.95	0.60	2.17
0.10	2.81	0.65	2.13
0.15	2.70	0.70	2.10
0.20	2.61	0.75	2.07
0.25	2.53	0.80	2.04
0.30	2.46	0.85	2.02
0.35	2.40	0.90	2.00
0.40	2.34	0.95	1.97
0.45	2.29	1.00	1.95

Figure 5.8. Optimal induced drag coefficient versus H/b_w.

5.4 Conclusion

The absolutely general minimization procedure has been used in the classical cantilever wing and in a biplane. The well known results of optimum, under elliptical distribution, for the classical wing have been found, and it has been demonstrated that, for a biplane under optimum conditions, the wings have the

same doublet distribution, which *in general*, is not elliptical, as reported in some papers. In subsequent chapters, closed wing systems and other non-planar wings will be analyzed, and it will be shown that the procedure used here is *general* and valid under the used hypotheses.

Nomenclature

α	angle of attack
α_i	induced angle of attack
ρ	fluid density
ϕ	small perturbation velocity potential
Ψ	small perturbation acceleration potential
Γ	vorticity
γ_x	distributed trailing vorticity
u_n	normalwash
$2b_w$	wing span
ϑ	angle of inclination of the lifting element
l	chord
H	distance between wing 1 and 2 (biplane case)
m	doublet distribution
$(m)_{\text{opt}}$	doublet distribution which minimizes the induced drag
$\overline{m}$	doublet distribution constant
L	lift
D_i	induced drag
C_L	coefficient of lift
C_{D_i}	coefficient of induced drag
F	aerodynamic force
$\overline{L}$	fixed value of the lifting force
$\overline{C}_L$	fixed value of the coefficient of lift
$(C_{D_i})_{\text{ref}}$	coefficient of minimum induced drag in a cantilever wing
$(C_{D_i})_{\text{opt}}$	coefficient of minimum induced drag
$(D_i)_{\text{opt}}$	minimum induced drag
$\delta_1(t), \delta_2(t)$	arbitrary functions
σ	parameter with the property $\sigma \in (-1, +1)$
λ	Lagrange multiplier
u, v, t, s	auxiliary variables
h	$\frac{H}{b_w}$
V_∞	velocity (freestream conditions)
$\fint$	Hadamard finite-part integral

Subscripts

∞	freestream conditions
1	wing 1
2	wing 2

Chapter 6

Closed Wing Systems: Annular Wings. Analytical Formulation

6.1 Introduction

Using the analytical procedure developed and tested in previous chapters, the following closed wing systems will be analyzed:

- *System 1*
  Circular annular wing with the wing span representing its *diameter*[1].
- *System 2*
  Elliptical annular wing with the wing span representing its *major* axis[2].
- *System 3*
  Elliptical annular wing with the wing span representing its *minor* axis[3].

For each wing, the following quantities will be found:

- *Quantity 1*
  The twist expressed as a function, which will be an integral equation, of the doublet distribution.
- *Quantity 2*
  The expression of the induced velocity (normalwash).
- *Quantity 3*
  The expression of the induced drag.

[1] In this case the radius is indicated by R_w; thus the wing span is $2R_w$.
[2] In this case the *major* semi-axis is indicated by b_w; thus the wing span is $2b_w$.
[3] In this case the *minor* semi-axis is indicated by b_w; thus the wing span is $2b_w$.

- *Quantity 4*
  The expression of the lift.

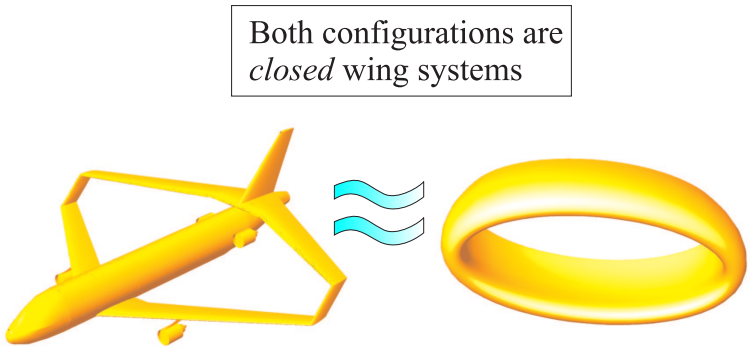

Figure 6.1. Joined wing and elliptical annular wing.

Why is studying the annular wing useful? Referring to figure 6.1, it is clear that both wings are closed wing systems and, therefore, they have similar aerodynamic properties. Thus, the results of the annular wings can not be considered exact for a joined wing, but, qualitatively, they can show some interesting properties of the closed wing systems and, as will be shown in chapter 9, they can have good correlations with the experimental results.

6.2 Circular Annular Wing with Wing Span Representing its Diameter

The geometry of the wing is displayed in figure 6.2. In figure 6.3, the reference coordinate system and a few useful notations are reported.

6.2.1 Coordinate Transformation

Because of the geometry of the wing, it is clear that a good coordinate system that is useful for this study is:

$$\begin{aligned} y &= R\cos\varphi \qquad 0 \leq \varphi \leq 2\pi, \\ z &= R\sin\varphi \qquad R > 0. \end{aligned} \tag{6.1}$$

Practically, each point which in the $y-z$ plane was characterized by the coordinates (y,z), is now characterized by the coordinates (R,φ). The circle representing the

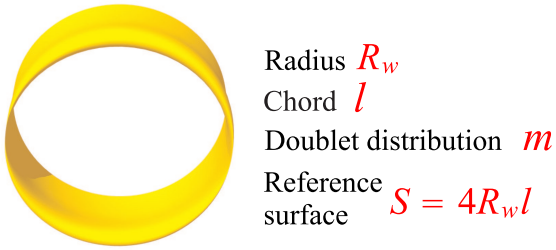

Figure 6.2. Circular annular wing.

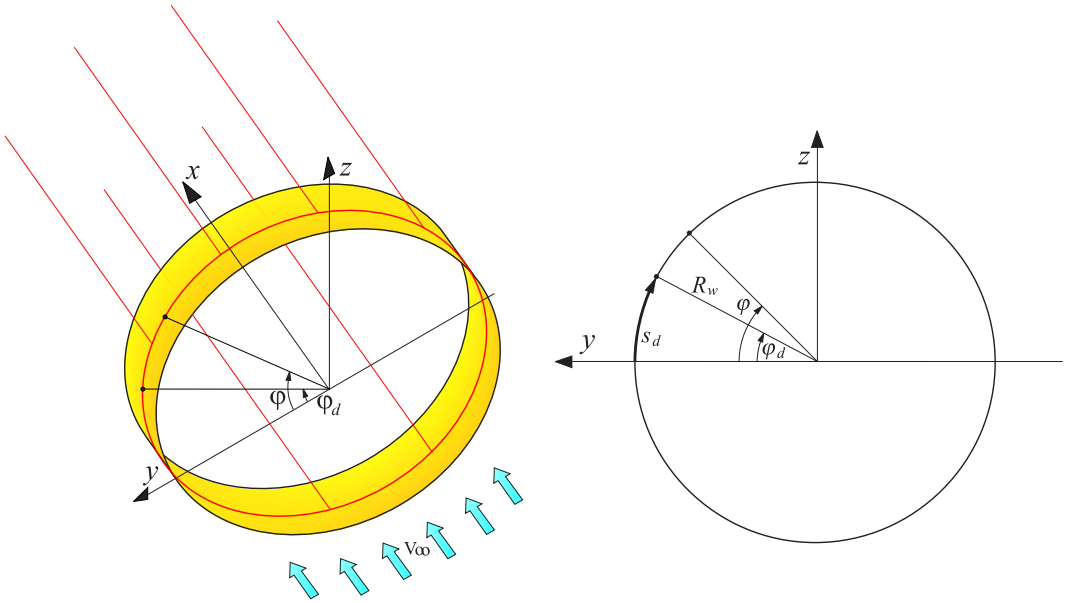

Figure 6.3. Circular annular wing: reference coordinate system.

wing has the equation:

$$\begin{aligned} y &= R_w \cos\varphi \qquad 0 \le \varphi \le 2\pi, \\ z &= R_w \sin\varphi \qquad R_w > 0, \end{aligned} \tag{6.2}$$

where R_w is the radius of the circular lifting line used to represent the wing. Differentiating equation (6.1):

$$\begin{aligned} \mathrm{d}y &= \cos\varphi\,\mathrm{d}R - R\sin\varphi\,\mathrm{d}\varphi, \\ \mathrm{d}z &= \sin\varphi\,\mathrm{d}R + R\cos\varphi\,\mathrm{d}\varphi. \end{aligned} \tag{6.3}$$

Squaring and summing:

$$\mathrm{d}s^2 = \mathrm{d}x^2 + \mathrm{d}y^2 = h_R^2 \mathrm{d}R^2 + h_\varphi^2 \mathrm{d}\varphi^2 = \mathrm{d}R^2 + R^2 \mathrm{d}\varphi^2. \tag{6.4}$$

Clearly, on the wing, $R = R_w = \text{constant} \Rightarrow \mathrm{d}R = 0$. Hence:

$$\mathrm{d}s_d = R_w \mathrm{d}\varphi_d. \tag{6.5}$$

6.2.2 Small Perturbation Acceleration Potential

In order to write the acceleration potential, the distance between a generic point $P(x,y,z)$ in space and a point $P_d(x_d,y_d,z_d)$ on the lifting line w (the point is characterized by $\varphi = \varphi_d$), where a generic doublet is positioned (see figure 6.4), is needed. The distance is:

$$D = \sqrt{(x - x_d)^2 + (y - y_d)^2 + (z - z_d)^2}. \tag{6.6}$$

The lifting line is contained in the $y-z$ plane, thus $x_d = 0$. Using the transformation

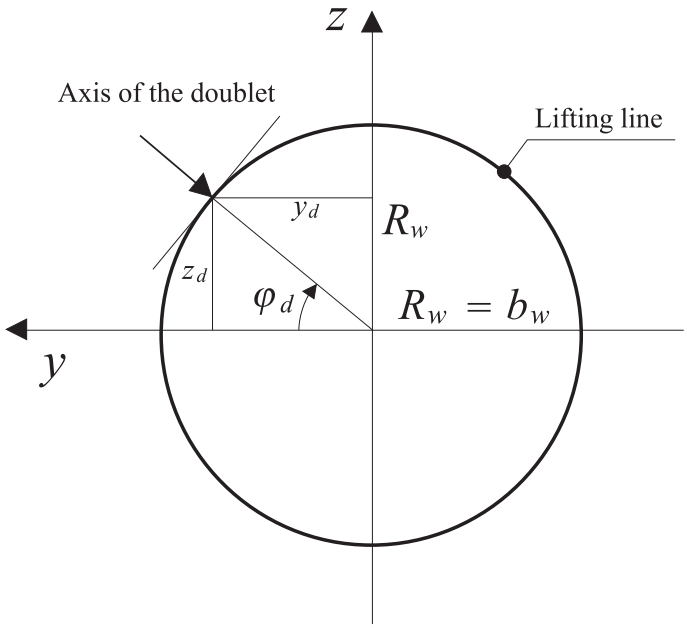

Figure 6.4. Positive direction of the doublet's axis.

seen above:

$$D = \sqrt{\left(R_w^2 X^2 + (R\cos\varphi - R_w\cos\varphi_d)^2 + (R\sin\varphi - R_w\sin\varphi_d)^2\right)}. \tag{6.7}$$

The previous relation can be written in a different way:

$$D = \left[\Delta\left(X,R,\varphi,R_w,\varphi_d\right)\right]^{\frac{1}{2}}, \tag{6.8}$$

where

$$\Delta = R_w^2 X^2 + R^2 + R_w^2 - 2RR_w \cos(\varphi - \varphi_d). \tag{6.9}$$

Using the generic formula (1.49), the small perturbation acceleration potential of a doublet $M = m(s_d)\,\mathrm{d}s_d$, positioned at a point on the lifting line characterized by $\varphi = \varphi_d$, is:

$$\Psi = -\frac{1}{4\pi} M \frac{n_{dx}(x - x_d) + n_{dy}(y - y_d) + n_{dz}(z - z_d)}{\left[(x - x_d)^2 + (y - y_d)^2 + (z - z_d)^2\right]^{\frac{3}{2}}}. \tag{6.10}$$

It is very easy to see that

$$\begin{aligned} n_{dx} &= 0, \\ n_{dy} &= -\cos\varphi_d, \\ n_{dz} &= -\sin\varphi_d. \end{aligned} \tag{6.11}$$

Hence, the expression of the small perturbation acceleration potential of a doublet is:

$$\mathrm{d}\Psi(X,R,\varphi,R_w) = -\frac{m(\varphi_d)}{4\pi} \frac{-\cos\varphi_d(R\cos\varphi - R_w\cos\varphi_d) - \sin\varphi_d(R\sin\varphi - R_w\sin\varphi_d)}{\Delta^{\frac{3}{2}}} R_w \mathrm{d}\varphi_d. \tag{6.12}$$

Integrating over the circle representing the lifting line yields:

$$\Psi = \frac{1}{4\pi R_w^2} \int_0^{2\pi} \frac{m(\varphi_d)\left(R\cos(\varphi - \varphi_d) - R_w\right)}{\left(X^2 + \frac{R^2}{R_w^2} + 1 - 2\frac{R}{R_w}\cos(\varphi - \varphi_d)\right)^{\frac{3}{2}}} \mathrm{d}\varphi_d \tag{6.13}$$

6.2.3 Small Perturbation Velocity Potential

In order to write the integral equation, Weissinger's condition has to be imposed. Therefore, the velocity perpendicular to the lifting line is needed, but, to get this velocity, the small perturbation velocity potential is required.
The relation that can be used to derive the velocity potential from the acceleration potential is:

$$\phi(x,R,\varphi,R_w) = \frac{1}{V_\infty} \int_{-\infty}^{x} \Psi(\xi,R,\varphi,R_w)\,\mathrm{d}\xi. \tag{6.14}$$

Changing the variables in order to use the non-dimensional variable X instead of x:

$$\xi = R_w\tau \Rightarrow \tau = \frac{\xi}{R_w} \Rightarrow d\tau = \frac{d\xi}{R_w}, \tag{6.15}$$

$$\phi(X,R,\varphi,R_w) = \frac{R_w}{V_\infty} \int_{-\infty}^{X} \Psi(\tau,R,\varphi,R_w)\,\mathrm{d}\tau. \tag{6.16}$$

Recalling the small perturbation acceleration potential:

$$\phi\left(X,R,\varphi,R_w\right)=\frac{R_w}{V_\infty}\int\limits_{-\infty}^{X}\left(\frac{1}{4\pi R_w^2}\int\limits_{0}^{2\pi}\frac{m\left(\varphi_d\right)\left(R\cos\left(\varphi-\varphi_d\right)-R_w\right)}{\left(\tau^2+\frac{R^2}{R_w^2}+1-2\frac{R}{R_w}\cos\left(\varphi-\varphi_d\right)\right)^{\frac{3}{2}}}\,\mathrm{d}\varphi_d\right)\mathrm{d}\tau. \tag{6.17}$$

Changing the order of integration:

$$\phi\left(X,R,\varphi,R_w\right)=\frac{1}{4\pi V_\infty R_w}\int\limits_{0}^{2\pi}\mathrm{d}\varphi_d\int\limits_{-\infty}^{X}\frac{m\left(\varphi_d\right)\left(R\cos\left(\varphi-\varphi_d\right)-R_w\right)}{\left(\tau^2+\frac{R^2}{R_w^2}+1-2\frac{R}{R_w}\cos\left(\varphi-\varphi_d\right)\right)^{\frac{3}{2}}}\,\mathrm{d}\tau. \tag{6.18}$$

The inner integral of expression (6.18) is of the type

$$\int\limits_{-\infty}^{X}\frac{f}{\left(\sqrt{\tau^2+g}\right)^3}\,\mathrm{d}\tau=f\frac{X+\sqrt{\left(X^2+g\right)}}{g\sqrt{\left(X^2+g\right)}}=\frac{f}{g}\left(\frac{X}{\sqrt{\left(X^2+g\right)}}+1\right), \tag{6.19}$$

where

$$\begin{aligned} f&=m\left(\varphi_d\right)\left(R\cos\left(\varphi-\varphi_d\right)-R_w\right),\\ g&=\tfrac{R^2}{R_w^2}+1-2\tfrac{R}{R_w}\cos\left(\varphi-\varphi_d\right). \end{aligned} \tag{6.20}$$

Substituting:

$$\begin{aligned} \phi\left(X,R,\varphi,R_w\right)=&\tfrac{1}{4\pi V_\infty R_w}\int\limits_{0}^{2\pi}\tfrac{m(\varphi_d)(R\cos(\varphi-\varphi_d)-R_w)}{\frac{R^2}{R_w^2}+1-2\frac{R}{R_w}\cos(\varphi-\varphi_d)}\cdot\\ &\cdot\left(\frac{X}{\sqrt{\left(X^2+\frac{R^2}{R_w^2}+1-2\frac{R}{R_w}\cos(\varphi-\varphi_d)\right)}}+1\right)\mathrm{d}\varphi_d. \end{aligned} \tag{6.21}$$

6.2.4 Imposition of Weissinger's Condition

Weissinger's condition consists of the WTC imposed in $X_0=\frac{l}{2R_w}$:

$$-\alpha\left(\varphi\right)=\frac{1}{V_\infty}\left(\frac{1}{h_R}\frac{\partial\phi\left(X,R,\varphi,R_w\right)}{\partial R}\right)_{X=X_0;\,R=R_w}. \tag{6.22}$$

The small perturbation velocity potential is written in the form

$$\begin{aligned} \phi\left(X,R,\varphi,R_w\right)\;=\;&\frac{1}{4\pi V_\infty R_w}\int\limits_{0}^{2\pi}m\left(\varphi_d\right)f_1\left(R,\varphi,\varphi_d,R_w\right)\cdot\\ &\cdot f_2\left(R,\varphi,\varphi_d,R_w\right)\cdot f_3\left(X,R,\varphi,\varphi_d,R_w\right)\mathrm{d}\varphi_d, \end{aligned} \tag{6.23}$$

where:

$$
\begin{aligned}
&f_1\left(R,\varphi,\varphi_d,R_w\right) = \left(R\cos\left(\varphi-\varphi_d\right)-R_w\right),\\
&f_2\left(R,\varphi,\varphi_d,R_w\right) = \frac{1}{\frac{R^2}{R_w^2}+1-2\frac{R}{R_w}\cos(\varphi-\varphi_d)} = \frac{1}{D(R,\varphi,\varphi_d,R_w)},\\
&f_3\left(X,R,\varphi,\varphi_d,R_w\right) = \frac{X}{\sqrt{\left(X^2+\frac{R^2}{R_w^2}+1-2\frac{R}{R_w}\cos(\varphi-\varphi_d)\right)}}+1 = \frac{X}{\sqrt{X^2+D(R,\varphi,\varphi_d,R_w)}}+1.
\end{aligned}
\tag{6.24}
$$

Therefore, to calculate the small perturbation velocity potential derivatives, the following quantity is required:

$$
\left[\frac{\partial}{\partial R}\left(f_1\cdot f_2\cdot f_3\right)\right]_{R=R_w;\,X=X_0} = \left[\frac{\partial f_1}{\partial R}\cdot f_2 f_3 + f_1\frac{\partial f_2}{\partial R}f_3 + f_1 f_2\frac{\partial f_3}{\partial R}\right]_{R=R_w;\,X=X_0}.
\tag{6.25}
$$

It is easy to show that

$$
\begin{aligned}
&[f_1]_{R=R_w} = -R_w\left(1-\cos\left(\varphi-\varphi_d\right)\right),\\
&[f_2]_{R=R_w} = \tfrac{1}{2}\frac{1}{1-\cos(\varphi-\varphi_d)},\\
&[f_3]_{R=R_w,X=X_0} = \frac{X_0}{\sqrt{\left(X_0^2+2(1-\cos(\varphi-\varphi_d))\right)}}+1,\\
&\left[\tfrac{\partial f_1}{\partial R}\right]_{R=R_w} = \cos\left(\varphi-\varphi_d\right),\\
&\left[\tfrac{\partial f_2}{\partial R}\right]_{R=R_w} = -\tfrac{1}{2R_w}\frac{1}{(1-\cos(\varphi-\varphi_d))},\\
&\left[\tfrac{\partial f_3}{\partial R}\right]_{R=R_w,X=X_0} = -\tfrac{1}{R_w}X_0\frac{(1-\cos(\varphi-\varphi_d))}{\left(\sqrt{\left(X_0^2+2(1-\cos(\varphi-\varphi_d))\right)}\right)^3},\\
&\left[\tfrac{\partial f_1}{\partial R}f_2 f_3\right]_{R=R_w,X=X_0} = \tfrac{1}{2}\frac{\cos(\varphi-\varphi_d)}{1-\cos(\varphi-\varphi_d)}\left(\frac{X_0}{\sqrt{\left(X_0^2+2(1-\cos(\varphi-\varphi_d))\right)}}+1\right),\\
&\left[f_1\tfrac{\partial f_2}{\partial R}f_3\right]_{R=R_w,X=X_0} = \tfrac{1}{2}\left(\frac{X_0}{\sqrt{\left(X_0^2+2(1-\cos(\varphi-\varphi_d))\right)}}+1\right),\\
&\left[f_1 f_2\tfrac{\partial f_3}{\partial R}\right]_{R=R_w,X=X_0} = \tfrac{1}{2}X_0\frac{(1-\cos(\varphi-\varphi_d))}{\left(\sqrt{\left(X_0^2+2(1-\cos(\varphi-\varphi_d))\right)}\right)^3}.
\end{aligned}
\tag{6.26}
$$

Notice that the term $\left[\frac{\partial f_1}{\partial R}f_2 f_3\right]_{R=R_w,X=X_0}$ is singular when $\varphi=\varphi_d$.

Treatment of the Singular Term

The singular term can be isolated through some algebraic manipulations. To achieve this, the definition

$$\left[\frac{\partial f_1}{\partial R} f_2 f_3\right]_{R=R_w, X=X_0} = \frac{\cos(\varphi - \varphi_d)\, F(X_0, \varphi, \varphi_d, R_w)}{1 - \cos(\varphi - \varphi_d)}, \tag{6.27}$$

where

$$F(X_0, \varphi, \varphi_d, R_w) = \frac{1}{2}\left(\frac{X_0}{\sqrt{(X_0^2 + 2(1 - \cos(\varphi - \varphi_d)))}} + 1\right), \tag{6.28}$$

is used. Summing and subtracting the term $F(X_0, \varphi, \varphi, R_w)$:

$$\begin{aligned}\frac{\cos(\varphi-\varphi_d)F(X_0,\varphi,\varphi_d,R_w)}{1-\cos(\varphi-\varphi_d)} &= \frac{\cos(\varphi-\varphi_d)(F(X_0,\varphi,\varphi_d,R_w)-F(X_0,\varphi,\varphi,R_w))}{1-\cos(\varphi-\varphi_d)} + \\ &+ \frac{\cos(\varphi-\varphi_d)F(X_0,\varphi,\varphi,R_w)}{1-\cos(\varphi-\varphi_d)},\end{aligned} \tag{6.29}$$

where

$$F(X_0, \varphi, \varphi, R_w) = \frac{1}{2}\left(\frac{X_0}{\sqrt{(X_0^2 + 2(1 - \cos(\varphi - \varphi)))}} + 1\right) = 1. \tag{6.30}$$

Simplifying equation (6.29):

$$\left[\frac{\partial f_1}{\partial R} f_2 f_3\right]_{R=R_w, X=X_0} = \cos(\varphi - \varphi_d)\, \frac{F(X_0,\varphi,\varphi_d,R_w) - F(X_0,\varphi,\varphi,R_w)}{1-\cos(\varphi-\varphi_d)} + \frac{\cos(\varphi-\varphi_d)}{(1-\cos(\varphi-\varphi_d))}. \tag{6.31}$$

But:

$$\frac{\cos(\varphi - \varphi_d)}{(1 - \cos(\varphi - \varphi_d))} = -1 + \frac{1}{(1 - \cos(\varphi - \varphi_d))}, \tag{6.32}$$

and

$$\begin{aligned}&F(X_0, \varphi, \varphi_d, R_w) - F(X_0, \varphi, \varphi, R_w) = \\ &= \frac{-(1-\cos(\varphi-\varphi_d))}{\left(X_0+\sqrt{\left(X_0^2+2(1-\cos(\varphi-\varphi_d))\right)}\right)\sqrt{\left(X_0^2+2(1-\cos(\varphi-\varphi_d))\right)}}.\end{aligned} \tag{6.33}$$

Thus, it can be concluded that

$$\begin{aligned}\left[\frac{\partial f_1}{\partial R} f_2 f_3\right]_{R=R_w, X=X_0} &= \frac{-\cos(\varphi-\varphi_d)}{\left(X_0+\sqrt{\left(X_0^2+2(1-\cos(\varphi-\varphi_d))\right)}\right)\sqrt{\left(X_0^2+2(1-\cos(\varphi-\varphi_d))\right)}} + \\ &-1 + \frac{1}{(1-\cos(\varphi-\varphi_d))}.\end{aligned} \tag{6.34}$$

Using this last relation, Weissinger's condition leads to introducing the integral equation reported in the next section.

6.2.5 Integral Equation with the Variables φ, φ_d

Using the relations found in the previous section, the integral equation containing the unknown doublet distribution m is:

$$-\alpha(\varphi) = \frac{1}{4\pi V_\infty^2 R_w} \oint_0^{2\pi} m(\varphi_d) \left[\frac{-\cos(\varphi-\varphi_d)}{\left(X_0+\sqrt{\left(X_0^2+2(1-\cos(\varphi-\varphi_d))\right)}\right)\sqrt{\left(X_0^2+2(1-\cos(\varphi-\varphi_d))\right)}} + \right.$$
$$-1+\boxed{\frac{1}{(1-\cos(\varphi-\varphi_d))}}+\frac{1}{2}\left(\frac{X_0}{\sqrt{\left(X_0^2+2(1-\cos(\varphi-\varphi_d))\right)}}+1\right)+$$
$$\left.+\frac{1}{2}X_0\frac{(1-\cos(\varphi-\varphi_d))}{\left(\sqrt{\left(X_0^2+2(1-\cos(\varphi-\varphi_d))\right)}\right)^3}\right]\mathrm{d}\varphi_d. \tag{6.35}$$

Notice that, since the equation contains a singular term (as shown inside the box), the integral has to be defined as Hadamard finite-part integral.

6.2.6 Integral Equation with the Variables t, s

For numerical approaches, it is useful to extend the integration domain between -1 and +1. Therefore, the following transformations are used:

$$\varphi_d = \pi(t+1), \varphi = \pi(s+1), \tag{6.36}$$

$$\begin{aligned} &\mathrm{d}\varphi_d = \pi \mathrm{d}t, \\ &\varphi - \varphi_d = \pi(s-t). \end{aligned} \tag{6.37}$$

Substituting into the integral equation obtained in the previous section:

$$-\alpha(s) = \frac{1}{4V_\infty^2 R_w} \oint_{-1}^{+1} m(t) \left[\frac{-\cos(\pi(t-s))}{\left(X_0+\sqrt{\left(X_0^2+2(1-\cos(\pi(t-s)))\right)}\right)\sqrt{\left(X_0^2+2(1-\cos(\pi(t-s)))\right)}} + \right.$$
$$-1+\boxed{\frac{1}{(1-\cos(\pi(t-s)))}}+\frac{1}{2}\left(\frac{X_0}{\sqrt{\left(X_0^2+2(1-\cos(\pi(t-s)))\right)}}+1\right)+$$
$$\left.+\frac{1}{2}X_0\frac{(1-\cos(\pi(t-s)))}{\left(\sqrt{\left(X_0^2+2(1-\cos(\pi(t-s)))\right)}\right)^3}\right]\mathrm{d}t. \tag{6.38}$$

6.2.7 Total Lifting Force

Remembering the convention for the positive sign of the doublet axis, the aerodynamic force which acts outward from the center is (see figure 6.5):

$$F(\varphi_d) = -\left(-\rho_\infty m(\varphi_d)\right) = \rho_\infty m(\varphi_d). \tag{6.39}$$

The *local lifting force* is:

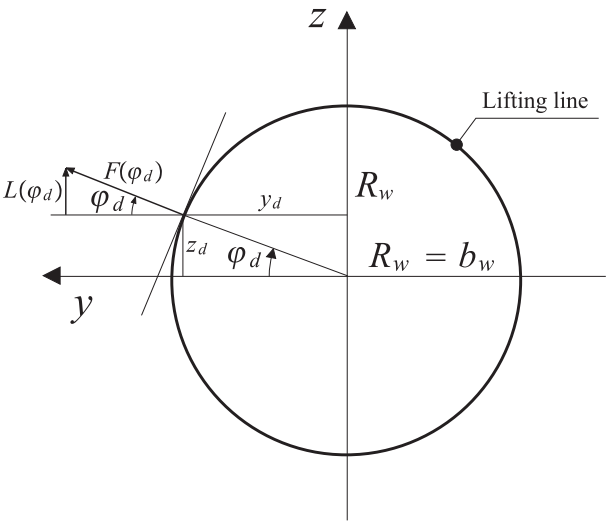

Figure 6.5. Calculation of the lifting force.

$$L\left(\varphi_d\right) = F\left(\varphi_d\right)\sin\varphi_d = \rho_\infty m\left(\varphi_d\right)\sin\varphi_d. \tag{6.40}$$

The total lifting force is obtained by integrating[4]:

$$L = \int_{ll} L\left(s_d\right)\mathrm{d}s_d. \tag{6.41}$$

Using the expression $\mathrm{d}s_d = R_w\mathrm{d}\varphi_d$:

$$L = \int_0^{2\pi} R_w L\left(\varphi_d\right)\mathrm{d}\varphi_d = \int_0^{2\pi} \rho_\infty R_w m\left(\varphi_d\right)\sin\varphi_d\mathrm{d}\varphi_d = \rho_\infty R_w \int_0^{2\pi} m\left(\varphi_d\right)\sin\varphi_d\mathrm{d}\varphi_d. \tag{6.42}$$

Introducing the coefficient of lift (reference surface defined as $S = 4R_w l$):

$$C_L = \frac{L}{\frac{1}{2}\rho_\infty\left(4R_w l\right)V_\infty^2} = \frac{1}{2lV_\infty^2}\int_0^{2\pi} m\left(\varphi_d\right)\sin\varphi_d\,\mathrm{d}\varphi_d. \tag{6.43}$$

Expressing equation (6.43) using variables t and s yields

$$C_L = -\frac{\pi}{2lV_\infty^2}\int_{-1}^{+1} m\left(t\right)\sin\left(\pi t\right)\,\mathrm{d}t. \tag{6.44}$$

[4] ll indicates "lifting line".

6.2.8 Normalwash $[u_n(\varphi)]_{X=0}$

Recalling the definition of the small perturbation velocity potential, the normalwash is:

$$[u_n(\varphi)]_{X=0} = \left(\frac{1}{h_R} \frac{\partial \phi(X,R,\varphi,R_w)}{\partial R} \right)_{R=R_w;\, X=0}. \tag{6.45}$$

Notice that this expression is formally similar to the expression used in Weissinger's condition. Hence:

$$\begin{aligned}
[u_n(\varphi)]_{X=0} = {} & \tfrac{1}{4\pi V_\infty R_w} \oint_0^{2\pi} m(\varphi_d) \cdot \\
& \cdot \lim_{X\to 0} \left\{ \left[\frac{-\cos(\varphi-\varphi_d)}{\left(X+\sqrt{(X^2+2(1-\cos(\varphi-\varphi_d)))}\right)\sqrt{(X^2+2(1-\cos(\varphi-\varphi_d)))}} + \right.\right. \\
& -1 + \tfrac{1}{(1-\cos(\varphi-\varphi_d))} + \tfrac{1}{2}\left(\frac{X}{\sqrt{(X^2+2(1-\cos(\varphi-\varphi_d)))}} + 1 \right) + \\
& \left.\left. + \tfrac{1}{2} X \frac{(1-\cos(\varphi-\varphi_d))}{\left(\sqrt{(X^2+2(1-\cos(\varphi-\varphi_d)))}\right)^3} \right] \right\} \mathrm{d}\varphi_d.
\end{aligned} \tag{6.46}$$

Simplifying:

$$[u_n(\varphi)]_{X=0} = \frac{1}{8\pi V_\infty R_w} \oint_0^{2\pi} \frac{m(\varphi_d)}{(1-\cos(\varphi-\varphi_d))} \mathrm{d}\varphi_d. \tag{6.47}$$

Observation 25 It is easy to show that

$$[u_n(\varphi)]_{X=0} = \frac{1}{2}[u_n(\varphi)]_{X\to\infty}. \tag{6.48}$$

The following comments can be made about this relation:

- *Comment 1*
  The result was predictable because the wing is positioned in a vertical plane[5].
- *Comment 2*
  This is also a verification of the theory: the formulation leads to correct results.

6.2.9 Normalwash $[u_n(s)]_{X=0}$

Using the expression of u_n found in the previous section, it is easy to show that

$$[u_n(s)]_{X=0} = \frac{1}{8V_\infty R_w} \oint_{-1}^{+1} \frac{m(t)}{(1-\cos(\pi(t-s)))} \mathrm{d}t. \tag{6.49}$$

[5]This result is valid also in a classical wing, where it is well known that the induced velocity in the Trefftz plane is twice the induced velocity on the wing [2].

6.2.10 Normalwash $[u_n(\varphi)]_{X=0}$: a Geometrical Approach

Suppose that the circulation $\Gamma(\varphi)$ on the lifting line is known. Referring to figure 6.6, the modulus of the induced velocity in a point on the circle characterized by the angle φ is indicated by V_{γ_x} . This velocity is induced by the trailing vortex $\gamma_x \mathrm{d}s_d$ positioned in correspondence to the angle φ_d. Moreover, the radial component of the induced velocity is indicated by $\mathrm{d}u_n$. From figure 6.6, it is clear that[6]

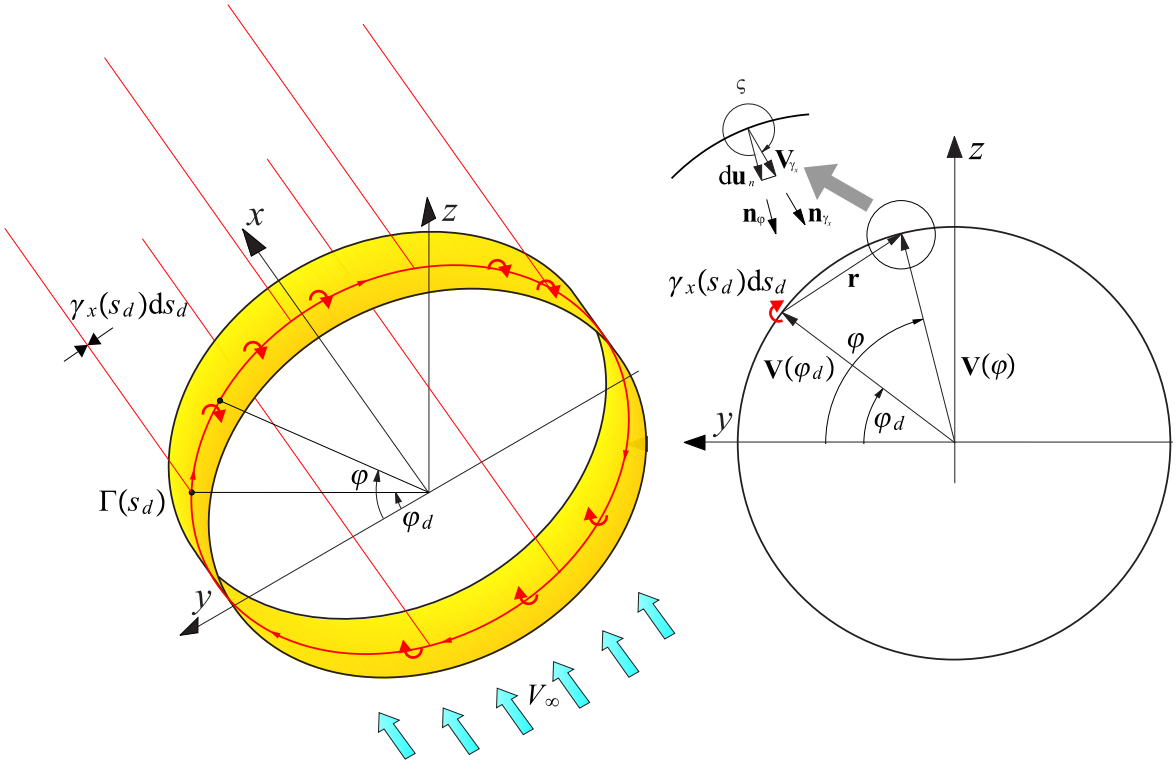

Figure 6.6. Induced velocity by the vortex $\gamma_x \mathrm{d}s_d$.

$$\mathrm{d}u_n = V_{\gamma_x} \cos\varsigma. \tag{6.50}$$

Writing the induced velocity in an explicit form:

$$\mathrm{d}u_n = \frac{\gamma_x(s_d)}{4\pi r} \cos\varsigma \, \mathrm{d}s_d, \tag{6.51}$$

where r is the modulus of the vector $\mathbf{r}$. $\mathbf{r}$ is obtainable as the difference between the position vectors as follows:

$$\mathbf{r} = \mathbf{V}(\varphi) - \mathbf{V}(\varphi_d) = (R_w \cos\varphi - R_w \cos\varphi_d)\ \mathbf{j} + (R_w \sin\varphi - R_w \sin\varphi_d)\ \mathbf{k}. \tag{6.52}$$

[6]Clearly, the positive direction for u_n acts toward the centre. Notice that in the previous analytical derivation the convention was the opposite.

Therefore, the modulus is

$$r = \sqrt{r_y^2 + r_z^2} = R_w \sqrt{2\left(1 - \cos\left(\varphi - \varphi_d\right)\right)}. \tag{6.53}$$

Clearly, $\mathbf{n}_{\gamma_x}$ has the expression

$$\mathbf{n}_{\gamma_x} = \mathbf{i} \times \frac{\mathbf{r}}{r} = -\frac{\left(\sin\varphi - \sin\varphi_d\right)}{\sqrt{2\left(1 - \cos\left(\varphi - \varphi_d\right)\right)}}\,\mathbf{j} + \frac{\left(\cos\varphi - \cos\varphi_d\right)}{\sqrt{2\left(1 - \cos\left(\varphi - \varphi_d\right)\right)}}\,\mathbf{k}. \tag{6.54}$$

The vector with unitary modulus acting toward the center and characterized by φ has the expression:

$$\mathbf{n}_{\varphi} = -\cos\varphi\,\mathbf{j} - \sin\varphi\,\mathbf{k}. \tag{6.55}$$

Therefore, it is possible to determine $\cos\varsigma$ as a scalar product of $\mathbf{n}_{\gamma_x}$ and $\mathbf{n}_{\varphi}$:

$$\begin{aligned}\cos\varsigma = \mathbf{n}_{\gamma_x} \cdot \mathbf{n}_{\varphi} &= -\tfrac{(\sin\varphi - \sin\varphi_d)}{\sqrt{2(1-\cos(\varphi-\varphi_d))}}(-\cos\varphi) + \tfrac{(\cos\varphi - \cos\varphi_d)}{\sqrt{2(1-\cos(\varphi-\varphi_d))}}(-\sin\varphi) = \\ &= \tfrac{\sin(\varphi-\varphi_d)}{\sqrt{2(1-\cos(\varphi-\varphi_d))}}.\end{aligned} \tag{6.56}$$

Substituting into equation (6.51):

$$\mathrm{d}u_n = \frac{\gamma_x\left(s_d\right)}{4\pi r}\left(\frac{\sin\left(\varphi - \varphi_d\right)}{\sqrt{2\left(1 - \cos\left(\varphi - \varphi_d\right)\right)}}\right)\mathrm{d}s_d. \tag{6.57}$$

Notice that, here, the induced velocity is considered positive when it acts toward the center. Considering figure 6.7:

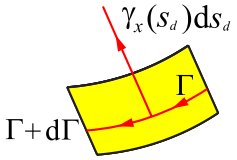

Figure 6.7. Bounded Vortex and trailing vortex.

$$\begin{aligned}\gamma_x\left(s_d\right) &= -\tfrac{d\Gamma(s_d)}{ds_d}, \\ \mathrm{d}s_d &= R_w \mathrm{d}\varphi_d.\end{aligned} \tag{6.58}$$

Using the expression used for r:

$$\mathrm{d}u_n = \frac{-\frac{\mathrm{d}\Gamma(\varphi_d)}{\mathrm{d}\varphi_d}}{4\pi R_w\sqrt{2(1-\cos(\varphi-\varphi_d))}}\frac{\sin(\varphi-\varphi_d)}{\sqrt{2(1-\cos(\varphi-\varphi_d))}}\,\mathrm{d}\varphi_d. \tag{6.59}$$

Integrating over the circle:

$$u_n = -\frac{1}{8\pi R_w} \oint_0^{2\pi} \frac{\frac{\mathrm{d}\Gamma(\varphi_d)}{\mathrm{d}\varphi_d} \sin(\varphi - \varphi_d)}{(1 - \cos(\varphi - \varphi_d))} \mathrm{d}\varphi_d. \tag{6.60}$$

Using the identity $\frac{\sin(\varphi-\varphi_d)}{(1-\cos(\varphi-\varphi_d))} = \frac{1}{\tan\frac{\varphi-\varphi_d}{2}}$, yields

$$u_n = -\frac{1}{8\pi R_w} \oint_0^{2\pi} \frac{\frac{d\Gamma(\varphi_d)}{d\varphi_d}}{\tan\frac{\varphi-\varphi_d}{2}} \mathrm{d}\varphi_d. \tag{6.61}$$

Changing the variables in a way to calculate the integrals in the interval -1,+1:

$$u_n = \frac{1}{8\pi R_w} \oint_{-1}^{+1} \frac{\frac{\mathrm{d}\Gamma(t)}{\mathrm{d}t}}{\tan\frac{\pi(t-s)}{2}} \mathrm{d}t. \tag{6.62}$$

Now it has to be demonstrated that equation (6.62) is the same as the normalwash formula (equation (6.49)) reported below[7]:

$$[u_n(s)]_{X=0} = \frac{1}{8V_\infty R_w} \oint_{-1}^{+1} m(t) \left(\frac{1}{(1 - \cos(\pi(t-s)))} \right) \mathrm{d}t. \tag{6.63}$$

Integrating equation (6.63) by parts:

$$[u_n(s)]_{X=0} = \left[m(t) \left(-\frac{1}{\pi \tan\frac{(\pi(t-s))}{2}} \right) \right]_{-1}^{+1} - \oint_{-1}^{+1} \frac{\mathrm{d}m}{\mathrm{d}t} \left(-\frac{1}{\pi \tan\frac{(\pi(t-s))}{2}} \right). \tag{6.64}$$

But $m(-1) = m(+1)$ in the annular wing, thus, expression (6.64) becomes

$$[u_n(s)]_{X=0} = \frac{1}{8V_\infty R_w} \oint_{-1}^{+1} \frac{dm}{dt} \left(\frac{1}{\pi \tan\frac{(\pi(t-s))}{2}} \right). \tag{6.65}$$

Observing that m and Γ are directly related:

$$m(t) = -V_\infty \Gamma(t), \tag{6.66}$$

and remembering the sign convention used for u_n, it is clear that the expressions (6.62) and (6.49) are the same. Therefore, the geometric approach yielded the same equation for normalwash as was obtained using the analytical procedure.

[7] In equation (6.63), u_n is positive when it acts outward from the center, while in equation (6.62) u_n is positive when it acts toward the center.

6.2.11 Evaluation of the Induced Drag

As seen in chapter 4, under the assumption made, the local contribute of the induced drag is

$$D_i(\varphi_d) = F(\varphi_d)\tan(\alpha_i(\varphi_d)) \simeq F(\varphi_d)\,\alpha_i(\varphi_d), \tag{6.67}$$

where

$$F(\varphi_d) = -(-\rho_\infty m(\varphi_d)) = \rho_\infty m(\varphi_d). \tag{6.68}$$

The induced incidence is

$$\alpha_i(\varphi_d) = -\frac{[u_n(\varphi_d)]_{X=0}}{V_\infty}, \tag{6.69}$$

where $[u_n(\varphi_d)]_{X=0}$ has been calculated before. Integrating over the entire lifting line[8]:

$$D_i = \oint_{ll} F(s_d)\,\alpha_i(s_d)\,\mathrm{d}s_d. \tag{6.70}$$

Using the expression of $\mathrm{d}s_d$:

$$D_i = \rho_\infty R_w \oint_0^{2\pi} m(\varphi_d)\left(-\frac{[u_n(\varphi_d)]_{X=0}}{V_\infty}\right)\mathrm{d}\varphi_d. \tag{6.71}$$

The corresponding coefficient of induced drag is

$$C_{D_i} = \frac{1}{2lV_\infty^3}\oint_0^{2\pi} m(\varphi_d)\left(-[u_n(\varphi_d)]_{X=0}\right)\mathrm{d}\varphi_d. \tag{6.72}$$

The coefficient of induced drag expressed with the variables t and s is:

$$C_{D_i} = \frac{\pi}{2lV_\infty^3}\oint_{-1}^{+1} m(t)\left(-[u_n(t)]_{X=0}\right)\mathrm{d}t. \tag{6.73}$$

Observation 26 Notice that the external integral in the expression of the induced drag has to be defined in the Cauchy sense. The reason is that the curve representing the lifting line is closed and, thus, the singularity is always inside the interval of integration. This last property guarantees that the external integral can be defined as a Cauchy integral instead of a Hadamard integral.

[8] ll means that the integrals have to be calculated over the lifting line representing the wing.

6.3 Elliptical Annular Wing with Wing Span Representing its Major Axis

The analytical procedure that will be used here is similar to the procedure adopted in the circular annular wing case. However, the mathematical expressions are different. Therefore, for the aim of completeness, the details of the derivations are not omitted. The reader not interested in mathematical derivations, could skip to chapter 7.

The geometry of the wing is shown in figure 6.8. In figure 6.9, the reference

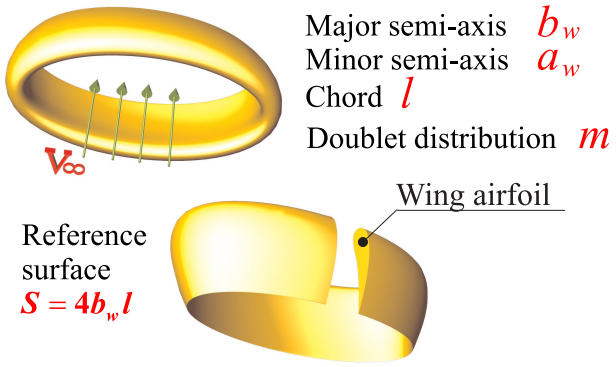

Figure 6.8. Elliptical annular wing with $b_w > a_w$.

coordinate system and a few useful notations are reported. Like the circular annular wing, the calculation of the *normalwash* is important. Thus, the derivatives along the perpendicular directions of the ellipse are required. This is done using a particular transformation of coordinates shown in the next subsection.

6.3.1 Coordinate Transformation

Is it possible to transform the coordinate system in order to define the same point using two directions which are tangent and perpendicular to an ellipse? The answer is yes. It is sufficient to write

$$\begin{aligned} y &= c\cosh\psi\cos\varphi \qquad 0 \le \varphi \le 2\pi, \\ z &= c\sinh\psi\sin\varphi \qquad \psi > 0. \end{aligned} \tag{6.74}$$

It can observed that the ellipse with semi-axes a_w and b_w is obtainable when

$$\begin{aligned} a_w &= c\sinh\psi_w, \\ b_w &= c\cosh\psi_w. \end{aligned} \tag{6.75}$$

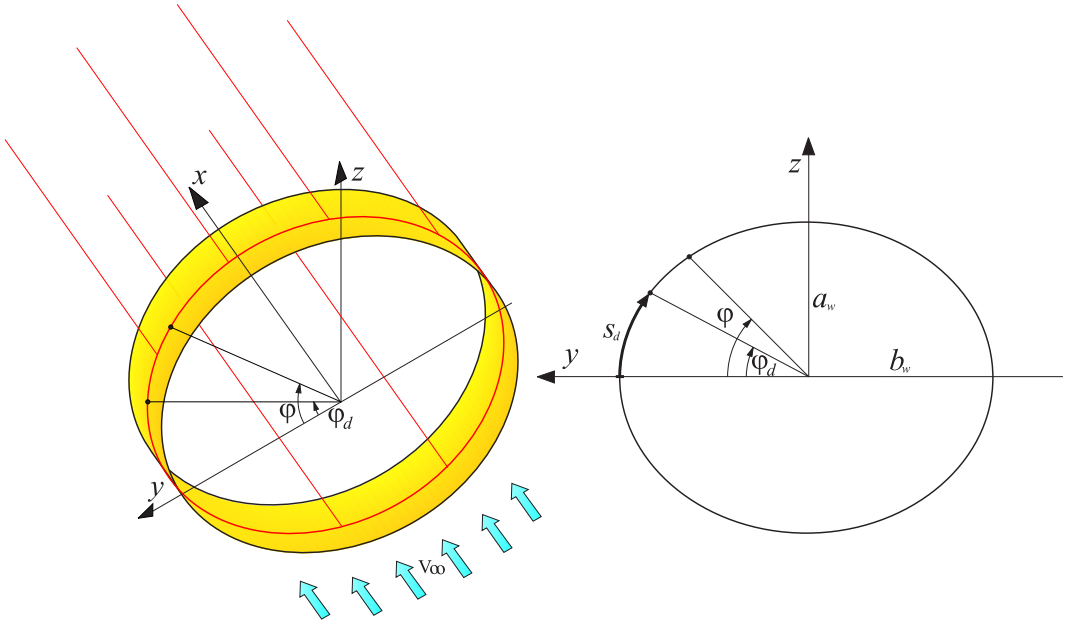

Figure 6.9. Elliptical annular wing: reference coordinate system.

From the last equations:

$$\begin{aligned} c^2 &= b_w^2 - a_w^2, \\ \cosh^2 \psi_w &= \tfrac{b_w^2}{b_w^2 - a_w^2}. \end{aligned} \tag{6.76}$$

The *ellipse representing the lifting line*[9] is

$$\begin{aligned} y &= c \cosh \psi_w \cos \varphi \qquad 0 \leq \varphi \leq 2\pi, \\ z &= c \sinh \psi_w \sin \varphi \qquad \psi_w > 0. \end{aligned} \tag{6.77}$$

Now consider the *generic ellipse*. It is easy to show that

$$\begin{aligned} \mathrm{d}y &= c \sinh \psi \cos \varphi \, \mathrm{d}\psi - c \cosh \psi \sin \varphi \, \mathrm{d}\varphi, \\ \mathrm{d}z &= c \cosh \psi \sin \varphi \, \mathrm{d}\psi + c \sinh \psi \cos \varphi \, \mathrm{d}\varphi. \end{aligned} \tag{6.78}$$

Squaring and summing:

$$\mathrm{d}s^2 = \mathrm{d}y^2 + \mathrm{d}z^2 = c^2 \left(\cosh^2 \psi - \cos^2 \varphi \right) \left(\mathrm{d}\psi^2 + \mathrm{d}\varphi^2 \right) = h^2 \left(\mathrm{d}\psi^2 + \mathrm{d}\varphi^2 \right). \tag{6.79}$$

From this equation, it is not difficult to understand that, for the ellipse representing the lifting line, the infinitesimal arc has the length[10]:

$$\mathrm{d}s_d = c \sqrt{\cosh^2 \psi_w - \cos^2 \varphi} \, \mathrm{d}\varphi_d. \tag{6.80}$$

[9] That ellipse is obtained by setting $\psi = \psi_w$.

[10] On the ellipse w (the lifting line), $\psi = \psi_w = \text{const} \Rightarrow \mathrm{d}\psi = 0$. Notice, the subscript d is used because a doublet will be positioned on the infinitesimal arc (see next derivations).

In figure 6.10, the transformation of the coordinate system can been seen. Each

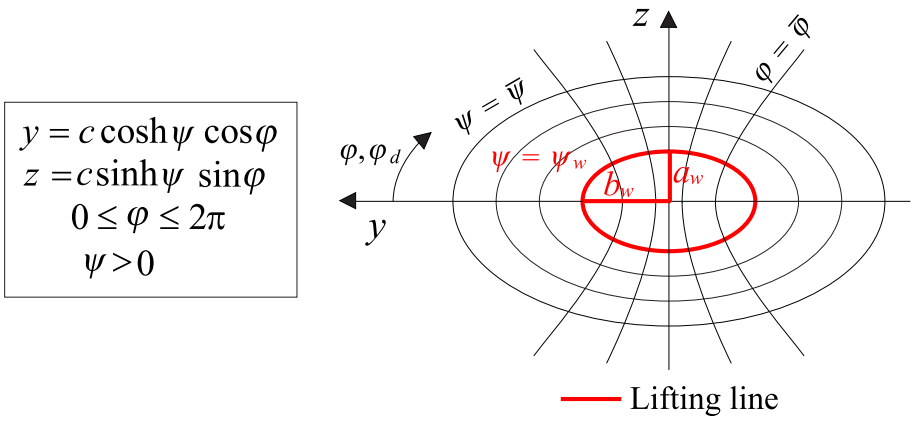

Figure 6.10. Transformation of the coordinate system.

point is uniquely determined as the intersection of an ellipse (each curve with $\psi =$ const is an ellipse) and a hyperbola (each curve with $\varphi =$ const is a hyperbola). Notice that in each intersection of an ellipse and a hyperbola, the tangent of the ellipse is perpendicular to the tangent of the hyperbola. This is shown in appendix D.

6.3.2 Small Perturbation Acceleration Potential

In order to write the acceleration potential, the following quantities are needed:

- *Quantity 1*
  The distance between a generic point $P(x,y,z)$ in space and a point $P_d(x_d,y_d,z_d)$ on the lifting line w.

- *Quantity 2*
  The cosine direction of the normal on the lifting line. The normal acts toward the local center of curvature.

These quantities are calculated in appendix E. Using the generic formula (1.49), the small perturbation acceleration potential of a doublet $M = m\,(s_d)\,\mathrm{d}s_d$ positioned at a point on the ellipse characterized by $\varphi = \varphi_d$ is:

$$\mathrm{d}\Psi\,(x,\psi,\varphi,\psi_w) = \tfrac{m(\varphi_d)\mathrm{d}\varphi_d}{4\pi c}\tfrac{H_1}{H_2^{3/2}}, \tag{6.81}$$

where

$$\begin{aligned} H_1 &= \cos\varphi_d \sinh\psi_w \left(\cosh\psi\cos\varphi - \cosh\psi_w\cos\varphi_d\right) + \\ &\quad + \sin\varphi_d \cosh\psi_w \left(\sinh\psi\sin\varphi - \sinh\psi_w\sin\varphi_d\right), \\ H_2 &= X^2 + \left(\cosh\psi\cos\varphi - \cosh\psi_w\cos\varphi_d\right)^2 + \\ &\quad + \left(\sinh\psi\sin\varphi - \sinh\psi_w\sin\varphi_d\right)^2. \end{aligned} \tag{6.82}$$

In equation (6.81), the following relations have been used:

$$\begin{aligned} x_d &= 0, \\ y_d &= c\cosh\psi_w\cos\varphi_d, \\ z_d &= c\sinh\psi_w\sin\varphi_d, \\ y &= c\cosh\psi\cos\varphi, \\ z &= c\sinh\psi_w\sin\varphi, \\ \mathrm{d}s_w &= c\sqrt{\cosh^2\psi_w - \cos^2\varphi_d}\,\mathrm{d}\varphi_d. \end{aligned} \tag{6.83}$$

Finally, using the relation

$$\begin{aligned} &\tfrac{1}{2}\left(\sinh\left(\psi+\psi_w\right)\cos\left(\varphi-\varphi_d\right) - \sinh\left(\psi-\psi_w\right)\cos\left(\varphi+\varphi_d\right) - \sinh 2\psi_w\right) = \\ &= \left(\cos\varphi_d\sinh\psi_w\right)\left(\cosh\psi\cos\varphi - \cosh\psi_w\cos\varphi_d\right) + \\ &+ \left(\sin\varphi_d\cosh\psi_w\right)\left(\sinh\psi\sin\varphi - \sinh\psi_w\sin\varphi_d\right), \end{aligned} \tag{6.84}$$

and integrating over the lifting line yields:

$$\Psi\left(x,\psi,\varphi,\psi_w\right) = \tfrac{1}{8\pi c}\int_0^{2\pi} m\left(\varphi_d\right)\tfrac{H_3}{H_4^{3/2}}\,\mathrm{d}\varphi_d, \tag{6.85}$$

where

$$\begin{aligned} H_3 &= \left(\sinh\left(\psi+\psi_w\right)\cos\left(\varphi-\varphi_d\right) - \sinh\left(\psi-\psi_w\right)\cos\left(\varphi+\varphi_d\right) - \sinh 2\psi_w\right), \\ H_4 &= X^2 + \sinh^2\psi + \cos^2\varphi - \cosh\left(\psi-\psi_w\right)\cos\left(\varphi+\varphi_d\right) + \\ &\quad - \cosh\left(\psi+\psi_w\right)\cos\left(\varphi-\varphi_d\right) + \sinh^2\psi_w + \cos^2\varphi_d. \end{aligned} \tag{6.86}$$

Equation (6.85) represents the small perturbation acceleration potential of all doublets positioned on the elliptical lifting line.

6.3.3 Small Perturbation Velocity Potential

Using the procedure adopted for the circular annular wing, it is possible to obtain the small perturbation velocity potential:

$$\phi = \frac{1}{8\pi V_\infty} \int_0^{2\pi} m\left(\varphi_d\right) \frac{H_3}{H_4 - X^2} \left(\frac{X}{\sqrt{H_4}} + 1\right) \mathrm{d}\varphi_d. \tag{6.87}$$

This expression is very useful, because by deriving it, the velocity perpendicular to the ellipse can be written and, therefore, Weissinger's condition can be imposed. This operation is done in the next subsection.

6.3.4 Imposition of Weissinger's Condition

Weissinger's condition consists of the WTC imposed in $X_0 = \frac{l}{2c}$:

$$-\alpha\left(\varphi\right) = \frac{1}{V_\infty} \left(\frac{1}{h} \frac{\partial \phi\left(X, \psi, \varphi, \psi_w\right)}{\partial \psi}\right)_{X = X_0;\, \psi = \psi_w}. \tag{6.88}$$

The explicit form of the derivatives and the treatment of the consequent singular term are given in appendix F.

6.3.5 Integral Equation with the Variables φ, φ_d

Using the relations found above, the final expression of Weissinger's condition can be written. It is represented by an integral equation containing the unknown function $m(\varphi)$, which is the doublet distribution on the elliptical lifting line. Thus[11]:

$$\begin{aligned} -\alpha\left(\varphi\right) = {} & \frac{1}{8\pi c V_\infty^2 \sqrt{\left(\cosh^2 \psi_w - \cos^2 \varphi\right)}} \oint_0^{2\pi} m\left(\varphi_d\right) \Big(\Big[f_2 \frac{\partial f_3}{\partial \psi} \Big]_{\psi = \psi_w, X = X_0} + \\ & + \Big(\Big[\frac{\partial f_2}{\partial \psi} \Big] f_3 \Big)_{\psi = \psi_w, X = X_0} \Big) \mathrm{d}\varphi_d, \end{aligned} \tag{6.89}$$

[11] Notice that the integral has to be defined as a Hadamard finite-part integral because the integral contains the singular term $\frac{2}{1 - \cos(\varphi - \varphi_d)}$.

where

$$
\begin{aligned}
&\left[f_2 \frac{\partial f_3}{\partial \psi}\right]_{\psi=\psi_w, X=X_0} = \frac{X_0 \cosh^2\psi_w \sinh^2\psi_w (1-\cos(\varphi-\varphi_d))}{(H_5)(H_6)^{\frac{3}{2}}},\\
&\left(\left[\frac{\partial f_2}{\partial \psi}\right] f_3\right)_{\psi=\psi_w, X=X_0} = \left(\left[\frac{\partial f_2}{\partial \psi}\right]^R f_3\right)_{\psi=\psi_w, X=X_0} + \left(\left[\frac{\partial f_2}{\partial \psi}\right]^S f_3\right)_{\psi=\psi_w, X=X_0},\\
&\left(\left[\frac{\partial f_2}{\partial \psi}\right]^S f_3\right)_{\psi=\psi_w, X=X_0} = \frac{\cosh^2\psi_w \cos(\varphi-\varphi_d) - \cos\varphi\cos\varphi_d}{(H_5)} \cdot f_I - \frac{\cosh(2\psi_w)}{(H_5)} + \\
&\qquad\qquad + \boxed{\frac{2}{1-\cos(\varphi-\varphi_d)}},\\
&\left(\left[\frac{\partial f_2}{\partial \psi}\right]^R f_3\right)_{\psi=\psi_w, X=X_0} = \frac{\sinh^2\psi_w \cosh^2\psi_w}{(H_5)^2} \cdot \left(\frac{X_0}{\sqrt{H_6}} + 1\right),\\
&f_I = \frac{-2(H_5)}{\left(X_0+\sqrt{H_6}\right)\sqrt{H_6}},\\
&H_5 = \sinh^2\psi_w + \sin^2\frac{\varphi+\varphi_d}{2},\\
&H_6 = X_0^2 + 2\left(\sinh^2\psi_w + \sin^2\frac{\varphi+\varphi_d}{2}\right)(1-\cos(\varphi-\varphi_d)).
\end{aligned}
\tag{6.90}
$$

The term inside the box is the singular term.

6.3.6 Integral Equation with the Variables t, s

The new variables t and s are defined as

$$
\varphi_d = \pi(t+1)\ ,\varphi = \pi(s+1). \tag{6.91}
$$

Observing the previous equation, it can be deduced that:

$$
\begin{aligned}
&\mathrm{d}\varphi_d = \pi \mathrm{d}t\\
&\varphi - \varphi_d = \pi(s-t),\\
&\cos(\pi(s+1)) = \cos(\pi s + \pi) = -\cos(\pi s),\\
&\cos(\pi(t+1)) = \cos(\pi t + \pi) = -\cos(\pi t).
\end{aligned}
\tag{6.92}
$$

Substituting into the integral equation yields:

$$
\begin{aligned}
-\alpha(s) = \frac{1}{8cV_\infty^2} \frac{1}{\sqrt{\left(\cosh^2\psi_w - \cos^2(\pi s)\right)}} \oint_{-1}^{+1} m(t) \Big(&\left[f_2 \frac{\partial f_3}{\partial \psi}\right]_{\psi=\psi_w, X=X_0} + \\
&+ \left(\left[\frac{\partial f_2}{\partial \psi}\right] f_3\right)_{\psi=\psi_w, X=X_0} \Big)\, \mathrm{d}t,
\end{aligned}
\tag{6.93}
$$

where

$$
\begin{aligned}
&\left[f_2 \frac{\partial f_3}{\partial \psi}\right]_{\psi=\psi_w, X=X_0} = \frac{X_0 \cosh^2\psi_w \sinh^2\psi_w (1-\cos(\pi(t-s)))}{(H_5)(H_6)^{\frac{3}{2}}},\\
&\left(\left[\frac{\partial f_2}{\partial \psi}\right] f_3\right)_{\psi=\psi_w, X=X_0} = \left(\left[\frac{\partial f_2}{\partial \psi}\right]^R f_3\right)_{\psi=\psi_w, X=X_0} + \left(\left[\frac{\partial f_2}{\partial \psi}\right]^S f_3\right)_{\psi=\psi_w, X=X_0},\\
&\left(\left[\frac{\partial f_2}{\partial \psi}\right]^S f_3\right)_{\psi=\psi_w, X=X_0} = \frac{\cosh^2\psi_w \cos(\pi(t-s)) - \cos(\pi s)\cos(\pi t)}{(H_5)} \cdot f_I - \frac{\cosh(2\psi_w)}{(H_5)} + \\
&\qquad\qquad + \boxed{\frac{2}{1-\cos(\pi(t-s))}},\\
&\left(\left[\frac{\partial f_2}{\partial \psi}\right]^R f_3\right)_{\psi=\psi_w, X=X_0} = \frac{\sinh^2\psi_w \cosh^2\psi_w}{(H_5)^2}\left(\frac{X_0}{\sqrt{H_6}} + 1\right),\\
&f_I = \frac{-2(H_5)}{\left(X_0+\sqrt{H_6}\right)\sqrt{H_6}},\\
&H_5 = \sinh^2\psi_w + \sin^2\left(\frac{\pi(t+s)}{2}\right),\\
&H_6 = X_0^2 + 2\left(\sinh^2\psi_w + \sin^2\left(\frac{\pi(t+s)}{2}\right)\right)(1-\cos(\pi(t-s))).
\end{aligned}
\tag{6.94}
$$

6.3.7 Total Lifting Force

Remembering the convention for the positive sign of the doublet axis, the aerodynamic force, which acts outward from the local center of curvature, is

$$F(\varphi_d) = -(-\rho_\infty m(\varphi_d)) = \rho_\infty m(\varphi_d). \tag{6.95}$$

The local normal direction is the aerodynamic force direction. Recalling the expression of the unit vector which acts outward from the local center of curvature:

$$\mathbf{N}_d = -\mathbf{n}_d = \frac{\cos\varphi_d \sinh\psi_w}{\sqrt{\cosh^2\psi_w - \cos^2\varphi_d}}\mathbf{j} + \frac{\sin\varphi_d \cosh\psi_w}{\sqrt{\cosh^2\psi_w - \cos^2\varphi_d}}\mathbf{k}, \tag{6.96}$$

it is easy to obtain (see figure 6.11)[12]:

$$\sin\beta = (\mathbf{N}_d)_z = \frac{\sin\varphi_d \cosh\psi_w}{\sqrt{\cosh^2\psi_w - \cos^2\varphi_d}}. \tag{6.97}$$

The *local* lift is:

$$L(\varphi_d) = F(\varphi_d)\sin\beta = \rho_\infty m(\varphi_d)\frac{\cosh\psi_w \sin\varphi_d}{\sqrt{\cosh^2\psi_w - \cos^2\varphi_d}}. \tag{6.98}$$

[12]Notice that vector $\mathbf{N}_d$ has modulus equal to one.

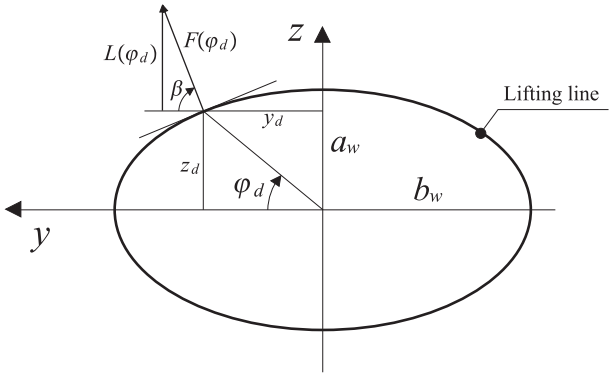

Figure 6.11. Calculation of the lifting force.

The total lifting force is determined by integrating

$$L = \int_{ll} L\left(s_d\right)\,\mathrm{d}s_d. \tag{6.99}$$

But it has been demonstrated that $\mathrm{d}s_d = c\sqrt{\cosh^2\psi_w - \cos^2\varphi_d}\,\mathrm{d}\varphi_d$; thus[13]

$$L = c\int_0^{2\pi} L\left(\varphi_d\right)\sqrt{\cosh^2\psi_w - \cos^2\varphi_d}\,\mathrm{d}\varphi_d = \rho_\infty b_w \int_0^{2\pi} m\left(\varphi_d\right)\sin\varphi_d\,\mathrm{d}\varphi_d. \tag{6.100}$$

Using the variable t instead of φ_d:

$$L = -\rho_\infty \pi b_w \int_{-1}^{+1} m\left(t\right)\sin\left(\pi t\right)\,\mathrm{d}t. \tag{6.101}$$

The corresponding coefficient of lift (using the reference surface $S = 4b_w l$) is

$$C_L = \frac{L}{\frac{1}{2}\rho_\infty S V_\infty^2} = -\frac{\pi}{2lV_\infty^2}\int_{-1}^{+1} m\left(t\right)\sin\left(\pi t\right)\,\mathrm{d}t. \tag{6.102}$$

6.3.8 Normalwash $\left[u_n\left(\varphi\right)\right]_{X=0}$

The induced velocity perpendicular to the lifting line is very important in the induced drag calculation. It is not difficult to analytically determine the expression of the induced velocity. It is sufficient to use the small perturbation velocity potential as following:

$$\left[u_n\left(\varphi\right)\right]_{X=0} = \left(\frac{1}{h}\frac{\partial\phi\left(X,\psi,\varphi,\psi_w\right)}{\partial\psi}\right)_{\psi=\psi_w;\,X=0}. \tag{6.103}$$

[13] Notice that $c\cosh\psi_w = b_w$.

Obviously, the positive direction of the induced velocity acts outward from the local center of curvature. Using the previous expressions, the normalwash equation is obtained:

$$\begin{aligned}[u_n(\varphi)]_{X=0} = \frac{1}{8\pi c V_\infty \sqrt{\left(\cosh^2\psi_w - \cos^2\varphi\right)}} \oint_0^{2\pi} m(\varphi_d) \Big(\Big[f_2 \frac{\partial f_3}{\partial \psi} \Big]_{\psi=\psi_w, X=0} + \\ + \Big(\Big[\frac{\partial f_2}{\partial \psi} \Big] f_3 \Big)_{\psi=\psi_w, X=0} \Big) \, \mathrm{d}\varphi_d,\end{aligned} \tag{6.104}$$

where

$$\begin{aligned}&\Big[f_2 \frac{\partial f_3}{\partial \psi} \Big]_{\psi=\psi_w, X=0} = 0 \\ &\Big(\Big[\frac{\partial f_2}{\partial \psi} \Big] f_3 \Big)_{\psi=\psi_w, X=0} = \Big(\Big[\frac{\partial f_2}{\partial \psi} \Big]^R f_3 \Big)_{\psi=\psi_w, X=0} + \Big(\Big[\frac{\partial f_2}{\partial \psi} \Big]^S f_3 \Big)_{\psi=\psi_w, X=0}, \\ &\Big(\Big[\frac{\partial f_2}{\partial \psi} \Big]^S f_3 \Big)_{\psi=\psi_w, X=0} = -\frac{\frac{1}{2}\cosh(2\psi_w)}{\left(\sinh^2\psi_w + \sin^2\frac{\varphi+\varphi_d}{2}\right)} + \boxed{\frac{1}{1-\cos(\varphi-\varphi_d)}}, \\ &\Big(\Big[\frac{\partial f_2}{\partial \psi} \Big]^R f_3 \Big)_{\psi=\psi_w, X=0} = \frac{\sinh^2\psi_w \cosh^2\psi_w}{\left(\sinh^2\psi_w + \sin^2\frac{\varphi+\varphi_d}{2}\right)^2}.\end{aligned} \tag{6.105}$$

Expressing the normalwash equation with the variables t and s yields:

$$\begin{aligned}[u_n(s)]_{X=0} = \frac{1}{8 c V_\infty \sqrt{\left(\cosh^2\psi_w - \cos^2(\pi s)\right)}} \oint_{-1}^{+1} m(t) \Big(\Big[f_2 \frac{\partial f_3}{\partial \psi} \Big]_{\psi=\psi_w, X=0} + \\ + \Big(\Big[\frac{\partial f_2}{\partial \psi} \Big] f_3 \Big)_{\psi=\psi_w,\, X=0} \Big) \, \mathrm{d}t,\end{aligned} \tag{6.106}$$

where

$$\begin{aligned}&\Big[f_2 \frac{\partial f_3}{\partial \psi} \Big]_{\psi=\psi_w, X=0} = 0 \\ &\Big(\Big[\frac{\partial f_2}{\partial \psi} \Big] f_3 \Big)_{\psi=\psi_w, X=0} = \Big(\Big[\frac{\partial f_2}{\partial \psi} \Big]^R f_3 \Big)_{\psi=\psi_w, X=0} + \Big(\Big[\frac{\partial f_2}{\partial \psi} \Big]^S f_3 \Big)_{\psi=\psi_w, X=0}, \\ &\Big(\Big[\frac{\partial f_2}{\partial \psi} \Big]^S f_3 \Big)_{\psi=\psi_w, X=0} = -\frac{\frac{1}{2}\cosh(2\psi_w)}{\left(\sinh^2\psi_w + \sin^2\left(\frac{\pi(t+s)}{2}\right)\right)} + \boxed{\frac{1}{(1-\cos(\pi(t-s)))}}, \\ &\Big(\Big[\frac{\partial f_2}{\partial \psi} \Big]^R f_3 \Big)_{\psi=\psi_w, X=0} = \frac{\sinh^2\psi_w \cosh^2\psi_w}{\left(\sinh^2\psi_w + \sin^2\left(\frac{\pi(t+s)}{2}\right)\right)^2}.\end{aligned} \tag{6.107}$$

Observation 27 The normalwash satisfies the following relation:

$$[u_n(\varphi)]_{X=0} = \frac{1}{2}[u_n(\varphi)]_{X\to\infty}, \tag{6.108}$$

as was shown in the circular annular wing case.

Observation 28 The induced velocity can be easily determined geometrically as has been done for the biplane and the circular annular wing. Details can be found in appendix G.

6.3.9 Evaluation of the Induced Drag

Under the assumption made, the local contribute of the induced drag is:

$$D_i(\varphi_d) = F(\varphi_d)\tan(\alpha_i(\varphi_d)) \simeq F(\varphi_d)\,\alpha_i(\varphi_d), \tag{6.109}$$

where

$$F(\varphi_d) = -(-\rho_\infty m(\varphi_d)) = \rho_\infty m(\varphi_d). \tag{6.110}$$

The induced incidence is

$$\alpha_i(\varphi_d) = -\frac{[u_n(\varphi_d)]_{X=0}}{V_\infty}. \tag{6.111}$$

Integrating over the entire lifting line:

$$D_i = \oint_{ll} F(s_d)\,\alpha_i(s_d)\,\mathrm{d}s_d. \tag{6.112}$$

Using the expression of $\mathrm{d}s_d$, the equation of induced drag is obtained:

$$D_i = \int_0^{2\pi} \rho_\infty c m(\varphi_d)\left(-\frac{[u_n(\varphi_d)]_{X=0}}{V_\infty}\right)\sqrt{\cosh^2\psi_w - \cos^2\varphi_d}\,\mathrm{d}\varphi_d. \tag{6.113}$$

The corresponding coefficient of induced drag is

$$C_{D_i} = \frac{c}{2b_w l V_\infty^3}\oint_0^{2\pi} m(\varphi_d)\sqrt{\cosh^2\psi_w - \cos^2\varphi_d}\,(-[u_n(\varphi_d)]_{X=0})\,\mathrm{d}\varphi_d. \tag{6.114}$$

Expressing the coefficient of induced drag with the variables t and s:

$$C_{D_i} = \frac{\pi c}{2b_w l V_\infty^3}\oint_{-1}^{+1} m(t)\sqrt{\cosh^2\psi_w - \cos^2(\pi t)}\,(-[u_n(t)]_{X=0})\,\mathrm{d}t. \tag{6.115}$$

6.4 Elliptical Annular Wing with Wing Span Representing its Minor Axis

The geometry of the wing is shown in figure 6.12. The reference coordinate system

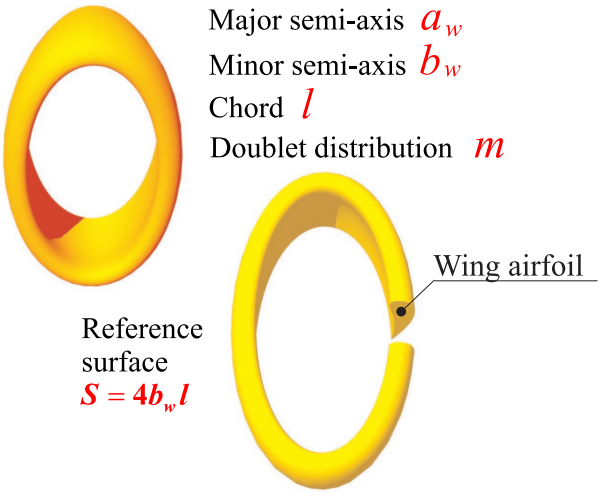

Figure 6.12. Elliptical annular wing with $b_w < a_w$.

is similar to the reference coordinate system seen in previous cases. Here, the transformation of variables is different. The same transformation used when $b_w > a_w$ can not be used. In particular, now

$$\begin{aligned} y &= c \sinh\psi \cos\varphi \qquad 0 \le \varphi \le 2\pi, \\ z &= c \cosh\psi \sin\varphi \qquad \psi > 0. \end{aligned} \tag{6.116}$$

It can be observed that the ellipse with semi-axes a_w and b_w is obtainable when

$$\begin{aligned} a_w &= c \cosh\psi_w, \\ b_w &= c \sinh\psi_w. \end{aligned} \tag{6.117}$$

From the last equations:

$$\begin{aligned} c^2 &= a_w^2 - b_w^2, \\ \cosh^2\psi_w &= \tfrac{a_w^2}{a_w^2 - b_w^2}, \\ \sinh^2\psi_w &= \tfrac{b_w^2}{a_w^2 - b_w^2}. \end{aligned} \tag{6.118}$$

The *ellipse representing the lifting line*[14] is

$$\begin{aligned} y &= c \sinh\psi_w \cos\varphi \qquad 0 \le \varphi \le 2\pi, \\ z &= c \cosh\psi_w \sin\varphi \qquad \psi_w > 0. \end{aligned} \tag{6.119}$$

[14] That ellipse is obtained by setting $\psi = \psi_w$.

As has been done for the case in which $b_w > a_w$, it is possible to find the relation

$$\mathrm{d}s^2 = \mathrm{d}y^2 + \mathrm{d}z^2 = c^2\left(\sinh^2\psi + \cos^2\varphi\right)\left(\mathrm{d}\psi^2 + \mathrm{d}\varphi^2\right) = h^2\left(\mathrm{d}\psi^2 + \mathrm{d}\varphi^2\right). \quad (6.120)$$

Now consider the ellipse w. It is easy to show that the infinitesimal arc has the dimension

$$\mathrm{d}s_d = c\sqrt{\sinh^2\psi + \cos^2\varphi}\,\mathrm{d}\varphi_d. \quad (6.121)$$

Figure 6.13 shows the transformation of the coordinate system. Each point in the

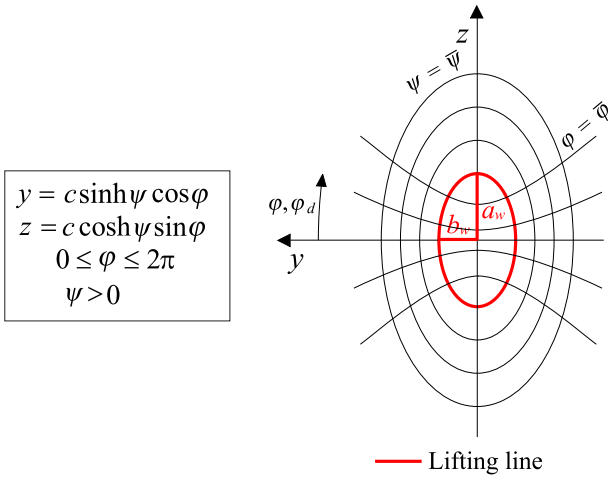

Figure 6.13. Transformation of the coordinate system.

plane $y - z$ is uniquely determined as the intersection of an ellipse (each curve with $\psi = \text{const}$ is an ellipse) and a hyperbola (each curve with $\varphi = \text{const}$ is a hyperbola). Notice that in each intersection of an ellipse and a hyperbola, the tangent of the ellipse is perpendicular to the tangent of the hyperbola, as it was for the ellipse with $b_w > a_w$.

6.4.1 Small Perturbation Acceleration Potential

In order to write the acceleration potential, the following quantities are needed:

- *Quantity 1*
  The distance between a generic point $P(x,y,z)$ in space and a point $P_d(x_d,y_d,z_d)$ on the lifting line w.

- *Quantity 2*
  The cosine directions of the normal to the lifting line. The normal acts toward the local center of curvature.

These quantities are calculated in appendix H. Using the generic formula (1.49), the small perturbation acceleration potential of a doublet $M = m\,(s_d)\,\mathrm{d}s_d$ positioned at a point on the ellipse characterized by $\varphi = \varphi_d$ is

$$\mathrm{d}\Psi\,(x,\psi,\varphi,\psi_w) = \tfrac{m(\varphi_d)\mathrm{d}\varphi_d}{4\pi c}\tfrac{H_1}{H_2^{3/2}}, \tag{6.122}$$

where

$$\begin{aligned} H_1 &= \cos\varphi_d \cosh\psi_w\,(\sinh\psi\cos\varphi - \sinh\psi_w\cos\varphi_d) + \\ &\quad + \sin\varphi_d \sinh\psi_w\,(\cosh\psi\sin\varphi - \cosh\psi_w\sin\varphi_d)\,, \\ H_2 &= X^2 + (\sinh\psi\cos\varphi - \sinh\psi_w\cos\varphi_d)^2 + \\ &\quad + (\cosh\psi\sin\varphi - \cosh\psi_w\sin\varphi_d)^2\,. \end{aligned} \tag{6.123}$$

In equation (6.122), the following relations have been used:

$$\begin{aligned} x_d &= 0, \\ y_d &= c\sinh\psi_w\cos\varphi_d, \\ z_d &= c\cosh\psi_w\sin\varphi_d, \\ y &= c\sinh\psi\cos\varphi, \\ z &= c\cosh\psi_w\sin\varphi, \\ \mathrm{d}s_d &= c\sqrt{\sinh^2\psi_w + \cos^2\varphi_d}\;\mathrm{d}\varphi_d. \end{aligned} \tag{6.124}$$

Integrating over the lifting line yields the small perturbation acceleration potential of all doublets positioned on the elliptical lifting line:

$$\Psi\,(x,\psi,\varphi,\psi_w) = \tfrac{1}{8\pi c}\int_0^{2\pi} m\,(\varphi_d)\,\tfrac{H_3}{H_4^{\frac{3}{2}}}\,\mathrm{d}\varphi_d, \tag{6.125}$$

where

$$\begin{aligned} H_3 &= (\sinh(\psi+\psi_w)\cos(\varphi-\varphi_d) + \sinh(\psi-\psi_w)\cos(\varphi+\varphi_d) - \sinh 2\psi_w)\,, \\ H_4 &= X^2 + \sinh^2\psi + \sin^2\varphi + \sinh^2\psi_w + \sin^2\varphi_d + \\ &\quad - \cosh(\psi+\psi_w)\cos(\varphi-\varphi_d) + \cosh(\psi-\psi_w)\cos(\varphi+\varphi_d)\,. \end{aligned} \tag{6.126}$$

6.4.2 Small Perturbation Velocity Potential

Using the procedure adopted in the previous sections, it is possible to obtain the small perturbation velocity potential:

$$\phi = \tfrac{1}{8\pi V_\infty}\int_0^{2\pi} m\,(\varphi_d)\,\tfrac{H_3}{H_4 - X^2}\left(\tfrac{X}{\sqrt{H_4}} + 1\right)\mathrm{d}\varphi_d. \tag{6.127}$$

6.4.3 Imposition of Weissinger's Condition

Weissinger's condition consists of the WTC imposed in $X_0 = \frac{l}{2c}$:

$$-\alpha(\varphi) = \frac{1}{V_\infty}\left(\frac{1}{h}\frac{\partial\phi(X,\psi,\varphi,\psi_w)}{\partial\psi}\right)_{X=X_0;\,\psi=\psi_w}. \tag{6.128}$$

The explicit form of the derivatives and the treatment of the consequent singular term are given in appendix I.

6.4.4 Integral Equation with the Variables φ, φ_d

Using the relations found above, the final expression of Weissinger's condition can be written. It is represented by an integral equation containing the unknown function $m(\varphi)$, which is the doublet distribution on the elliptical lifting line. Thus:

$$\begin{aligned}-\alpha(\varphi) = \tfrac{1}{8\pi c V_\infty^2}\frac{1}{\sqrt{\left(\sinh^2\psi_w+\cos^2\varphi\right)}}\fint_0^{2\pi} m(\varphi_d)\Big(\Big[f_2\tfrac{\partial f_3}{\partial\psi}\Big]_{\psi=\psi_w,X=X_0}+\\ +\left(\left[\tfrac{\partial f_2}{\partial\psi}\right]f_3\right)_{\psi=\psi_w,X=X_0}\Big)\,\mathrm{d}\varphi_d,\end{aligned} \tag{6.129}$$

where

$$\begin{aligned}
&\Big[f_2\tfrac{\partial f_3}{\partial\psi}\Big]_{\psi=\psi_w,X=X_0} = \tfrac{X_0\cosh^2\psi_w\sinh^2\psi_w(1-\cos(\varphi-\varphi_d))}{(H_5)(H_6)^{\frac{3}{2}}},\\
&\left(\left[\tfrac{\partial f_2}{\partial\psi}\right]f_3\right)_{\psi=\psi_w,X=X_0} = \left(\left[\tfrac{\partial f_2}{\partial\psi}\right]^R f_3\right)_{\psi=\psi_w,X=X_0} + \left(\left[\tfrac{\partial f_2}{\partial\psi}\right]^S f_3\right)_{\psi=\psi_w,X=X_0},\\
&\left(\left[\tfrac{\partial f_2}{\partial\psi}\right]^S f_3\right)_{\psi=\psi_w,X=X_0} = \tfrac{\cosh^2\psi_w\cos(\varphi-\varphi_d)-\sin\varphi\sin\varphi_d}{(H_5)}\cdot f_I - \tfrac{\cosh(2\psi_w)}{(H_5)}+\\
&\qquad\qquad +\boxed{\tfrac{2}{1-\cos(\varphi-\varphi_d)}},\\
&\left(\left[\tfrac{\partial f_2}{\partial\psi}\right]^R f_3\right)_{\psi=\psi_w,X=X_0} = \tfrac{\sinh^2\psi_w\cosh^2\psi_w}{(H_5)^2}\left(\tfrac{X_0}{\sqrt{H_6}}+1\right),\\
&f_I = \tfrac{-2(H_5)}{\left(X_0+\sqrt{H_6}\right)\sqrt{H_6}},\\
&H_5 = \sinh^2\psi_w+\cos^2\tfrac{\varphi+\varphi_d}{2},\\
&H_6 = X_0^2+2\left(\sinh^2\psi_w+\cos^2\tfrac{\varphi+\varphi_d}{2}\right)(1-\cos(\varphi-\varphi_d)).
\end{aligned} \tag{6.130}$$

The term inside the box is the singular term: when $\varphi \to \varphi_d$ the term becomes infinite. In the next section, the same equation written in terms of the new variables

t and s, which have the property to transform all intervals of integration in the manner: [0,2π] $\rightarrow$ [$-1, +1$], will be seen.

6.4.5 Integral Equation with the Variables t, s

The new variables t and s are defined as

$$\varphi_d = \pi\left(t+1\right) ,\varphi = \pi\left(s+1\right). \tag{6.131}$$

Observing the previous equation, it can be deduced that:

$$\begin{aligned} &\mathrm{d}\varphi_d = \pi \mathrm{d}t, \\ &\varphi - \varphi_d = \pi\left(s-t\right), \\ &\sin\left(\pi\left(s+1\right)\right) = \sin\left(\pi s+\pi\right) = -\sin\left(\pi s\right), \\ &\sin\left(\pi\left(t+1\right)\right) = \sin\left(\pi t+\pi\right) = -\sin\left(\pi t\right). \end{aligned} \tag{6.132}$$

Substituting into the integral equation yields:

$$\begin{aligned} -\alpha\left(s\right) = \frac{1}{8cV_\infty^2\sqrt{\left(\sinh^2\psi_w+\cos^2(\pi s)\right)}} \oint_{-1}^{+1} m\left(t\right)\Big(\Big[f_2\frac{\partial f_3}{\partial\psi}\Big]_{\psi=\psi_w,X=X_0} + \\ +\Big(\Big[\frac{\partial f_2}{\partial\psi}\Big]f_3\Big)_{\psi=\psi_w,X=X_0}\Big)\mathrm{d}t, \end{aligned} \tag{6.133}$$

where

$$\begin{aligned} &\Big[f_2\frac{\partial f_3}{\partial\psi}\Big]_{\psi=\psi_w,X=X_0} = \frac{X_0\cosh^2\psi_w\sinh^2\psi_w(1-\cos(\pi(t-s)))}{(H_5)(H_6)^{3/2}}, \\ &\Big(\Big[\frac{\partial f_2}{\partial\psi}\Big]f_3\Big)_{\psi=\psi_w,X=X_0} = \Big(\Big[\frac{\partial f_2}{\partial\psi}\Big]^R f_3\Big)_{\psi=\psi_w,X=X_0} + \Big(\Big[\frac{\partial f_2}{\partial\psi}\Big]^S f_3\Big)_{\psi=\psi_w,X=X_0}, \\ &\Big(\Big[\frac{\partial f_2}{\partial\psi}\Big]^S f_3\Big)_{\psi=\psi_w,X=X_0} = \frac{\cosh^2\psi_w\cos(\pi(t-s))-\sin(\pi s)\sin(\pi t)}{(H_5)}f_I - \frac{\cosh(2\psi_w)}{(H_5)} + \\ &\qquad\qquad + \boxed{\frac{2}{(1-\cos(\pi(t-s)))}}, \\ &\Big(\Big[\frac{\partial f_2}{\partial\psi}\Big]^R f_3\Big)_{\psi=\psi_w,X=X_0} = \frac{\sinh^2\psi_w\cosh^2\psi_w}{(H_5)^2}\Big(\frac{X_0}{\sqrt{H_6}}+1\Big), \\ &f_I = \frac{-2(H_5)}{\left(X_0+\sqrt{H_6}\right)\sqrt{H_6}}, \\ &H_5 = \sinh^2\psi_w + \cos^2\Big(\frac{\pi(t+s)}{2}\Big), \\ &H_6 = X_0^2 + 2\Big(\sinh^2\psi_w + \cos^2\Big(\frac{\pi(t+s)}{2}\Big)\Big)\left(1-\cos\left(\pi\left(t-s\right)\right)\right). \end{aligned} \tag{6.134}$$

6.4.6 Total Lifting Force

Recalling the convention for the positive sign of the doublet axis, the aerodynamic force, which acts outward from the local center of curvature, is

$$F(\varphi_d) = -(-\rho m(\varphi_d)) = \rho m(\varphi_d). \tag{6.135}$$

The local normal direction is the aerodynamic force direction. Recalling the expression of the unit vector, which acts outward from the local center of curvature:

$$\mathbf{N}_d = -\mathbf{n}_d = \frac{\cos\varphi_d \cosh\psi_w}{\sqrt{\sinh^2\psi_w + \cos^2\varphi_d}}\mathbf{j} + \frac{\sin\varphi_d \sin\psi_w}{\sqrt{\sinh^2\psi_w + \cos^2\varphi_d}}\mathbf{k}, \tag{6.136}$$

It easy to obtain (see figure 6.14)[15]:

$$\sin\beta = (\mathbf{N}_d)_z = \frac{\sin\varphi_d \sin\psi_w}{\sqrt{\sinh^2\psi_w + \cos^2\varphi_d}}. \tag{6.137}$$

The *local* lift is:

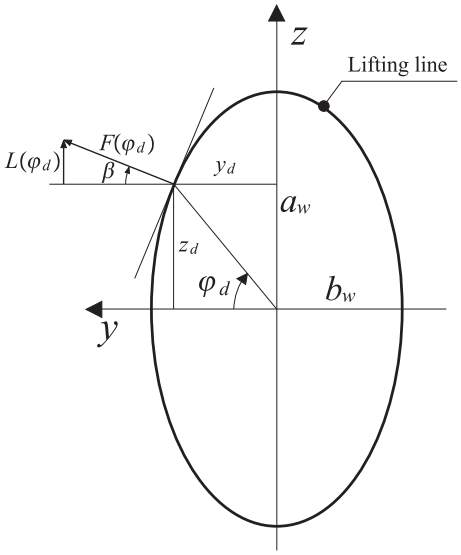

Figure 6.14. Calculation of the lifting force.

$$L(\varphi_d) = F(\varphi_d)\sin\beta = \rho_\infty m(\varphi_d)\frac{\sin\varphi_d \sin\psi_w}{\sqrt{\sinh^2\psi_w + \cos^2\varphi_d}}. \tag{6.138}$$

[15]Notice that vector $\mathbf{N}_d$ has modulus equal to one.

The total lifting force is determined by integrating

$$L = \int_{ll} L\left(s_d\right)\, \mathrm{d}s_d. \tag{6.139}$$

But it has been demonstrated that $\mathrm{d}s_d = c\sqrt{\sinh^2\psi_w + \cos^2\varphi_d}\,\mathrm{d}\varphi_d$; thus[16],

$$L = c\int_0^{2\pi} L\left(\varphi_d\right)\sqrt{\sinh^2\psi_w + \cos^2\varphi_d}\,\mathrm{d}\varphi_d = \rho_\infty b_w \int_0^{2\pi} m\left(\varphi_d\right)\sin\varphi_d\,\mathrm{d}\varphi_d. \tag{6.140}$$

Using the variable t instead of φ_d:

$$L = -\rho_\infty \pi b_w \int_{-1}^{+1} m\left(t\right)\sin\left(\pi t\right)\,\mathrm{d}t. \tag{6.141}$$

The corresponding coefficient of lift (using the reference surface $S = 4b_w l$) is

$$C_L = \frac{L}{\frac{1}{2}\rho_\infty S V_\infty^2} = -\frac{\pi}{2lV_\infty^2}\int_{-1}^{+1} m\left(t\right)\sin\left(\pi t\right)\,\mathrm{d}t. \tag{6.142}$$

6.4.7 Normalwash $\left[u_n\left(\varphi\right)\right]_{X=0}$

The induced velocity perpendicular to the lifting line is very important in the induced drag calculation. It is not difficult to analytically find the expression of the induced velocity. It is sufficient to use the small perturbation velocity potential:

$$\left[u_n\left(\varphi\right)\right]_{X=0} = \left(\frac{1}{h}\frac{\partial\phi\left(X,\psi,\varphi,\psi_w\right)}{\partial\psi}\right)_{\psi=\psi_w;\,X=0}. \tag{6.143}$$

Obviously, the positive direction of the induced velocity acts outward from the local center of curvature. Using the previous expressions, the normalwash equation is obtained:

$$\begin{aligned}\left[u_n\left(\varphi\right)\right]_{X=0} = {} & \frac{1}{8\pi c V_\infty\sqrt{\sinh^2\psi_w+\cos^2\varphi_d}} \oint_0^{2\pi} m\left(\varphi_d\right)\Big(\left[f_2\tfrac{\partial f_3}{\partial\psi}\right]_{\psi=\psi_w,X=0} + \\ & + \left(\left[\tfrac{\partial f_2}{\partial\psi}\right]f_3\right)_{\psi=\psi_w,X=0}\Big)\,\mathrm{d}\varphi_d,\end{aligned} \tag{6.144}$$

[16] Notice that $c\sinh\psi_w = b_w$.

where

$$\begin{aligned}
&\left[f_2 \frac{\partial f_3}{\partial \psi}\right]_{\psi=\psi_w, X=0} = 0 \\
&\left(\left[\frac{\partial f_2}{\partial \psi}\right] f_3\right)_{\psi=\psi_w, X=0} = \left(\left[\frac{\partial f_2}{\partial \psi}\right]^R f_3\right)_{\psi=\psi_w, X=0} + \left(\left[\frac{\partial f_2}{\partial \psi}\right]^S f_3\right)_{\psi=\psi_w, X=0}, \\
&\left(\left[\frac{\partial f_2}{\partial \psi}\right]^S f_3\right)_{\psi=\psi_w, X=0} = -\frac{\frac{1}{2}\cosh(2\psi_w)}{\left(\sinh^2\psi_w + \cos^2\frac{\varphi+\varphi_d}{2}\right)} + \boxed{\frac{1}{1-\cos(\varphi-\varphi_d)}}, \\
&\left(\left[\frac{\partial f_2}{\partial \psi}\right]^R f_3\right)_{\psi=\psi_w, X=0} = \frac{\sinh^2\psi_w \cosh^2\psi_w}{\left(\sinh^2\psi_w + \cos^2\frac{\varphi+\varphi_d}{2}\right)^2}.
\end{aligned} \tag{6.145}$$

Expressing the normalwash equation with the variables t and s yields:

$$\begin{aligned}
[u_n(s)]_{X=0} = \frac{1}{8cV_\infty\sqrt{\sinh^2\psi_w + \cos^2(\pi t)}} \oint_{-1}^{+1} m(t) \Big(&\left[f_2 \frac{\partial f_3}{\partial \psi}\right]_{\psi=\psi_w, X=0} + \\
&+ \left(\left[\frac{\partial f_2}{\partial \psi}\right] f_3\right)_{\psi=\psi_w,\, X=0} \Big)\, \mathrm{d}t,
\end{aligned} \tag{6.146}$$

where

$$\begin{aligned}
&\left[f_2 \frac{\partial f_3}{\partial \psi}\right]_{\psi=\psi_w, X=0} = 0 \\
&\left(\left[\frac{\partial f_2}{\partial \psi}\right] f_3\right)_{\psi=\psi_w, X=0} = \left(\left[\frac{\partial f_2}{\partial \psi}\right]^R f_3\right)_{\psi=\psi_w, X=0} + \left(\left[\frac{\partial f_2}{\partial \psi}\right]^S f_3\right)_{\psi=\psi_w, X=0}, \\
&\left(\left[\frac{\partial f_2}{\partial \psi}\right]^S f_3\right)_{\psi=\psi_w, X=0} = -\frac{\frac{1}{2}\cosh(2\psi_w)}{\left(\sinh^2\psi_w + \cos^2\left(\frac{\pi(t+s)}{2}\right)\right)} + \boxed{\frac{1}{(1-\cos(\pi(t-s)))}}, \\
&\left(\left[\frac{\partial f_2}{\partial \psi}\right]^R f_3\right)_{\psi=\psi_w, X=0} = \frac{\sinh^2\psi_w \cosh^2\psi_w}{\left(\sinh^2\psi_w + \cos^2\left(\frac{\pi(t+s)}{2}\right)\right)^2}.
\end{aligned} \tag{6.147}$$

Observation 29 It is easy to demonstrate that

$$[u_n(\varphi)]_{X=0} = \frac{1}{2}[u_n(\varphi)]_{X\to\infty}, \tag{6.148}$$

as has been found for the other cases.

6.4.8 Evaluation of the Induced Drag

Using the same procedure adopted for the other annular wings, it possible to obtain the induced drag and the coefficient of induced drag equations:

$$D_i = \oint_0^{2\pi} \rho_\infty c m(\varphi_d) \left(-\frac{[u_n(\varphi_d)]_{X=0}}{V_\infty}\right) \sqrt{\sinh^2\psi_w + \cos^2\varphi_d}\, \mathrm{d}\varphi_d, \tag{6.149}$$

$$C_{D_i} = \frac{c}{2b_w l V_\infty^3} \oint_0^{2\pi} m\left(\varphi_d\right) \sqrt{\sinh^2 \psi_w + \cos^2 \varphi_d} \left(-\left[u_n\left(\varphi_d\right)\right]_{X=0}\right) \, \mathrm{d}\varphi_d. \tag{6.150}$$

Expressing the equation with the variables t and s yields:

$$C_{D_i} = \frac{\pi c}{2b_w l V_\infty^3} \oint_{-1}^{+1} m\left(t\right) \sqrt{\sinh^2 \psi_w + \cos^2\left(\pi t\right)} \, \left(-\left[u_n\left(t\right)\right]_{X=0}\right) \, \mathrm{d}t. \tag{6.151}$$

Nomenclature

α	angle of attack
α_i	induced angle of attack
ρ	fluid density
ϕ	small perturbation velocity potential
Ψ	small perturbation acceleration potential
Γ	circulation
γ_x	distributed trailing vorticity
u_n	normalwash
$2b_w$	wing span
l	chord
M	doublet
m	doublet distribution
L	lift
D_i	induced drag
C_L	coefficient of lift
C_{D_i}	coefficient of induced drag
F	algebraic expression, aerodynamic force
t, s	auxiliary variables
V_∞	velocity (freestream conditions)
$\fint$	Hadamard finite-part integral
$\int\!\!\!\!\!\!-$	integral defined in the Cauchy principal values sense
b_w	semi-axis elliptical annular wing
a_w	semi-axis elliptical annular wing
R_w	radius of a circular annular wing
$\mathrm{d}s, \mathrm{d}s_d$	infinitesimal length
R, φ	coordinates used in the circular annular wing
ψ, φ	coordinates used in the elliptical annular wing
c	$\sqrt{b_w^2 - a_w^2}$, $\sqrt{a_w^2 - b_w^2}$
X	$\frac{x}{R_w}$, $\frac{x}{c}$
X_0	$\frac{l}{2R_w}$, $\frac{l}{2c}$
D	distance between a generic point and a point on the wing
$\boldsymbol{i}, \boldsymbol{j}, \boldsymbol{k}$	unit vectors
$\boldsymbol{n}_\varphi, \boldsymbol{n}_{\gamma_x}$	unit vectors
$\boldsymbol{n}_d, \boldsymbol{N}_d$	unit vectors
WTC	Wall Tangency Condition

Subscripts

∞	freestream conditions
d	doublet
w	quantity referred to the wing

Chapter 7

Elliptical Lifting Arcs. Analytical Formulation

7.1 Introduction

Chapter 6 introduced the theory related to the annular wings. But it is interesting to see, from an aerodynamic point of view, *what happens if a closed wing system with a non-planar wing system like an arc is compared*. To illustrate this concept, the differences between the elliptical annular wing (see wing 1 in figure 7.1) and elliptical lifting arcs (see wings 2-4 in figure 7.1) should be understood. In this chapter, the

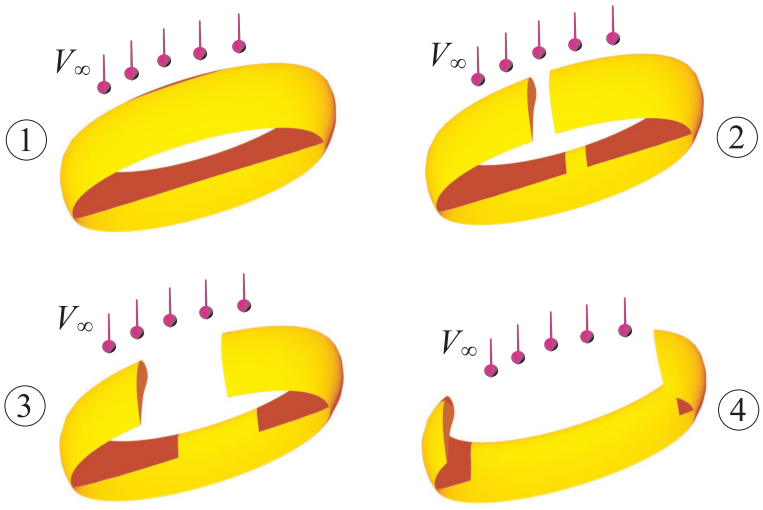

Figure 7.1. A few examples of elliptical annular wing and elliptical lifting arcs.

elliptical lifting arcs obtained from an annular wing with $b_w > a_w$ will be analyzed.

Obviously, the formulation reported here is extendable to the cases in which $b_w = a_w$ or $b_w < a_w$[1]. Notice that with this mathematical model winglets and C-wings can be described as well. It is important to know that future analyses are valid only from an aerodynamic point of view. Other aspects of the design (aeroelasticity, for example) have to be taken into account when studying a wing system [14].

7.2 Convex Elliptical Lifting Arcs

The convex elliptical lifting arcs (see figure 7.2) can be studied similarly, as have been done for the other wings. This means using a doublet distribution, writing

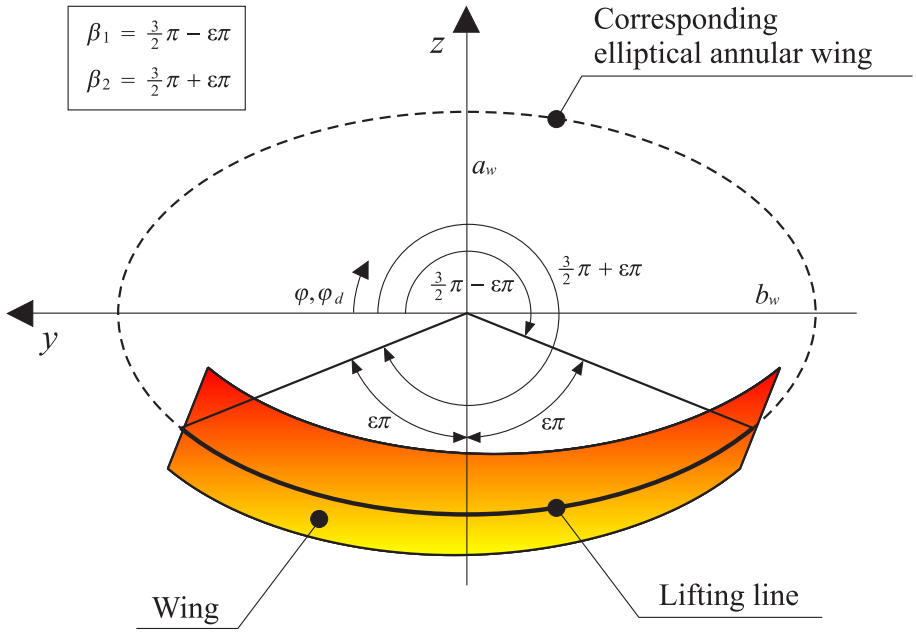

Figure 7.2. Convex Elliptical Lifting Arcs. Geometry and notations.

the small perturbation acceleration potential, imposing Weissinger's condition and finding the integral equation. But there is a simple way to achieve the same goal: the same equations (opportunely modified) used for the corresponding annular wings can be used. Consider an annular wing. It has been found that the total lift and induced drag have the expressions:

$$L = \rho_\infty b_w \int_0^{2\pi} m\left(\varphi_d\right) \sin\varphi_d \, \mathrm{d}\varphi_d, \tag{7.1}$$

[1]Clearly, the corresponding annular wings will be circular and elliptical (with $b_w < a_w$), respectively.

$$D_i = -\frac{\rho_\infty}{8\pi V_\infty^2} \int_0^{2\pi} m(\varphi_d) \int_0^{2\pi} m(\varphi) \left(\frac{\sinh^2\psi_w \cosh^2\psi_w}{\left(\sinh^2\psi_w + \sin^2\frac{\varphi+\varphi_d}{2}\right)^2} - \frac{\frac{1}{2}\cosh(2\psi_w)}{\left(\sinh^2\psi_w + \sin^2\frac{\varphi+\varphi_d}{2}\right)} \right) \mathrm{d}\varphi\, \mathrm{d}\varphi_d + \\ -\frac{\rho_\infty}{8\pi V_\infty^2} \int_0^{2\pi} m(\varphi_d) \, \Xint=_0^{2\pi} \frac{m(\varphi)}{1-\cos(\varphi-\varphi_d)} \mathrm{d}\varphi\, \mathrm{d}\varphi_d. \tag{7.2}$$

What is the difference between the annular wing and the elliptical arc wing? Because of the supposed linearity, the difference is only in the integration domain. Therefore, it can be concluded that for elliptical arcs (see figure 7.2)[2]:

$$L = \rho_\infty b_w \int_{\beta_1}^{\beta_2} m(\varphi_d) \sin\varphi_d \, \mathrm{d}\varphi_d, \tag{7.3}$$

$$D_i = -\frac{\rho_\infty}{8\pi V_\infty^2} \int_{\beta_1}^{\beta_2} m(\varphi_d) \int_{\beta_1}^{\beta_2} m(\varphi) \left(\frac{\sinh^2\psi_w \cosh^2\psi_w}{\left(\sinh^2\psi_w + \sin^2\frac{\varphi+\varphi_d}{2}\right)^2} - \frac{\frac{1}{2}\cosh(2\psi_w)}{\left(\sinh^2\psi_w + \sin^2\frac{\varphi+\varphi_d}{2}\right)} \right) \mathrm{d}\varphi\, \mathrm{d}\varphi_d + \\ -\frac{\rho_\infty}{8\pi V_\infty^2} \int_{\beta_1}^{\beta_2} m(\varphi_d) \, \Xint=_{\beta_1}^{\beta_2} \frac{m(\varphi)}{1-\cos(\varphi-\varphi_d)} \mathrm{d}\varphi\, \mathrm{d}\varphi_d, \tag{7.4}$$

where

$$\begin{aligned} \beta_1 &= \tfrac{3}{2}\pi - \varepsilon\pi, \\ \beta_2 &= \tfrac{3}{2}\pi + \varepsilon\pi. \end{aligned} \tag{7.5}$$

For a numerical analysis, it is useful to convert the domain of integration. Thus[3]:

$$\begin{aligned} \varphi_d &= \tfrac{3}{2}\pi + \varepsilon\pi t, \\ \varphi &= \tfrac{3}{2}\pi + \varepsilon\pi s. \end{aligned} \tag{7.6}$$

With this transformation, it can be concluded that

$$L = -\varepsilon\pi\rho_\infty b_w \int_{-1}^{+1} m(t) \cos(\varepsilon\pi t) \, \mathrm{d}t, \tag{7.7}$$

$$D_i = -\frac{\rho_\infty \varepsilon^2 \pi}{8 V_\infty^2} \int_{-1}^{+1} m(s) \int_{-1}^{+1} m(t) \left(\frac{\sinh^2\psi_w \cosh^2\psi_w}{\left(\sinh^2\psi_w + \cos^2\left(\varepsilon\pi\frac{t+s}{2}\right)\right)^2} - \frac{\frac{1}{2}\cosh(2\psi_w)}{\left(\sinh^2\psi_w + \cos^2\left(\varepsilon\pi\frac{t+s}{2}\right)\right)} \right) \mathrm{d}t\, \mathrm{d}s + \\ -\frac{\rho_\infty \varepsilon^2 \pi}{8 V_\infty^2} \int_{-1}^{+1} m(s) \, \Xint=_{-1}^{+1} \frac{m(t)}{1-\cos(\varepsilon\pi(t-s))} \mathrm{d}t\, \mathrm{d}s. \tag{7.8}$$

[2]Notice that, now, the external integral in the expression of D_i is neither a Hadamard finite-part integral nor a Cauchy integral *because the doublet distribution must be zero at the tips.*

[3]The variables t and s *are not* the same variables t and s used for the elliptical annular wing.

The corresponding coefficients of lift and induced drag are, respectively,

$$C_L = -\frac{2\varepsilon\pi b_w}{SV_\infty^2}\int_{-1}^{+1} m\left(t\right)\cos\left(\varepsilon\pi t\right)\,\mathrm{d}t, \tag{7.9}$$

$$\begin{aligned} C_{D_i} = &-\frac{\varepsilon^2\pi}{4SV_\infty^4}\int_{-1}^{+1} m\left(s\right)\int_{-1}^{+1} m\left(t\right)\left(\frac{\sinh^2\psi_w\cosh^2\psi_w}{\left(\sinh^2\psi_w+\cos^2\left(\varepsilon\pi\frac{t+s}{2}\right)\right)^2}-\frac{\frac{1}{2}\cosh(2\psi_w)}{\left(\sinh^2\psi_w+\cos^2\left(\varepsilon\pi\frac{t+s}{2}\right)\right)}\right)\mathrm{d}t\,\mathrm{d}s+\\ &-\frac{\varepsilon^2\pi}{4SV_\infty^4}\int_{-1}^{+1} m\left(s\right)\,\#\!\!\!\!\!\!\int_{-1}^{+1}\frac{m(t)}{1-\cos(\varepsilon\pi(t-s))}\,\mathrm{d}t\,\mathrm{d}s. \end{aligned} \tag{7.10}$$

S is the reference surface, and it can be chosen as the projection of the wing on plane $x-y$:

$$\begin{aligned} S &= 2lb_w\sin\varepsilon\pi \qquad \text{if } \varepsilon < \tfrac{1}{2},\\ S &= 2lb_w \qquad\quad \text{if } \varepsilon \geq \tfrac{1}{2}. \end{aligned} \tag{7.11}$$

S can also be chosen to be equal to $4b_w l$, in order to have an easy comparison with the elliptical annular wing.

7.3 Concave Elliptical Lifting Arcs

The concave elliptical lifting arcs (see figure 7.3) can be studied similarly, as in the previous section. In a formal point of view, equations (7.3) and (7.4) are still valid. Only the definition of β_1 and β_2 (see figure 7.3) are different:

$$\begin{aligned} \beta_1 &= \tfrac{\pi}{2}-\varepsilon\pi,\\ \beta_2 &= \tfrac{\pi}{2}+\varepsilon\pi. \end{aligned} \tag{7.12}$$

The new variables t and s are now defined as

$$\begin{aligned} \varphi_d &= \tfrac{\pi}{2}+\varepsilon\pi t,\\ \varphi &= \tfrac{\pi}{2}+\varepsilon\pi s. \end{aligned} \tag{7.13}$$

Therefore, the expressions for the lifting force and induced drag are

$$L = \varepsilon\pi\rho_\infty b_w\int_{-1}^{+1} m\left(t\right)\cos\left(\varepsilon\pi t\right)\,\mathrm{d}t, \tag{7.14}$$

$$\begin{aligned} D_i = &-\frac{\rho_\infty\varepsilon^2\pi}{8V_\infty^2}\int_{-1}^{+1} m\left(s\right)\int_{-1}^{+1} m\left(t\right)\left(\frac{\sinh^2\psi_w\cosh^2\psi_w}{\left(\sinh^2\psi_w+\cos^2\left(\varepsilon\pi\frac{t+s}{2}\right)\right)^2}-\frac{\frac{1}{2}\cosh(2\psi_w)}{\left(\sinh^2\psi_w+\cos^2\left(\varepsilon\pi\frac{t+s}{2}\right)\right)}\right)\mathrm{d}t\,\mathrm{d}s+\\ &-\frac{\rho_\infty\varepsilon^2\pi}{8V_\infty^2}\int_{-1}^{+1} m\left(s\right)\,\#\!\!\!\!\!\!\int_{-1}^{+1}\frac{m(t)}{1-\cos(\varepsilon\pi(t-s))}\,\mathrm{d}t\,\mathrm{d}s. \end{aligned} \tag{7.15}$$

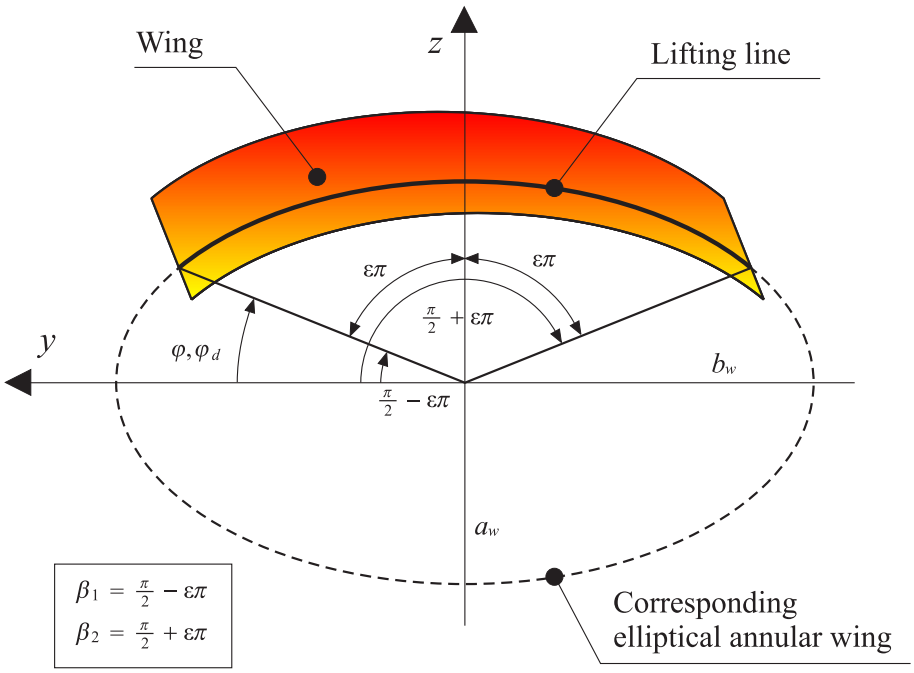

Figure 7.3. Concave Elliptical Lifting Arcs. Geometry and notations.

Notice that in the expression of the lifting force only the sign is changed, while in the expression of the induced drag nothing is changed. Thus, the non-dimensional coefficient will be the same as before, except the fact that now the sign of the coefficient of lift is changed. Also, the reference surface expressions are the same (see equation (7.11)).

Nomenclature

ρ	fluid density
l	chord
m	doublet distribution
L	lift
D_i	induced drag
C_L	coefficient of lift
C_{D_i}	coefficient of induced drag
V_∞	velocity (freestream conditions)
$\fint$	Hadamard finite-part integral
$\int\!\!\!\!\!\!-$	integral defined in the Cauchy principal values sense
b_w	semi-axis of the corresponding elliptical annular wing
a_w	semi-axis of the corresponding elliptical annular wing
ψ, φ	coordinates used in the elliptical annular wing
ε	see figures 7.2 and 7.3
β_1, β_2	see figures 7.2 and 7.3

Subscripts

∞	freestream conditions
d	doublet
w	quantity referred to the wing

Chapter 8

Numerical Validation

8.1 Introduction

In chapter 6 the analytical expression for the total lifting force and induced drag of annular wings were obtained. Also, from Weissinger's condition, the integral equation containing the unknown doublet distribution on the lifting line representing the wing was obtained. It is clear that the present approach for solving the aerodynamic problem consists of the following steps:

- *Step 1*
  Writing of Weissinger's condition and the integral equation containing the unknown m (see chapter 6 for the annular wings and chapter 5 for the biplane).

- *Step 2*
  Solving of the integral equation which contains Hadamard finite-part integrals (see chapter 2).

- *Step 3*
  Determining of the total lifting force using the calculated doublet distribution m.

- *Step 4*
  Determining of the induced drag using the calculated doublet distribution m.

In the discussion of biplane and minimum induced drag conditions in chapter 5, not all related issues were explicitly considered. This chapter will analyze those issues and show how they can be solved.

8.2 Integral Equation: Numerical Solution

Consider the elliptical annular wing with $b_w > a_w$[1]. As was seen in chapter 6, the integral equation with the unknown doublet distribution is in the form of

$$-\alpha(s) = \frac{1}{8cV_\infty^2\sqrt{\left(\cosh^2\psi_w - \cos^2(\pi s)\right)}} \oint_{-1}^{+1} m(t)\left(f_{\text{int}}^R(t,s) + f_{\text{int}}^S(t,s)\right) \mathrm{d}t, \quad (8.1)$$

where f_{int}^R and f_{int}^S are the regular and singular[2] functions, respectively. In chapter 2, the numerical methods available to solve that equation were discussed. In particular, the collocation method and a few particular techniques to manipulate the Hadamard finite-part integrals were discussed.
When using the collocation method, the functions f_{int}^R and f_{int}^S have to be calculated at some points. Thus, the integrals[3] must be calculated numerically. Particularly difficult is the calculation of the *regular integrals* involving function f_{int}^R, because this function shows very high gradients; hence, the Gaussian quadrature is not always very accurate. In order to analyze this problem in more detail, consider an elliptical annular wing with the following data[4]:

$$\begin{aligned} &l = 1,\ V_\infty = 2,\ b_w = 12,\ a_w = 10,\ c^2 = b_w^2 - a_w^2 = 44, \\ &\cosh^2\psi_w = \tfrac{b_w^2}{b_w^2 - a_w^2} = \tfrac{36}{11},\ \ \sinh^2\psi_w = \tfrac{a_w^2}{b_w^2 - a_w^2} = \tfrac{25}{11},\ \ X_0 = \tfrac{l}{2c} = \tfrac{1}{44}\sqrt{11}. \end{aligned} \quad (8.2)$$

In figures 8.1 and 8.2, the behavior of the function f_{int}^R versus the variable t with fixed s is illustrated. As can be seen, *the Gaussian quadrature* is not a very good method to integrate this function. This problem is particularly evident in the *induced drag computation.* Therefore, an adaptive subroutine (H2A1D from the ABACI library) has been used.

8.2.1 Collocation Method: Numerical Study

The collocation method has been discussed. But the important question to answer is: how many points are required in order to have a good accuracy? As will be seen later, 20 points give sufficient precision of the results. In order to show that, consider the following case.

[1] The numerical issues that will be analyzed are, also, valid for the other annular wings, elliptical lifting arcs, biplane and, in general, for all wings studied using the present procedure.
[2] See chapter 6 for their explicit form.
[3] Regular integrals for the function f_{int}^R and Hadamard integrals for the function f_{int}^S.
[4] All lengths are expressed in meters.

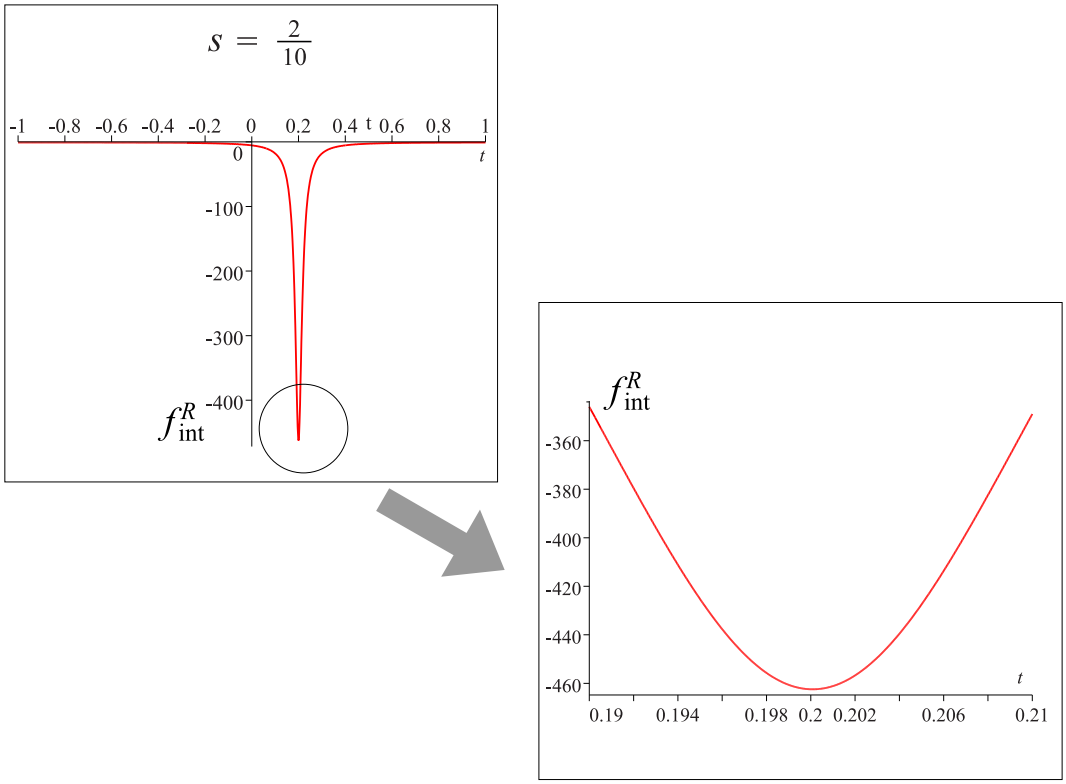

Figure 8.1. f^R_{int} versus t with $s = \frac{2}{10}$.

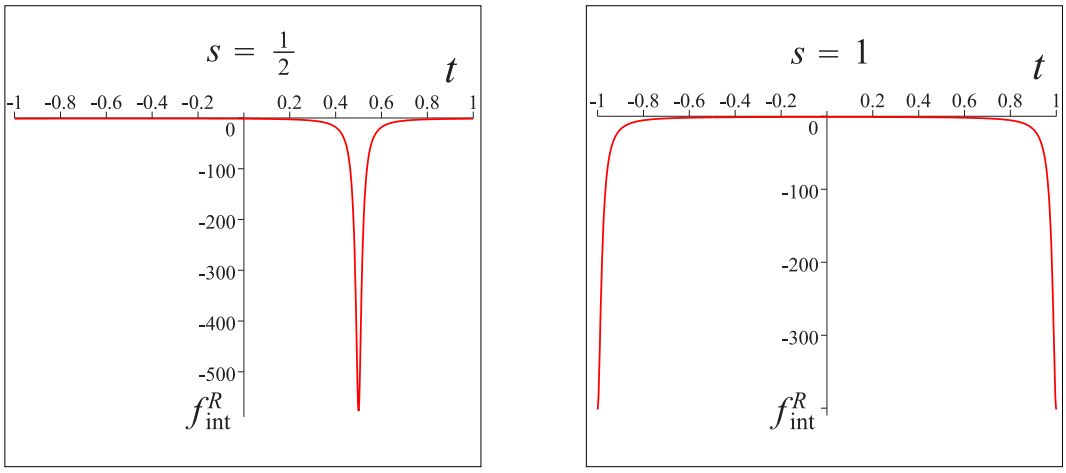

Figure 8.2. f^R_{int} versus t with $s = \frac{1}{2}$ and $s = 1$.

Elliptical Annular Wing with Twist Corresponding to a Rigid Rotation Along the y Axis

The elliptical annular wing with *twist* $\alpha(\varphi)$ corresponding to a *rigid rotation* Ω along the y axis will be analyzed. Recalling the expression

$$\sin\beta = \frac{\sin\varphi\cosh\psi_w}{\sqrt{\cosh^2\psi - \cos^2\varphi}}, \tag{8.3}$$

and considering figure 8.3, the twist corresponding to the rigid rotation Ω can be found:

$$\alpha(\varphi) = \Omega\sin\beta = \Omega\frac{\sin\varphi\cosh\psi_w}{\sqrt{\cosh^2\psi - \cos^2\varphi}}. \tag{8.4}$$

Now consider the particular case in which $\Omega = 1$[5]. The convergence test for two

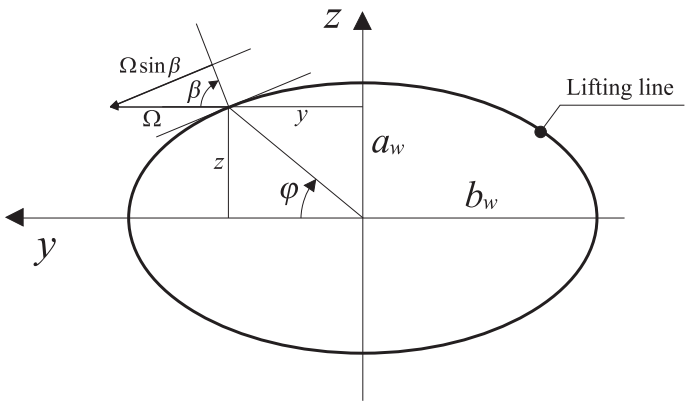

Figure 8.3. Incidence corresponding to a rigid rotation Ω along y.

different cases (ellipse and ellipse close to a circle[6]) is shown in figure 8.4. As illustrated in figure 8.4, 20 collocation points are sufficient in practical applications. Notice that in the biplane study (see chapter 5), 20 points were used as well.

8.3 Numerical Evaluation of the Induced Drag

Once the doublet distribution is found via integral equation solution, the lifting force can be calculated using a simple integration. Usually, this operation is not

[5]Because of the unitary value of Ω, the coefficient of lift could be seen as an angular coefficient of lift.

[6]Notice that the circular annular wing can be studied as a particular case of an elliptical annular wing in which $a_w \to b_w$.

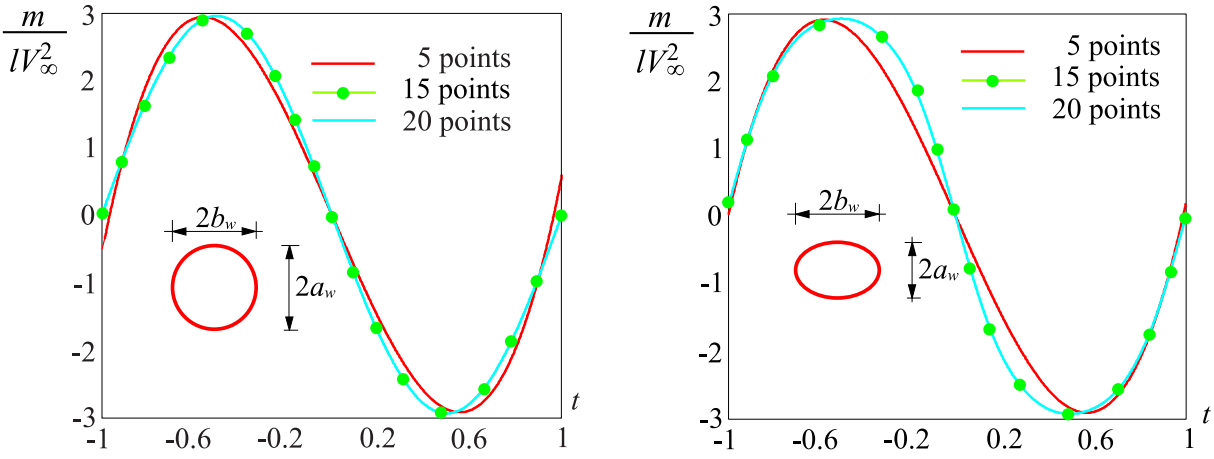

Figure 8.4. Convergence test when $\frac{a_w}{b_w} \to \frac{12}{12}$ and $\frac{a_w}{b_w} = \frac{8}{12}$.

difficult and the integral expressing the lift can be numerically computed using the Gaussian quadrature formula. For the induced drag, the calculation is less simple. In order to better understand the problem, consider the coefficient of induced drag in an elliptical annular wing with $b_w > a_w$[7]:

$$D_i = -\frac{\rho_\infty}{8\pi V_\infty^2} \int_0^{2\pi} m\left(\varphi_d\right) \int_0^{2\pi} m\left(\varphi\right) \left(\frac{\sinh^2\psi_w \cosh^2\psi_w}{\left(\sinh^2\psi_w + \sin^2\frac{\varphi+\varphi_d}{2}\right)^2} - \frac{\frac{1}{2}\cosh(2\psi_w)}{\left(\sinh^2\psi_w + \sin^2\frac{\varphi+\varphi_d}{2}\right)} \right) \mathrm{d}\varphi\, \mathrm{d}\varphi_d + \\ -\frac{\rho_\infty}{8\pi V_\infty^2} \int_0^{2\pi} m\left(\varphi_d\right) \fint_0^{2\pi} \frac{m(\varphi)}{1-\cos(\varphi-\varphi_d)} \mathrm{d}\varphi\, \mathrm{d}\varphi_d. \tag{8.5}$$

Observing the integrand function inside the inner integral, it can be understood that it is of the same type of the integrand function appeared in the integral equation (figures 8.1 and 8.2 illustrate the behavior of that function). Therefore, it can be understood that:

- The Gaussian rule is not a good method to evaluate the inner integral due to high gradients of the function.
- The induced drag is a very small number compared to the magnitude of the other quantities (for example, C_L). Thus, a small error in the calculation of the doublet distribution m can create significant errors in the evaluation of the double integral used for the induced drag coefficient.

[7]Note that, here, the Cauchy integral is not used. The reason is that this dissertation analyzes only two cases: annular wing with a twist corresponding to a rigid rotation along y and annular wing under optimal conditions. In both cases, the doublet distribution is zero at both endpoints of the integral; as a result, the Cauchy integral becomes a standard integral.

Several different numerical approaches and techniques could be applied in this case.

- *Approach 1*
  The singular term in the integral equation (8.1) (now, m is a known function and, therefore, all integrals are easily calculable) is eliminated. In this method, the Hadamard integral does not have to be addressed, and this is the main advantage. But there is the numerical cancellation issue (round-off error), since, as it is possible to see, two terms with the same order of magnitude are algebraically added.
  Using this approach, three different methods have been developed:

  - *Method 1*
    Both of the integrals in the C_{D_i} expression are seen like integral in one variable and are calculated using an adaptive method (see chapter 2). The precision of the computation is very good[8], but the CPU usage, in terms of time, is slightly expensive.
  - *Method 2*
    The internal integral (which contains the non-smooth function) is calculated using the adaptive procedure, while the external integral is calculated using the classical Gaussian rule. Compared to method 1, this method is faster in terms of CPU time.
  - *Method 3*
    The internal and external integrals are calculated using a subroutine designed for double integrals (H2B2A from the ABACI library).

- *Approach 2*
  The Hadamard integral *is not* eliminated. This method is the only possible method if there is no interest in the solution of the direct problem[9] or if it can not be solved. A typical case is the minimum induced drag problem: the function $\alpha(s)$ is not known a priori; therefore, it can not be used to eliminate the Hadamard integral[10]. Using this approach, two different methods have been developed:

  - *Method 4*
    Both of the regular integrals (internal and external) are calculated using

[8] But the cancellation problem is more severe because the Hadamard integral is eliminated using the integral equation.

[9] The direct problem is represented by the integral equation (8.1).

[10] The Hadamard integral is not eliminated, but the cancellation issue is still present (but less significant), because equation (8.5) contains the term $\frac{\sinh^2\psi_w \cosh^2\psi_w}{\left(\sinh^2\psi_w + \sin^2\frac{\varphi+\varphi_d}{2}\right)^2} - \frac{\frac{1}{2}\cosh(2\psi_w)}{\left(\sinh^2\psi_w + \sin^2\frac{\varphi+\varphi_d}{2}\right)}$, which presents cancellation problem.

an adaptive procedure[11]. The Hadamard internal integral is calculated using the method shown in chapter 2.

– *Method 5*
The internal integral (the regular part) is computed using an adaptive procedure, while the external integral is calculated using a Gaussian rule. The external integral in the double integral that contains the Hadamard integral[12] is calculated using a Gaussian rule with a number of points coinciding with the number of the collocation points[13]. In the biplane study (see chapter 5), this method has been used.

Now consider a practical case in which the annular wing has $\frac{a_w}{b_w} \to \frac{12}{12}$, $\frac{b_w}{l} = 12$, $\Omega = 1$ and $\alpha(\varphi) = \Omega \frac{\sin\varphi \cosh\psi_w}{\sqrt{\cosh^2\psi - \cos^2\varphi}}$. In figure 8.5, the results of all five methods[14] are reported. From figure 8.5, it can be understood that, with the present formulation,

$\frac{a_w}{b_w} \to \frac{12}{12}$ $\frac{b_w}{l} = 12$	$10\, C_{D_i}$
Method 1	2.83
Method 2	2.83
Method 3	2.81
Method 4	2.87
Method 5	2.83

Figure 8.5. Coefficient of induced drag calculated using five different methods.

the coefficient of induced drag has two digits accuracy. This is not a problem if the nature of this dissertation is considered: the aim is to formulate an innovative, analytical approach for non-planar wings, and, for this objective the accuracy of the present method is acceptable. For more accurate results the concepts exposed in chapter 4 should be applied.

[11] The subroutine H2A1D was used.

[12] Obviously, the Hadamard integral is computed using the method shown in chapter 2.

[13] Because, in the Gaussian rule, the nodes are the zeros of the Legendre polynomials and because the collocation method with the points calculated as zeros of the Legendre polynomial was used, it can be understood that using the Gaussian rule can minimize the error in this case.

[14] In the Gaussian quadrature formula, 200 points were used, except in case 5, where, for the external integral containing the Hadamard integral, 20 points were used (notice that in the collocation method as well 20 points were used). 200 Gauss points were used because, with the matured experience for these particular analyses, using the empirical relation $N_{\text{Gauss Points}} = 10 \cdot N_{\text{Collocation Points}}$ yielded good results. The required high number of Gauss points is clear if the complexity of the functions that have to be integrated is considered.

8.4 Effect of the Aspect Ratio

In this section, the effect of the aspect ratio on the induced drag as well as a few related numerical problems will be analyzed.
When the ratio of $\frac{a_w}{b_w}$ decreases, the function f^R_{int} nearly becomes singular. Clearly, this creates a problem in the evaluation of the lift and induced drag[15]. This problem can partially be avoided by increasing the number of collocation points, but when a_w/b_w is too small even this method does not work well.
Figure 8.6 illustrates the effect of the aspect ratio, when the incidence is correspondent to an unitary rigid rotation of the ellipse along the y axis (in all cases, $\frac{b_w}{l} = 12$). As can be seen, the induced drag increases as $\frac{a_w}{b_w}$ becomes smaller. In

a_w/b_w	C_L	$10\ C_{D_i}$
8/12	4.92	3.9
9/12	4.85	3.6
10/12	4.77	3.3
11/12	4.70	3.0
12/12	4.63	2.8

Figure 8.6. Coefficient of lift and induced drag. Aspect ratio effects

theory, it could not be concluded that the aerodynamics of the ellipse is worse when $\frac{a_w}{b_w}$ becomes smaller, because *the comparison is not done with fixed lift*. But, observing the numbers in figure 8.6 shows that the coefficient of lift increases from 4.63 to 4.92 (difference: +6%). From a qualitative point of view, considering a quadratic dependence from the lift, a variation of the coefficient of induced drag should be expected to be $\frac{4.92^2-4.63^2}{4.63^2} = 13\%$. But *this is not true*; as shown in figure 8.6, the coefficient of induced drag increases from 0.28 to 0.39 (difference: +39%>13%).
A comparison between the two different aspect ratios is reported in figure 8.7. Notice that, in a rigorous point of view, the curves in figure 8.7 could not be superimposed, because the variables t and s are different in such cases.

[15] Fortunately, these problems are less evident when the wing under optimal conditions is studied. This is because the analytical expressions are much simpler.

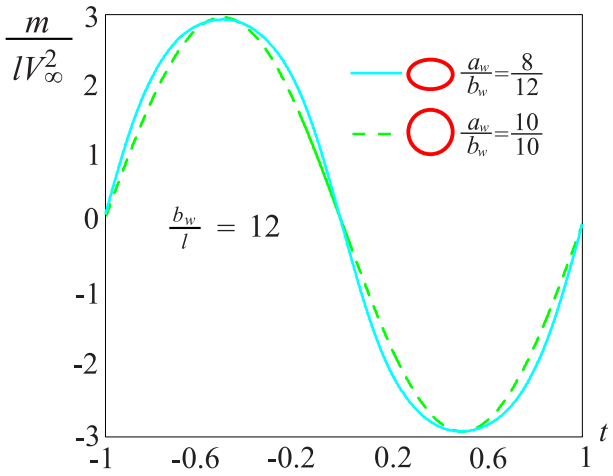

Figure 8.7. Aspect ratio effect on the doublet distribution

Nomenclature

ρ	fluid density
l	chord
m	doublet distribution
L	lift
D_i	induced drag
C_L	coefficient of lift
C_{D_i}	coefficient of induced drag
V_∞	velocity (freestream conditions)
$\nexists$	Hadamard finite-part integral
b_w	semi-axis of the elliptical annular wing
a_w	semi-axis of the elliptical annular wing
ψ, φ	coordinates used in the elliptical annular wing
c	$\sqrt{b_w^2 - a_w^2}$
β, Ω	see figure 8.3
f^R_{int}	regular function in the integral equation (direct problem)
f^S_{int}	singular function in the integral equation (direct problem)

Subscripts

∞	freestream conditions
d	doublet
w	quantity referred to the wing

Chapter 9

Annular Wings: Minimum Induced Drag

9.1 Introduction

In chapter 6, the analytical formulation for the annular wings was discussed. Chapter 2, also, discussed the procedure to find the Euler-Lagrange equation and its numerical solution. In chapter 5, the procedure studying the classical cantilever wing and the biplane was validated.
For all annular wings examined in this dissertation, the following quantities can now be calculated analytically and numerically:

- *Quantity 1*
  Optimal doublet distribution.
- *Quantity 2*
  Coefficient of minimum induced drag
- *Quantity 3*
  Induced velocity (normalwash) under the condition of minimum induced drag

Munk's Minimum Induced Drag Theorems will be applied to test the quality of the solutions, and a comparison with some available results [15] will be done.
The same analytical procedure is used in all cases. However, the mathematical expressions are different. Therefore, for the aim of completeness, the details of the derivations are not omitted.

9.2 Minimum Induced Drag in a Circular Annular Wing

The coefficient of induced drag has the expression:

$$C_{D_i} = -\frac{\pi}{16 R_w l V_\infty^4} \int_{-1}^{+1} m(s) \, \fint_{-1}^{+1} m(t) \left(\frac{1}{1 - \cos(\pi(t-s))} \right) \mathrm{d}t \, \mathrm{d}s. \tag{9.1}$$

The goal is to minimize the coefficient by considering the following conditions:

- *Condition 1*
  The coefficient of lift is *fixed*:

$$-\frac{\pi}{2 l V_\infty^2} \int_{-1}^{+1} m(t) \sin(\pi t) \, \mathrm{d}t = \overline{C}_L \tag{9.2}$$

- *Condition 2*
  The wing span $2b_w = 2R_w$ is *fixed*

Before proceeding, the following important observation can be made.

Observation 30 When the biplane under optimal condition was studied in chapter 5, it was found that the wings had the same doublet distribution, which was zero at the tips. If, with an ideal experiment, it was possible to curve the wings symmetrically, an elliptical annular wing could be obtained. It is intuitive that this process would lead to an unknown doublet distribution, but it is reasonable to think that it has to be zero at the points $y = \pm b_w$[1]. If this hypothesis is considered, the external integral can be considered as a normal integral, *but the final distribution must satisfy the conditions seen above: m has to be zero at $y = \pm b_w$.*

Observing expression (9.1), it can be understood that it is of the same type of the functional minimized in chapter 2. Now, the kernel is

$$\overline{Y}(t,s) = \frac{1}{1 - \cos(\pi(t-s))}. \tag{9.3}$$

To use the procedure developed in chapter 2, the kernel has to be in the form

$$Y(t,s) = \frac{1}{(t-s)^2}. \tag{9.4}$$

[1] In chapter 4, it was shown that in a closed wing system a constant distribution can be added without drag penalty. If the arbitrary constant is assumed zero (under that condition the doublet distribution is called *fundamental distribution*) and the wing has some symmetries (like an elliptical annular wing) then the *fundamental* doublet distribution has to be zero at $y = \pm b_w$.

But it is not difficult to understand that multiplying and dividing equation (9.3) by $(t-s)^2$, a kernel of the type (9.4) is obtained. Therefore:

$$\frac{1}{1-\cos(\pi(t-s))} = \frac{(t-s)^2}{1-\cos(\pi(t-s))}\frac{1}{(t-s)^2} = \frac{(t-s)^2}{1-\cos(\pi(t-s))}Y(t,s). \quad (9.5)$$

Now it has been shown that the same procedure shown in chapter 2[2] can be used. Observing expressions (9.1) and (9.2) and comparing them with equations (2.82) and (2.84), it is deduced that, in this case,

$$\begin{aligned} &C_1 = -\tfrac{\pi}{16R_w l V_\infty^4}, \quad C_2 = -\tfrac{\pi}{2lV_\infty^2}, \\ &\overline{C} = \overline{C}_L, \quad g(t) = \sin(\pi t). \end{aligned} \quad (9.6)$$

Using equation (2.101)[3], the Euler-Lagrange equation is obtained:

$$\begin{aligned} &2C_1 \oint_{-1}^{+1} m_{\text{opt}}(s)\,\overline{Y}(t,s)\,\mathrm{d}s - C_2\lambda g(t) = 0 \Rightarrow \\ &\Rightarrow -\tfrac{\pi}{8R_w l V_\infty^4} \oint_{-1}^{+1} \tfrac{m_{\text{opt}}(s)}{1-\cos(\pi(t-s))}\,\mathrm{d}s + \tfrac{\pi}{2lV_\infty^2}\lambda\sin(\pi t) = 0. \end{aligned} \quad (9.7)$$

Therefore, this concludes that, in order to find the optimal distribution m_{opt}, the system shown below has to be solved:

$$\begin{cases} \frac{1}{4R_w V_\infty^2} \oint_{-1}^{+1} \frac{m_{\text{opt}}(s)}{1-\cos(\pi(t-s))}\,\mathrm{d}s - \lambda\sin(\pi t) = 0, \\ -\frac{\pi}{2lV_\infty^2} \int_{-1}^{+1} m_{\text{opt}}(t)\sin(\pi t)\,\mathrm{d}t = \overline{C}_L. \end{cases} \quad (9.8)$$

9.2.1 Analytical Solution of the Euler-Lagrange Equation

Observing the system of equations (9.8), notice that the function $\sin(\pi t)$ appears explicitly in both equations. Moreover, this function has the property to be a continuous and periodical function, as it should be for m_{opt}. Furthermore, the function is zero when $t = -1$ and $t = 0$ (which corresponds to $y = \pm b_w$), as is expected. Therefore, the aim is to verify whether this function satisfies the system (9.8). From a practical point of view, the following expression of the optimal distribution can be used:

$$m_{\text{opt}}(t) = k\sin(\pi t) \qquad k \text{ real number.} \quad (9.9)$$

[2] This is possible because the property demonstrated in appendix A is valid also for the kernel $\overline{Y}(t,s)$.

[3] In this case $\overline{Y}(t,s)$ has to be used instead of $Y(t,s)$.

Substituting equation (9.9) into the system (see appendix J) yields:

$$\lambda = \frac{l\overline{C}_L}{\pi R_w}, \tag{9.10}$$

$$k = -\frac{2lV_\infty^2 \overline{C}_L}{\pi}. \tag{9.11}$$

Because the system has been satisfied, it can be concluded that the *optimal doublet distribution* is:

$$m_{\text{opt}}(t) = -\frac{2lV_\infty^2 \overline{C}_L}{\pi} \sin(\pi t). \tag{9.12}$$

In the original variable:

$$\boxed{m_{\text{opt}}(\varphi) = \frac{2lV_\infty^2 \overline{C}_L}{\pi} \sin(\varphi)}. \tag{9.13}$$

It is possible to calculate the normalwash under optimal conditions[4] as:

$$\left[(u_n)_{\text{opt}}\right]_{X=0} = \frac{1}{8V_\infty R_w} \fint_{-1}^{+1} \frac{m_{\text{opt}}(t)}{(1-\cos(\pi(t-s)))} \,\mathrm{d}t = \frac{1}{8V_\infty R_w} \left[2\frac{2lV_\infty^2 \overline{C}_L}{\pi} \sin(\pi s)\right]. \tag{9.14}$$

Simplifying:

$$\left[(u_n)_{\text{opt}}\right]_{X=0} = \frac{lV_\infty \overline{C}_L}{2\pi R_w} \sin(\pi s). \tag{9.15}$$

In the original variables:

$$\boxed{\left[(u_n)_{\text{opt}}\right]_{X=0} = -\frac{lV_\infty \overline{C}_L}{2\pi R_w} \sin\varphi}. \tag{9.16}$$

The coefficient of minimum induced drag is[5]:

$$\left[(C_{D_i})_{\text{opt}}\right]_{\frac{b_w}{a_w}=1} = -\frac{\pi}{16 R_w l V_\infty^4} \int_{-1}^{1} m_{\text{opt}}(s) \fint_{-1}^{1} m_{\text{opt}}(t) \left(\frac{1}{1-\cos(\pi(t-s))}\right) \mathrm{d}t \,\mathrm{d}s. \tag{9.17}$$

Calculating the integral (see appendix J for the Hadamard integral):

$$\left[(C_{D_i})_{\text{opt}}\right]_{\frac{b_w}{a_w}=1} = \frac{l\overline{C}_L^2}{2\pi R_w}. \tag{9.18}$$

[4] See appendix J for the value of the integral.

[5] The subscript $\frac{b_w}{a_w} = 1$ is used to underline that the coefficient is referred to the circular annular wing, where $a_w = b_w = R_w$.

The corresponding induced drag is[6]:

$$\boxed{\left[(D_i)_{\text{opt}}\right]_{\frac{b_w}{a_w}=1} = \frac{\overline{L}^2}{2\pi q(2R_w)^2}}, \tag{9.19}$$

while the aerodynamic efficiency is

$$\boxed{\left[(E)_{\text{opt}}\right]_{\frac{b_w}{a_w}=1} = \frac{2\pi q(2R_w)^2}{\overline{L}}}. \tag{9.20}$$

Now consider a classical cantilever wing with *the same total lifting force* and the same wing span $2b_w$[7]. The efficiency under *optimal condition* is[8]:

$$\left[(E)_{\text{opt}}\right]_{\text{ref}} = \frac{\pi q\,(2b_w)^2}{\overline{L}}. \tag{9.21}$$

Hence, it is deduced that

$$\boxed{\frac{\left[(E)_{\text{opt}}\right]_{\frac{b_w}{a_w}=1}}{\left[(E)_{\text{opt}}\right]_{\text{ref}}} = 2}. \tag{9.22}$$

This last result shows the great aerodynamic advantage of the closed wing system. It is also in perfect accord with the known value found by Cone [15].
The Euler-Lagrange equation can be solved numerically by following the steps illustrated in chapter 2. The comparison between the analytical and numerical solutions is shown in figure 9.1. As can be seen, the numerical solution shows good correlations with the analytical results.

9.2.2 Verification of Munk's Minimum Induced Drag Theorem

If the doublet distribution m_{opt} is effectively the optimum distribution, Munk's Minimum Induced Drag Theorem has to be satisfied (see figure 9.2). Thus:

$$\frac{\left[(u_n)_{\text{opt}}\right]_{X=0}}{\cos\vartheta} = \frac{-\frac{lV_\infty \overline{C}_L \sin\varphi}{2\pi R_w}}{\sin\varphi} = -\frac{lV_\infty \overline{C}_L}{2\pi R_w} = \text{const.} \tag{9.23}$$

[6] q indicates the dynamic pressure: $q = \frac{1}{2}\rho_\infty V_\infty^2$.
[7] Notice that $b_w = R_w$ for circular wing.
[8] The subscript "ref" indicates that the classical wing is used as a reference wing.

$\frac{R_w}{l}$	$100 \cdot \left[(C_{D_i})_{\text{opt}} \right]_{\frac{b_w}{a_w}=1}$	
	Analytical	Numerical
10	1.59	1.59
15	1.06	1.06
20	0.80	0.79
25	0.64	0.64
30	0.53	0.53
50	0.32	0.32
100	0.16	0.16

Figure 9.1. Circular annular wing: coefficient of minimum induced drag ($\overline{C}_L = 1$).

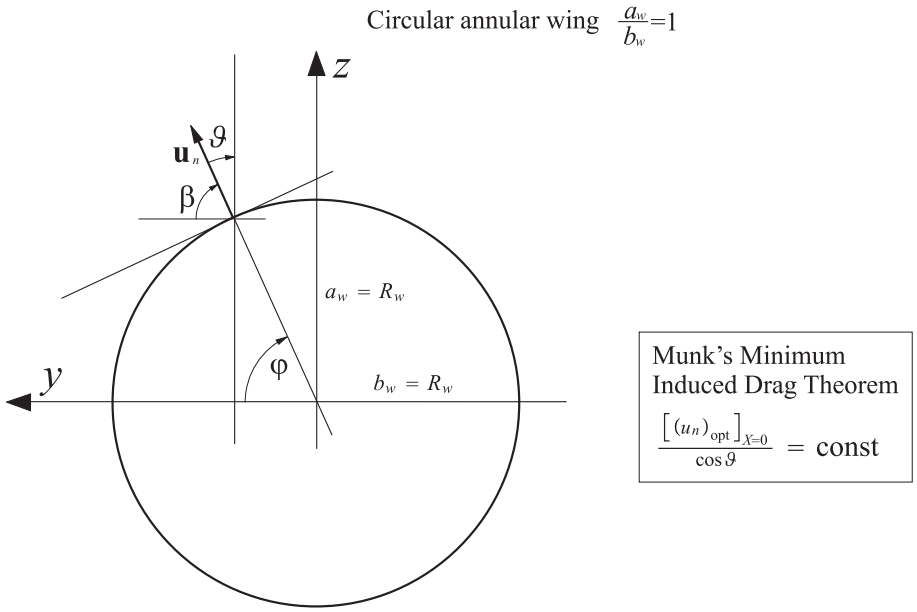

Figure 9.2. Circular annular wing and Munk's Minimum Induced Drag Theorem.

9.3 Minimum Induced Drag in an Elliptical Annular Wing with $b_w > a_w$

The coefficient of induced drag has the expression[9]:

$$C_{D_i} = -\frac{\pi}{16 b_w l V_\infty^4} \int_{-1}^{+1} m(s) \, \Xint= _{-1}^{+1} m(t) \, \overline{Y}(t,s) \, \mathrm{d}t \, \mathrm{d}s. \tag{9.24}$$

$\overline{Y}(t,s)$ is the *symmetric kernel*:

$$\overline{Y}(t,s) = \frac{\sinh^2 \psi_w \cosh^2 \psi_w}{\left(\sinh^2 \psi_w + \sin^2\left(\frac{\pi(t+s)}{2}\right)\right)^2} - \frac{\frac{1}{2}\cosh(2\psi_w)}{\left(\sinh^2 \psi_w + \sin^2\left(\frac{\pi(t+s)}{2}\right)\right)} + \frac{1}{(1-\cos(\pi(t-s)))}. \tag{9.25}$$

The goal is to minimize the coefficient of induced drag by considering the following conditions:

- *Condition 1*
  The coefficient of lift is *fixed*:

$$\overline{C}_L = -\frac{\pi}{2 l V_\infty^2} \int_{-1}^{+1} m(t) \sin(\pi t) \, \mathrm{d}t. \tag{9.26}$$

- *Condition 2*
  The wing span $2b_w$ is *fixed.*

Using the usual notation (see previous sections and chapter 2):

$$\begin{aligned} &C_1 = -\tfrac{\pi}{16 b_w l V_\infty^4}, \quad C_2 = -\tfrac{\pi}{2 l V_\infty^2}, \\ &\overline{C} = \overline{C}_L, \quad g(t) = \sin(\pi t). \end{aligned} \tag{9.27}$$

Using equation (2.101), the Euler-Lagrange equation becomes:

$$\begin{aligned} &2C_1 \, \Xint= _{-1}^{+1} m_{\text{opt}}(s) \, \overline{Y}(t,s) \, \mathrm{d}s - C_2 \lambda g(t) = 0 \Rightarrow \\ &\Rightarrow -\tfrac{\pi}{8 b_w l V_\infty^4} \, \Xint= _{-1}^{+1} m_{\text{opt}}(s) \, \overline{Y}(t,s) \, \mathrm{d}s + \tfrac{\pi}{2 l V_\infty^2} \lambda \sin(\pi t) = 0. \end{aligned} \tag{9.28}$$

[9] Considered here is the particular case in which the doublet distribution is zero at $y = \pm b_w$, as has been done above for the circular annular wing. Therefore, the external integral is not a Cauchy integral.

Therefore, it is deduced that, in order to find the optimal distribution m_{opt}, the system that has to be solved is

$$\begin{cases} \frac{1}{4b_w V_\infty^2} \oint_{-1}^{+1} m_{\text{opt}}(s)\, \overline{Y}(t,s)\, \mathrm{d}s - \lambda \sin(\pi t) = 0, \\ -\frac{\pi}{2lV_\infty^2} \int_{-1}^{+1} m_{\text{opt}}(t) \sin(\pi t)\, \mathrm{d}t = \overline{C}_L. \end{cases} \tag{9.29}$$

9.3.1 Analytical Solution of the Euler-Lagrange Equation

Observing the system of equations (9.29), and thinking as has been done for the circular annular wing, the following optimal distribution candidate is used:

$$m_{\text{opt}}(t) = k \sin(\pi t) \qquad k \ \text{ real number.} \tag{9.30}$$

Substituting equation (9.30) into the system (see appendix K) yields:

$$\lambda = \frac{2l\overline{C}_L}{\pi (b_w + a_w)}, \tag{9.31}$$

$$k = -\frac{2lV_\infty^2}{\pi} \overline{C}_L. \tag{9.32}$$

Thus, it is deduced that the *optimal doublet distribution* is:

$$m_{\text{opt}}(t) = -\frac{2lV_\infty^2 \overline{C}_L}{\pi} \sin(\pi t)\,. \tag{9.33}$$

In the original variable:

$$\boxed{m_{\text{opt}}(\varphi) = \frac{2lV_\infty^2 \overline{C}_L}{\pi} \sin(\varphi)}. \tag{9.34}$$

In figure 9.3, the optimal doublet distribution is shown. It is possible to calculate the normalwash under optimal conditions (see appendix K for details about the integrals I_A, I_B and I_C):

$$\left[(u_n)_{\text{opt}}\right]_{X=0} = \frac{1}{8cV_\infty \sqrt{\left(\cosh^2 \psi_w - \cos^2(\pi s)\right)}} \left(I_A - I_B + I_C\right). \tag{9.35}$$

Simplifying:

$$\left[(u_n)_{\text{opt}}\right]_{X=0} = \frac{\sin(\pi s) \cosh \psi_w}{\sqrt{\left(\cosh^2 \psi_w - \cos^2(\pi s)\right)}} \frac{lV_\infty \overline{C}_L \left(\cosh \psi_w - \sinh \psi_w\right)}{c\pi}. \tag{9.36}$$

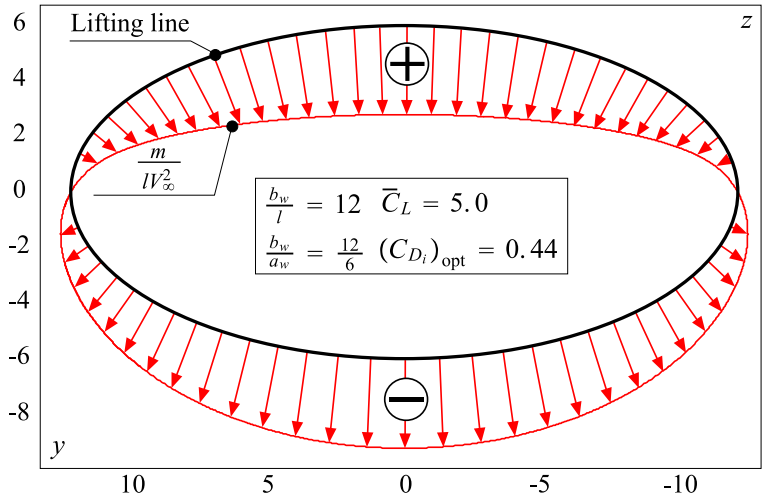

Figure 9.3. Elliptical annular wing with $b_w > a_w$. Doublet distribution under optimal conditions.

In the original variables:

$$\boxed{\left[(u_n)_{\text{opt}}\right]_{X=0} = -\frac{\sin\varphi\cosh\psi_w}{\sqrt{\left(\cosh^2\psi_w - \cos^2\varphi\right)}}\frac{lV_\infty\overline{C}_L(\cosh\psi_w - \sinh\psi_w)}{c\pi}}. \tag{9.37}$$

The coefficient of minimum induced drag is[10]:

$$\left[(C_{D_i})_{\text{opt}}\right]_{\frac{b_w}{a_w}>1} = -\frac{l\overline{C}_L^2}{4\pi b_w}\int_{-1}^{+1}\sin(\pi s)\left(\frac{I_A(s)}{k} - \frac{I_B(s)}{k} + \frac{I_C(s)}{k}\right)\mathrm{d}s. \tag{9.38}$$

Calculating the integral (see appendix K for details about the integrals):

$$\left[(C_{D_i})_{\text{opt}}\right]_{\frac{b_w}{a_w}>1} = \frac{l\overline{C}_L^2}{\pi(b_w + a_w)}. \tag{9.39}$$

The corresponding induced drag is:

$$\boxed{\left[(D_i)_{\text{opt}}\right]_{\frac{b_w}{a_w}>1} = \frac{\overline{L}^2}{\pi q\left(\frac{b_w+a_w}{b_w}\right)(2b_w)^2}}, \tag{9.40}$$

while the aerodynamic efficiency is

$$\boxed{\left[(E)_{\text{opt}}\right]_{\frac{b_w}{a_w}>1} = \frac{\pi q\left(\frac{b_w+a_w}{b_w}\right)(2b_w)^2}{\overline{L}}}. \tag{9.41}$$

[10]The subscript $\frac{b_w}{a_w} > 1$ is used to show that the coefficient is related to the elliptical annular wing with $b_w > a_w$.

Using the expression of efficiency in a classical cantilever wing with *the same total lifting force* and the same wing span $2b_w$:

$$\boxed{\frac{\left[(E)_{\text{opt}}\right]_{\frac{b_w}{a_w}>1}}{\left[(E)_{\text{opt}}\right]_{\text{ref}}} = \frac{b_w+a_w}{b_w} = 1+\frac{a_w}{b_w}}. \tag{9.42}$$

Observation 31 From the previous equation, it is clear that $1 < \frac{\left[(E)_{\text{opt}}\right]_{\frac{b_w}{a_w}>1}}{\left[(E)_{\text{opt}}\right]_{\text{ref}}} < 2$. It is also clear that

$$\lim_{a_w\to 0} \frac{\left[(E)_{\text{opt}}\right]_{\frac{b_w}{a_w}>1}}{\left[(E)_{\text{opt}}\right]_{\text{ref}}} = 1, \tag{9.43}$$

$$\lim_{a_w\to b_w} \frac{\left[(E)_{\text{opt}}\right]_{\frac{b_w}{a_w}>1}}{\left[(E)_{\text{opt}}\right]_{\text{ref}}} = 2. \tag{9.44}$$

The elliptical annular wing with $b_w > a_w$ has the same induced drag (under optimal condition) as a cantilever classical wing when $a_w \to 0$. Moreover, the elliptical annular wing with $b_w > a_w$ has the same induced drag (under optimal condition) as a circular annular wing when $a_w \to b_w$.

The Euler-Lagrange equation can also be solved numerically. Figure 9.4 shows the comparison between the analytical and numerical solution (in all cases, $\frac{b_w}{l} = 1$ and $\overline{C}_L = 1$).

9.3.2 Verification of Munk's Minimum Induced Drag Theorem

If the doublet distribution m_{opt} is effectively the optimum distribution, Munk's Minimum Induced Drag Theorem has to be satisfied (see figure 9.5). Therefore[11]:

$$\frac{\left[(u_n)_{\text{opt}}\right]_{X=0}}{\cos\vartheta} = \frac{-\frac{\cosh\psi_w\sin\varphi}{\sqrt{\cosh^2\psi_w-\cos^2\varphi}}\frac{lV_\infty\overline{C}_L(\cosh\psi_w-\sinh\psi_w)}{\pi c}}{\frac{\cosh\psi_w\sin\varphi}{\sqrt{\cosh^2\psi_w-\cos^2\varphi}}} = -\frac{lV_\infty\overline{C}_L(\cosh\psi_w-\sinh\psi_w)}{\pi c} = \text{const.} \tag{9.45}$$

Thus, the theorem is satisfied and the doublet distribution is effectively the distribution of minimum induced drag.

[11] Notice that

$$\cos\vartheta = \sin\beta = \frac{\cosh\psi_w\sin\varphi}{\sqrt{\cosh^2\psi_w-\cos^2\varphi}}.$$

$\frac{b_w}{a_w}$	$100 \cdot \left[(C_{D_i})_{\text{opt}} \right]_{\frac{b_w}{a_w}>1}$	
	Analytical	Numerical
12/1	2.45	2.45
12/2	2.27	2.27
12/3	2.12	2.12
12/4	1.99	1.99
12/5	1.87	1.87
12/6	1.77	1.77
12/7	1.67	1.67
12/8	1.59	1.59
12/9	1.51	1.51
12/10	1.45	1.44
12/11	1.38	1.38
12/12	1.33	1.32

Figure 9.4. Elliptical annular wing with $b_w > a_w$. Comparison between analytical and numerical results.

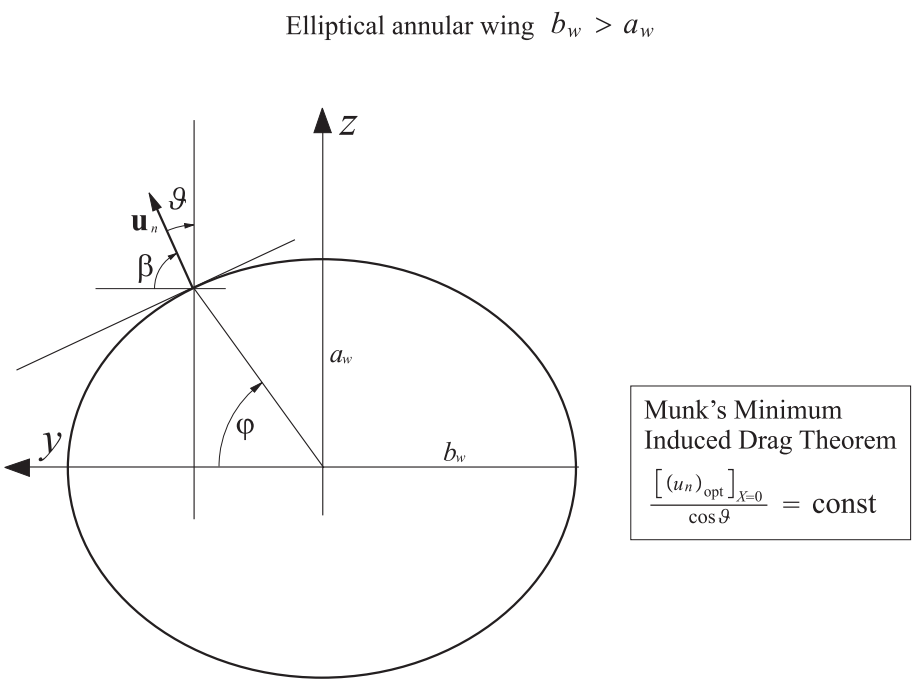

Figure 9.5. Elliptical annular wing with $b_w > a_w$ and Munk's Minimum Induced Drag Theorem.

9.4 Minimum Induced Drag in an Elliptical Annular Wing with $b_w < a_w$

The coefficient of induced drag has the expression[12]:

$$C_{D_i} = -\frac{\pi}{16 b_w l V_\infty^4} \int_{-1}^{+1} m(s) \, \Xint= _{-1}^{+1} m(t) \, \overline{Y}(t,s) \, \mathrm{d}t \, \mathrm{d}s. \tag{9.46}$$

$\overline{Y}(t,s)$ is the *symmetric kernel*:

$$\overline{Y}(t,s) = \frac{\sinh^2 \psi_w \cosh^2 \psi_w}{\left(\sinh^2 \psi_w + \cos^2\left(\frac{\pi(t+s)}{2}\right)\right)^2} - \frac{\frac{1}{2}\cosh(2\psi_w)}{\left(\sinh^2 \psi_w + \cos^2\left(\frac{\pi(t+s)}{2}\right)\right)} + \frac{1}{1-\cos(\pi(t-s))}. \tag{9.47}$$

The goal is to minimize the coefficient of induced drag by considering the following conditions:

- *Condition 1*
  The coefficient of lift is *fixed*:

$$\overline{C}_L = -\frac{\pi}{2 l V_\infty^2} \int_{-1}^{+1} m(t) \sin(\pi t) \, \mathrm{d}t \tag{9.48}$$

- *Condition 2*
  The wing span $2b_w$ is *fixed*.

Using the usual notation (see previous sections and chapter 2):

$$\begin{aligned} &C_1 = -\tfrac{\pi}{16 b_w l V_\infty^4}, \quad C_2 = -\tfrac{\pi}{2 l V_\infty^2}, \\ &\overline{C} = \overline{C}_L, \quad g(t) = \sin(\pi t). \end{aligned} \tag{9.49}$$

Using equation (2.101), the Euler-Lagrange equation becomes:

$$\begin{aligned} &2C_1 \, \Xint= _{-1}^{+1} m_{\text{opt}}(s) \, \overline{Y}(t,s) \, \mathrm{d}s - C_2 \lambda g(t) = 0 \Rightarrow \\ &\Rightarrow -\tfrac{\pi}{8 b_w l V_\infty^4} \, \Xint= _{-1}^{+1} m_{\text{opt}}(s) \, \overline{Y}(t,s) \, \mathrm{d}s + \tfrac{\pi}{2 l V_\infty^2} \lambda \sin(\pi t) = 0. \end{aligned} \tag{9.50}$$

[12] Considered here is the particular case in which the doublet distribution is zero at $y = \pm b_w$, as has been done above for the other annular wings. Therefore, the external integral is not a Cauchy integral.

Therefore, this deduces that, in order to find the optimal distribution m_{opt}, the following system has to be solved:

$$\begin{cases} \frac{1}{4b_w V_\infty^2} \oint\limits_{-1}^{+1} m_{\text{opt}}(s)\, \overline{Y}(t,s)\, \mathrm{d}s - \lambda \sin(\pi t) = 0, \\ -\frac{\pi}{2lV_\infty^2} \int\limits_{-1}^{+1} m_{\text{opt}}(t) \sin(\pi t)\, \mathrm{d}t = \overline{C}_L. \end{cases} \tag{9.51}$$

9.4.1 Analytical Solution of the Euler-Lagrange Equation

Observing the system of equations (9.51), and thinking as has been done for the circular annular wing and the elliptical annular wing with $b_w > a_w$, the following optimal distribution candidate is used:

$$m_{\text{opt}}(t) = k \sin(\pi t) \qquad k \text{ real number.} \tag{9.52}$$

Substituting equation (9.52) into the system (9.51) (see appendix L):

$$\lambda = \frac{2l\overline{C}_L}{\pi (b_w + a_w)}, \tag{9.53}$$

$$k = -\frac{2lV_\infty^2}{\pi}\overline{C}_L. \tag{9.54}$$

Thus, this deduces that the *optimal doublet distribution* is:

$$m_{\text{opt}}(t) = -\frac{2lV_\infty^2 \overline{C}_L}{\pi} \sin(\pi t)\,. \tag{9.55}$$

In the physical variable:

$$\boxed{m_{\text{opt}}(\varphi) = \tfrac{2lV_\infty^2 \overline{C}_L}{\pi} \sin(\varphi)}. \tag{9.56}$$

It is possible to calculate the normalwash under optimal conditions (see appendix L for details on integrals I_A, I_B and I_C):

$$\left[(u_n)_{\text{opt}}\right]_{X=0} = \frac{1}{8cV_\infty} \frac{1}{\sqrt{\left(\sinh^2\psi_w + \cos^2(\pi s)\right)}} (I_A - I_B + I_C)\,. \tag{9.57}$$

Simplifying:

$$\left[(u_n)_{\text{opt}}\right]_{X=0} = \frac{\sin(\pi s)\sinh\psi_w}{\sqrt{\left(\sinh^2\psi_w + \cos^2(\pi s)\right)}} \frac{lV_\infty \overline{C}_L (\cosh\psi_w - \sinh\psi_w)}{c\pi}. \tag{9.58}$$

In the original variables:

$$\boxed{\left[(u_n)_{\text{opt}}\right]_{X=0} = -\frac{\sin\varphi\sinh\psi_w}{\sqrt{\left(\sinh^2\psi_w+\cos^2\varphi\right)}}\frac{lV_\infty\overline{C}_L(\cosh\psi_w-\sinh\psi_w)}{c\pi}}. \tag{9.59}$$

The coefficient of minimum induced drag is[13]:

$$\left[(C_{D_i})_{\text{opt}}\right]_{\frac{b_w}{a_w}<1} = -\frac{l\overline{C}_L^2}{4\pi b_w}\int_{-1}^{+1}\sin(\pi s)\left(\frac{I_A(s)}{k}-\frac{I_B(s)}{k}+\frac{I_C(s)}{k}\right)\mathrm{d}s. \tag{9.60}$$

Calculating the integral (see appendix L for details on the integral):

$$\left[(C_{D_i})_{\text{opt}}\right]_{\frac{b_w}{a_w}<1} = \frac{l\overline{C}_L^2}{\pi(b_w+a_w)}. \tag{9.61}$$

The corresponding induced drag is:

$$\boxed{\left[(D_i)_{\text{opt}}\right]_{\frac{b_w}{a_w}<1} = \frac{\overline{L}^2}{\pi q\left(\frac{b_w+a_w}{b_w}\right)(2b_w)^2}}, \tag{9.62}$$

while the aerodynamic efficiency is

$$\boxed{\left[(E)_{\text{opt}}\right]_{\frac{b_w}{a_w}<1} = \frac{\pi q\left(\frac{b_w+a_w}{b_w}\right)(2b_w)^2}{\overline{L}}}. \tag{9.63}$$

Using the expression of efficiency in a classical cantilever wing with *the same total lifting force* and the same wing span $2b_w$:

$$\boxed{\frac{\left[(E)_{\text{opt}}\right]_{\frac{b_w}{a_w}<1}}{\left[(E)_{\text{opt}}\right]_{\text{ref}}} = \frac{b_w+a_w}{b_w} = 1+\frac{a_w}{b_w}}. \tag{9.64}$$

Observation 32 In the previous equation, notice that $2 < \frac{\left[(E)_{\text{opt}}\right]_{\frac{b_w}{a_w}<1}}{\left[(E)_{\text{opt}}\right]_{\text{ref}}} < \infty$. It is also clear that

$$\lim_{a_w\to b_w}\frac{\left[(E)_{\text{opt}}\right]_{\frac{b_w}{a_w}<1}}{\left[(E)_{\text{opt}}\right]_{\text{ref}}} = 2, \tag{9.65}$$

$$\lim_{a_w\to\infty}\frac{\left[(E)_{\text{opt}}\right]_{\frac{b_w}{a_w}<1}}{\left[(E)_{\text{opt}}\right]_{\text{ref}}} = \infty. \tag{9.66}$$

[13]The subscript $\frac{b_w}{a_w} < 1$ is used to show that the coefficient is related to the elliptical annular wing with $b_w < a_w$.

The elliptical annular wing with $b_w < a_w$ has the same induced drag (under optimal condition) as a circular wing when $a_w \to b_w$. Moreover, the elliptical annular wing with $b_w < a_w$ has infinite efficiency when $a_w \to \infty$.
But this does not mean that, effectively, this condition can be reached, because other aspects of the problem should be considered. For example, the weight of the wing was not taken into account. If it was then, clearly, the condition $a_w \to \infty$ would imply infinite weight and this is not acceptable. However, these analyses show that the aerodynamic of the closed wing system is very good.

As has been done for the other cases, the Euler-Lagrange equation can also be solved numerically.

9.4.2 Verification of Munk's Minimum Induced Drag Theorem

If the doublet distribution m_{opt} is effectively the optimum distribution, Munk's Minimum Induced Drag Theorem has to be satisfied (see figure 9.6).

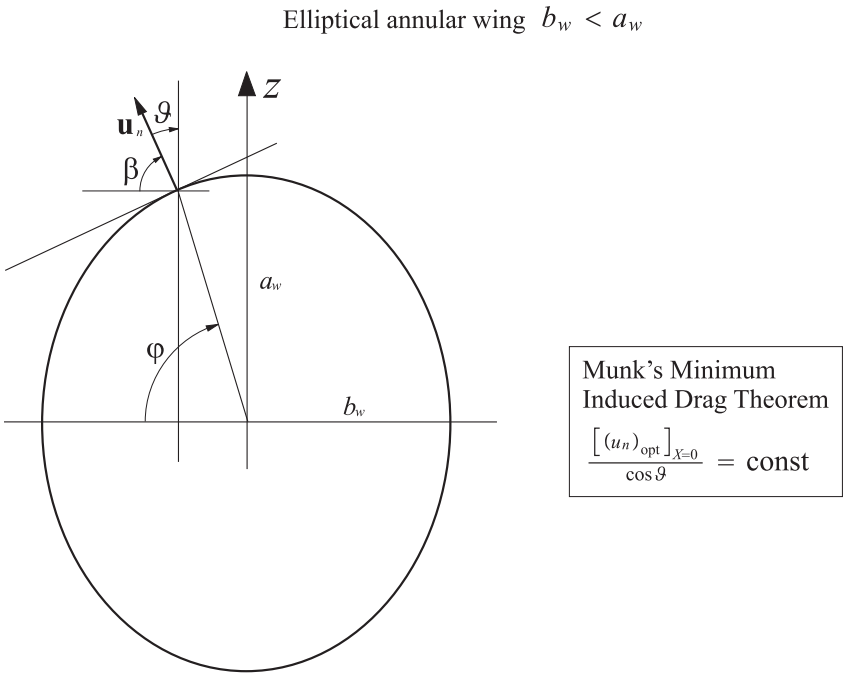

Figure 9.6. Elliptical annular wing with $b_w < a_w$ and Munk's Minimum Induced Drag Theorem.

Therefore[14]:

$$\frac{\left[(u_n)_{\text{opt}}\right]_{X=0}}{\cos\vartheta} = \frac{-\frac{\sinh\psi_w\sin\varphi}{\sqrt{\sinh^2\psi_w+\cos^2\varphi}}\frac{lV_\infty\overline{C}_L(\cosh\psi_w-\sinh\psi_w)}{\pi c}}{\frac{\sinh\psi_w\sin\varphi}{\sqrt{\sinh^2\psi_w+\cos^2\varphi}}} = -\frac{lV_\infty\overline{C}_L(\cosh\psi_w-\sinh\psi_w)}{\pi c} = \text{const.} \tag{9.67}$$

Thus, the theorem is satisfied and the doublet distribution is effectively the distribution of minimum induced drag.

9.5 Doublet Distribution of Minimum Induced Drag. Non-uniqueness of the Solution

Is the optimal doublet distribution unique? Remembering the contents of chapter 4, the answer is: no. The solution is not unique. In particular, if m_{opt} is a solution for the minimization problem, the distribution $m'_{\text{opt}} = m_{\text{opt}} + \text{const}$ is a solution too. This property can be verified for the annular wings[15].

9.5.1 Circular Annular Wing Case

In order to demonstrate the property, it is sufficient to show that for a constant doublet distribution the lift and induced drag are zero. The first verification is very simple and is omitted here. The second property, however, will be verified.
Suppose that $m = \text{const} = \overline{m}$. The induced drag is[16]:

$$C_{D_i} = -\frac{\overline{m}^2\pi}{16R_w lV_\infty^4}\int_{-1}^{+1}\!\!\!\!\!\!=\int_{-1}^{+1}\left(\frac{1}{1-\cos\left(\pi\left(t-s\right)\right)}\right)\mathrm{d}t\,\mathrm{d}s. \tag{9.68}$$

But the indefinite integral can be calculated as:

$$\int\left(\frac{1}{\left(1-\cos\left(\pi\left(t-s\right)\right)\right)}\right)\mathrm{d}t = -\frac{1}{\pi\tan\frac{(\pi(t-s))}{2}}. \tag{9.69}$$

Using this result, the Hadamard integral becomes zero. Because the internal integral is zero, the following is found:

$$C_{D_i} = 0. \tag{9.70}$$

Thus, the property is demonstrated.

[14]Notice that

$$\cos\vartheta = \sin\beta = \frac{\sinh\psi_w\sin\varphi}{\sqrt{\sinh^2\psi_w+\cos^2\varphi}}.$$

[15]This is another way to demonstrate that the formulation is correct.

[16]Now the external integral must be defined as a Cauchy integral. That is because the *doublet distribution is not zero at the endpoints of the integral.*

9.5.2 Elliptical Annular Wing Case

Consider the case in which $b_w > a_w$ (similar to the method for the case $b_w < a_w$). This case is a little more complicated than the previous one. If $m = \overline{m}$, the coefficient of induced drag can be written as

$$C_{D_i} = -\frac{\overline{m}^2 \pi}{16 b_w l V_\infty^4} \oint_{-1}^{+1} (I'_A - I'_B + I'_C)\, \mathrm{d}s, \tag{9.71}$$

where:

$$\begin{aligned}
I'_A &= \int_{-1}^{+1} \frac{\sinh^2\psi_w \cosh^2\psi_w}{\left(\sinh^2\psi_w + \sin^2\left(\frac{\pi(t+s)}{2}\right)\right)^2}\,\mathrm{d}s = \sinh^2\psi_w \cosh^2\psi_w \int_{-1}^{+1} \frac{1}{\left(\sinh^2\psi_w + \sin^2\left(\frac{\pi(t+s)}{2}\right)\right)^2}\,\mathrm{d}s, \\
I'_B &= \int_{-1}^{+1} \frac{\frac{1}{2}\cosh(2\psi_w)}{\left(\sinh^2\psi_w + \sin^2\left(\frac{\pi(t+s)}{2}\right)\right)}\,\mathrm{d}s = \frac{1}{2}\cosh(2\psi_w) \int_{-1}^{+1} \frac{1}{\left(\sinh^2\psi_w + \sin^2\left(\frac{\pi(t+s)}{2}\right)\right)}\,\mathrm{d}s, \\
I'_C &= \oint_{-1}^{+1} \frac{1}{(1-\cos(\pi(t-s)))}\,\mathrm{d}s.
\end{aligned} \tag{9.72}$$

I'_C has already been calculated and has been shown that it is zero. The other two integrals (i.e., I'_B and I'_C) are calculated in appendix M. Referring to appendix M:

$$I'_A = I'_B = \frac{\cosh(2\psi_w)}{\sinh\psi_w \cosh\psi_w}, \tag{9.73}$$

therefore, $C_{D_i} = 0$. Thus, the property is demonstrated.

9.6 Annular Wings and Classical Wings. Comparison Under Optimal Conditions

The obtained results are summarized in this section. The ratio between the aerodynamic efficiency of the annular wings and the efficiency of the classical cantilever wings is reported in figure 9.7.

9.7 Annular Wings Under Optimal Conditions. Twist of Minimum Induced Drag

What is the twist that creates the optimal doublet distribution? In order to answer this question, $m = m_{\text{opt}}$ should be inserted into the integral equation to find the

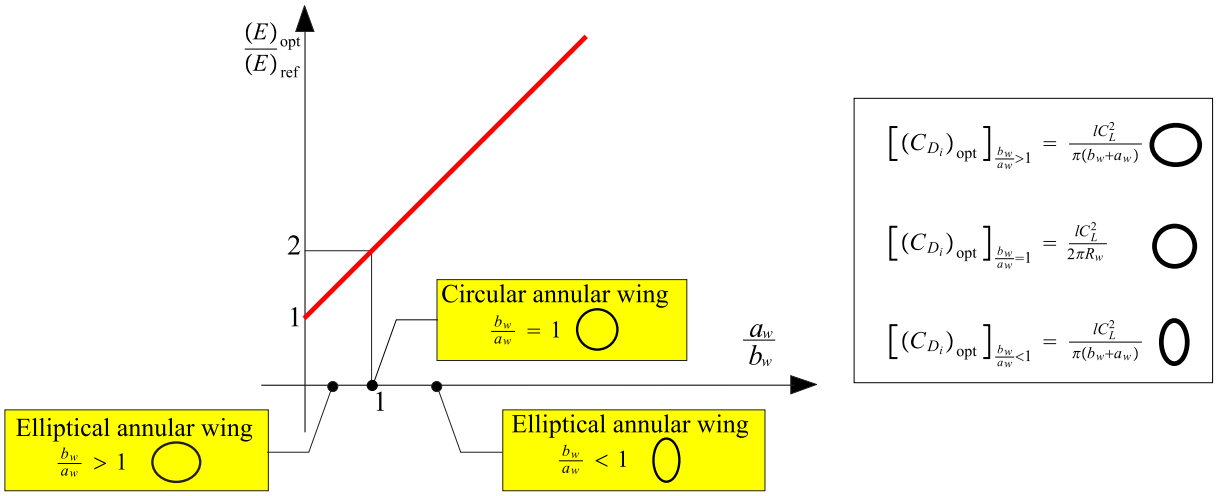

Figure 9.7. Efficiency of annular wings under optimal conditions.

twist $\alpha(s)$. But, from *a practical point of view*, observing figure 8.6 and applying the formula

$$\left[(C_{D_i})_{\text{opt}}\right]_{\frac{b_w}{a_w}<1} = \frac{l\overline{C}_L^2}{\pi\,(b_w + a_w)},$$

almost the same coefficient of induced drag is found. Thus, from a practical point of view, *if $a_w \approx b_w$, the twist corresponding to a rigid rotation of the ellipse along the y axis is the twist of minimum induced drag.* Figure 9.8 illustrates this concept. As can be seen, the optimal distribution and the distribution corresponding to a rigid rotation along the y axis are almost the same if $b_w \approx a_w$. This figure also shows that the optimal distribution has lesser gradient than the distribution in the rigid rotation case, in correspondence to the points $t = \pm 1{,}0$. Notice that the two curves are almost coincident when $a_w \to b_w$, but when a_w is different than b_w this is no longer true. Concluding, *the twist corresponding to a rigid rotation is not the optimal incidence law if $\frac{a_w}{b_w}$ is small.*

9.8 Elliptical Annular Wing and Biplane. Comparison Under Optimal Conditions

The annular wings and the biplane have been analyzed. The conditions that guarantee the minimum induced drag were found under fixed wing span. But it is interesting to understand when an elliptical annular wing is better than a biplane (both under the condition of minimum induced drag). First of all, it must be decided

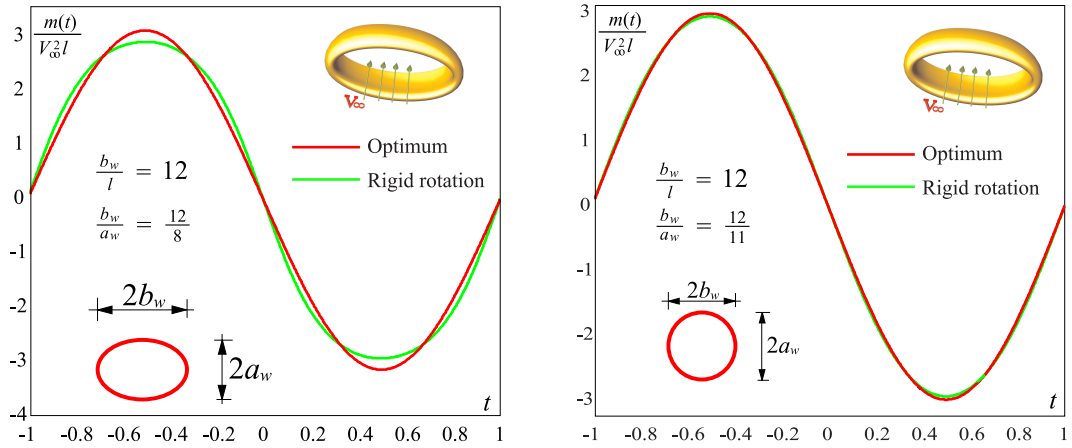

Figure 9.8. Comparison of doublet distributions.

which is the best ellipse to compare with the biplane. Considering the fact that the ellipse has curved extremities, a biplane with the distance between the wings equal to H can be compared with an elliptical annular wing with $a_w = H$ (this is not the only possible choice). The geometry of the wings is reported in figure 9.9. The

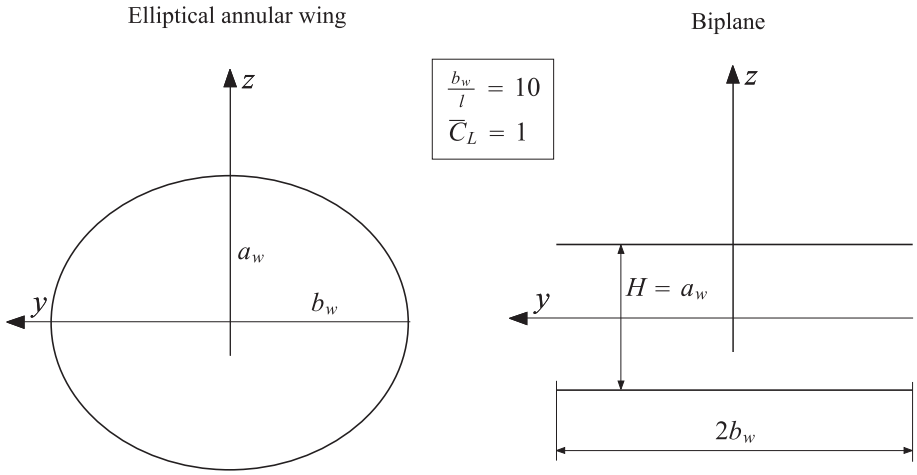

Figure 9.9. Geometry of the wings.

comparison between the wings is reported in figure 9.10. From figure 9.10, it is clear that, *for small aspect ratio, the annular wing and biplane show similar behavior*,

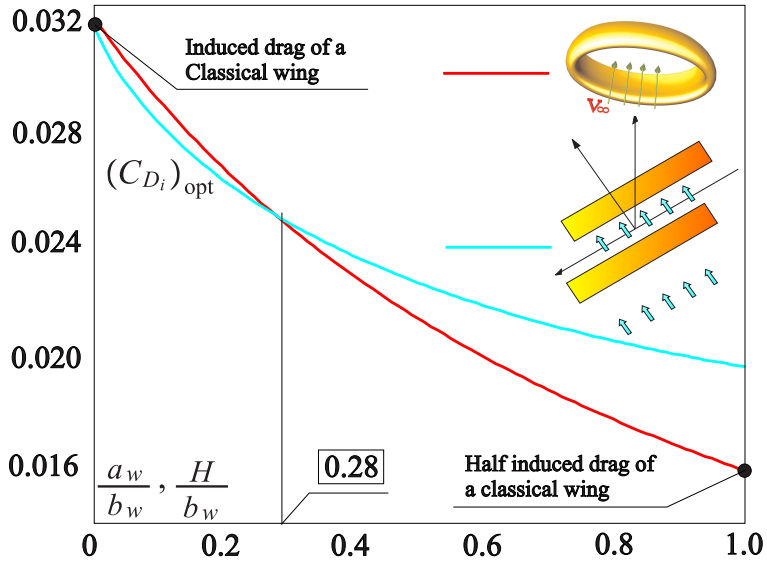

Figure 9.10. Biplane and elliptical annular wing under optimal conditions ($\overline{C}_L = 1$). Coefficient of minimum induced drag.

while for high aspect ratio the tendency is the opposite[17].

9.8.1 Closed Wing System and Biplane. An Experimental Comparison

The results shown above have a simple experimental verification. Consider the wind tunnel model of the Prandtlplane made by Alenia Aeronautica (see chapter 4). The model was built with the main purpose of better understanding the difference between joined wing and the corresponding biplane obtained by removing the vertical joining wings. As shown in figure 9.11, the induced drag in the closed system is practically the same as the induced drag of the corresponding biplane. This is in perfect accord with figure 9.10: for the range of aspect ratio used in the test (0.23 and 0.34), the closed wing system and biplane do not show big difference in their induced drag[18].

[17]The biplane has a minimum value of induced drag equal to 1/2 the induced drag of a classical wing (when the wings are indefinitely distant), while an elliptical annular wing does not have this limit.

[18]Notice that Alenia's model was not tested under optimal conditions. Therefore, the results shown in figure 9.10 can not be applied in the real case. However, they can be accepted in a qualitative way.

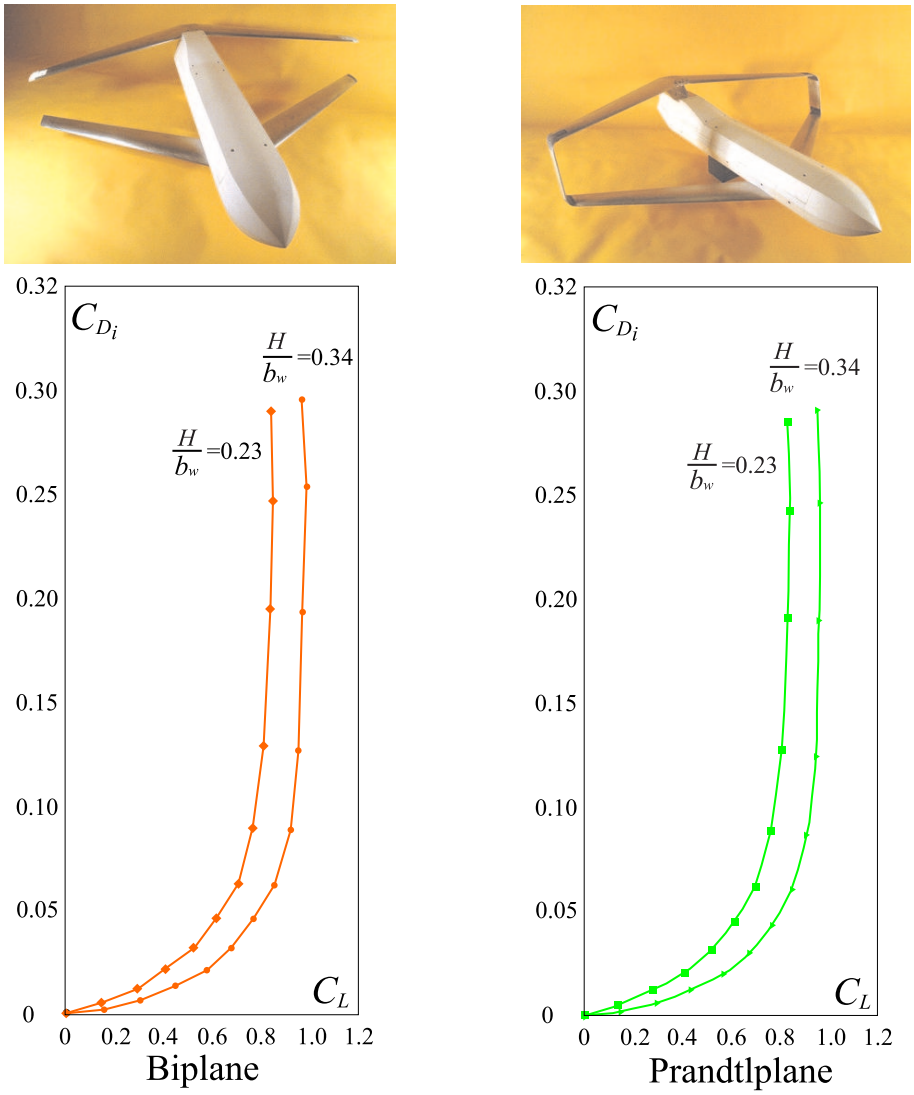

Figure 9.11. Alenia's Prandtlplane model. Coefficient of induced drag versus coefficient of lift (see [68]).

Nomenclature

α	twist
ρ	fluid density
u_n	normalwash
$2b_w$	wing span
ϑ	angle of inclination of the lifting element
l	chord
m	doublet distribution
$\overline{m}$	constant doublet distribution
L	lift
D_i	induced drag
C_L	coefficient of lift
C_{D_i}	coefficient of induced drag
F	aerodynamic force
$\overline{L}$	fixed value of the lifting force
$\overline{C}_L$	fixed value of the coefficient of lift
λ	Lagrange multiplier
V_∞	velocity (freestream conditions)
q	aerodynamic pressure
$\fint$	Hadamard finite-part integral
$\fint$	integral defined in the Cauchy principal values sense
H	distance between wings 1 and 2 (biplane case)
E	aerodynamic efficiency
$Y, \overline{Y}$	kernels

Subscripts

∞	freestream conditions
ref	referred to a cantilever wing with the same lift and wing span
opt	optimal condition (minimum induced drag)
$\frac{b_w}{a_w} < 1$	referred to an elliptical annular wing with $\frac{b_w}{a_w} < 1$
$\frac{b_w}{a_w} = 1$	referred to a circular annular wing with $R_w = b_w = a_w$
$\frac{b_w}{a_w} > 1$	referred to an elliptical annular wing with $\frac{b_w}{a_w} > 1$

Chapter 10

Elliptical Lifting Arcs: Minimum Induced Drag

10.1 Introduction

The analytical formulation for the elliptical lifting arcs was seen in chapter 7. In this chapter, the condition corresponding to a minimum induced drag will be studied, as was done for the annular wings (see chapter 9). The results will be compared with the classical cantilever wing and with the corresponding annular wing. It will be understood which is the most advantageous point to close the wing and what are the differences between annular wings and C-wings.
Some theoretical considerations can be found in [14], [15] and in chapter 4.
The following quantities will be calculated:

- *Quantity 1*
  Optimal doublet distribution.
- *Quantity 2*
  Coefficient of minimum induced drag.

Kroo's results will be confirmed: the C-wings have similar induced drag to that of the closed wing systems. But note that the purpose of these analyses is to demonstrate that this formulation is a good tool for the preliminary study of a new configuration. Also, very interesting properties of the annular (and, in general, closed) wings will be found.

10.2 Minimum Induced Drag in a Convex Elliptical Lifting Arc

The coefficient of induced drag has the expression (see chapter 7)[1]:

$$C_{D_i} = -\frac{\varepsilon^2\pi}{4SV_\infty^4}\int_{-1}^{+1} m(s)\int_{-1}^{+1} m(t)\left(\frac{\sinh^2\psi_w\cosh^2\psi_w}{\left(\sinh^2\psi_w+\cos^2\left(\varepsilon\pi\frac{t+s}{2}\right)\right)^2}-\frac{\frac{1}{2}\cosh(2\psi_w)}{\left(\sinh^2\psi_w+\cos^2\left(\varepsilon\pi\frac{t+s}{2}\right)\right)}\right)\mathrm{d}t\,\mathrm{d}s+$$
$$-\frac{\varepsilon^2\pi}{4SV_\infty^4}\int_{-1}^{+1} m(s)\,\fint_{-1}^{+1}\frac{m(t)}{1-\cos(\varepsilon\pi(t-s))}\mathrm{d}t\,\mathrm{d}s=-\frac{\varepsilon^2\pi}{4SV_\infty^4}\int_{-1}^{+1} m(s)\,\fint_{-1}^{+1} m(t)\,\overline{Y}(t,s)\,\mathrm{d}t\,\mathrm{d}s. \tag{10.1}$$

The goal is to minimize the coefficient of induced drag by considering the following conditions:

- *Condition 1*
  The coefficient of lift is *fixed*:

$$-\frac{2\varepsilon\pi b_w}{SV_\infty^2}\int_{-1}^{+1} m(t)\cos(\varepsilon\pi t)\,\mathrm{d}t=\overline{C}_L. \tag{10.2}$$

- *Condition 2*
  The wing span $2b_w$ is *fixed*.

Observing expression (10.1), it is clear that the expression is of the same type of the functional J minimized in chapter 2. Observing expressions (10.1) and (10.2) and comparing with equations (2.82) and (2.84), it can be deduced that, in this case,

$$\begin{aligned} &C_1=-\frac{\varepsilon^2\pi}{4SV_\infty^4},\quad C_2=-\frac{2\varepsilon\pi b_w}{SV_\infty^2},\\ &\overline{C}=\overline{C}_L,\quad g(t)=\cos(\varepsilon\pi t). \end{aligned} \tag{10.3}$$

Using equation (2.101), the Euler-Lagrange equation becomes:

$$\begin{aligned} &2C_1\,\fint_{-1}^{+1} m_{\text{opt}}(s)\,\overline{Y}(t,s)\,\mathrm{d}s-C_2\lambda g(t)=0\Rightarrow\\ &\Rightarrow-\frac{\varepsilon^2\pi}{2SV_\infty^4}\,\fint_{-1}^{+1} m_{\text{opt}}(s)\,\overline{Y}(t,s)\,\mathrm{d}s+\frac{2\varepsilon\pi b_w}{SV_\infty^2}\lambda\cos(\varepsilon\pi t)=0. \end{aligned} \tag{10.4}$$

[1] If $b_w < a_w$, the following equation is almost the same. Only $\cos^2\left(\varepsilon\pi\frac{t+s}{2}\right)$ has to be substituted with $\sin^2\left(\varepsilon\pi\frac{t+s}{2}\right)$.

Therefore, it is deduced that in order to find the optimal distribution m_{opt}, the system that has to be solved is:

$$\begin{cases} \frac{\varepsilon}{2V_\infty^2} \oint_{-1}^{+1} m_{\text{opt}}(s)\, \overline{Y}(t,s)\, \mathrm{d}s - 2b_w\lambda \cos(\varepsilon\pi t) = 0, \\ -\frac{2\varepsilon\pi b_w}{SV_\infty^2} \int_{-1}^{+1} m_{\text{opt}}(t) \cos(\varepsilon\pi t)\, \mathrm{d}t = \overline{C}_L. \end{cases} \tag{10.5}$$

Unlike the annular wings, this system can be solved only numerically, which will be performed later.

10.3 Minimum Induced Drag in a Concave Elliptical Lifting Arc

The coefficient of induced drag is the same as the case of a convex arc. The coefficient of lift is the same except for a sign. Therefore, this concludes that in order to determine the minimum induced drag, the system that has to be solved is:

$$\begin{cases} \frac{\varepsilon}{2V_\infty^2} \oint_{-1}^{+1} m_{\text{opt}}(s)\, \overline{Y}(t,s)\, \mathrm{d}s + 2b_w\lambda \cos(\varepsilon\pi t) = 0, \\ +\frac{2\varepsilon\pi b_w}{SV_\infty^2} \int_{-1}^{+1} m_{\text{opt}}(t) \cos(\varepsilon\pi t)\, \mathrm{d}t = \overline{C}_L. \end{cases} \tag{10.6}$$

Observation 33 Consider the systems (10.6) and (10.5). Let the optimal distribution in a concave arc be indicated by $[m_{\text{opt}}]_{\text{concave}}$ and the optimal distribution in a convex arc be indicated by $[m_{\text{opt}}]_{\text{convex}}$. Comparing the lift constraints (the second equation in both systems) deduces that

$$[m_{\text{opt}}]_{\text{concave}} = -[m_{\text{opt}}]_{\text{convex}}. \tag{10.7}$$

Substituting the last expression into the Euler-Lagrange equation of a concave arc (system (10.6)), in a formal point of view, the Euler-Lagrange equation of a convex arc (system (10.5)) is the obtained result. This concludes that *the convex arc and the concave arc have the same optimal induced drag.* Obviously, the two arcs must be perfectly identical (i.e., ε must be the same). The only difference between the two cases is in the *induced lift* not considered here (see chapter 4 for details).

10.4 Results

First, the present method is validated using a result from [15]. In that paper, Cone investigates circular arcs using conformal transformations. Cone plots the efficiency

ratio $\frac{(E)_{\text{opt}}}{(E)_{\text{ref}}}$ against the $\frac{a}{b}$ ratio. As shown in figure 10.1, the present optimization procedure shows very good correlation. In figure 10.2, the arcs with $\frac{b_w}{a_w} \approx 1$ are

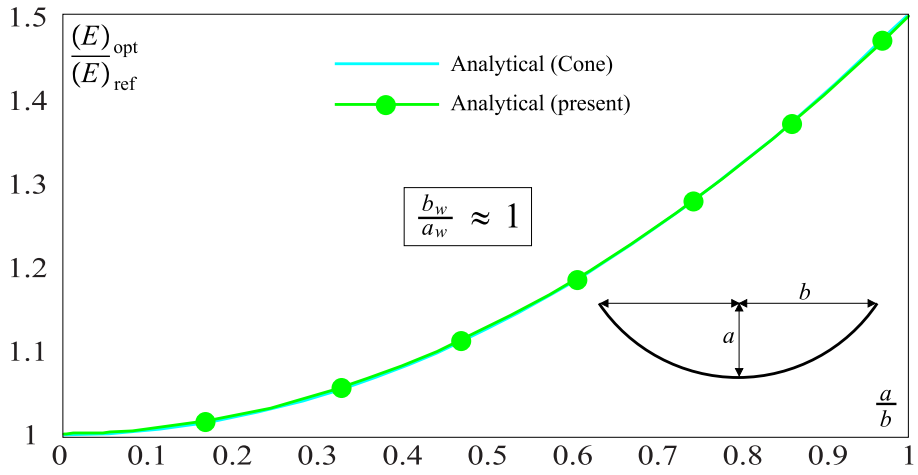

Figure 10.1. Elliptical lifting arcs. Comparison with the literature results.

studied. In particular, the efficiency ratio with the angle $2\varepsilon\pi$ is analyzed. Clearly, when $2\varepsilon\pi \approx 0$, *the curvature effects are negligible, and the efficiency is almost the same as the optimally loaded classical wing.* But when the angle is increased, an increment of the efficiency can be observed. This is particularly evident in the range $\frac{150}{180}\pi \leq 2\varepsilon\pi \leq \frac{210}{180}\pi$, where the efficiency ratio increases by 33%. Moreover, it can be noticed that, when the arcs tend to be a closed curve, the induced drag is practically the same as the induced drag of the corresponding circular annular wing[2]. Now it is of interest to answer the following questions: how does the optimal doublet distribution change when the angle $2\varepsilon\pi$ is changed? What is the difference between the doublet distribution in the annular wing and the arc with $2\varepsilon\pi \approx 2\pi$? In order to answer these questions, consider figures 10.3, 10.4, 10.5, 10.6 and 10.7. The following results can be noticed[3]:

- *Result 1*
  The elliptical lifting arcs (and, in general, all arcs) have the same efficiency (under optimal conditions) as an optimally loaded classical wing when ε is

[2]Remember that, in figure (10.2), $\frac{b_w}{a_w} \approx 1$.

[3]If it is not said otherwise, consider, in all cases, $\overline{C}_L = 1$.

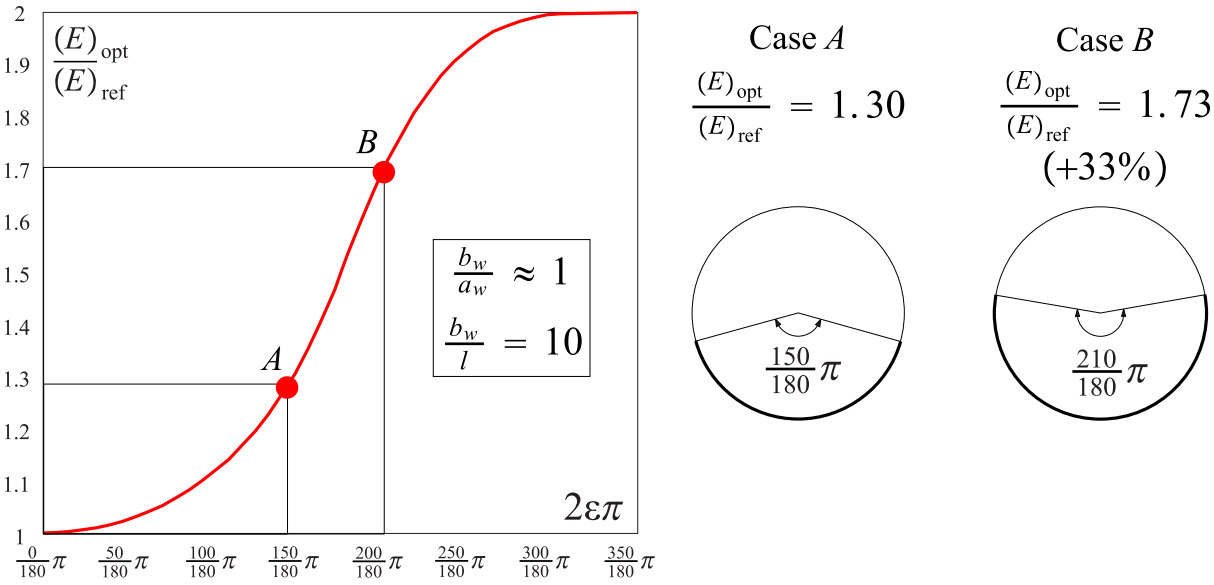

Figure 10.2. Elliptical lifting arcs under optimal conditions. Comparison with a classical wing with the same lift and wing span.

small. Moreover, the doublet distribution is almost elliptical (figure 10.3). This is an intuitive result: when $\varepsilon \to 0$, the curvature effects are negligible and the elliptical lifting arcs are practically a classical wing.

- *Result 2*
  When ε is not small, the efficiency increases and the doublet distribution is not an ellipse anymore (figures 10.4, 10.5, 10.6 and 10.7). This is particularly true when the arc is almost a closed curve (figures 10.6 and 10.7). This behavior does not change if the $\frac{b_w}{a_w}$ ratio is changed (figures 10.6 and 10.7).

- *Result 3*
  When the arc is almost a closed curve (*but still an arc*) the induced drag is the same as the induced drag of the corresponding annular wing (figures 10.6 and 10.7).

- *Result 4*
  The optimal doublet distribution *is always different than zero,* except at the tip of the wing. This is a very different situation with respect to what have been seen in the annular wings, where the distribution was sinusoidal. This property is also valid when the arc is almost a closed curve.

Figures 10.8, 10.9 and 10.10 show the non-dimensional optimal doublet distribution on the lifting arcs[4].

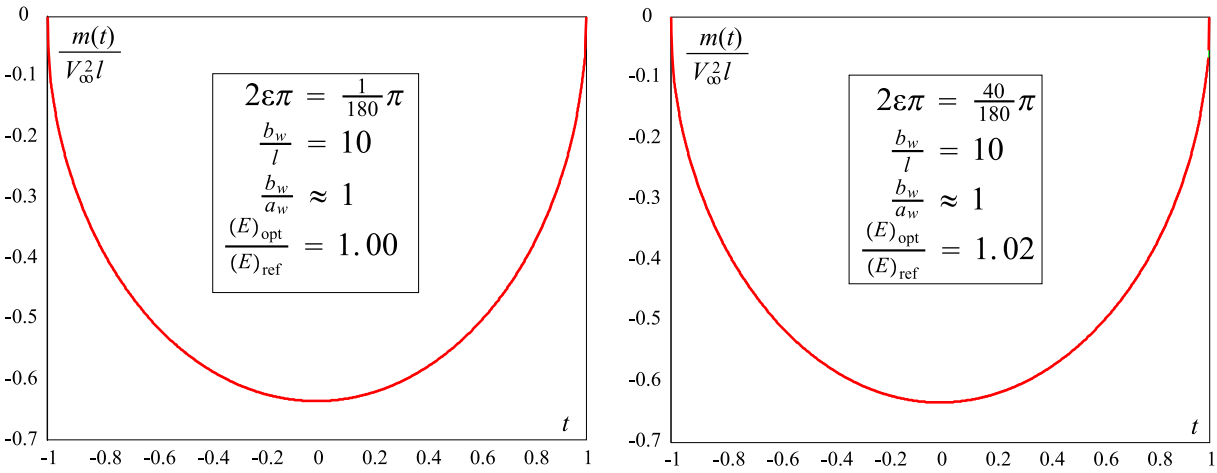

Figure 10.3. Optimal doublet distribution. $2\varepsilon\pi = \frac{1}{180}\pi$ and $2\varepsilon\pi = \frac{40}{180}\pi$ cases.

[4]The reference surface used to calculate the coefficient of lift is the following:

$$S = 2lb_w \sin\varepsilon\pi \qquad \text{if } \varepsilon < \tfrac{1}{2},$$
$$S = 2lb_w \qquad \text{if } \varepsilon \geq \tfrac{1}{2}.$$

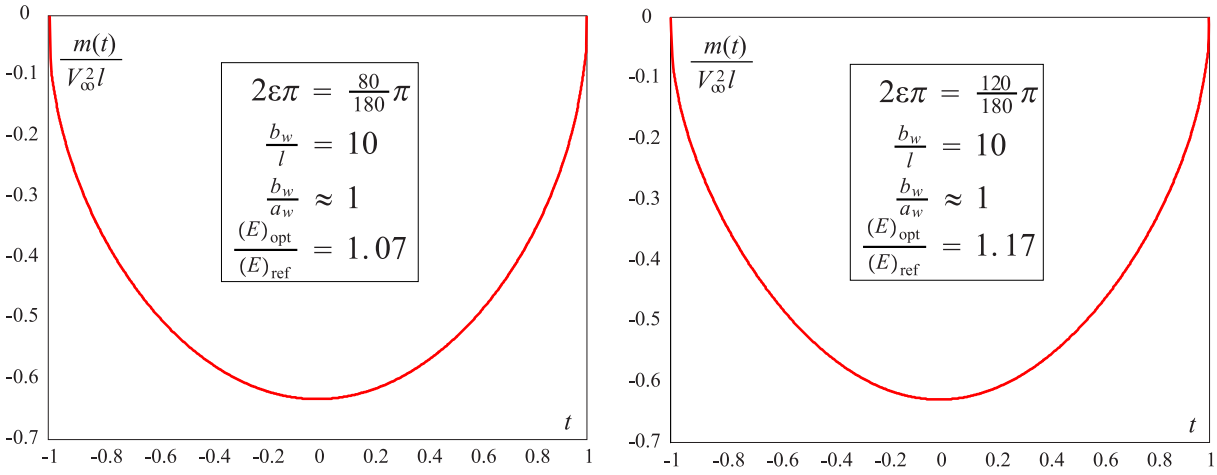

Figure 10.4. Optimal doublet distribution. $2\varepsilon\pi = \frac{80}{180}\pi$ and $2\varepsilon\pi = \frac{120}{180}\pi$ cases.

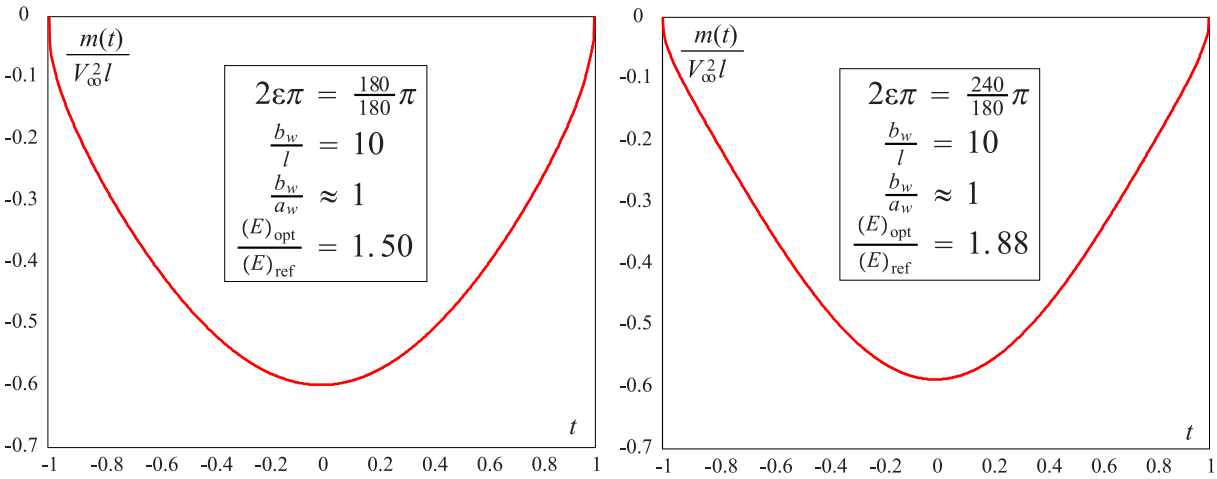

Figure 10.5. Optimal doublet distribution. $2\varepsilon\pi = \frac{180}{180}\pi$ and $2\varepsilon\pi = \frac{240}{180}\pi$ cases.

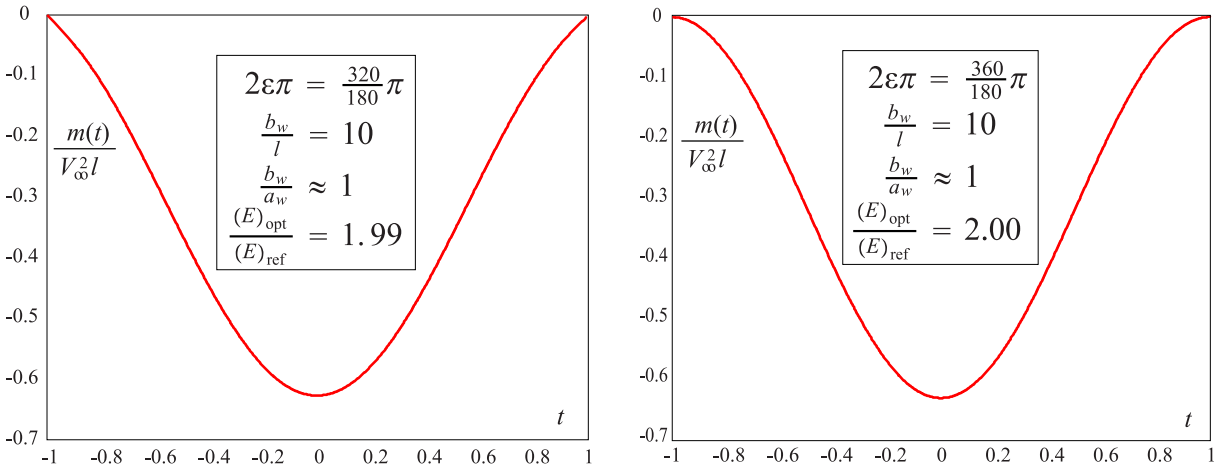

Figure 10.6. Optimal doublet distribution. $2\varepsilon\pi = \frac{320}{180}\pi$ and $2\varepsilon\pi = \frac{360}{180}\pi$ cases.

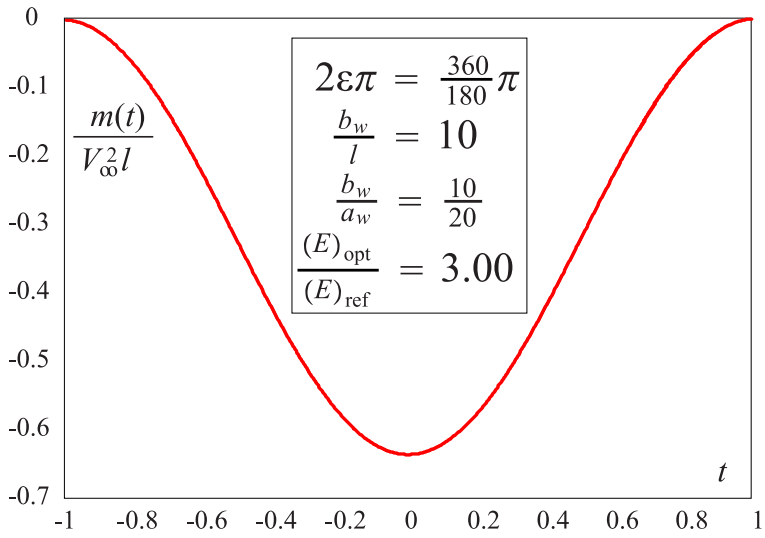

Figure 10.7. Optimal doublet distribution. $2\varepsilon\pi = \frac{360}{180}\pi$ case.

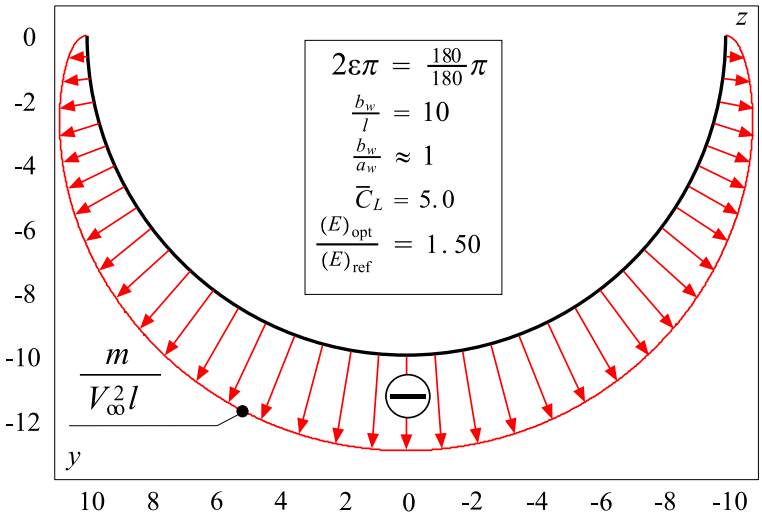

Figure 10.8. Optimal doublet distribution. $2\varepsilon\pi = \frac{180}{180}\pi$ case.

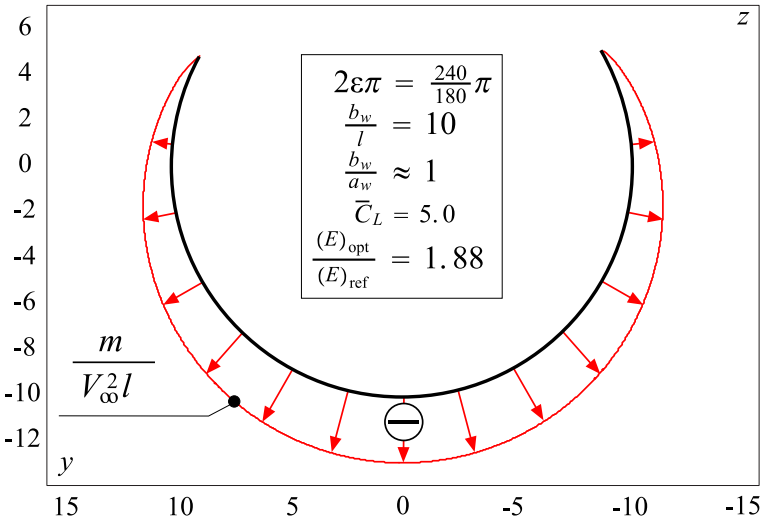

Figure 10.9. Optimal doublet distribution. $2\varepsilon\pi = \frac{240}{180}\pi$ case.

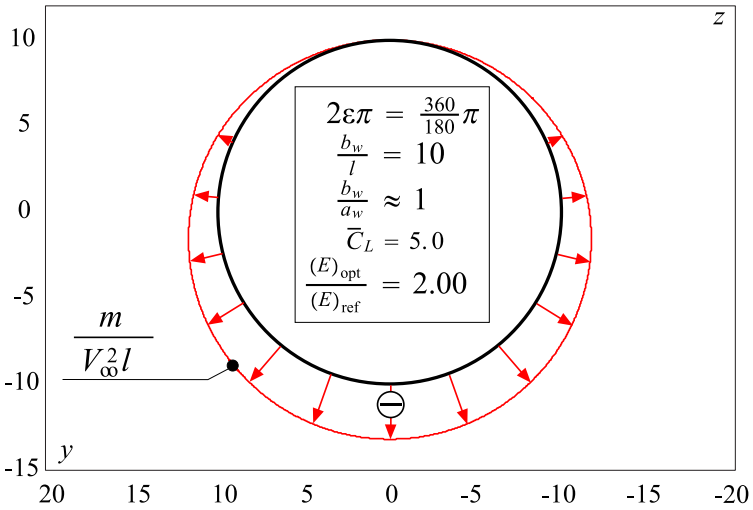

Figure 10.10. Optimal doublet distribution. $2\varepsilon\pi = \frac{360}{180}\pi$ case.

Nomenclature

$2b_w$	wing span
m	doublet distribution
C_L	coefficient of lift
C_{D_i}	coefficient of induced drag
F	aerodynamic force
$\overline{C}_L$	fixed value of the coefficient of lift
λ	Lagrange multiplier
V_∞	velocity (freestream conditions)
E	aerodynamic efficiency
$\overline{Y}$	kernel
S	reference surface

Subscripts

∞	freestream conditions
ref	referred to a cantilever wing with the same lift and wing span
concave	referred to a concave lifting arc
convex	referred to a convex lifting arc
opt	optimal condition (minimum induced drag)

Part III

Structural Model

Chapter 11

A Nonlinear Structural Model for the Nonlinear Aeroelastic Analysis of Joined Wings

11.1 Introduction

The work reported in this chapter is a result of the collaboration between the universities Politecnico di Torino (Turin, Italy) and University of Washington (Seattle, USA) about the joined wing analyses and studies.
A structural nonlinear code has been developed by the writer with the supervision of professor Livne. Here, a few details of this work (see, also, [70]) are reported.
A structural/structural-dynamic method for the modeling of general assemblies of thin plate segments is described. The method is based on Ritz functions approximations using complete polynomials as generalized coordinates per plate segment. A penalty function approach is used to impose boundary conditions and compatibility of motion between adjacent segments. The method is flexible in that it allows configuration-dependent selection of large segments with high order Ritz functions or small segments with low order Ritz functions or combinations of both for the efficient modeling of different configurations. No numerical integration is required. Test results obtained by the present method for a variety of plate structures show good correlation with published results and results by other computer codes.
As is widely recognized by now, structural nonlinearity has a major effect on the aeroelastic behavior of Joined-Wing configurations. When significant compressive loads are present in the rear wing (which supports the main wing) its effective stiffness (linear + geometric) varies. Aeroelastic mechanisms can involve buckling (or divergence) of the rear wing or flutter. As axial loads in the rear wing change, when the airplane maneuvers, its effective stiffness varies, and with it its flutter

mechanisms. The nonlinear structure might develop limit cycle oscillations or other nonlinear dynamic mechanisms. The fact that the two wings (rear and main) are joined complicates things. The type of joint and its location will be important. And then, of course, whether linearized or nonlinear aerodynamic modeling is used might make a difference too, depending on how large the deformations of the configuration are.
The fundamental nature of such questions, and the lack of thorough understanding of joined-wing aeroelasticity issues, call for basic research using mathematical models that can capture the important physics of the problem and that yet are simple enough to allow quick and user-friendly generation and provide guidance during the development of possible simple scaled-models for experiments.
Here, a simple and efficient nonlinear structural modeling capability developed for the fundamental study of simple plate-like lifting surface configurations undergoing moderate nonlinear deformation and oscillation is presented. General 3-dimensional configurations made of lifting surfaces and control surfaces can be modeled. The discretization of the differential equations describing the structure is based on a Ritz technique, using global function bases for the different lifting surface segment. With the capability to calculate deflections and rotations at any point on the structure using the global Ritz functions, the problem of transformation between structural and aerodynamic grids - one of the fundamental problems of Aeroelasticity - is greatly simplified.

11.2 Description of the Structural Model

The mathematical model is built by assembling nonlinear solid-plate elements (denoted as wing segments). Boundary conditions and compatibility constraints used to connect different segments to one another are imposed by a penalty function method [71]. The physical meaning of the weights used for the penalty terms is that of physical springs. This discretization is shown in figure 11.1. Wing segments are modeled as solid thin plates, with planar cross sections remaining planar and staying perpendicular to the plate's reference surface. Nonlinear behavior is studied using the von-Karman plate theory for moderately-large displacements:

$$\begin{aligned} \varepsilon_{xx} &= u_{,_x} + \tfrac{1}{2} w_{,_x}^2 \,, \\ \varepsilon_{yy} &= v_{,_y} + \tfrac{1}{2} w_{,_y}^2 \,, \\ \varepsilon_{xy} &= \tfrac{1}{2} \left(u_{,_y} + v_{,_x} \right) + \tfrac{1}{2} w_{,_x} w_{,_y} . \end{aligned} \tag{11.1}$$

In accordance with the Classical Plate Theory, it is also assumed that each layer (lamina) of the plate is in plane strain:

$$\varepsilon_{zx} = \varepsilon_{zy} = \varepsilon_{zz} = 0. \tag{11.2}$$

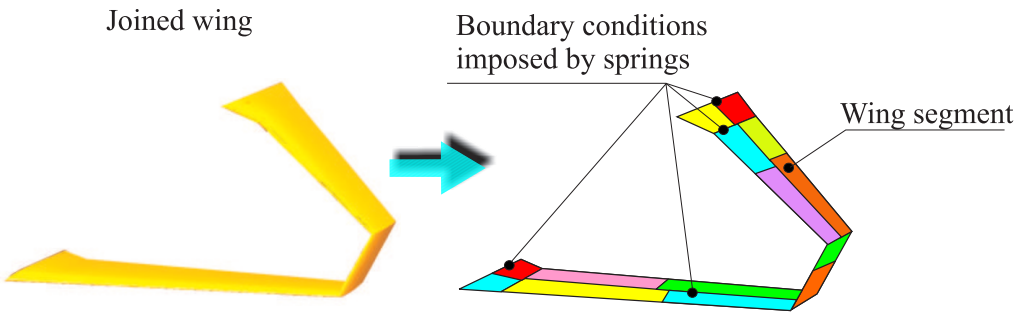

Figure 11.1. Joined wing discretization using trapezoidal wing segments.

For the displacement field, CLPT (Classical Plate Theory) is based on:

$$\begin{aligned} u\,(x,y,z,t) &= u_0\,(x,y,t) - z w_{0,x}\,(x,y,t)\ , \\ v\,(x,y,z,t) &= v_0\,(x,y,t) - z w_{0,y}\,(x,y,t)\ , \\ w\,(x,y,z,t) &= w_0\,(x,y,t)\,. \end{aligned} \tag{11.3}$$

Multiplication of the equations of equilibrium by virtual displacements, and integration over the plate's volume lead to the virtual work principle in the form

$$\int_V \sigma_{ij}\delta\varepsilon_{ij}\,\mathrm{d}v + \int_V \rho\ddot{u}_i\delta u_i\,\mathrm{d}v = \int_S T_i\delta u_i\,\mathrm{d}s, \tag{11.4}$$

where T_i is the traction force per unit of area. For the layer-by-layer plane stress case, the last equation can be written as

$$\begin{aligned} &\int_V \left(\sigma_{xx}\delta\varepsilon_{xx} + \sigma_{yy}\delta\varepsilon_{yy} + \sigma_{xy}\delta\gamma_{xy}\right)\mathrm{d}v + \int_V \rho\left(\ddot{u}\delta u + \ddot{v}\delta v + \ddot{w}\delta w\right)\mathrm{d}v = \\ &= \int_S \left(T_x\delta u + T_y\delta v + T_z\delta w\right)\mathrm{d}s. \end{aligned} \tag{11.5}$$

Using a general linear material law for plane-stress[1], the previous equation becomes:

$$\int_V \delta\boldsymbol{\varepsilon}^T\,\overline{\boldsymbol{Q}}\,\boldsymbol{\varepsilon}\,\mathrm{d}v + \int_V \rho\delta\boldsymbol{u}^T\ddot{\boldsymbol{u}}\,\mathrm{d}v = \int_S \delta\boldsymbol{u}^T\boldsymbol{T}\,\mathrm{d}s. \tag{11.6}$$

[1] The Hooke law is:

$$\boldsymbol{\sigma} = \overline{\boldsymbol{Q}}\boldsymbol{\varepsilon},$$

where:

$$\boldsymbol{\sigma} = \left[\sigma_{xx}\ \ \sigma_{yy}\ \ \sigma_{xy}\right]^T, \qquad \boldsymbol{\varepsilon} = \left[\varepsilon_{xx}\ \ \varepsilon_{yy}\ \ \gamma_{xy}\right]^T,$$

$$\overline{\mathbf{Q}} = \begin{bmatrix} \overline{Q}_{11} & \overline{Q}_{12} & \overline{Q}_{16} \\ \overline{Q}_{12} & \overline{Q}_{22} & \overline{Q}_{26} \\ \overline{Q}_{16} & \overline{Q}_{26} & \overline{Q}_{66} \end{bmatrix}.$$

The strains can be written as (equations (11.1) and (11.3))

$$\boldsymbol{\varepsilon} = \boldsymbol{\varepsilon}_{l_0} - z\boldsymbol{\varepsilon}_{l_1} + \boldsymbol{\varepsilon}_{nl}, \tag{11.7}$$

where:

$$\boldsymbol{\varepsilon}_{l_0} = \begin{bmatrix} u_{0,_x} \\ v_{0,_y} \\ u_{0,_y} + v_{0,_x} \end{bmatrix}, \quad \boldsymbol{\varepsilon}_{l_1} = \begin{bmatrix} w_{0,_{xx}} \\ w_{0,_{yy}} \\ 2w_{0,_{xy}} \end{bmatrix}, \quad \boldsymbol{\varepsilon}_{nl} = \begin{bmatrix} \frac{1}{2}w_{0,_x}^2 \\ \frac{1}{2}w_{0,_y}^2 \\ w_{0,_x} w_{0,_y} \end{bmatrix}. \tag{11.8}$$

Carrying out the volume integration, first with respect to z and then with respect to x and y and using the matrices:

$$\begin{aligned} \boldsymbol{A} &= \int_z \overline{\boldsymbol{Q}} \mathrm{d}z, \\ \boldsymbol{D} &= \int_z z^2 \, \overline{\boldsymbol{Q}} \mathrm{d}z, \end{aligned} \tag{11.9}$$

yields, in the case of symmetric layups[2],

$$\begin{aligned} \int_V \delta\boldsymbol{\varepsilon}^T \, \overline{\boldsymbol{Q}} \, \boldsymbol{\varepsilon} \, \mathrm{d}v \;=\; & \int_{x,y} \delta\boldsymbol{\varepsilon}_{l_0}^T \boldsymbol{A} \boldsymbol{\varepsilon}_{l_0} \, \mathrm{d}x\mathrm{d}y + \int_{x,y} \delta\boldsymbol{\varepsilon}_{l_0}^T \boldsymbol{A} \boldsymbol{\varepsilon}_{nl} \, \mathrm{d}x\mathrm{d}y + \int_{x,y} \delta\boldsymbol{\varepsilon}_{l_1}^T \boldsymbol{D} \boldsymbol{\varepsilon}_{l_1} \, \mathrm{d}x\mathrm{d}y + \\ & \int_{x,y} \delta\boldsymbol{\varepsilon}_{nl}^T \boldsymbol{A} \boldsymbol{\varepsilon}_{l_0} \, \mathrm{d}x\mathrm{d}y + \int_{x,y} \delta\boldsymbol{\varepsilon}_{nl}^T \boldsymbol{A} \boldsymbol{\varepsilon}_{nl} \, \mathrm{d}x\mathrm{d}y. \end{aligned} \tag{11.10}$$

11.3 Ritz Discretization

Solutions for the displacement field are sought by using a set of Ritz functions as generalized coordinates:

$$\begin{aligned} u_0\,(x,y,t) &= F_1^u\,(x,y)\,q_{u_1}\,(t) + F_2^u\,(x,y)\,q_{u_2}\,(t) + \ldots + F_{N_u}^u\,(x,y)\,q_{u_{N_u}}\,(t)\,, \\ v_0\,(x,y,t) &= F_1^v\,(x,y)\,q_{v_1}\,(t) + F_2^v\,(x,y)\,q_{v_2}\,(t) + \ldots + F_{N_v}^v\,(x,y)\,q_{v_{N_v}}\,(t)\,, \\ w_0\,(x,y,t) &= F_1^w\,(x,y)\,q_{w_1}\,(t) + F_2^w\,(x,y)\,q_{w_2}\,(t) + \ldots + F_{N_w}^w\,(x,y)\,q_{w_{N_w}}\,(t)\,. \end{aligned} \tag{11.11}$$

Here, following [72]-[77], polynomials of the type $x^s y^r$ are used as Ritz functions to create complete-polynomials.
It is well known that simple polynomials lead to ill-conditioning when used as Ritz functions, as terms with high powers r and s are present alongside low-order terms. However, simple polynomials lead to a greatly simplified problem formulation, and, if a configuration is divided into small segments where low-order polynomials are

[2] The reference plane x,y is the middle plane of the plate.

used, ill-conditioning is not a problem.
Using a more compact notation, the displacement field (equation (11.11)) is expressed as

$$\begin{bmatrix} u_0 \\ v_0 \\ w_0 \end{bmatrix} = \begin{bmatrix} \boldsymbol{F}^{u\,T} & \boldsymbol{0}^{v\,T} & \boldsymbol{0}^{w\,T} \\ \boldsymbol{0}^{u\,T} & \boldsymbol{F}^{v\,T} & \boldsymbol{0}^{w\,T} \\ \boldsymbol{0}^{u\,T} & \boldsymbol{0}^{v\,T} & \boldsymbol{F}^{w\,T} \end{bmatrix} \cdot \begin{bmatrix} \boldsymbol{q}_u \\ \boldsymbol{q}_v \\ \boldsymbol{q}_w \end{bmatrix}. \tag{11.12}$$

Substitution into equations (11.8) and (11.10) leads to

$$\begin{aligned} \int_V \delta\boldsymbol{\varepsilon}^T \overline{\boldsymbol{Q}}\, \boldsymbol{\varepsilon}\, \mathrm{d}v &= \delta\boldsymbol{q}^T \boldsymbol{K}_{l_0 l_0} \boldsymbol{q} + \delta\boldsymbol{q}^T \boldsymbol{K}_{l_0 nl} \boldsymbol{q} + \delta\boldsymbol{q}^T \boldsymbol{K}_{l_1 l_1} \boldsymbol{q} + \\ &+ \delta\boldsymbol{q}^T \boldsymbol{K}_{nl\,l_0} \boldsymbol{q} + \delta\boldsymbol{q}^T \boldsymbol{K}_{nl\,nl} \boldsymbol{q}. \end{aligned} \tag{11.13}$$

The details of the computation of the different stiffness matrices are given in appendices N and O. Because of the simple-polynomial nature of the Ritz function used, all volume integrals over trapezoidal plate segments can be carried out analytically without any need for numerical integration.
For a symmetric layup and uniform density, the inertial terms are

$$\int_V \rho \delta\boldsymbol{u}^T \ddot{\boldsymbol{u}}\, \mathrm{d}v = \delta\boldsymbol{q}^T \boldsymbol{M}^1 \ddot{\boldsymbol{q}} + \delta\boldsymbol{q}^T \boldsymbol{M}^2 \ddot{\boldsymbol{q}}. \tag{11.14}$$

The virtual work equation (equations (11.10) and (11.13)) now takes the form

$$\delta\boldsymbol{q}^T \left[\boldsymbol{K}_{l_0 l_0} + \boldsymbol{K}_{l_0 nl} + \boldsymbol{K}_{l_1 l_1} + \boldsymbol{K}_{nl\,l_0} + \boldsymbol{K}_{nl\,nl}\right] \boldsymbol{q} + \delta\boldsymbol{q}^T \left[\boldsymbol{M}^1 + \boldsymbol{M}^2\right] \ddot{\boldsymbol{q}} = \delta L_e, \tag{11.15}$$

where δL_e is the external virtual work.

11.4 Imposition of the Boundary Conditions

Stiffness and mass matrices are calculated for each wing segment separately in local coordinate axes for the segment. In assembling a configuration from segments, boundary conditions have to be imposed as well as compatibility conditions between segments. The following boundary conditions have to be imposed:

- *Boundary Condition 1*
  Displacements and rotations between two adjacent wing segments must be the same[3].

[3] There is an important exception. In some joined wing studies, it could be interesting, for example, to impose only the same displacements in the joint and compare the results with a case where the rotations are also imposed.

- *Boundary Condition 2*
  Displacement and/or rotations have to be zero at points or along the lines attached to the ground.

One of the essential features of the finite element method is that generalized displacements are actual physical displacements and rotations of element nodes. By adding to the proper locations on the global stiffness and mass matrices stiffness and mass contributions of elements that share the same nodes, compatibility of motion is guaranteed at those nodes. But compatibility of motion is not guaranteed along the common edges of elements, and what convergence characteristics "compatible" or "incompatible" various plate elements have is one of the most challenging problems of plate and shell finite elements.
By using a penalty function technique (Ref. [71]) to impose compatibility along the sides of adjacent plate elements, relating the Ritz functions to nodal motions is not needed. Any order of Ritz functions can be used over a plate segment, while element-to-element attachments are enforced by lines of stiff springs - the physical meaning of the penalty terms used to enforce the compatibility constraints.
To do that, it is sufficient to put adequate number of springs along the edges between two adjacent wing segments. In order to impose compatibility of the rotations between two wing segments, if only translational springs are used, it is sufficient to place translational springs in different positions along the thickness.
Consider a simple case where two points, 1_A on wing segment A and 1_B on wing segment B, have to be linked by springs (figure 11.2). The procedure is based on these steps:

- *Step 1*
  The displacement field at point 1_A in the *local coordinate system* on the wing segment A is considered.

- *Step 2*
  The *global coordinates* of the same point are determined by multiplying the local coordinates by the geometric transformation matrix from local A axes to global axes.

- *Step 3*
  The same procedure is applied to point 1_B on the wing segment B.

- *Step 4*
  The *potential energy* of springs linking the $x-y-z$ motions of points 1_A and 1_B is written as

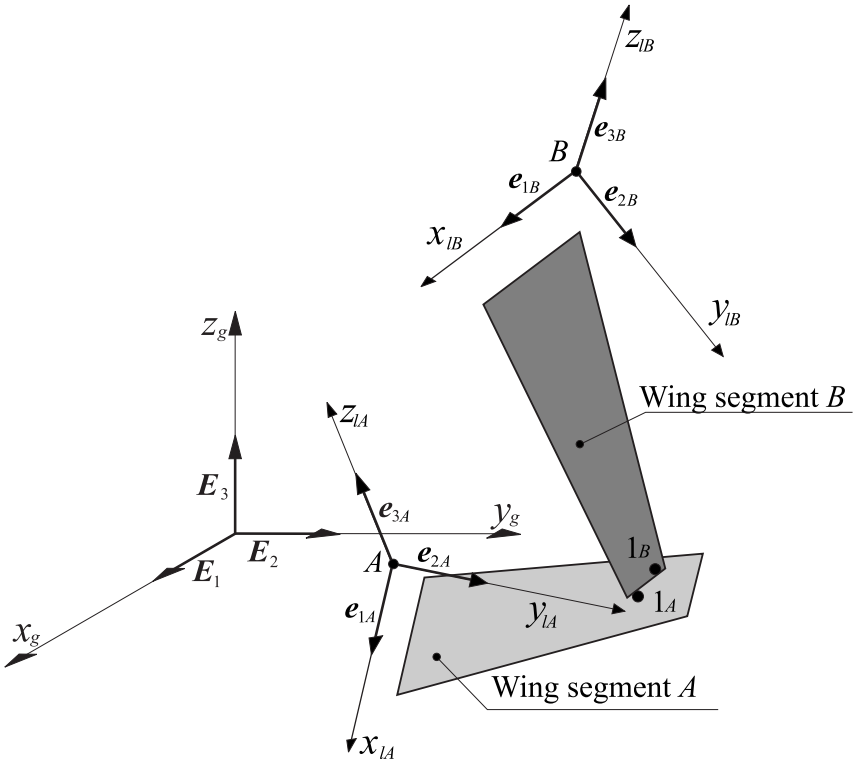

Figure 11.2. Imposition of boundary conditions by springs.

$$U = \frac{1}{2}\left[\begin{bmatrix} u_{1_A} \\ v_{1_A} \\ w_{1_A} \end{bmatrix}_g - \begin{bmatrix} u_{1_B} \\ v_{1_B} \\ w_{1_B} \end{bmatrix}_g\right]^T \begin{bmatrix} k_x^1 & 0 & 0 \\ 0 & k_y^1 & 0 \\ 0 & 0 & k_z^1 \end{bmatrix} \left[\begin{bmatrix} u_{1_A} \\ v_{1_A} \\ w_{1_A} \end{bmatrix}_g - \begin{bmatrix} u_{1_B} \\ v_{1_B} \\ w_{1_B} \end{bmatrix}_g\right]. \tag{11.16}$$

The subscripts g in the previous equation indicate that the displacements have to be referred to the *global coordinate system.*

- *Step 5*
  Substituting the Ritz function series approximations for the displacements of 1_A and 1_B in axes A and B, respectively (equations (11.11) and (11.12)), and using the subscripts A and B for the generalized coordinates on the wing segments A and B, the potential energy can be rewritten as

$$U = \frac{1}{2}\left[\boldsymbol{q}_A^T\left(\boldsymbol{K}_{AA}^{s1}\right)\boldsymbol{q}_A + \boldsymbol{q}_A^T\left(\boldsymbol{K}_{AB}^{s1}\right)\boldsymbol{q}_B + \boldsymbol{q}_B^T\left(\boldsymbol{K}_{BA}^{s1}\right)\boldsymbol{q}_A + \boldsymbol{q}_B^T\left(\boldsymbol{K}_{BB}^{s1}\right)\boldsymbol{q}_B\right]. \tag{11.17}$$

The quantities $\boldsymbol{K}^{s1}_{AA}$, $\boldsymbol{K}^{s1}_{AB}$, $\boldsymbol{K}^{s1}_{BA}$ and $\boldsymbol{K}^{s1}_{BB}$ are the stiffness matrices that have to be added to the total stiffness matrix in locations corresponding to generalized coordinates $\boldsymbol{q}_A$ and $\boldsymbol{q}_B$ (figure 11.3).

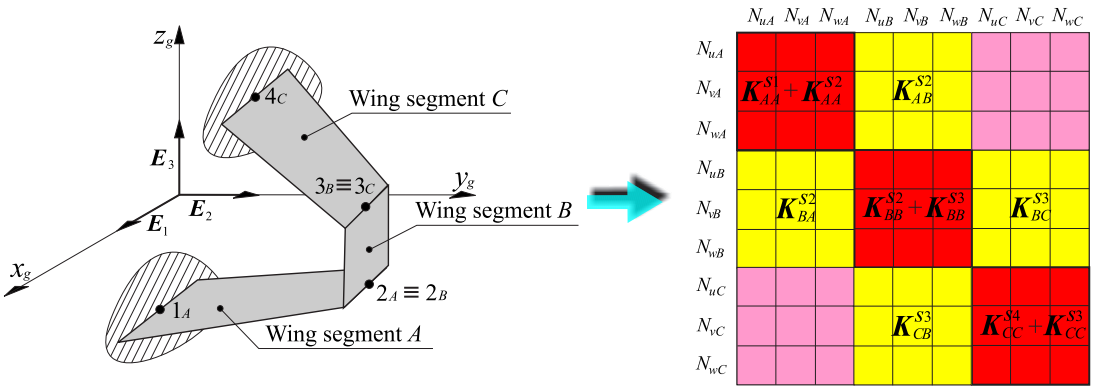

Figure 11.3. Example of imposition of boundary conditions by springs.

11.5 Analytical Integration

One important advantage of the usage of Ritz functions in the form $x^s y^r$ is that it is possible to use *analytical* integration to calculate the integrals over a trapezoidal domain (the middle surface of the wing segment).
Consider a wing segment in which two edges are parallel to the local x axis[4], as shown in figure 11.4. The front and rear (aft) lines depend on the coordinates of the vertices of the trapezoid and are defined by the equations:

$$\begin{aligned} x_F(y) &= F_1 y + F_2, \\ x_A(y) &= A_1 y + A_2, \end{aligned} \tag{11.18}$$

where:

$$\begin{aligned} F_1 &= \tfrac{x_{FR} - x_{FL}}{y_R - y_L}, \\ F_2 &= \tfrac{x_{FL} y_R - x_{FR} y_L}{y_R - y_L}, \\ A_1 &= \tfrac{x_{AR} - x_{AL}}{y_R - y_L}, \\ A_2 &= \tfrac{x_{AL} y_R - x_{AR} y_L}{y_R - y_L}. \end{aligned} \tag{11.19}$$

[4]It is always possible to divide the wing into segments with this characteristic without losing generality.

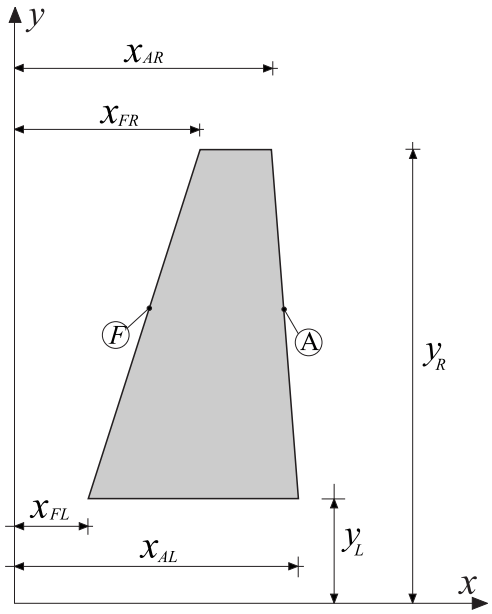

Figure 11.4. Analytical integration.

The integral of any simple-polynomial term with powers r and s over the wing is of the type:

$$\begin{aligned} I_{\mathrm{TR}}(r,s) &= \int_{y=y_L}^{y=y_R} y^r \int_{x=x_F(y)}^{x=x_A(y)} x^s \mathrm{d}\,x \mathrm{d}\,y = \tfrac{1}{s+1} \int_{y=y_L}^{y=y_R} y^r \left[x_A(y)^{s+1} - x_F(y)^{s+1} \right] \mathrm{d}y = \\ &= \tfrac{1}{s+1} \int_{y=y_L}^{y=y_R} y^r (A_1 y + A_2)^{s+1} \,\mathrm{d}y - \tfrac{1}{s+1} \int_{y=y_L}^{y=y_R} y^r (F_1 y + F_2)^{s+1} \,\mathrm{d}y = \\ &= \tfrac{1}{S} \int_{y=y_L}^{y=y_R} y^R (A_1 y + A_2)^S \,\mathrm{d}y - \tfrac{1}{S} \int_{y=y_L}^{y=y_R} y^R (F_1 y + F_2)^S \,\mathrm{d}y. \end{aligned} \tag{11.20}$$

The last two integrals can be calculated by using the recursive formulas:

$$\int y^R (A_1 y + A_2)^S \,\mathrm{d}y = \frac{y^{R+1} (A_1 y + A_2)^S}{R+S+1} + \frac{S A_2}{R+S+1} \int y^R (A_1 y + A_2)^{S-1} \,\mathrm{d}y, \tag{11.21}$$

$$\int y^R (F_1 y + F_2)^S \,\mathrm{d}y = \frac{y^{R+1} (F_1 y + F_2)^S}{R+S+1} + \frac{S F_2}{R+S+1} \int y^R (F_1 y + F_2)^{S-1} \,\mathrm{d}y. \tag{11.22}$$

A table of integrals of simple-polynomial functions of increasing order is prepared once for each trapezoidal segments at the start of a simulation run up to the highest

order needed. Integrals of $x^s\ y^r$ over the trapezoid are then taken from such tables in the stiffness and mass matrix assembly process.

11.6 Solution of the Nonlinear System

Several methods are presented in literature for the integration and solution of fully nonlinear structural analysis problems ([78]-[87]). In the formulation used here for the moderately-small deformations of plates, the *direct iteration method* and *Newton-Raphson method are adopted*. While the linear parts of the stiffness matrix are computed once, the nonlinear parts, which depend on the motion $\boldsymbol{q}$, have to be repetitively calculated during simulation. This is done by pulling out of the integral tables needed integrals of polynomial functions and using them to compute new nonlinear stiffness matrices (appendices N and O).

11.7 The Selected Test Problems

A number of test cases were selected for evaluation of the nonlinear structural plate analysis described here. Results of the present capability are compared with the reported results from literature and with MSC-NASTRAN solutions. In all MSC-NASTRAN cases, CQUAD4 plate elements were used. The following cases are analyzed:

- *Case 1*
  Isotropic cantilever plate under uniform pressure (figure 11.5). Static loading. This case is used to study the convergence of the present method. It is also used to study the effect of the stiffness of the constraint springs on final results.

- *Case 2*
  Isotropic squared plate supported along its circumference (figure 11.5). Static loading. All edges have $u_0 = v_0 = w_0 = 0$. A uniform pressure load is applied.

- *Case 3*
  Isotropic rhombic cantilever plate (figure 11.6), on which uniform pressure is applied. The analysis is linear.

- *Case 4*
  Typical joined-wing configuration (figure 11.6). Linear and nonlinear behavior are analyzed under uniform loading, as shown in figure 11.6. Natural modes are also calculated.

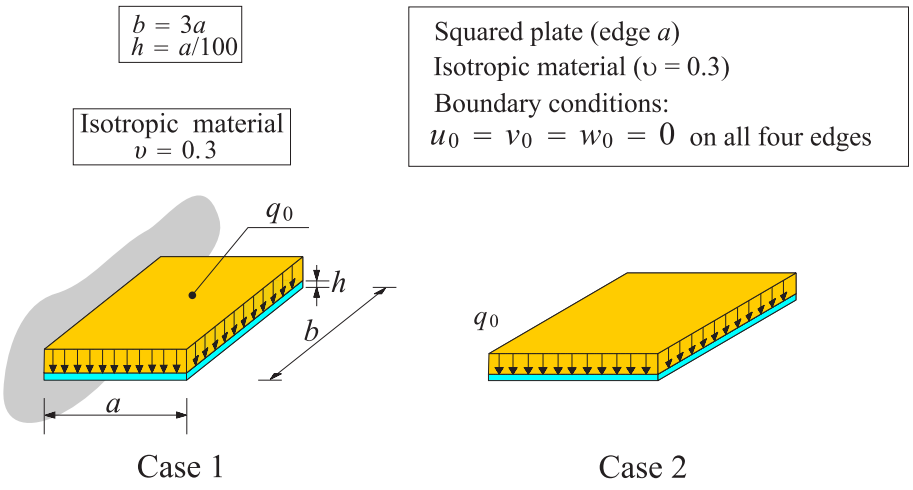

Figure 11.5. Case 1 and case 2: geometry and notations.

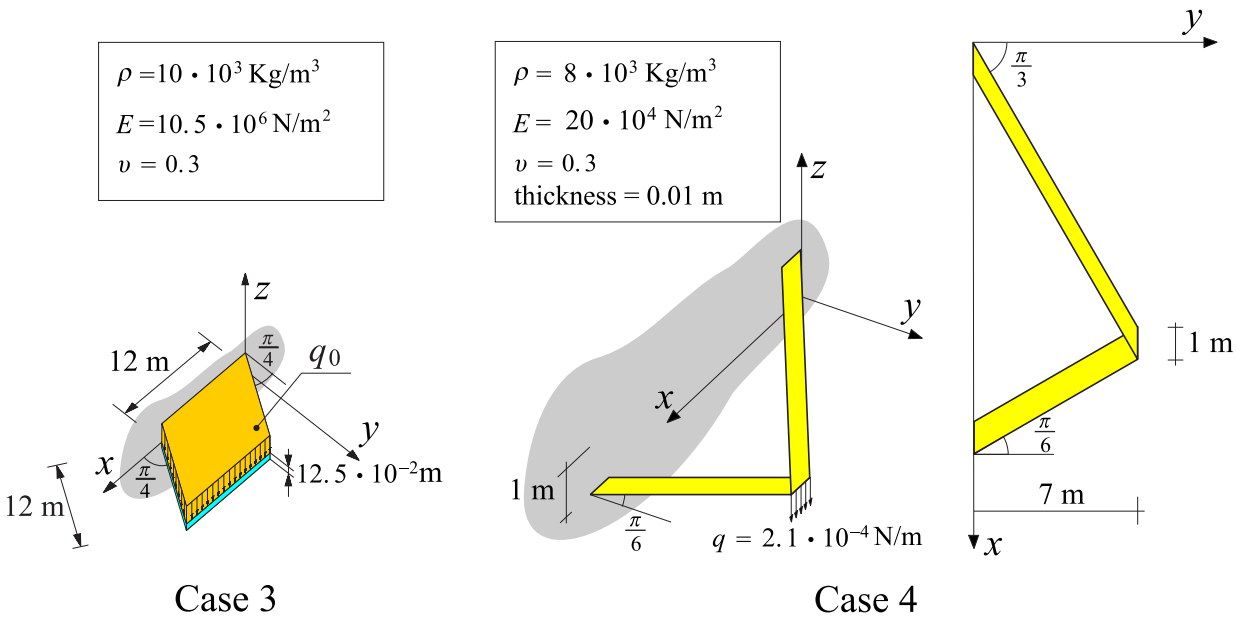

Figure 11.6. Case 3 and case 4: geometry and notations.

11.8 Convergence Test

As shown in figure 11.7, an increased number of wing segments with low-order Ritz polynomials per segments lead to results that are more close to a solution obtained by the ADINA code [76] and [77]. It should be noted that the ADINA solution is fully

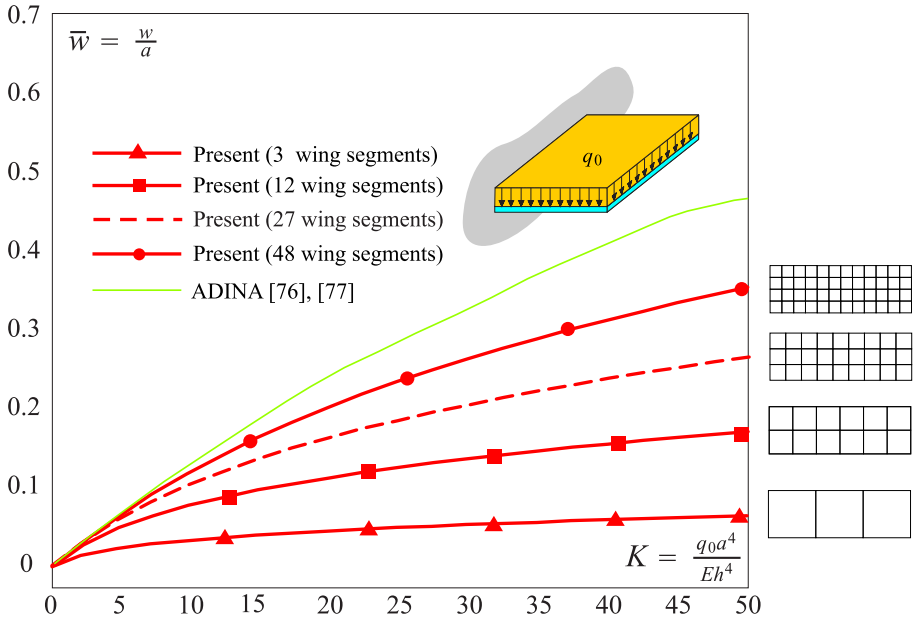

Figure 11.7. Case 1: effect of the number of wing segments.

nonlinear and allows large deformation. That is, nodes are allowed to move when the load is increased. The present solution, based on von-Karman's plate theory, assumes fixed local coordinates for segments, and, thus, as expected, it cannot follow the large-deformation case beyond a certain load level. In the cases shown in figure 11.7, the present modeling technique captures the nonlinear behavior of the plate up to a normalized load factor of about K=7.

In figure 11.7, 6 Ritz functions are used for the displacements u_0, v_0 and w_0 of each segment. Hence, the Ritz function used are $F_1^u = F_1^v = F_1^w = 1$, $F_2^u = F_2^v = F_2^w = x$, $F_3^u = F_3^v = F_3^w = y$, $F_4^u = F_4^v = F_4^w = x^2$, $F_5^u = F_5^v = F_5^w = xy$ and $F_6^u = F_6^v = F_6^w = y^2$.

Figure 11.8 shows the effect of the stiffness of the springs used for boundary conditions and compatibility enforcement. As is evident, the solution is not sensitive to the stiffness of the springs, as long as the springs (penalty weights) are stiff enough but not too stiff to cause ill-conditioning [71].

Values of $k_x = k_y = k_z = aE$ are, thus, used for all springs. Figure 11.9 shows that selection of the order of expansion used is very important. A good correlation

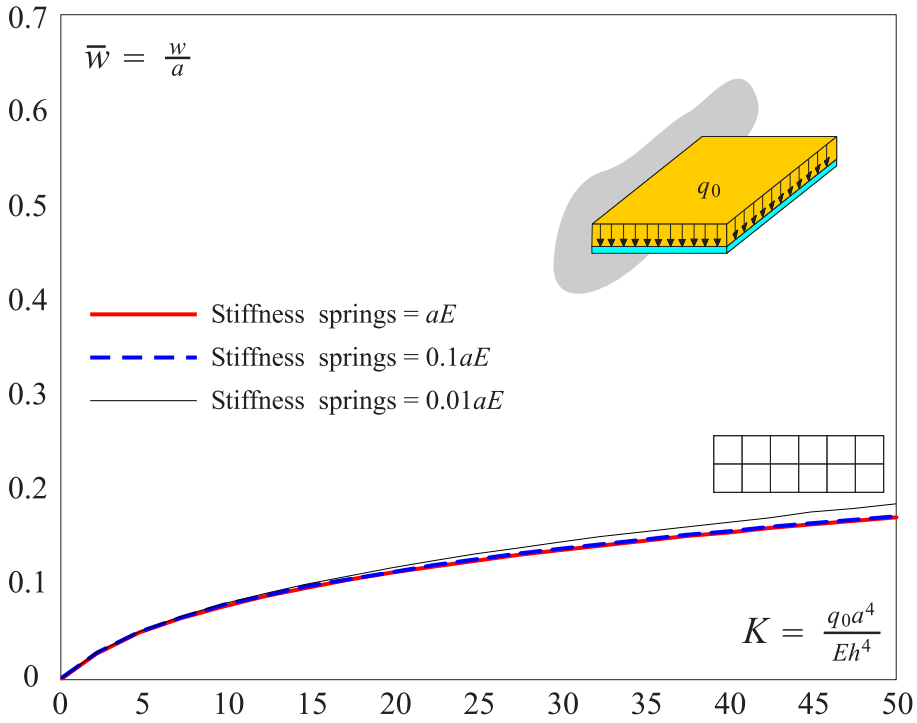

Figure 11.8. Case 1: effect of springs' stiffness.

with ADINA is obtained by using 12 wing segments, where, for each segment, 6 Ritz functions (quadratic complete polynomials) are used for u_0 and v_0 and 15 Ritz functions are used for w_0 (4^{th} order complete polynomial).
Note the difference in results between ADINA and MSC-NASTRAN, due, possibly, to a difference between the plate element formulations used.

11.9 Comparison with Published Results

In figures 11.10 and 11.11, results obtained by the present capability are compared with results presented in the literature ([88]-[92]). In figure 11.10, four wing segments are used, with 6 Ritz functions for u_0 and v_0 and 15 Ritz functions for w_0 of each segment. Results obtained by the present capability are denoted by "Present MATLAB". In figure 11.11, the same Ritz functions are used, but nine wing segments had to be used to have a good convergence for the linear case of the rhombic wing.

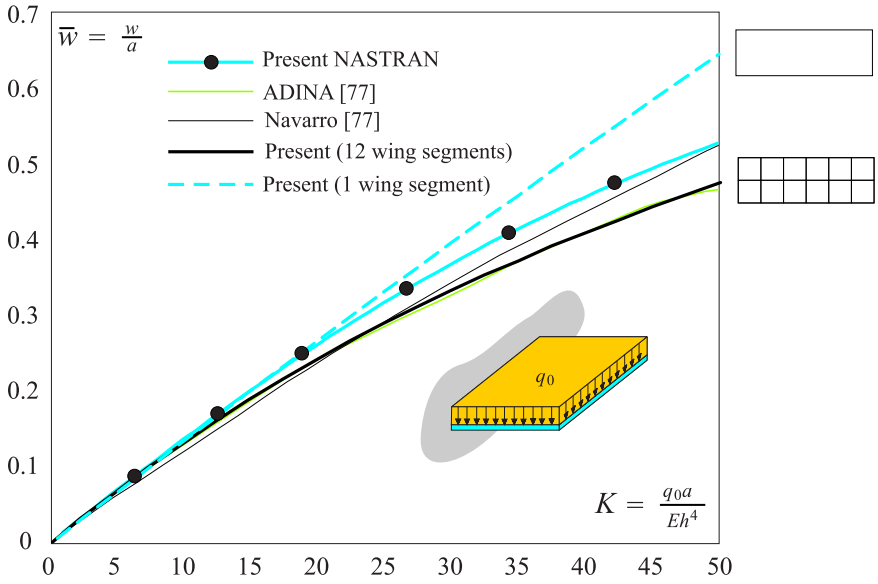

Figure 11.9. Case 1: effect of the number of Ritz functions.

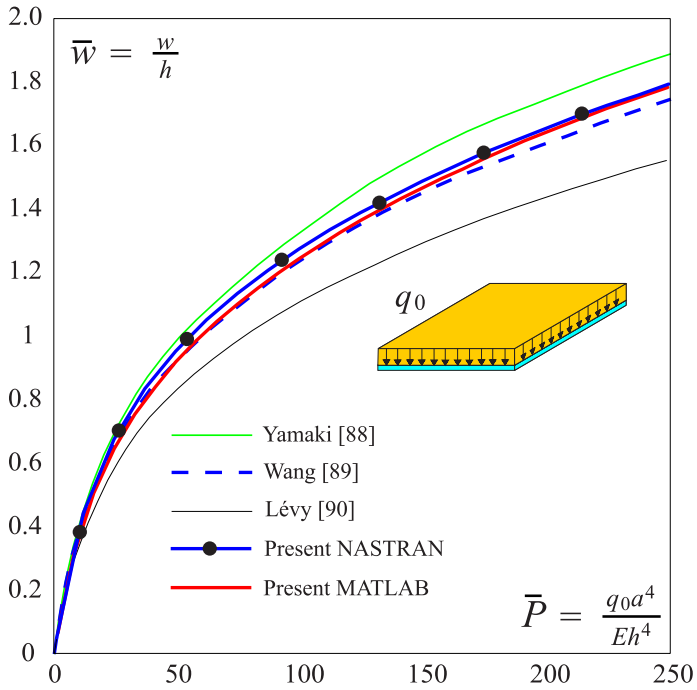

Figure 11.10. Case 2: nonlinear displacements.

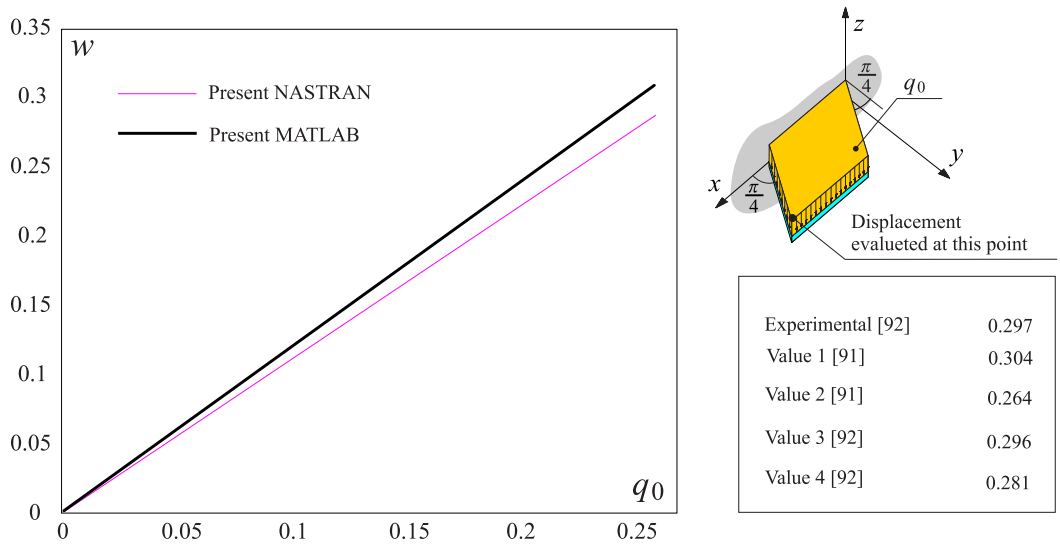

Figure 11.11. Case 3: linear displacements.

11.10 Structural Analysis of a Joined Wing Configuration

Fourty two wing segments (21 for each wing) have been used to model the Joined-Wing configuration of case 4 (figure 11.6).
Six Ritz functions for u_0 and v_0 and 15 Ritz functions for w_0 were used.
Figures 11.13, 11.14 and 11.15 show the natural modes and frequencies obtained by the present capability and NASTRAN. The correlation is good up to quite a high natural frequency.
Comparison of static linear and nonlinear displacements under tip load between the present capability and MSC-NASTRAN is shown in figure 11.12.
Results by NASTRAN and the present code deviate slightly from one another, starting with the linear case, due, possibly, to the differences in modeling classical plates between the CQUAD4 element formulation and the formulation used here. This is not surprising given the sensitivity of nonlinear structural simulations to element selection, especially in the case of plates and shells. Overall, the present capability captures the nonlinear deformation quite well.

11.11 Conclusion

The structural model presented here is capable of well capturing displacements (linear and nonlinear) and natural modes and frequencies of multi-segment plate configurations. Several different geometries have been analyzed. In all cases, results obtained in present study showed good agreement with the published results and NASTRAN runs. The present capability can capture vibration modes and nonlinear deformation, including buckling of joined wings configurations. It is general in that it allows modeling using different sizes of wing segments (from small to large) and different orders of Ritz polynomials per segment (from high order to low-order). Some experimentation with paneling (division into segments) and Ritz function order selection per panel is required when a new configuration is studied for the first time to determine the best paneling/Ritz function order necessary.

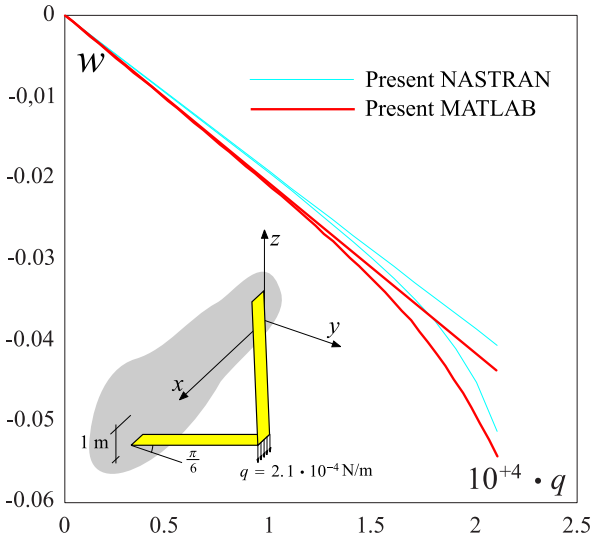

Figure 11.12. Case 4: nonlinear results.

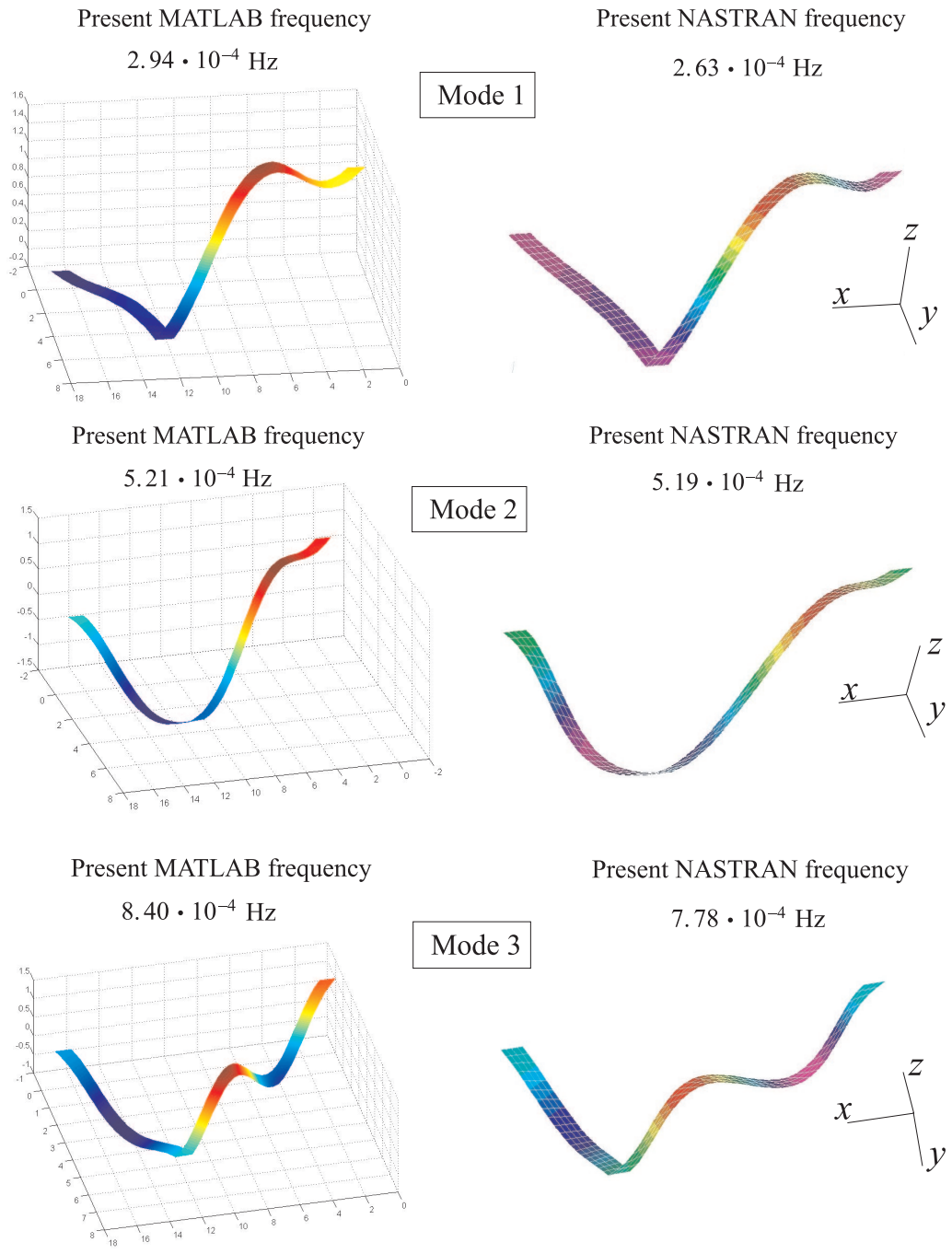

Figure 11.13. Case 4: modes 1, 2, 3 compared with NASTRAN.

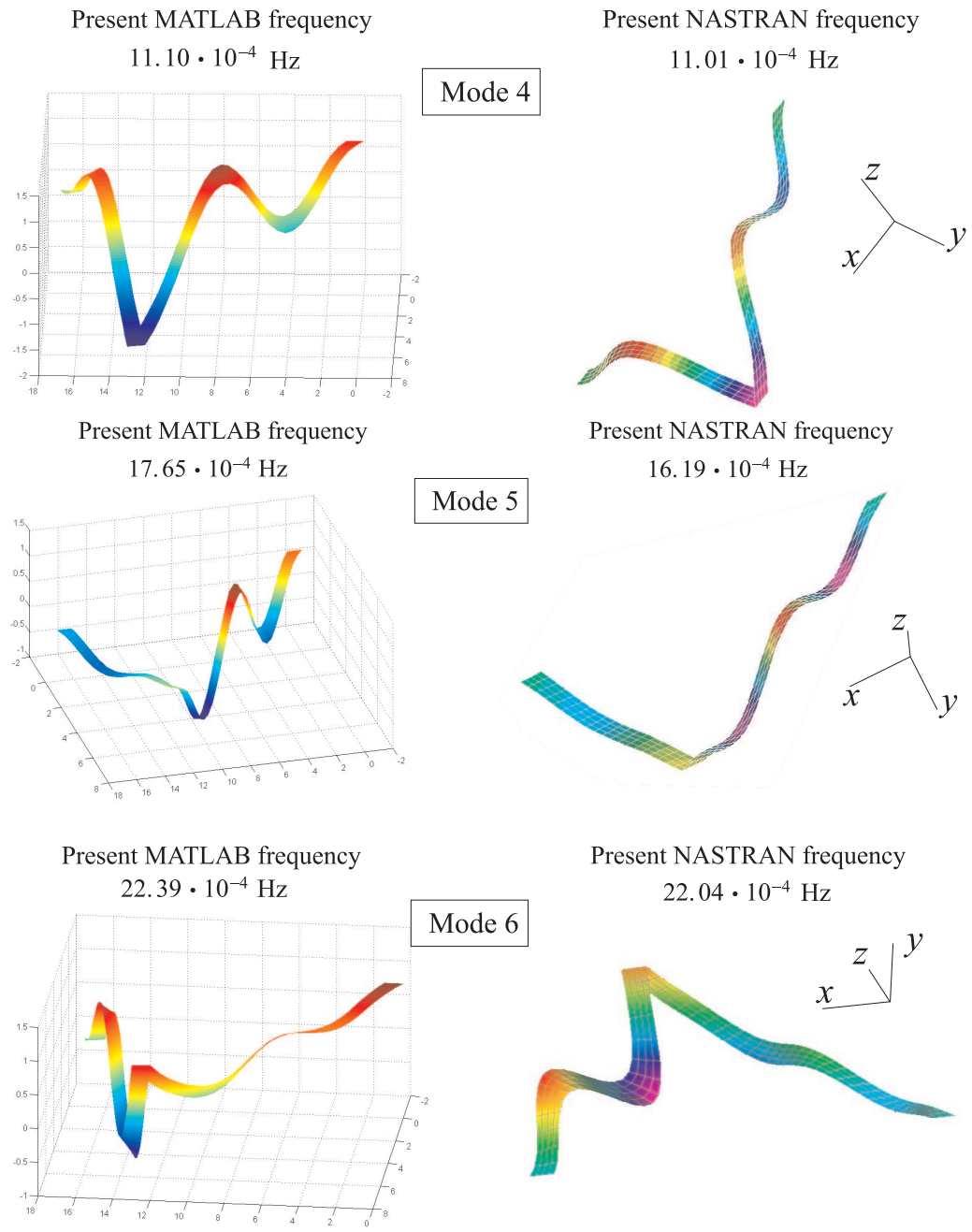

Figure 11.14. Case 4: modes 4, 5, 6 compared with NASTRAN.

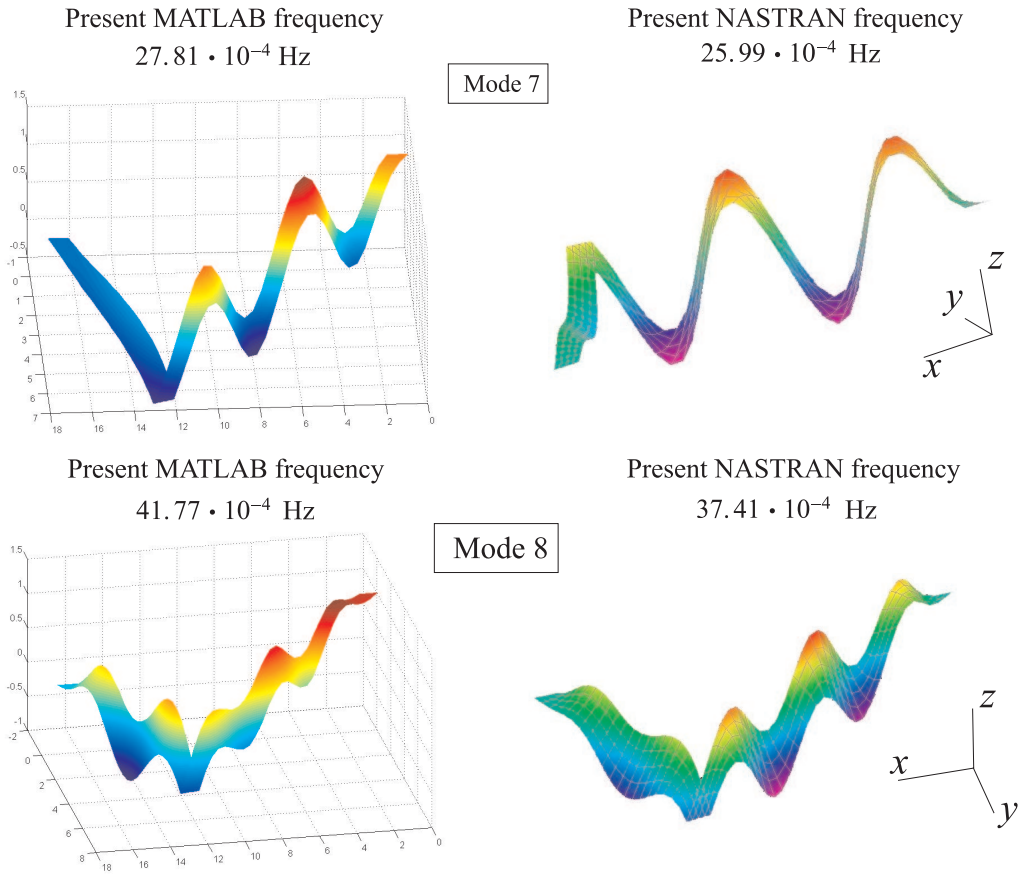

Figure 11.15. Case 4: modes 7, 8 compared with NASTRAN.

Nomenclature

t	time
$u\,(x,y,z,t)$	x-component displacement
$v\,(x,y,z,t)$	y-component displacement
$w\,(x,y,z,t)$	w-component displacement
$\mathrm{d}s$	infinitesimal area
$\mathrm{d}v$	infinitesimal volume
$\ddot{u}$	$\frac{\partial^2 u}{\partial t^2}$
$\ddot{v}$	$\frac{\partial^2 v}{\partial t^2}$
$\ddot{w}$	$\frac{\partial^2 w}{\partial t^2}$
ρ	material density
V	volume
S	surface
E	modulus of elasticity
ν	Poisson's ratio
U	potential energy
k_x, k_y, k_z	spring stiffness
$\boldsymbol{q}$	generalized coordinates
$\boldsymbol{F}^{u\,T}, \boldsymbol{F}^{v\,T}, \boldsymbol{F}^{w\,T}$	Ritz functions
$\boldsymbol{M} = \boldsymbol{M}^1 + \boldsymbol{M}^2$	mass matrix
$\boldsymbol{K}_{l_0\,l_0}, \boldsymbol{K}_{l_1\,l_1}$	stiffness matrices
$\boldsymbol{K}_{l_0\,nl}, \boldsymbol{K}_{nl\,l_0}$	stiffness matrices (linear dependence from $\boldsymbol{q}$)
$\boldsymbol{K}_{nl\,nl}$	stiffness matrix (quadratic dependence from $\boldsymbol{q}$)
q_0	distributed constant pressure

Subscripts

$,x$	derivative with respect to x
$,y$	derivative with respect to y
$,xx$	second derivative with respect to x
$,yy$	second derivative with respect to y
0	referred to the middle surface of the plate

Bibliography

[1] J. Anderson, Jr.: "*Fundamentals of Aerodynamics*", McGraw-Hill, Inc. 1991.

[2] F. Quori, "*Aerodinamica*", Levrotto & bella, 1993.

[3] G. Chiocchia, "*Lezioni di Aerodinamica Instazionaria*", Notes, 1997.

[4] L. Prandtl, "*Beitrag zur Theorie der tragenden Fläche*", ZAMM, Vol. 16, n.6, pp.360-361, 1936

[5] G. Monegato, "*Numerical evaluation of hypersingular integrals*", Journal of Computational and Applied Mathematics 50, 9-31, 1994

[6] D. Zwillinger, " *Standard Mathematical Tables and Formulae*", CRC Press 30$^{\text{th}}$ Edition, 1996.

[7] G. Monegato, " *Fondamenti di Calcolo Numerico*", CLUT, 1996.

[8] S. Chakraborty, V. Jandhyala, "*A Modified Adaptive Quadrature Scheme for Continuous Piecewise-Smooth Functions*", UWEE Technical Report Number UWEETR-2002-0015, August 2 2002.

[9] W. Gander, W. Gautschi, "*Adaptive quadrature-revised*", Technical Report 306, Department Informatik, ETH Zürich, August 1998.

[10] J. Hadamard, "*Lectures on Cauchy's Problem in Linear Partial Differential Equations*", Yale Univ. Press, New Haven, CT, 1923 / Dover, Newy York, 1952

[11] A. Bacciotti, "*Teoria matematica dei controlli*", CELID, Torino, 1998

[12] E. Pistolesi, "*Betrachtungen über die gegenseitige Beeinflussung von Tragflügelsystemen*", in Gesammelte Vorträge der Hauptversammlung 1937 der Lilienthal-Gesellschaft, Berlin, 1937

[13] J. Weissinger, "*Über die Auftriebverteilung von Pfeilflügeln*", Forsch. Ber. d. Zentr. f. wiss. Berichtswesen 1553, Berlin-Adlershof, 1942

[14] I. Kroo, "*Drag due to Lift: Concepts for Prediction and Reduction*", Annual Reviews Fluid Mechanics Vol. 33, pp. 587-617, 2001

[15] C. Cone, "*Theory of Induced Lift and Minimum Induced Drag of Nonplanar Lifting Systems*", NASA TR R-139, 1962

[16] J. E. Yates, C. D. Donaldson, "*A Fundamental Study of Drag and an Assessment of Conventional Drag-Due-to-Lift Reduction Devices*", NASA Contractor Report 4004, 1986

[17] C. Cone, "*A Theoretical Investigation of Vortex-Sheet Deformation Behind a Highly Loaded Wing and Its Effect on Lift*", NASA TN D-657, 1961

[18] K. Mortara, D. M. Straussfogel, M. D. Maughmer, "*Analysis and Design of Planar and Non-planar Wings for Induced Drag Minimization*", Annual Progress Report NASA-CR-189509, December 1991

[19] D.J. Butter, G.J. Hancock, "*A Numerical Method for Calculating the Trailing Vortex System behind a Swept Wing at Low Speed*", The Aeronautical Journal of the Royal Aeronautical Society, Vol. 75, pp. 564-568, August 1971

[20] S. C Smith, "*A Computational and Experimental Study of Nonlinear Aspects of Induced Drag*", Ph.D. Dissertation, Department of Aeronautics and Astronautics, Stanford University, CA, June 1995

[21] S. C Smith, "*A Computational and Experimental Study of Nonlinear Aspects of Induced Drag*", Ames Research Center, Moffett Field, California, NASA Technical Paper 3598, 1996

[22] I. Kroo, S.C. Smith, "*Computation of induced drag with nonplanar and deformed wakes*", SAE 901933, Soc. Automot. Eng., Warrendale, Pa 1990

[23] E. Trefftz, "*Prandtlshe Tragflächen und Propellertheorie*", Z. angew. Math. mech. Vol.1, p. 206, 1921

[24] http://www.desktopaero.com/appliedaero/potential3d/induceddrag.html

[25] L. Prandtl, "*Applications of Modern Hydrodynamics to Aeronautics*", NACA Report No. 116, 1921

[26] E. Eppler, "*Die Entwicklung der Tragflügeltheorie*", Z. Flugwiss, pp. 133-144, November 1987

[27] V.M. Falkner, "*The Calculation of Aerodynamic Loading on Surfaces of Any Shape*", ARC R&M 1910, 1943

[28] H. Schlichting, H.H.B.M. Thomas "*Note on the Calculation of the Lift Distribution of Swept Wings*", R.A.E. Report No. AERO 2236, December 1947

[29] A. Robinson, M.A. Laurmann"*Wing Theory*", Cambridge University Press, Cambridge, 1956

[30] H. Schlichting, E. Truckenbrodt, "*Aerodynamics of the Airplane*", McGraw-Hill, New York, 1979

[31] R. T. Jones, D. Cohen "*High-Speed Wing Theory*", Princeton University Press, Princeton, 1960

[32] Z. Mittelman, "*Prediction of Unsteady Aerodynamics and Control of Delta Wings with Tangential Leading Edge Blowing*", Ph.D. Dissertation, SUDDAR 580, Department of Aeronautics and Astronautics, Stanford University, 1989

[33] T.R. Quackenbush, D.B. Bliss, D.A. Wachspress, C.C. Ong "*Free Wake Analysis of Hover Performance Using a New Influence Coefficient Method*", NASA CR-4150, 1988

[34] H. Lamb, "*Hydrodynamics*", Dover, 6th ed., 1945

[35] K. Ramachandran, C. Tung, F.X. Caradonna, "*The Free-Wake Prediction of Rotor Hover Performance Using a Vortex-Embedding Method*", AIAA Paper 89-0638, presented at AIAA 27th Aerospace Sciences Meeting and Exhibit, Reno, Nev., Jan. 1989

[36] M.G. Nagati, J.D. Iverson, J.M. Vogel, "*Vortex Sheet Modeling with Curved Higher-Order Panels*", J. Aircraft, vol 24, pp. 776-781, Nov. 1987

[37] R.S. Ribeiro, "*Analysis of Wing Wake Roll-Up Using a Vortex-In-Cell Method*", Ph.D. Dissertation Department of Aeronautics and Astronautics, Stanford University, Stanford, Calif., May 1992

[38] E. Albano, W. Rodden, "*A Doublet Lattice Method for Calculating Lifting Distributions on Oscillating Surfaces in Subsonic Flows* ", AIAA Journal, Vol. 7, No. 2, pp. 279-285, 1969

[39] J. Katz, A. Plotkin, "*Low-Speed Wing Aerodynamics*", McGraw-Hill, New York, 1991

[40] B. Maskew, "*Prediction of Subsonic Aerodynamic Characteristics: A Case for Low-Order Panel Methods*", Journal of Aircraft, Vol. 19, pp. 157-163, Feb. 1982

[41] M. Munk, "*The minimum induced drag in airfoils*", NACA Report 121, 1921

[42] S. Inglesias, W.H. Mason, "*Optimum Spanloads Incorporating Wing Structural Weight*", First AIAA Aircraft Technology, Integration, and Operation Forum 16-18, Los Angeles, October 2001

[43] RT. Jones, "*The spanwise distribution of lift for minimum induced drag of wings having a given lift and a given bending moment*", NACA TN 2249, Natl. Advis. Comm. Aeronaut., Hampton, VA 1950

[44] I. Kroo, "*A General Approach to Multiple Lifting Surface Analysis and Design*", AIAA 84-2507, Oct. 1984

[45] A. Frediani, G. Montanari, M. Pappalardo, "*Sul problema di Prandtl della minima resistenza indotta di un sistema portante*", XV Congr. Naz. AIDAA, Torino 1999

[46] L. Prandtl, "*Induced drag of multiplanes*", NACA TN 182, 1924

[47] La Roche Consulting, "*Wing-grid-The Substitute for Span*", http://www.winggrid.ch/index.htm

[48] U. La Roche, S. Palffy, "*Wing-grid a Novel Device for Reduction of Induced Drag on Wings*", Proceedings ICAS 96, Sorrento, Italy, 1996

[49] U. La Roche, La Roche Consulting, H.R, Meyer Piening, I Stengele, B.T Bitanx, "*Developement, Qualification and Flight Testing of a Winggrid on a jetpowered testbed*", Proceedings ICAS 98, Melbourne, Australia, 1996

[50] Urlich and U. La Roche, La Roche Consulting, "*Induced Drag Reduction with the Winggrid Device*", http://www.winggrid.ch/ceas00.pdf

[51] U. La Roche and H.L La Roche, "*A Fanned Winglet Wingtip with parallel blades, Fluid Dynamics and Design*", http://www.winggrid.ch/Fluid%20dynamics%20and%20design%20of%20winggrids.pdf

[52] J. Wolkovitch, "*The joined wing aircraft: an overview*", Journal of Aircraft, n. 23, 1986

[53] E. Livne, "*Aeroelasticity of Joined-Wing Airplane Configurations: Past Work and Future Challenges - a Survey*", AIAA Paper 2001-1370, 42nd AIAA / ASME / ASCE / AHS / ASC Structures, Structural Dynamics, and Materials Conference, Seattle, WA, April 2001.

[54] http://aero.stanford.edu/reports/nonplanarwings/ClosedSystems.html

[55] I. Kroo, J. McMasters, S.C. Smith, "*Highly Nonplanar Lifting Systems*", http://aero.stanford.edu/reports/nonplanarwings/nonplanarwings.html

[56] R.H. Lange et alii, "*Feasibility study of the transonic biplane concept for transport aircraft applications*", CR–132462, Lockheed–Georgia Company, 1974

[57] G. Chiocchia, E. Carrera, L. Barbieri, C. Maggi, "*Alcune Analisi Sulle Strutture di una Configurazione Prandtlplano*", XVI Congresso Nazionale AIDAA, Palermo, 2001

[58] G. Chiocchia, E. Carrera, D. Spinello, "*Risultati di un modello FEM per l'analisi aeroelastica di architetture alari non convenzionali*", XIV Congresso AIDAA, Napoli, 1997

[59] A.Frediani, "*Sviluppo di una configurazione innovativa di un velivolo da trasporto*", XVI Congresso Nazionale AIDAA, Palermo, 2001

[60] G. Chiocchia, G. Iuso, E. Carrera, A. Frediani, "*A Wind Tunnel Model of a ULM Configuration of Prandtplane: Design, Manufactoring and Aerodynamic Testing*", XVII Congresso AIDAA, Roma, 2003

[61] A. Frediani, M. Gasperini, G. Saporito, A. Rimondi, "*Development of a prandtlplane aircraft configuration*", XVII Congresso AIDAA, Roma, 2003

[62] G. Chiocchia, E. Carrera, L. Demasi, "*Studio aerodinamico di un'ala anulare ellittica*", Italian Conference AIDAA, Palermo (Italy), 2001

[63] L. Demasi, G. Chiocchia, E. Carrera," *Aerodinamica dei sistemi portanti chiusi: ala anulare ellittica*", Italian Conference AIDAA, Roma (Italy), 2003

[64] G. Chiocchia, "*A Reflection on Induced Drag*", "Design challenges and mathematical methods in aircraft and spacecraft" 39th Workshop International School of Mathematics "G. Stampacchia" at Ettore Majorana Foundation and Center for Scientific Culture Erice (TP), Italy, 1-10 July 2003

[65] L. Demasi," *Ala Anulare Ellittica: Distribuzione di Circolazione di Minima Resistenza Indotta*", Italian Conference AIDAA, Roma (Italy), 2003

[66] A. Frediani, G. Montanari, "*On the Prandtl best wing system*", in: A. Frediani, A. Miele (Eds.), Advanced design problems in aerospace engineering, Plenum Press, NY, 2001

[67] G. Chiocchia, "*Carichi aerodinamici e divergenza statica in un'ala anulare*", Italian Conference AIDAA, Torino (Italy), 1999

[68] D Muhlpacker, D Bruti, "*Prandtl Box Wing layout Application to UAV configuration: wind tunnel computational data comparison.*", CEAS Aerospace

Aerodynamics Research Conference Royal Aeronautical Society, London (UK), 10-12 June 2003

[69] Web site useful in the calculation of integrals: "*http://integrals.wolfram.com/*",

[70] L. Demasi, E. Livne, "*A Plate Modeling Structural Modeling Capability for the Nonlinear Aeroelastic Analysis of Joined-Wing Configurations*", Italian Conference AIDAA, Roma (Italy), 2003

[71] C.A. Felippa, "*Error Analysis of Penalty Function Techniques for Constraint Definition in Linear Algebraic System*", Structural Mechanics Laboratory, Lokheed Palo Alto Research Laboratory, Palo Alto, California, USA, 1977

[72] G.L. Giles, "*Equivalent Plate Analysis of Aircraft Wing Box Structures with General Planform Geometry*", Journal of Aircraft, Vol. 23, No. 11, pp. 859-864, 1986

[73] E. Livne, "*Equivalent Plate Structural Modeling for Wing Shape Optimization Including Transverse Shear*", AIAA Journal, Vol. 32, No. 6, pp. 1278-1288, 1994

[74] G.L. Giles, "*Equivalent Plate Modeling for Conceptual Design of Aircraft Wing Structures*", AIAA Paper 95-3945, 1st AIAA Aircraft Engineering, Technology and Operations Congress, Los Angeles, CA, September 1995

[75] E. Livne, R. A. Sels, K.G. Bhatia, "*Lessons from Application of Equivalent Plate Structural Modeling to an HASCT Wing*", Journal of Aircraft Vol. 31, No. 4, pp. 953-960, 1994

[76] E. Livne , I. Navarro, "*Nonlinear Equivalent Plate Modeling of Wing-Box Structures*", Journal of Aircraft Vol. 36, No. 5, September-October 1999

[77] I. Navarro, "*Nonlinear Equivalent Plate Modeling of Wing Structures*", M.S. Thesis, Dept. of Aeronautics, Univ. of Washington, Seattle, WA, 1997

[78] E. Ramm, "*Strategies for Tracing the Nonlinear Response Near Limit Points*", Nonlinear Finite Element Analysis in Structural Mechanics, W. Wunderlich et al.(eds.), Springer-Verlag, Berlin, 63-89 1981

[79] E. Riks, "*An Incremental Approach to the Solution of Snapping and Buckling Problem*", International Journal of Solids and Structures 15, 529-551, 1979

[80] J.L. Batoz, G. Dhatt, "*Incremental Displacement Algorithms for Nonlinear Problems*", International Journal for Numerical Methods in Engineering 14, 1262-1266, 1979

[81] M.A. Crisfield, "*A Fast Incremental/Iterative Solution Procedure That Handles Snap-Through* ", Computer and Structures 13, 55-62, 1981

[82] G.A. Wempner, "*Discrete Approximations Related to Nonlinear Theories of Solids* ", International Journal of Solids and Structures 7, 1581-1599, 1981

[83] K.-J. Bathe, "*Finite Element Procedures*", Prentice Hall, Englewood Cliffs, NJ, USA, 1996.

[84] Carrera E., "*Nonlinear response of axisymmetrical laminated plates in cylindrical bending*", AIAA J., 31 (7), pp. 1353-57, 1993.

[85] E. Carrera, "*Comportamento Postcritico di Gusci Multistrato*", Tesi di dottorato (Ph.D. Dissertation), Dottorato in Ingegneria Aerospaziale Politecnico di Milano- Politecnico di Torino - Università di Pisa, 1991.

[86] E. Carrera, B. Kroeplin, "*Zigzag and interlaminar equilibria effects in large deflection and postbuckling analysis of multilayered plates*", Mechanics of Composite Materials and Structures, Vol. 4, pp. 69-94, 1997.

[87] E. Carrera, H. Parish, "*Evaluation of geometrical nonlinear effects of thin and moderately thick multilayered shells*", Composite Structures, Vol. 40, pp. 11-24, 1998.

[88] N. Yamaki, "*Influence of Large Amplitudes on Flexural Vibrations of elastic Plates*", ZAMM 41, 501-510, 1967

[89] C.T. Wang, "*Bending of Rectangular Plates with Large Deflections*", Report No. 1462, NACA, 1948

[90] S. Levy, "*Bending of Rectangular Plated with Large Deflections*", Report No. 737, NACA, 1942

[91] J-L Batoz, K-J Bathe, L-W Ho, "*A study of Three-Node Triangular Plate Bending Elements*", International Journal for Numerical methods in Engineering, Vol. 15, 1771-1812, 1980

[92] R. W. Clough, J.L. Tocher, "*Finite Element Stiffness Matrices for Analysis of plate bending*", Proc. Conf. on Matrix Methods in Structural Mechanics, WPAFB, Ohio, 515-545, 1965

Appendix A

Exchange Property in a Double Integral Defined in the Hadamard Finite-part Sense

Reported here is an original demonstration of the following property:

$$\oint_{-1}^{+1}\left(\oint_{-1}^{+1}\frac{f\left(t,s\right)}{\left(t-s\right)^{2}}\,\mathrm{d}t\right)\,\mathrm{d}s=\oint_{-1}^{+1}\left(\oint_{-1}^{+1}\frac{f\left(t,s\right)}{\left(t-s\right)^{2}}\,\mathrm{d}s\right)\,\mathrm{d}t. \tag{A.1}$$

To achieve this goal, the integrals defined in the Cauchy principal value sense have to be considered (see next section).

A.1 Proof for Integrals Defined in the Cauchy Principal Value Sense

The following property has to be demonstrated:

$$\int_{-1}^{+1}\left(\oint_{-1}^{+1}\frac{f\left(t,s\right)}{t-s}\,\mathrm{d}t\right)\,\mathrm{d}s=\int_{-1}^{+1}\left(\oint_{-1}^{+1}\frac{f\left(t,s\right)}{t-s}\,\mathrm{d}s\right)\,\mathrm{d}t. \tag{A.2}$$

Suppose that the function f is not a constant. Suppose also that f is not constant with respect to variable t. Adding and subtracting the term $f\left(s,s\right)$, it is possible to write

$$\int_{-1}^{+1}\left(\oint_{-1}^{+1}\frac{f\left(t,s\right)}{t-s}\,\mathrm{d}t\right)\,\mathrm{d}s=\int_{-1}^{+1}\left(\int_{-1}^{+1}\left(\frac{f\left(t,s\right)-f\left(s,s\right)}{t-s}\right)\,\mathrm{d}t+f\left(s,s\right)\oint_{-1}^{+1}\frac{1}{t-s}\,\mathrm{d}t\right)\,\mathrm{d}s. \tag{A.3}$$

Notice that the assumption of f *being not constant with respect to variable* t does not reduce the generality of the demonstration. Even *if* the function *was constant with respect to* t, but not with respect to s, instead of expression (A.2), the following equivalent statement should be demonstrated:

$$\int_{-1}^{+1}\left(\oint_{-1}^{+1}\frac{f\left(t,s\right)}{t-s}\,\mathrm{d}s\right)\,\mathrm{d}t=\int_{-1}^{+1}\left(\oint_{-1}^{+1}\frac{f\left(t,s\right)}{t-s}\,\mathrm{d}t\right)\,\mathrm{d}s, \tag{A.4}$$

and instead of equation (A.3), the following identity should be considered:

$$\int_{-1}^{+1}\left(\oint_{-1}^{+1}\tfrac{f(t,s)}{t-s}\,\mathrm{d}s\right)\,\mathrm{d}t=\int_{-1}^{+1}\left(\int_{-1}^{+1}\left(\tfrac{f(t,s)-f(t,t)}{t-s}\right)\,\mathrm{d}s+f\left(t,t\right)\oint_{-1}^{+1}\tfrac{1}{t-s}\,\mathrm{d}s\right)\,\mathrm{d}t. \tag{A.5}$$

Back to equation (A.3). The first double integral is regular, therefore, the order of integration can be exchanged:

$$\int_{-1}^{+1}\left(\oint_{-1}^{+1}\tfrac{f(t,s)}{t-s}\,\mathrm{d}t\right)\,\mathrm{d}s=\int_{-1}^{+1}\left(\int_{-1}^{+1}\left(\tfrac{f(t,s)-f(s,s)}{t-s}\right)\,\mathrm{d}s\right)\,\mathrm{d}t+\int_{-1}^{+1}\left(f\left(s,s\right)\oint_{-1}^{+1}\tfrac{1}{t-s}\,\mathrm{d}t\right)\,\mathrm{d}s. \tag{A.6}$$

But

$$\oint_{-1}^{+1}\frac{1}{t-s}\,\mathrm{d}t=\ln\left|1-s\right|-\ln\left|-1-s\right|, \tag{A.7}$$

and using the fact that t and s are included in the interval -1,1:

$$\int_{-1}^{+1}\left(\oint_{-1}^{+1}\tfrac{f(t,s)}{t-s}\,\mathrm{d}t\right)\,\mathrm{d}s=\int_{-1}^{+1}\left(\int_{-1}^{+1}\left(\tfrac{f(t,s)-f(s,s)}{t-s}\right)\,\mathrm{d}s\right)\,\mathrm{d}t+\int_{-1}^{+1}f\left(s,s\right)\ln\tfrac{1-s}{1+s}\,\mathrm{d}s. \tag{A.8}$$

Elaborating the first integral:

$$\begin{aligned}\int_{-1}^{+1}\left(\oint_{-1}^{+1}\tfrac{f(t,s)}{t-s}\,\mathrm{d}t\right)\,\mathrm{d}s=&\int_{-1}^{+1}\mathrm{d}t\oint_{-1}^{+1}\tfrac{f(t,s)}{t-s}\,\mathrm{d}s-\int_{-1}^{+1}\mathrm{d}t\oint_{-1}^{+1}\tfrac{f(s,s)}{t-s}\,\mathrm{d}s+\\&+\int_{-1}^{+1}f\left(s,s\right)\ln\tfrac{1-s}{1+s}\,\mathrm{d}s,\end{aligned} \tag{A.9}$$

$$\begin{aligned}\int_{-1}^{+1}\left(\oint_{-1}^{+1}\tfrac{f(t,s)}{t-s}\,\mathrm{d}t\right)\,\mathrm{d}s=&\int_{-1}^{+1}\mathrm{d}t\oint_{-1}^{+1}\tfrac{f(t,s)}{t-s}\,\mathrm{d}s-\int_{-1}^{+1}\left(\tfrac{\mathrm{d}}{\mathrm{d}t}\int_{-1}^{+1}f\left(s,s\right)\ln\left|t-s\right|\,\mathrm{d}s\right)\,\mathrm{d}t+\\&+\int_{-1}^{+1}f\left(s,s\right)\ln\tfrac{1-s}{1+s}\,\mathrm{d}s.\end{aligned} \tag{A.10}$$

Hence:

$$\int_{-1}^{+1}\left(\oint_{-1}^{+1}\frac{f(t,s)}{t-s}\,\mathrm{d}t\right)\mathrm{d}s=\int_{-1}^{+1}\mathrm{d}t\oint_{-1}^{+1}\frac{f(t,s)}{t-s}\,\mathrm{d}s-\left[\int_{-1}^{+1}f\left(s,s\right)\ln\left|t-s\right|\,\mathrm{d}s\right]_{-1}^{+1}+\\+\int_{-1}^{+1}f\left(s,s\right)\ln\frac{1-s}{1+s}\,\mathrm{d}s. \tag{A.11}$$

Rearranging:

$$\int_{-1}^{+1}\left(\oint_{-1}^{+1}\frac{f\left(t,s\right)}{t-s}\,\mathrm{d}t\right)\mathrm{d}s=\int_{-1}^{+1}\mathrm{d}t\oint_{-1}^{+1}\frac{f\left(t,s\right)}{t-s}\,\mathrm{d}s. \tag{A.12}$$

This relation demonstrates that exchanging the variables of integration is correct *if the function is not a constant*. Now consider $f\left(t,s\right)=\text{const}=a$. Hence:

$$\int_{-1}^{+1}\left(\oint_{-1}^{+1}\frac{a}{t-s}\,\mathrm{d}t\right)\mathrm{d}s=a\int_{-1}^{+1}\ln\frac{1-s}{1+s}\,\mathrm{d}s=0. \tag{A.13}$$

Similarly:

$$\int_{-1}^{+1}\left(\oint_{-1}^{+1}\frac{a}{t-s}\,\mathrm{d}s\right)\mathrm{d}t=0. \tag{A.14}$$

Thus, it has been demonstrated that

$$\int_{-1}^{+1}\left(\oint_{-1}^{+1}\frac{f\left(t,s\right)}{t-s}\,\mathrm{d}t\right)\mathrm{d}s=\int_{-1}^{+1}\left(\oint_{-1}^{+1}\frac{f\left(t,s\right)}{t-s}\,\mathrm{d}s\right)\mathrm{d}t \tag{A.15}$$

in all cases.

A.2 Proof for Integrals Defined in the Hadamard Finite-part Sense

In this case, it has to be supposed that $f(t,s)$ is not constant, and verify with direct calculation that the exchange of variables is possible when $f(t,s)$ is constant. Suppose $f(t,s)$ *is not constant*. Summing and subtracting the term $f\left(s,s\right)$, yields a Cauchy integral:

$$\oint_{-1}^{+1}\left(\oint_{-1}^{+1}\frac{f(t,s)}{(t-s)^2}\,\mathrm{d}t\right)\mathrm{d}s=\int_{-1}^{+1}\left(\oint_{-1}^{+1}\frac{f(t,s)-f(s,s)}{(t-s)^2}\,\mathrm{d}t\right)\mathrm{d}s+\oint_{-1}^{+1}\left(f\left(s,s\right)\oint_{-1}^{+1}\frac{1}{(t-s)^2}\,\mathrm{d}t\right)\mathrm{d}s. \tag{A.16}$$

But it has previously been demonstrated that the exchange operation is possible for the Cauchy integrals, therefore:

$$\oint\!\!\!\!\!\!-_{-1}^{+1}\left(\oint\!\!\!\!\!\!-_{-1}^{+1}\frac{f(t,s)}{(t-s)^2}\,\mathrm{d}t\right)\mathrm{d}s=\int_{-1}^{+1}\left(\oint\!\!\!\!\!\!-_{-1}^{+1}\frac{f(t,s)-f(s,s)}{(t-s)^2}\,\mathrm{d}s\right)\mathrm{d}t+\oint\!\!\!\!\!\!-_{-1}^{+1}\left(f\left(s,s\right)\oint\!\!\!\!\!\!-_{-1}^{+1}\frac{1}{(t-s)^2}\,\mathrm{d}t\right)\mathrm{d}s. \tag{A.17}$$

Now a few algebraic manipulations are reported:

$$\begin{aligned}\oint\!\!\!\!\!\!-_{-1}^{+1}\left(\oint\!\!\!\!\!\!-_{-1}^{+1}\frac{f(t,s)}{(t-s)^2}\,\mathrm{d}t\right)\mathrm{d}s=&\oint\!\!\!\!\!\!-_{-1}^{+1}\left(\oint\!\!\!\!\!\!-_{-1}^{+1}\frac{f(t,s)}{(t-s)^2}\,\mathrm{d}s\right)\mathrm{d}t-\oint\!\!\!\!\!\!-_{-1}^{+1}\left(\oint\!\!\!\!\!\!-_{-1}^{+1}\frac{f(s,s)}{(t-s)^2}\,\mathrm{d}s\right)\mathrm{d}t+\\&+\oint\!\!\!\!\!\!-_{-1}^{+1}\left(f\left(s,s\right)\oint\!\!\!\!\!\!-_{-1}^{+1}\frac{1}{(t-s)^2}\,\mathrm{d}t\right)\mathrm{d}s,\end{aligned} \tag{A.18}$$

$$\begin{aligned}\oint\!\!\!\!\!\!-_{-1}^{+1}\left(\oint\!\!\!\!\!\!-_{-1}^{+1}\frac{f(t,s)}{(t-s)^2}\,\mathrm{d}t\right)\mathrm{d}s=&\oint\!\!\!\!\!\!-_{-1}^{+1}\left(\oint\!\!\!\!\!\!-_{-1}^{+1}\frac{f(t,s)}{(t-s)^2}\,\mathrm{d}s\right)\mathrm{d}t+\int_{-1}^{+1}\frac{\mathrm{d}}{\mathrm{d}t}\left(\oint\!\!\!\!\!\!-_{-1}^{+1}\frac{f(s,s)}{(t-s)}\,\mathrm{d}s\right)\mathrm{d}t+\\&+\oint\!\!\!\!\!\!-_{-1}^{+1}\left(f\left(s,s\right)\oint\!\!\!\!\!\!-_{-1}^{+1}\frac{1}{(t-s)^2}\,\mathrm{d}t\right)\mathrm{d}s,\end{aligned} \tag{A.19}$$

$$\begin{aligned}\oint\!\!\!\!\!\!-_{-1}^{+1}\left(\oint\!\!\!\!\!\!-_{-1}^{+1}\frac{f(t,s)}{(t-s)^2}\,\mathrm{d}t\right)\mathrm{d}s=&\oint\!\!\!\!\!\!-_{-1}^{+1}\left(\oint\!\!\!\!\!\!-_{-1}^{+1}\frac{f(t,s)}{(t-s)^2}\,\mathrm{d}s\right)\mathrm{d}t+\left[\oint\!\!\!\!\!\!-_{-1}^{+1}\frac{f(s,s)}{(t-s)}\,\mathrm{d}s\right]_{-1}^{+1}+\\&+\oint\!\!\!\!\!\!-_{-1}^{+1}\left(f\left(s,s\right)\left[-\tfrac{1}{1-s}+\tfrac{1}{-1-s}\right]\right)\mathrm{d}s.\end{aligned} \tag{A.20}$$

Hence,

$$\oint\!\!\!\!\!\!-_{-1}^{+1}\left(\oint\!\!\!\!\!\!-_{-1}^{+1}\frac{f\left(t,s\right)}{\left(t-s\right)^2}\,\mathrm{d}t\right)\mathrm{d}s=\oint\!\!\!\!\!\!-_{-1}^{+1}\left(\oint\!\!\!\!\!\!-_{-1}^{+1}\frac{f\left(t,s\right)}{\left(t-s\right)^2}\,\mathrm{d}s\right)\mathrm{d}t, \tag{A.21}$$

at least for non-constant functions. Now suppose $f(t,s)=a$. The integral becomes:

$$\oint\!\!\!\!\!\!-_{-1}^{+1}\left(\oint\!\!\!\!\!\!-_{-1}^{+1}\frac{a}{\left(t-s\right)^2}\,\mathrm{d}t\right)\mathrm{d}s=\oint\!\!\!\!\!\!-_{-1}^{+1}\frac{2a}{\left(-1+s\right)\left(1+s\right)}\,\mathrm{d}s=-\ln 2. \tag{A.22}$$

Similarly:

$$\oint\!\!\!\!\!\!-_{-1}^{+1}\left(\oint\!\!\!\!\!\!-_{-1}^{+1}\frac{a}{\left(t-s\right)^2}\,\mathrm{d}s\right)\mathrm{d}t=\oint\!\!\!\!\!\!-_{-1}^{+1}\frac{2a}{\left(-1+t\right)\left(1+t\right)}\,\mathrm{d}t=-\ln 2. \tag{A.23}$$

Thus, the property is demonstrated for all cases.

Observation 34 If the function f is zero at both endpoints, the following property is valid:

$$\int_{-1}^{+1}\left(\Xint=_{-1}^{+1}\frac{f\left(t,s\right)}{\left(t-s\right)^{2}}\,\mathrm{d}t\right)\,\mathrm{d}s=\int_{-1}^{+1}\left(\Xint=_{-1}^{+1}\frac{f\left(t,s\right)}{\left(t-s\right)^{2}}\,\mathrm{d}s\right)\,\mathrm{d}t. \tag{A.24}$$

This is possible because the external integral is not singular at the endpoints (the function is zero at those points). Therefore, the external integral does not have to be defined as Hadamard finite-part integral.

Appendix B

Normalwash in a Biplane. A Geometrical Approach

Consider figure B.1. At point P on wing 1, vortex $\gamma_{2x}(y_d)\,\mathrm{d}y_d$ induces the velocity

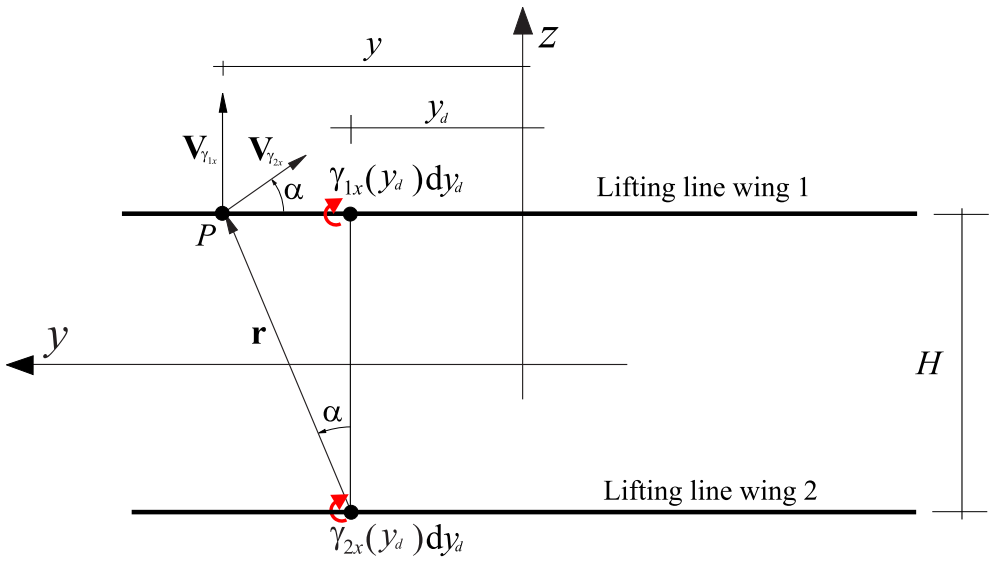

Figure B.1. Induced velocity calculation using geometric method.

$$\mathbf{V}_{\gamma_{x2}} = \gamma_{x2}\,\mathrm{d}y_d\mathbf{i} \times \frac{\mathbf{r}}{4\pi r} = \frac{\gamma_{x2}}{4\pi\sqrt{(y-y_d)^2+H^2}}\left(-\frac{H}{\sqrt{(y-y_d)^2+H^2}}\mathbf{j} + \frac{y-y_d}{\sqrt{(y-y_d)^2+H^2}}\mathbf{k}\right)\mathrm{d}y_d. \tag{B.1}$$

At the same point, vortex $\gamma_{1x}(y_d)\,\mathrm{d}y_d$ induces the velocity

$$\mathbf{V}_{\gamma_{x1}} = \frac{\gamma_{x1}\,\mathrm{d}y_d}{4\pi\,(y-y_d)}\mathbf{k}. \tag{B.2}$$

From these relations, it is deduced that:

$$\mathrm{d}\mathbf{u}_n\left(y\right) = \mathbf{V}_{\gamma_{x2}} \cdot \mathbf{k} + \mathbf{V}_{\gamma_{x1}}, \tag{B.3}$$

where $\mathrm{d}\mathbf{u}_n$ is directed along $+z$. Using the previous equations:

$$\mathrm{d}u_n\left(y\right) = \gamma_{x2}\,\mathrm{d}y_{d1}\frac{\left(y-y_d\right)}{4\pi\left(\left(y-y_d\right)^2+H^2\right)} + \gamma_{x1}\,\mathrm{d}y_d\frac{1}{4\pi\left(y-y_d\right)}. \tag{B.4}$$

Remembering that $\gamma_{x1} = -\frac{d\Gamma_1(y_d)}{\mathrm{d}y_d}$, $\gamma_{x2} = -\frac{d\Gamma_2(y_d)}{\mathrm{d}y_d}$, and integrating:

$$u_{n1}\left(y\right) = -\frac{1}{4\pi}\int_{-b_w}^{+b_w}\frac{\left(y-y_d\right)}{\left(\left(y-y_d\right)^2+H^2\right)}\frac{\mathrm{d}\Gamma\left(y_d\right)}{\mathrm{d}y_d}\mathrm{d}y_d - \frac{1}{4\pi}\oint_{-b_w}^{+b_w}\frac{\frac{\mathrm{d}\Gamma(y_d)}{\mathrm{d}y_d}}{\left(y-y_d\right)}\,\mathrm{d}y_d. \tag{B.5}$$

Integrating by parts:

$$\begin{aligned}\int_{-b_w}^{+b_w}\frac{(y-y_d)}{\left((y-y_d)^2+H^2\right)}\frac{\mathrm{d}\Gamma(y_d)}{\mathrm{d}y_{d1}}\,\mathrm{d}y_d = &\left[\Gamma\left(y_d\right)\frac{(y-y_d)}{\left((y-y_d)^2+H^2\right)}\right]_{-b_w}^{+b_w} + \\ &-\int_{-b_w}^{+b_w}\Gamma\left(y_d\right)\frac{\left((y-y_d)^2-H^2\right)}{\left((y-y_d)^2+H^2\right)^2}\,\mathrm{d}y_d,\end{aligned} \tag{B.6}$$

$$\oint_{-b_w}^{+b_w}\frac{\frac{\mathrm{d}\Gamma(y_d)}{\mathrm{d}y_d}}{\left(y-y_d\right)}\,\mathrm{d}y_d = \left[\frac{\Gamma\left(y_d\right)}{\left(y-y_d\right)}\right]_{-b_w}^{+b_w} - \oint_{-b_w}^{+b_w}\frac{\Gamma\left(y_d\right)}{\left(y-y_d\right)^2}\,\mathrm{d}y_d. \tag{B.7}$$

The circulation is zero at the tips and the following relation[1] is valid:

$$\rho V_\infty \Gamma\left(y_d\right) = -\rho m\left(y_d\right) \Rightarrow \Gamma\left(y_d\right) = -\frac{m\left(y_d\right)}{V_\infty}. \tag{B.8}$$

As a result,

$$\int_{-b_w}^{+b_w}\frac{\left(y-y_d\right)}{\left(\left(y-y_d\right)^2+H^2\right)}\frac{d\Gamma\left(y_d\right)}{\mathrm{d}y_d}\,\mathrm{d}y_d = \frac{1}{V_\infty}\int_{-b_w}^{+b_w} m\left(y_d\right)\frac{\left(\left(y-y_d\right)^2-H^2\right)}{\left(\left(y-y_d\right)^2+H^2\right)^2}\,\mathrm{d}y_d, \tag{B.9}$$

$$\oint_{-b_w}^{+b_w}\frac{1}{\left(y-y_d\right)}\frac{\mathrm{d}\Gamma\left(y_d\right)}{\mathrm{d}y_d}\,\mathrm{d}y_d = \frac{1}{V_\infty}\oint_{-b_w}^{+b_w} m\left(y_d\right)\frac{1}{\left(y-y_d\right)^2}\,\mathrm{d}y_d. \tag{B.10}$$

Substituting equations (B.9) and (B.10) into (B.5), the same relation as (5.34) is obtained. The same procedure can be applied for the velocity induced on the wing 2.

[1] Notice that the doublets have been chosen with axes along $+z$. This explains the negative sign in the next expression.

Appendix C

Minimum Induced Drag in a Biplane: Euler-Lagrange Equations

The functional is

$$J\left((m_1)_{\text{opt}}(\cdot)+\sigma\delta_1(\cdot),(m_2)_{\text{opt}}(\cdot)+\sigma\delta_2(\cdot)\right)=$$
$$=-\frac{\rho_\infty}{4\pi V_\infty^2}\int\limits_{-b_w}^{+b_w}\fint\limits_{-b_w}^{+b_w}\frac{\left[(m_1)_{\text{opt}}(y_d)+\sigma\delta_1(y_d)\right]\left[(m_1)_{\text{opt}}(y)+\sigma\delta_1(y)\right]}{(y-y_d)^2}\,\mathrm{d}y\,\mathrm{d}y_d+$$
$$-\frac{\rho_\infty}{4\pi V_\infty^2}\int\limits_{-b_w}^{+b_w}\int\limits_{-b_w}^{+b_w}\frac{\Big[\left[(m_1)_{\text{opt}}(y_d)+\sigma\delta_1(y_d)\right]\left[(m_2)_{\text{opt}}(y)+\sigma\delta_2(y)\right]+\left[(m_1)_{\text{opt}}(y)+\sigma\delta_1(y)\right]\left[(m_2)_{\text{opt}}(y_d)+\sigma\delta_2(y_d)\right]\Big]}{\left((y-y_d)^2+H^2\right)^2}\cdot$$
$$\cdot\left((y-y_d)^2-H^2\right)\,\mathrm{d}y\,\mathrm{d}y_d-\frac{\rho_\infty}{4\pi V_\infty^2}\int\limits_{-b_w}^{+b_w}\fint\limits_{-b_w}^{+b_w}\frac{\left[(m_2)_{\text{opt}}(y)+\sigma\delta_2(y)\right]\left[(m_2)_{\text{opt}}(y_d)+\sigma\delta_2(y_d)\right]}{(y-y_d)^2}\,\mathrm{d}y\,\mathrm{d}y_d. \tag{C.1}$$

The derivative with respect to σ of the functional is:

$$\begin{aligned}
&\tfrac{\mathrm{d}}{\mathrm{d}\sigma} J\left((m_1)_{\mathrm{opt}}(\cdot)+\sigma\delta_1(\cdot),(m_2)_{\mathrm{opt}}(\cdot)+\sigma\delta_2(\cdot)\right)= \\
&= -\tfrac{\rho_\infty}{4\pi V_\infty^2} \int\limits_{-b_w}^{+b_w} \fint\limits_{-b_w}^{+b_w} \tfrac{\delta_1(y_d)\left[\left((m_1)_{\mathrm{opt}}(y)+\sigma\delta_1(y)\right)\right]+\left[(m_1)_{\mathrm{opt}}(y_d)+\sigma\delta_1(y_d)\right]\delta_1(y)}{(y-y_d)^2}\,\mathrm{d}y\,\mathrm{d}y_d+ \\
&\quad -\tfrac{\rho_\infty}{4\pi V_\infty^2} \int\limits_{-b_w}^{+b_w} \int\limits_{-b_w}^{+b_w} \tfrac{\left[\delta_1(y_d)\left[(m_2)_{\mathrm{opt}}(y)+\sigma\delta_2(y)\right]+\left[(m_1)_{\mathrm{opt}}(y_d)+\sigma\delta_1(y_d)\right]\delta_2(y)\right]}{\left((y-y_d)^2+H^2\right)^2}\left((y-y_d)^2-H^2\right)\mathrm{d}y\,\mathrm{d}y_d+ \\
&\quad -\tfrac{\rho_\infty}{4\pi V_\infty^2} \int\limits_{-b_w}^{+b_w} \int\limits_{-b_w}^{+b_w} \tfrac{\left[\delta_1(y)\left[(m_2)_{\mathrm{opt}}(y_d)+\sigma\delta_2(y_d)\right]+\left[(m_1)_{\mathrm{opt}}(y)+\sigma\delta_1(y)\right]\delta_2(y_d)\right]}{\left((y-y_d)^2+H^2\right)^2}\left((y-y_d)^2-H^2\right)\mathrm{d}y\,\mathrm{d}y_d+ \\
&\quad -\tfrac{\rho_\infty}{4\pi V_\infty^2} \int\limits_{-b_w}^{+b_w} \fint\limits_{-b_w}^{+b_w} \left(\tfrac{\delta_2(y_d)\left[\left((m_2)_{\mathrm{opt}}(y)+\sigma\delta_2(y)\right)\right]+\left[(m_2)_{\mathrm{opt}}(y_d)+\sigma\delta_2(y_d)\right]\delta_2(y)}{(y-y_d)^2}\,\mathrm{d}y\right)\mathrm{d}y_d.
\end{aligned} \tag{C.2}$$

Setting $\sigma = 0$:

$$\begin{aligned}
\left[\tfrac{\mathrm{d}}{\mathrm{d}\sigma}J\right]_{\sigma=0} &= -\tfrac{\rho_\infty}{4\pi V_\infty^2} \int\limits_{-b_w}^{+b_w} \fint\limits_{-b_w}^{+b_w} \tfrac{\delta_1(y_d)(m_1)_{\mathrm{opt}}(y)+(m_1)_{\mathrm{opt}}(y_d)\delta_1(y)}{(y-y_d)^2}\,\mathrm{d}y\,\mathrm{d}y_d+ \\
&\quad -\tfrac{\rho_\infty}{4\pi V_\infty^2} \int\limits_{-b_w}^{+b_w} \int\limits_{-b_w}^{+b_w} \tfrac{\left[\delta_1(y_d)(m_2)_{\mathrm{opt}}(y)+(m_1)_{\mathrm{opt}}(y_d)\delta_2(y)+\delta_1(y)(m_2)_{\mathrm{opt}}(y_d)+(m_1)_{\mathrm{opt}}(y)\delta_2(y_d)\right]}{\left((y-y_d)^2+H^2\right)^2}\cdot \\
&\quad \cdot\left((y-y_d)^2-H^2\right)\mathrm{d}y\,\mathrm{d}y_d - \tfrac{\rho_\infty}{4\pi V_\infty^2} \int\limits_{-b_w}^{+b_w} \fint\limits_{-b_w}^{+b_w} \left(\tfrac{\delta_2(y_d)(m_2)_{\mathrm{opt}}(y)+(m_2)_{\mathrm{opt}}(y_d)\delta_2(y)}{(y-y_d)^2}\,\mathrm{d}y\right)\mathrm{d}y_d.
\end{aligned} \tag{C.3}$$

But it is easy to demonstrate the following equations (see chapter 2 and appendix A):

$$\int\limits_{-b_w}^{+b_w} \fint\limits_{-b_w}^{+b_w} \tfrac{\delta_1(y_d)(m_1)_{\mathrm{opt}}(y)+(m_1)_{\mathrm{opt}}(y_d)\delta_1(y)}{(y-y_d)^2}\,\mathrm{d}y\,\mathrm{d}y_d = \int\limits_{-b_w}^{+b_w} \fint\limits_{-b_w}^{+b_w} 2\tfrac{\delta_1(y_d)(m_1)_{\mathrm{opt}}(y)}{(y-y_d)^2}\,\mathrm{d}y\,\mathrm{d}y_d, \tag{C.4}$$

$$\int\limits_{-b_w}^{+b_w} \fint\limits_{-b_w}^{+b_w} \tfrac{\delta_2(y_d)(m_2)_{\mathrm{opt}}(y)+(m_2)_{\mathrm{opt}}(y_d)\delta_2(y)}{(y-y_d)^2}\,\mathrm{d}y\,\mathrm{d}y_d = \int\limits_{-b_w}^{+b_w} \fint\limits_{-b_w}^{+b_w} 2\tfrac{\delta_2(y_d)(m_2)_{\mathrm{opt}}(y)}{(y-y_d)^2}\,\mathrm{d}y\,\mathrm{d}y_d, \tag{C.5}$$

$$\begin{aligned}
&\int\limits_{-b_w}^{+b_w} \int\limits_{-b_w}^{+b_w} \tfrac{\left[\delta_1(y_d)(m_2)_{\mathrm{opt}}(y)+(m_1)_{\mathrm{opt}}(y_d)\delta_2(y)+\delta_1(y)(m_2)_{\mathrm{opt}}(y_d)+(m_1)_{\mathrm{opt}}(y)\delta_2(y_d)\right]\left((y-y_d)^2-H^2\right)}{\left((y-y_d)^2+H^2\right)^2}\,\mathrm{d}y\,\mathrm{d}y_d = \\
&= \int\limits_{-b_w}^{+b_w} \int\limits_{-b_w}^{+b_w} 2\tfrac{\left[\delta_1(y_d)(m_2)_{\mathrm{opt}}(y)+\delta_2(y_d)(m_1)_{\mathrm{opt}}(y)\right]\left((y-y_d)^2-H^2\right)}{\left((y-y_d)^2+H^2\right)^2}\,\mathrm{d}y\,\mathrm{d}y_d.
\end{aligned} \tag{C.6}$$

Therefore, the derivative is

$$\begin{aligned}\left[\frac{\mathrm{d}}{\mathrm{d}\sigma}J\right]_{\sigma=0} = &-\frac{\rho_\infty}{2\pi V_\infty^2}\int_{-b_w}^{+b_w}\!\!\!\!\!\!\diagup\!\!\!\!\!\!\int_{-b_w}^{+b_w}\left(\frac{\delta_1(y_d)(m_1)_{\mathrm{opt}}(y)}{(y-y_d)^2}+\frac{\delta_2(y_d)(m_2)_{\mathrm{opt}}(y)}{(y-y_d)^2}\right)\mathrm{d}y\,\mathrm{d}y_d+\\ &-\frac{\rho_\infty}{2\pi V_\infty^2}\int_{-b_w}^{+b_w}\int_{-b_w}^{+b_w}\frac{\left[\delta_1(y_d)(m_2)_{\mathrm{opt}}(y)+\delta_2(y_d)(m_1)_{\mathrm{opt}}(y)\right]\left((y-y_d)^2-H^2\right)}{\left((y-y_d)^2+H^2\right)^2}\mathrm{d}y\,\mathrm{d}y_d.\end{aligned} \tag{C.7}$$

Now the condition of fixed total lift is taken into account using the *Lagrange multiplier method.* The condition has to be manipulated as reported below[1]:

$$\begin{aligned}&\overline{L} = -\rho_\infty\int_{-b_w}^{+b_w} m_1(y_d)\,\mathrm{d}y_d - \rho_\infty\int_{-b_w}^{+b_w} m_2(y_d)\,\mathrm{d}y_d \Rightarrow\\ &l(y_d) = -\rho_\infty\int_{-b_w}^{y_d} m_1(\overline{y})\,\mathrm{d}\overline{y} - \rho_\infty\int_{-b_w}^{y_d} m_2(\overline{y})\,\mathrm{d}\overline{y} \Rightarrow\\ &l'(y_d) + \rho_\infty m_1(y_d) + \rho_\infty m_2(y_d) = 0.\end{aligned} \tag{C.8}$$

Setting

$$\begin{aligned}&l(\cdot) = l(\cdot)_{\mathrm{opt}} + \sigma\delta_3(\cdot) \qquad \sigma\in(-1,1),\\ &m_1(\cdot) = (m_1)_{\mathrm{opt}}(\cdot) + \sigma\delta_1(\cdot) \qquad \sigma\in(-1,1),\\ &m_2(\cdot) = (m_2)_{\mathrm{opt}}(\cdot) + \sigma\delta_2(\cdot) \qquad \sigma\in(-1,1),\end{aligned} \tag{C.9}$$

the condition becomes

$$l'(y_d)_{\mathrm{opt}} + \sigma\delta_3'(y_d) + \rho_\infty\left[(m_1)_{\mathrm{opt}}(y_d)+\sigma\delta_1(y_d)\right] + \rho_\infty\left[(m_2)_{\mathrm{opt}}(y_d)+\sigma\delta_2(y_d)\right] = 0. \tag{C.10}$$

Its derivative with respect to σ and calculated for $\sigma = 0$ yields:

$$\delta_3'(y_d) + \rho_\infty\delta_1(y_d) + \rho_\infty\delta_2(y_d) = 0. \tag{C.11}$$

Multiplying this expression by $\lambda(y_d)$, integrating by parts[2] the term containing $\delta_3'(y_d)$, and summing with equation (C.7), the result is:

$$\begin{aligned}0 = &-\frac{\rho_\infty}{2\pi V_\infty^2}\int_{-b_w}^{+b_w}\!\!\!\!\!\!\diagup\!\!\!\!\!\!\int_{-b_w}^{+b_w}\frac{\delta_1(y_d)(m_1)_{\mathrm{opt}}(y)+\delta_2(y_d)(m_2)_{\mathrm{opt}}(y)}{(y-y_d)^2}\mathrm{d}y\,\mathrm{d}y_d+\\ &-\frac{\rho_\infty}{2\pi V_\infty^2}\int_{-b_w}^{+b_w}\int_{-b_w}^{+b_w}\frac{\left[\delta_1(y_d)(m_2)_{\mathrm{opt}}(y)+\delta_2(y_d)(m_1)_{\mathrm{opt}}(y)\right]\left((y-y_d)^2-H^2\right)}{\left((y-y_d)^2+H^2\right)^2}\mathrm{d}y\,\mathrm{d}y_d - \int_{-b_w}^{+b_w}\lambda'(y_d)\,\delta_3(y_d)\,\mathrm{d}y_d+\\ &+\rho_\infty\int_{-b_w}^{+b_w}\lambda(y_d)\,\delta_1(y_d)\,\mathrm{d}y_d + \rho_\infty\int_{-b_w}^{+b_w}\lambda(y_d)\,\delta_2(y_d)\,\mathrm{d}y_d.\end{aligned} \tag{C.12}$$

[1] Notice that $l(\overline{y}=b_w) = \overline{L}$ and $l(\overline{y}=-b_w) = 0$.

[2] Notice that $\delta_3(+b_w) = \delta_3(-b_w) = 0$.

The Euler-Lagrange equation *leads to a system* of three equations containing the unknown functions $\lambda\left(y_d\right)$, $\left(m_2\right)_{\text{opt}}$ and $\left(m_1\right)_{\text{opt}}$. It can be observed that the functions $\delta_1\left(y_d\right)$, $\delta_2\left(y_d\right)$ and $\delta_3\left(y_d\right)$ are *arbitrary* functions. Thus, it can be written that

$$\delta_2\left(y_d\right) = \delta_1\left(y_d\right) \equiv 0 \Rightarrow \lambda'\left(y_d\right) = 0 \Rightarrow \lambda\left(y_d\right) = \text{cost}. \tag{C.13}$$

Using this result:

$$\begin{aligned} 0 = &-\frac{\rho_\infty}{2\pi V_\infty^2} \int\limits_{-b_w}^{+b_w} \!\!\!\!\!\!\diagup\!\!\!\!\!\!\int\limits_{-b_w}^{+b_w} \frac{\delta_1(y_d)(m_1)_{\text{opt}}(y)+\delta_2(y_d)(m_2)_{\text{opt}}(y)}{(y-y_d)^2}\,\mathrm{d}y\,\mathrm{d}y_d + \\ &-\frac{\rho_\infty}{2\pi V_\infty^2} \int\limits_{-b_w}^{+b_w} \int\limits_{-b_w}^{+b_w} \frac{\left[\delta_1(y_d)(m_2)_{\text{opt}}(y)+\delta_2(y_d)(m_1)_{\text{opt}}(y)\right]\left((y-y_d)^2-H^2\right)}{\left((y-y_d)^2+H^2\right)^2}\,\mathrm{d}y\,\mathrm{d}y_d + \\ &+\rho_\infty\lambda \int\limits_{-b_w}^{+b_w} \delta_1\left(y_d\right)\,\mathrm{d}y_d + \rho_\infty\lambda \int\limits_{-b_w}^{+b_w} \left(y_d\right)\delta_2\left(y_d\right)\,\mathrm{d}y_d. \end{aligned} \tag{C.14}$$

Now imposing $\delta_2\left(y_d\right) \equiv 0$:

$$\begin{aligned} &-\frac{\rho_\infty}{2\pi V_\infty^2} \int\limits_{-b_w}^{+b_w} \left(\!\!\!\!\!\!\diagup\!\!\!\!\!\!\int\limits_{-b_w}^{+b_w} \frac{\delta_1(y_d)(m_1)_{\text{opt}}(y)}{(y-y_d)^2}\,\mathrm{d}y + \int\limits_{-b_w}^{+b_w} \frac{\delta_1(y_d)(m_2)_{\text{opt}}(y)\left((y-y_d)^2-H^2\right)}{\left((y-y_d)^2+H^2\right)^2}\,\mathrm{d}y \right) \mathrm{d}y_d + \\ &+\rho_\infty\lambda \int\limits_{-b_w}^{+b_w} \delta_1\left(y_d\right)\,\mathrm{d}y_d = 0. \end{aligned} \tag{C.15}$$

Elaborating this expression yields

$$\int\limits_{-b_w}^{+b_w} \delta_1\left(y_d\right) \left[\left(-\frac{\rho_\infty}{2\pi V_\infty^2} \!\!\!\!\!\!\diagup\!\!\!\!\!\!\int\limits_{-b_w}^{+b_w} \frac{(m_1)_{\text{opt}}(y)}{(y-y_d)^2}\,\mathrm{d}y - \frac{\rho_\infty}{2\pi V_\infty^2} \int\limits_{-b_w}^{+b_w} \frac{(m_2)_{\text{opt}}(y)\left((y-y_d)^2-H^2\right)}{\left((y-y_d)^2+H^2\right)^2}\,\mathrm{d}y \right) + \rho_\infty\lambda \right] \mathrm{d}y_d = 0. \tag{C.16}$$

Because the function $\delta_1\left(y_d\right)$ is arbitrary, in order to satisfy the equation, the quantity in brackets must be equal to zero:

$$\boxed{ -\frac{\rho_\infty}{2\pi V_\infty^2} \!\!\!\!\!\!\diagup\!\!\!\!\!\!\int\limits_{-b_w}^{+b_w} \frac{(m_1)_{\text{opt}}(y)}{(y-y_d)^2}\,\mathrm{d}y - \frac{\rho_\infty}{2\pi V_\infty^2} \int\limits_{-b_w}^{+b_w} \frac{(m_2)_{\text{opt}}(y)\left((y-y_d)^2-H^2\right)}{\left((y-y_d)^2+H^2\right)^2}\,\mathrm{d}y + \rho_\infty\lambda = 0. } \tag{C.17}$$

Now imposing $\delta_1\left(y_d\right) \equiv 0$ and using similar algebraic manipulations:

$$\boxed{ -\frac{\rho_\infty}{2\pi V_\infty^2} \!\!\!\!\!\!\diagup\!\!\!\!\!\!\int\limits_{-b_w}^{+b_w} \frac{(m_2)_{\text{opt}}(y)}{(y-y_d)^2}\,\mathrm{d}y - \frac{\rho_\infty}{2\pi V_\infty^2} \int\limits_{-b_w}^{+b_w} \frac{(m_1)_{\text{opt}}(y)\left((y-y_d)^2-H^2\right)}{\left((y-y_d)^2+H^2\right)^2}\,\mathrm{d}y + \rho_\infty\lambda = 0. } \tag{C.18}$$

The last two expressions are the Euler-Lagrange equations for the biplane.

Appendix D

Elliptical Annular Wing with $b_w > a_w$. Orthogonality of the Used Coordinate System

In order to demonstrate this property, the tangent vectors at the intersection of an ellipse and a hyperbola have to be calculated, and the fact that they are perpendicular to each other have to be shown.
Consider the curve $\psi = \overline{\psi}$. It is an ellipse of equation

$$\frac{y^2}{\cosh^2 \overline{\psi}} + \frac{z^2}{\sinh^2 \overline{\psi}} = c^2. \tag{D.1}$$

Notice that the previous equation is always defined because $\overline{\psi} > 0$. Setting $\varphi = \overline{\varphi}$ and supposing $\overline{\varphi} \neq k\frac{\pi}{2}$, a hyperbola of equation

$$-\frac{y^2}{\cos^2 \overline{\varphi}} + \frac{z^2}{\sin^2 \overline{\varphi}} = -c^2 \tag{D.2}$$

is defined. The ellipse and hyperbola intersect at point

$$\begin{aligned} \overline{y} &= c \cosh \overline{\psi} \cos \overline{\varphi}, \\ \overline{z} &= c \sinh \overline{\psi} \sin \overline{\varphi}. \end{aligned} \tag{D.3}$$

The equation of the *tangent of the hyperbola* at that point is

$$-\frac{2\overline{y}}{\cos^2 \overline{\varphi}} (y - \overline{y}) + \frac{2\overline{z}}{\sin^2 \overline{\varphi}} (z - \overline{z}) = 0, \tag{D.4}$$

while the equation of the *tangent of the ellipse* at the same point is

$$\frac{2\overline{y}}{\cosh^2 \overline{\psi}} (y - \overline{y}) + \frac{2\overline{z}}{\sinh^2 \overline{\psi}} (z - \overline{z}) = 0. \tag{D.5}$$

The vectors parallel to the tangent lines are, respectively,

$$\begin{aligned} \mathbf{V}_{hyp} &= \tfrac{2\overline{z}}{\sin^2\overline{\varphi}}\mathbf{j} + \tfrac{2\overline{y}}{\cos^2\overline{\varphi}}\mathbf{k}, \\ \mathbf{V}_{el} &= \tfrac{2\overline{z}}{\sinh^2\overline{\psi}}\mathbf{j} - \tfrac{2\overline{y}}{\cosh^2\overline{\psi}}\mathbf{k}. \end{aligned} \tag{D.6}$$

Their scalar product is

$$\mathbf{V}_{hyp}\cdot\mathbf{V}_{el} = 4\left(\frac{\overline{z}^2}{\sin^2\overline{\varphi}\sinh^2\overline{\psi}} - \frac{\overline{y}^2}{\cos^2\overline{\varphi}\cosh^2\overline{\psi}}\right). \tag{D.7}$$

Using the expression of $\overline{y}$ and $\overline{z}$:

$$\mathbf{V}_{hyp}\cdot\mathbf{V}_{el} = 4c^2\left(\frac{\sinh^2\overline{\psi}\sin^2\overline{\varphi}}{\sin^2\overline{\varphi}\sinh^2\overline{\psi}} - \frac{\cosh^2\overline{\psi}\cos^2\overline{\varphi}}{\cos^2\overline{\varphi}\cosh^2\overline{\psi}}\right) = 0 \quad \forall\overline{\psi}\ ,\forall\overline{\varphi} \neq k\frac{\pi}{2}. \tag{D.8}$$

Thus, the orthogonality is demonstrated for all cases[1].

[1]In the particular condition of $\overline{\varphi} = k\frac{\pi}{2}$, there are horizontal or vertical lines, and they are perpendicular to a generic ellipse. Hence, the orthogonality is valid in all cases.

Appendix E

Elliptical Annular Wing with $b_w > a_w$. Some Useful Derivations

Cartesian Distance

In order to write the small perturbation acceleration potential, the cartesian distance between a generic point $P(x,y,z)$ and a point $P_d(x_d,y_d,z_d)$[1] on the lifting line w, where the generic *doublet is positioned*, is needed. The distance is

$$D = \sqrt{(x - x_d)^2 + (y - y_d)^2 + (z - z_d)^2}. \tag{E.1}$$

The lifting line is contained in the $y - z$ plane, thus $x_d = 0$. With the position $x = cX$ and using the new coordinate system:

$$D = c\sqrt{\left(X^2 + (\cosh\psi\cos\varphi - \cosh\psi_w\cos\varphi_d)^2 + (\sinh\psi\sin\varphi - \sinh\psi_w\sin\varphi_d)^2\right)}, \tag{E.2}$$

where the relations valid on the lifting line w have been used:

$$\begin{array}{ll} y_d = c\cosh\psi_w\cos\varphi_d & 0 \le \varphi_d \le 2\pi, \\ z_d = c\sinh\psi_w\sin\varphi_d & \psi_w > 0. \end{array} \tag{E.3}$$

The cartesian distance can be written in another way:

$$D = c\left[\Delta\left(X,\psi,\varphi,\psi_w,\varphi_d\right)\right]^{\frac{1}{2}}, \tag{E.4}$$

where

$$\begin{aligned} \Delta \;=\; & X^2 + \sinh^2\psi + \cos^2\varphi - \cosh\left(\psi - \psi_w\right)\cos\left(\varphi + \varphi_d\right) + \\ & - \cosh\left(\psi + \psi_w\right)\cos\left(\varphi - \varphi_d\right) + \sinh^2\psi_w + \cos^2\varphi_d. \end{aligned} \tag{E.5}$$

[1] The point P_d is characterized by $\varphi = \varphi_d$.

Cosine Directions of the Normal to the Lifting Line

The lifting line is studied considering a doublet distribution m. Each doublet has axis which has inward direction to the ellipse and is perpendicular to the lifting line (figure E.1). The straight line perpendicular to the ellipse, where the generic

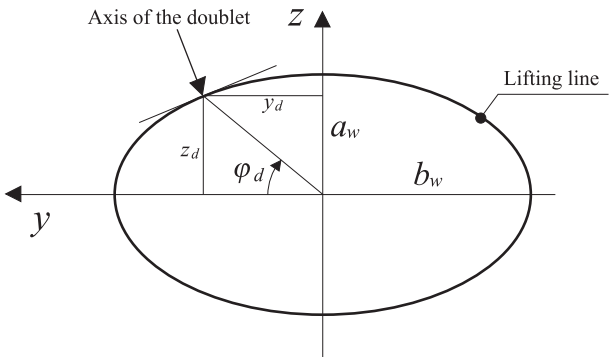

Figure E.1. Positive direction of the doublet's axis.

doublet is positioned, has the equation

$$-\frac{2y_d}{\cos^2\varphi_d}(y-y_d)+\frac{2z_d}{\sin^2\varphi_d}(z-z_d)=0. \tag{E.6}$$

From that relation, a vector perpendicular to the ellipse has the expression

$$\mathbf{V}_{\perp el}=\frac{z_d}{\sin^2\varphi_d}\mathbf{j}+\frac{y_d}{\cos^2\varphi_d}\mathbf{k}. \tag{E.7}$$

Using relation (E.3):

$$\mathbf{V}_{\perp el}=\frac{c\sinh\psi_w\sin\varphi_d}{\sin^2\varphi_d}\mathbf{j}+\frac{c\cosh\psi_w\cos\varphi_d}{\cos^2\varphi_d}\mathbf{k}. \tag{E.8}$$

Therefore, the vector

$$\mathbf{V}_{\perp el}=\frac{\sinh\psi_w}{\sin\varphi_d}\mathbf{j}+\frac{\cosh\psi_w}{\cos\varphi_d}\mathbf{k}, \tag{E.9}$$

is perpendicular to the ellipse at the point characterized by $y=y_d$, $x=x_d=0$, $z=z_d$ and $\varphi=\varphi_d$. Normalizing the vector expressed in equation (E.9):

$$V_{\perp el}=\frac{\sqrt{\cosh^2\psi_w-\cos^2\varphi_d}}{|\sin\varphi_d|\,|\cos\varphi_d|}; \tag{E.10}$$

$$\begin{aligned}
\mathbf{V}_{\perp el} &= \frac{\frac{\sinh\psi_w}{\sin\varphi_d}}{V_{\perp el}}\mathbf{j} + \frac{\frac{\cosh\psi_w}{\cos\varphi_d}}{V_{\perp el}}\mathbf{k} \Rightarrow \\
\mathbf{V}_{\perp el} &= \frac{|\sin\varphi_d|\,|\cos\varphi_d|}{\sqrt{\cosh^2\psi_w - \cos^2\varphi_d}}\frac{\sinh\psi_w}{\sin\varphi_d}\mathbf{j} + \frac{|\sin\varphi_d|\,|\cos\varphi_d|}{\sqrt{\cosh^2\psi_w - \cos^2\varphi_d}}\frac{\cosh\psi_w}{\cos\varphi_d}\mathbf{k}. \quad \text{(E.11)}
\end{aligned}$$

From this equation, it can be deduced that vector $\mathbf{n}_d$, perpendicular to the ellipse where the doublet is positioned, is

$$\mathbf{n}_d = -\frac{\cos\varphi_d \sinh\psi_w}{\sqrt{\cosh^2\psi_w - \cos^2\varphi_d}}\mathbf{j} - \frac{\sin\varphi_d \cosh\psi_w}{\sqrt{\cosh^2\psi_d - \cos^2\varphi_d}}\mathbf{k}. \quad \text{(E.12)}$$

It is easy to verify that the direction of vector $\mathbf{n}_d$ is in accord with figure E.1. Clearly, from the previous expression, it can be written that:

$$\begin{aligned}
n_{dx} &= 0, \\
n_{dy} &= -\frac{\cos\varphi_d \sinh\psi_w}{\sqrt{\cosh^2\psi_w - \cos^2\varphi_d}}, \quad \text{(E.13)} \\
n_{dz} &= -\frac{\sin\varphi_d \cosh\psi_w}{\sqrt{\cosh^2\psi_w - \cos^2\varphi_d}}.
\end{aligned}$$

Now, the small perturbation acceleration potential can be written.

Appendix F

Elliptical Annular Wing with $b_w > a_w$. Weissinger's Condition

F.1 Mathematical Derivation

Weissinger's condition is

$$-\alpha(\varphi) = \frac{1}{V_\infty}\left(\frac{1}{h}\frac{\partial\phi(X,\psi,\varphi,\psi_w)}{\partial\psi}\right)_{X=X_0;\,\psi=\psi_w}, \tag{F.1}$$

where $X_0 = \frac{l}{2c}$. In order to calculate the derivative of the small perturbation velocity potential, the small perturbation velocity potential is written as

$$\phi(X,\psi,\varphi,\psi_w) = \frac{1}{8\pi V_\infty}\int_0^{2\pi} m(\varphi_d)\cdot f_2(\psi,\varphi,\psi_w)\cdot f_3(X,\psi,\varphi,\psi_w)\,\mathrm{d}\varphi_d, \tag{F.2}$$

where:

$$\begin{aligned}
f_2 &= \tfrac{(\sinh(\psi+\psi_w)\cos(\varphi-\varphi_d)-\sinh(\psi-\psi_w)\cos(\varphi+\varphi_d)-\sinh 2\psi_w)}{\sinh^2\psi+\cos^2\varphi-\cosh(\psi-\psi_w)\cos(\varphi+\varphi_d)-\cosh(\psi+\psi_w)\cos(\varphi-\varphi_d)+\sinh^2\psi_w+\cos^2\varphi_d} = \tfrac{N}{D},\\
f_3 &= \tfrac{X}{\sqrt{X^2+D}}+1,\\
N &= (\sinh(\psi+\psi_w)\cos(\varphi-\varphi_d)-\sinh(\psi-\psi_w)\cos(\varphi+\varphi_d)-\sinh 2\psi_w),\\
D &= \sinh^2\psi+\cos^2\varphi-\cosh(\psi-\psi_w)\cos(\varphi+\varphi_d)+\\
&\quad-\cosh(\psi+\psi_w)\cos(\varphi-\varphi_d)+\sinh^2\psi_w+\cos^2\varphi_d.
\end{aligned} \tag{F.3}$$

In the derivative of the small perturbation velocity potential, the following quantity appears:

$$\left[\frac{\partial}{\partial\psi}(f_2\cdot f_3)\right]_{\psi=\psi_w;\,X=X_0} = \left[\frac{\partial f_2}{\partial\psi}f_3 + f_2\frac{\partial f_3}{\partial\psi}\right]_{\psi=\psi_w;\,X=X_0}. \tag{F.4}$$

Now, the principal algebraic operations are shown:

$$
\begin{aligned}
&[N]_{\psi=\psi_w} = -\sinh(2\psi_w)\left(1-\cos(\varphi-\varphi_d)\right),\\
&[D]_{\psi=\psi_w} = \sinh^2\psi_w + \cos^2\varphi - \cos(\varphi+\varphi_d) - \cosh(2\psi_w)\cos(\varphi-\varphi_d) + \\
&\qquad\qquad + \sinh^2\psi_w + \cos^2\varphi_d = 2(H_5)\left(1-\cos(\varphi-\varphi_d)\right),\\
&[f_2]_{\psi=\psi_w} = \tfrac{-\sinh(2\psi_w)}{2(H_5)},\\
&[f_3]_{\psi=\psi_w, X=X_0} = \tfrac{X_0}{\sqrt{H_6}} + 1,\\
&\left[\tfrac{\partial N}{\partial\psi}\right]_{\psi=\psi_w} = 2\left(\cosh^2\psi_w\cos(\varphi-\varphi_d) - \cos\varphi\cos\varphi_d\right),\\
&\left[\tfrac{\partial D}{\partial\psi}\right]_{\psi=\psi_w} = \sinh(2\psi_w)\left(1-\cos(\varphi-\varphi_d)\right) = -[N]_{\psi=\psi_w},\\
&\left[\tfrac{\partial f_2}{\partial\psi}\right]_{\psi=\psi_w} = \tfrac{\cosh^2\psi_w\cos(\varphi-\varphi_d)-\cos\varphi\cos\varphi_d}{(H_5)(1-\cos(\varphi-\varphi_d))} + \tfrac{\sinh^2\psi_w\cosh^2\psi_w}{(H_5)^2},\\
&\left[\tfrac{\partial f_3}{\partial\psi}\right]_{\psi=\psi_w, X=X_0} = -\tfrac{X_0\cosh\psi_w\sinh\psi_w(1-\cos(\varphi-\varphi_d))}{(H_6)^{\frac{3}{2}}},\\
&\left[f_2\tfrac{\partial f_3}{\partial\psi}\right]_{\psi=\psi_w, X=X_0} = \tfrac{X_0\cosh^2\psi_w\sinh^2\psi_w(1-\cos(\varphi-\varphi_d))}{(H_5)(H_6)^{\frac{3}{2}}},\\
&\left[\tfrac{\partial f_2}{\partial\psi}f_3\right]_{\psi=\psi_w, X=X_0} = \left(\tfrac{\cosh^2\psi_w\cos(\varphi-\varphi_d)-\cos\varphi\cos\varphi_d}{(H_5)(1-\cos(\varphi-\varphi_d))} + \tfrac{\sinh^2\psi_w\cosh^2\psi_w}{(H_5)^2}\right)\left(\tfrac{X_0}{\sqrt{H_6}}+1\right),\\
&H_5 = \sinh^2\psi_w + \sin^2\tfrac{\varphi+\varphi_d}{2},\\
&H_6 = X_0^2 + 2\left(\sinh^2\psi_w + \sin^2\tfrac{\varphi+\varphi_d}{2}\right)\left(1-\cos(\varphi-\varphi_d)\right).
\end{aligned}
\tag{F.5}
$$

Notice that the term $\left[\frac{\partial f_2}{\partial\psi}f_3\right]_{\psi=\psi_w, X=X_0}$ contains the *singular* term $\frac{X_0}{\sqrt{H_6}}$ (when $\varphi=\varphi_d$, it reaches infinity). Thus, $\left[\frac{\partial f_2}{\partial\psi}f_3\right]_{\psi=\psi_w, X=X_0}$ is rewritten in the form

$$
\left[\frac{\partial f_2}{\partial\psi}f_3\right]_{\psi=\psi_w, X=X_0} = \left(\left[\frac{\partial f_2}{\partial\psi}\right]^S f_3\right)_{\psi=\psi_w, X=X_0} + \left(\left[\frac{\partial f_2}{\partial\psi}\right]^R f_3\right)_{\psi=\psi_w, X=X_0}, \tag{F.6}
$$

where the superscripts "S" and "R" indicate "singular" and "regular", respectively.

F.2 Treatment of the Singularity

The is to isolate the singularity from the term $\left(\left[\frac{\partial f_2}{\partial \psi}\right]^S f_3\right)_{\psi=\psi_w, X=X_0}$. That term is:

$$\left(\left[\frac{\partial f_2}{\partial \psi}\right]^S f_3\right)_{\psi=\psi_w, X=X_0} = \frac{\cosh^2\psi_w \cos(\varphi-\varphi_d) - \cos\varphi\cos\varphi_d}{(H_5)(1-\cos(\varphi-\varphi_d))}\left(\frac{X_0}{\sqrt{H_6}}+1\right). \tag{F.7}$$

In a compact form:

$$\left(\left[\frac{\partial f_2}{\partial \psi}\right]^S f_3\right)_{\psi=\psi_w, X=X_0} = \frac{\cosh^2\psi_w \cos(\varphi-\varphi_d) - \cos\varphi\cos\varphi_d}{(H_5)} \cdot \frac{f_3(X_0,\varphi,\psi_w,\varphi_d)}{1-\cos(\varphi-\varphi_d)}. \tag{F.8}$$

Using the following identity:

$$\frac{f_3\left(X_0,\varphi,\psi_w,\varphi_d\right)}{1-\cos\left(\varphi-\varphi_d\right)} = \frac{f_3\left(X_0,\varphi,\psi_w,\varphi_d\right) - f_3\left(X_0,\varphi,\psi_w,\varphi\right)}{1-\cos\left(\varphi-\varphi_d\right)} + \frac{f_3\left(X_0,\varphi,\psi_w,\varphi\right)}{1-\cos\left(\varphi-\varphi_d\right)}, \tag{F.9}$$

where

$$f_3\left(X_0,\varphi,\psi_w,\varphi\right) = 2, \tag{F.10}$$

$$\frac{f_3\left(X_0,\varphi,\psi_w,\varphi_d\right) - f_3\left(X_0,\varphi,\psi_w,\varphi\right)}{1-\cos\left(\varphi-\varphi_d\right)} = f_I, \tag{F.11}$$

$$f_I = \frac{-2(H_5)}{\left(X_0+\sqrt{H_6}\right)\sqrt{H_6}}, \tag{F.12}$$

thus,

$$\frac{f_3\left(X_0,\varphi,\psi_w,\varphi_d\right)}{1-\cos\left(\varphi-\varphi_d\right)} = f_I + \frac{2}{1-\cos\left(\varphi-\varphi_d\right)}. \tag{F.13}$$

Using expression (F.13), equation (F.8) becomes:

$$\begin{aligned}\left(\left[\frac{\partial f_2}{\partial \psi}\right]^S f_3\right)_{\psi=\psi_w, X=X_0} &= \frac{\cosh^2\psi_w \cos(\varphi-\varphi_d) - \cos\varphi\cos\varphi_d}{(H_5)} f_I + \\ &+ 2\frac{\cosh^2\psi_w \cos(\varphi-\varphi_d) - \cos\varphi\cos\varphi_d}{(H_5)(1-\cos(\varphi-\varphi_d))}.\end{aligned} \tag{F.14}$$

The second term, which appears in the previous equation, can be simplified more. Considering the identities

$$2\frac{\cosh^2\psi_w \cos(\varphi-\varphi_d) - \cos\varphi\cos\varphi_d}{(H_5)(1-\cos(\varphi-\varphi_d))} = 2\frac{\cosh^2\psi_w \cos(\varphi-\varphi_d) - \cos\varphi\cos\varphi_d - (H_5)}{(H_5)(1-\cos(\varphi-\varphi_d))} + \frac{2}{1-\cos(\varphi-\varphi_d)}, \tag{F.15}$$

$$\cosh^2\psi_w \cos\left(\varphi-\varphi_d\right) - \cos\varphi\cos\varphi_d - (H_5) = \frac{-(\cosh(2\psi_w))(1-\cos(\varphi-\varphi_d))}{2}, \tag{F.16}$$

it can be deduced that

$$2\frac{\cosh^2\psi_w \cos\left(\varphi-\varphi_d\right) - \cos\varphi\cos\varphi_d}{(H_5)\left(1-\cos\left(\varphi-\varphi_d\right)\right)} = \frac{-\cosh\left(2\psi_w\right)}{(H_5)} + \frac{2}{1-\cos\left(\varphi-\varphi_d\right)}. \tag{F.17}$$

Finally, equation (F.14) is rewritten as

$$\left(\left[\frac{\partial f_2}{\partial \psi}\right]^S f_3\right)_{\psi=\psi_w, X=X_0} = \frac{\cosh^2\psi_w \cos(\varphi-\varphi_d)-\cos\varphi\cos\varphi_d}{(H_5)} \cdot f_I - \frac{\cosh(2\psi_w)}{(H_5)} + \frac{2}{1-\cos(\varphi-\varphi_d)}. \tag{F.18}$$

Appendix G

Normalwash in an Elliptical Annular Wing with $b_w > a_w$. A Geometrical Approach

Suppose that the *circulation* $\Gamma(\varphi)$ is known. The normalwash at a point on the ellipse induced by the vortex γ_x is

$$\mathrm{d}u_n = \frac{\gamma_x(s_d)}{4\pi r}\cos\varsigma\,\mathrm{d}s_d, \tag{G.1}$$

where r indicates the distance between the point characterized by φ_d (where the trailing vortex $\gamma_x(s_d)\,\mathrm{d}s_d$ is positioned) and the point characterized by φ (where the induced velocity is calculated). For more details see figure G.1.
But the following well known formula (see figure G.2) is valid:

$$\gamma_x(s_d) = -\frac{\mathrm{d}\Gamma(s_d)}{\mathrm{d}s_d}; \tag{G.2}$$

recalling the relation $\mathrm{d}s_d = c\sqrt{\cosh^2\psi_w - \cos^2\varphi_d}\,\mathrm{d}\varphi_d$, equation (G.1) becomes

$$\mathrm{d}u_n = -\frac{\frac{\mathrm{d}\Gamma(\varphi_d)}{\mathrm{d}\varphi_d}}{4\pi r}\cos\varsigma\,\mathrm{d}\varphi_d. \tag{G.3}$$

The following is a step by step calculation of all terms that appear in equation (G.3).

- *Step 1*
  Finding of the expression of distance r.
  It is seen as the modulus of the vector that links the points (see figure G.1). This vector is the difference between the position vectors as reported below:

$$\begin{aligned}\mathbf{r} = \mathbf{V}(\varphi) - \mathbf{V}(\varphi_d) = c(\cosh\psi_w)(\cos\varphi - \cos\varphi_d)\,\mathbf{j} + \\ + c(\sinh\psi_w)(\sin\varphi - \sin\varphi_d)\,\mathbf{k}.\end{aligned} \tag{G.4}$$

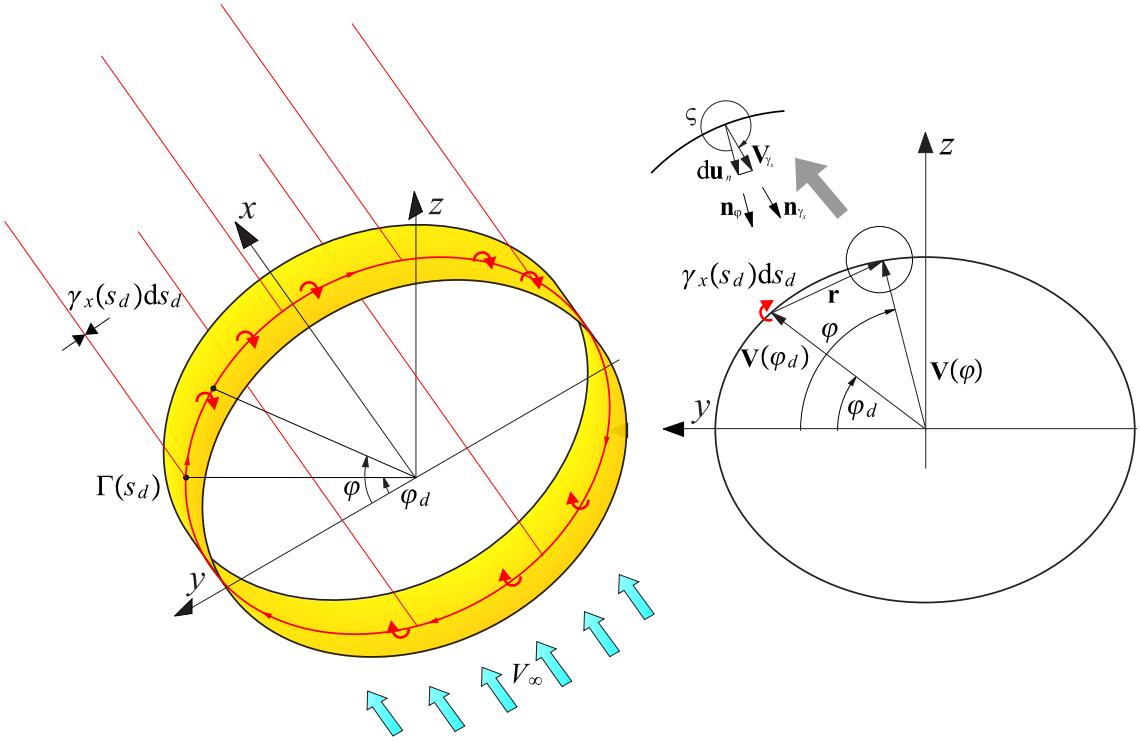

Figure G.1. Induced velocity by the vortex $\gamma_x(s_d)\,\mathrm{d}s_d$.

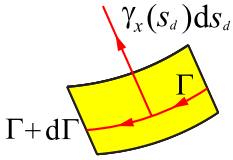

Figure G.2. Bounded vortex and trailing vortex.

Hence:

$$r = c\sqrt{2\left(\sinh^2\psi_w + \sin^2\frac{\varphi+\varphi_d}{2}\right)(1-\cos(\varphi-\varphi_d))}. \tag{G.5}$$

- *Step 2*
  Writing of the unitary vector $\mathbf{n}_{\gamma_x}$.

$$\mathbf{n}_{\gamma_x} = \mathbf{i}\times\frac{\mathbf{r}}{r} = -\frac{(\sinh\psi_w)(\sin\varphi-\sin\varphi_d)}{\sqrt{2\left(\sinh^2\psi_w+\sin^2\frac{\varphi+\varphi_d}{2}\right)(1-\cos(\varphi-\varphi_d))}}\,\mathbf{j}+ \\ +\frac{(\cosh\psi_w)(\cos\varphi-\cos\varphi_d)}{\sqrt{2\left(\sinh^2\psi_w+\sin^2\frac{\varphi+\varphi_d}{2}\right)(1-\cos(\varphi-\varphi_d))}}\,\mathbf{k}. \tag{G.6}$$

- *Step 3*
  Writing of the unitary vector $\mathbf{n}_\varphi$ perpendicular to the ellipse in φ[1].

$$\mathbf{n}_\varphi = -\frac{\cos\varphi \sinh\psi_w}{\sqrt{\cosh^2\psi_w - \cos^2\varphi}}\,\mathbf{j} - \frac{\sin\varphi\cosh\psi_w}{\sqrt{\cosh^2\psi_w - \cos^2\varphi}}\,\mathbf{k}. \tag{G.7}$$

- *Step 4*
  Calculation of $\cos\varsigma$.
  $\cos\varsigma$ is determined using the scalar product of the unitary vectors $\mathbf{n}_{\gamma_x}$ and $\mathbf{n}_\varphi$:

$$\cos\varsigma = \mathbf{n}_{\gamma_x}\cdot\mathbf{n}_\varphi = \frac{-\sin 2\varphi + \sin(\varphi+\varphi_d) - (\cosh 2\psi_w)\sin(-\varphi+\varphi_d)}{2\sqrt{\cosh^2\psi_w - \cos^2\varphi}\sqrt{2\left(\sinh^2\psi_w + \sin^2\frac{\varphi+\varphi_d}{2}\right)(1-\cos(\varphi-\varphi_d))}}. \tag{G.8}$$

Substituting these quantities into the expression of the induced velocity:

$$\mathrm{d}u_n = -\frac{\frac{\mathrm{d}\Gamma}{\mathrm{d}\varphi_d}(-\sin 2\varphi + \sin(\varphi+\varphi_d) - (\cosh 2\psi_w)\sin(-\varphi+\varphi_d))}{16\pi c\sqrt{\cosh^2\psi_w - \cos^2\varphi}\left(\sinh^2\psi_w + \sin^2\frac{\varphi+\varphi_d}{2}\right)(1-\cos(\varphi-\varphi_d))}\,\mathrm{d}\varphi_d. \tag{G.9}$$

Integrating over the lifting line:

$$u_n = -\frac{1}{16\pi c\sqrt{\cosh^2\psi_w - \cos^2\varphi}} \oint_0^{2\pi} \frac{\frac{\mathrm{d}\Gamma}{\mathrm{d}\varphi_d}(-\sin 2\varphi + \sin(\varphi+\varphi_d) - (\cosh 2\psi_w)\sin(-\varphi+\varphi_d))}{\left(\sinh^2\psi_w + \sin^2\frac{\varphi+\varphi_d}{2}\right)(1-\cos(\varphi-\varphi_d))}\,\mathrm{d}\varphi_d. \tag{G.10}$$

Now the variables t and s are changed because they are useful in the numerical approach and because the notation is more clean. Thus[2],

$$u_n = -\frac{1}{16\pi c\sqrt{\cosh^2\psi_w - \cos^2(\pi s)}} \oint_{-1}^{1} \frac{\frac{\mathrm{d}\Gamma}{\mathrm{d}t}(-\sin 2\pi s + \sin\pi(t+s) + (\cosh 2\psi_w)\sin\pi(s-t))}{\left(\sinh^2\psi_w + \sin^2\left(\frac{\pi(t+s)}{2}\right)\right)(1-\cos(\pi(t-s)))}\,\mathrm{d}t. \tag{G.11}$$

Now what remains is to show that the theoretical expression of the induced velocity (see chapter 6) leads to the equation reported above (equation G.11).
In chapter 6, the following expression was found:

$$u_n = \frac{1}{8cV_\infty}\frac{1}{\sqrt{\left(\cosh^2\psi_w - \cos^2(\pi s)\right)}} \oint_{-1}^{+1} m(t)\left[\frac{\sinh^2\psi_w\cosh^2\psi_w}{\left(\sinh^2\psi_w + \sin^2\left(\frac{\pi(t+s)}{2}\right)\right)^2} + \right.$$
$$\left. -\frac{\cosh(2\psi_w)}{2\left(\sinh^2\psi_w + \sin^2\left(\frac{\pi(t+s)}{2}\right)\right)} + \frac{1}{(1-\cos(\pi(t-s)))}\right]\mathrm{d}t. \tag{G.12}$$

[1] Notice that the vector acts towards the local center of curvature. This is the opposite of the convention used in the theory.

[2] Remember that the normalwash is considered positive if it has the same direction as $\mathbf{n}_\varphi$.

Integrating by parts and after a few algebraic operations:

$$u_n = \frac{1}{8cV_\infty}\frac{1}{\sqrt{\left(\cosh^2\psi_w - \cos^2(\pi s)\right)}}\left[m\left(t\right)\frac{-\sin(2\pi s)+\sin\pi(t+s)+\cosh 2\psi_w \sin\pi(s-t)}{2\pi\left(\sinh^2\psi_w+\sin^2\left(\frac{\pi(t+s)}{2}\right)\right)(1-\cos(\pi(t-s)))}\right]_{-1}^{+1} + \\ -\frac{1}{8cV_\infty}\frac{1}{\sqrt{\left(\cosh^2\psi_w - \cos^2(\pi s)\right)}} \; \cancel{\int}_{-1}^{+1} \frac{\mathrm{d}m(t)}{\mathrm{d}t}\frac{-\sin(2\pi s)+\sin\pi(t+s)+\cosh 2\psi_w \sin\pi(s-t)}{2\pi\left(\sinh^2\psi_w+\sin^2\left(\frac{\pi(t+s)}{2}\right)\right)(1-\cos(\pi(t-s)))}\,\mathrm{d}t. \tag{G.13}$$

But it is obvious that $m\left(-1\right) = m\left(+1\right)$[3]. Using this result, equation (G.13) becomes:

$$u_n = -\frac{1}{8cV_\infty\sqrt{\left(\cosh^2\psi_w - \cos^2(\pi s)\right)}} \int_{-1}^{+1} \frac{\mathrm{d}m(t)}{\mathrm{d}t}\frac{-\sin(2\pi s)+\sin\pi(t+s)+\cosh 2\psi_w \sin\pi(s-t)}{2\pi\left(\sinh^2\psi_w+\sin^2\left(\frac{\pi(t+s)}{2}\right)\right)(1-\cos(\pi(t-s)))}\,\mathrm{d}t. \tag{G.14}$$

Remembering the relation found in chapter 1:

$$\rho V_\infty \Gamma\left(\varphi_d\right) = -\rho m\left(\varphi_d\right) \Rightarrow m\left(\varphi_d\right) = -V_\infty \Gamma\left(\varphi_d\right), \tag{G.15}$$

and substituting into equation (G.14), expression (G.11)[4] is obtained.

[3] Therefore, the term $\left[\,\cdot\,\right]_{-1}^{+1}$, which appears in equation (G.13), can be written as

$$m\left(1\right)\left(\frac{-\sin(2\pi s)+\sin\pi(1+s)+\cosh 2\psi_w \sin\pi(s-1)}{2\pi\left(\sinh^2\psi_w+\sin^2\left(\frac{\pi(1+s)}{2}\right)\right)(1-\cos(\pi(1-s)))} - \frac{-\sin(2\pi s)+\sin\pi(-1+s)+\cosh 2\psi_w \sin\pi(s+1)}{2\pi\left(\sinh^2\psi_w+\sin^2\left(\frac{\pi(-1+s)}{2}\right)\right)(1-\cos(\pi(-1-s)))}\right) = 0,$$

because the following identities are valid:

$$-\sin\left(2\pi s\right) + \sin\pi\left(1+s\right) + \cosh 2\psi_w \sin\pi\left(s-1\right) =$$
$$= -\sin\left(2\pi s\right) + \sin\pi\left(-1+s\right) + \cosh 2\psi_w \sin\pi\left(s+1\right) = -2\sin\pi s\cos\pi s - 2\cosh^2\psi_w \sin\pi s;$$
$$2\pi\left(\sinh^2\psi_w + \sin^2\left(\tfrac{\pi(1+s)}{2}\right)\right)\left(1-\cos\left(\pi\left(1-s\right)\right)\right) =$$
$$= 2\pi\left(\sinh^2\psi_w + \sin^2\left(\tfrac{\pi(-1+s)}{2}\right)\right)\left(1-\cos\left(\pi\left(-1-s\right)\right)\right) =$$
$$= 2\pi\sinh^2\psi_w + 2\pi\sinh^2\psi_w\cos\pi s + 2\pi\cos^2\tfrac{1}{2}\pi s + 2\pi\cos^2\tfrac{1}{2}\pi s\cos\pi s.$$

[4] Remember that, here, a *different sign convention* for u_n is used.

Appendix H

Annular Wing with $b_w < a_w$. Some Useful Derivations

H.1 Cartesian Distance

In order to write the small perturbation acceleration potential, the cartesian distance between a generic point $P(x,y,z)$ and a point[1] $P_d(x_d,y_d,z_d)$ on the lifting line w,where the generic *doublet is positioned*, is needed. The distance is:

$$D = \sqrt{(x-x_d)^2 + (y-y_d)^2 + (z-z_d)^2}. \tag{H.1}$$

The lifting line is contained in the $y-z$ plane, thus $x_d = 0$. Setting $x = cX$ and using the new coordinate system:

$$D = c\sqrt{\left(X^2 + (\sinh\psi\cos\varphi - \sinh\psi_w\cos\varphi_d)^2 + (\cosh\psi\sin\varphi - \cosh\psi_w\sin\varphi_d)^2\right)}, \tag{H.2}$$

where the relations valid on the lifting line w have been used:

$$\begin{array}{ll} y_d = c\sinh\psi_w\cos\varphi_d & 0 \le \varphi_d \le 2\pi, \\ z_d = c\cosh\psi_w\sin\varphi_d & \psi_w > 0. \end{array} \tag{H.3}$$

The cartesian distance can be written in another form:

$$D = c\left[\Delta\left(X,\psi,\varphi,\psi_w,\varphi_d\right)\right]^{\frac{1}{2}}, \tag{H.4}$$

where

$$\begin{aligned} \Delta \;=\; & X^2 + \sinh^2\psi + \sin^2\varphi + \sinh^2\psi_w + \sin^2\varphi_d + \\ & - \cosh\left(\psi+\psi_w\right)\cos\left(\varphi-\varphi_d\right) + \cosh\left(\psi-\psi_w\right)\cos\left(\varphi+\varphi_d\right). \end{aligned} \tag{H.5}$$

[1]The point P_d is characterized by $\varphi = \varphi_d$.

H.2 Cosine Directions of the Normal to the Lifting Line

The lifting line is studied considering a doublet distribution m. Each doublet has axis which has inward direction to the ellipse and is perpendicular to the lifting line (figure H.1). Consider a point where the generic doublet is positioned. The straight

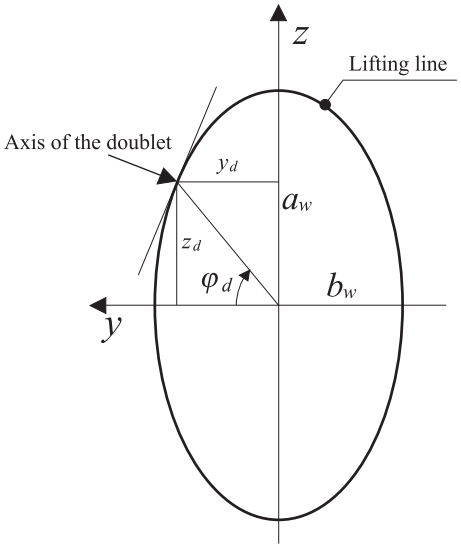

Figure H.1. Positive direction of the doublet's axis.

line perpendicular to the ellipse at that point has the equation:

$$-\frac{2y_d}{\cos^2\varphi_d}(y-y_d)+\frac{2z_d}{\sin^2\varphi_d}(z-z_d)=0. \tag{H.6}$$

From that relation, a vector perpendicular to the ellipse has the expression

$$\mathbf{V}_{\perp el}=\frac{z_d}{\sin^2\varphi_d}\mathbf{j}+\frac{y_d}{\cos^2\varphi_d}\mathbf{k}. \tag{H.7}$$

Using equation (H.3):

$$\mathbf{V}_{\perp el}=\frac{c\cosh\psi_w\sin\varphi_d}{\sin^2\varphi_d}\mathbf{j}+\frac{c\sinh\psi_w\cos\varphi_d}{\cos^2\varphi_d}\mathbf{k}. \tag{H.8}$$

Therefore, it is not difficult to understand that the vector

$$\mathbf{V}_{\perp el}=\frac{\cosh\psi_w}{\sin\varphi_d}\mathbf{j}+\frac{\sinh\psi_w}{\cos\varphi_d}\mathbf{k}, \tag{H.9}$$

is also perpendicular to the ellipse at the point characterized by $y = y_d$, $x = x_d = 0$, $z = z_d$ and $\varphi = \varphi_d$. Normalizing that vector:

$$V_{\perp el} = \frac{\sqrt{\sinh^2 \psi_w + \cos^2 \varphi_d}}{|\sin \varphi_d| \, |\cos \varphi_d|}; \tag{H.10}$$

$$\begin{aligned} \mathbf{V}_{\perp el} &= \frac{\frac{\cosh \psi_w}{\sin \varphi_d}}{V_{\perp el}} \mathbf{j} + \frac{\frac{\sinh \psi_w}{\cos \varphi_d}}{V_{\perp el}} \mathbf{k} \Rightarrow \\ \mathbf{V}_{\perp el} &= \frac{|\sin \varphi_d| \, |\cos \varphi_d|}{\sqrt{\sinh^2 \psi_w + \cos^2 \varphi_d}} \frac{\cosh \psi_w}{\sin \varphi_d} \mathbf{j} + \frac{|\sin \varphi_d| \, |\cos \varphi_d|}{\sqrt{\sinh^2 \psi_w + \cos^2 \varphi_d}} \frac{\sin \psi_w}{\cos \varphi_d} \mathbf{k}. \end{aligned} \tag{H.11}$$

From this equation, it can be deduced that vector $\mathbf{n}_d$ perpendicular to the ellipse, where the doublet is positioned, is:

$$\mathbf{n}_d = -\frac{\cos \varphi_d \cosh \psi_w}{\sqrt{\sinh^2 \psi_w + \cos^2 \varphi_d}} \mathbf{j} - \frac{\sin \varphi_d \sin \psi_w}{\sqrt{\sinh^2 \psi_w + \cos^2 \varphi_d}} \mathbf{k}. \tag{H.12}$$

It is easy to verify that the direction of vector $\mathbf{n}_d$ is in accordance with figure H.1. Clearly, from the previous expression, it can be written that

$$\begin{aligned} n_{dx} &= 0, \\ n_{dy} &= -\frac{\cos \varphi_d \cosh \psi_w}{\sqrt{\sinh^2 \psi_w + \cos^2 \varphi_d}}, \\ n_{dz} &= -\frac{\sin \varphi_d \sinh \psi_w}{\sqrt{\sinh^2 \psi_w + \cos^2 \varphi_d}}. \end{aligned} \tag{H.13}$$

Appendix I

Elliptical Annular Wing with $b_w < a_w$. Weissinger's Condition

I.1 Mathematical Derivation

Weissinger's condition is:

$$-\alpha(\varphi) = \frac{1}{V_\infty}\left(\frac{1}{h}\frac{\partial\phi(X,\psi,\varphi,\psi_w)}{\partial\psi}\right)_{X=X_0;\,\psi=\psi_w}, \tag{I.1}$$

where $X_0 = \frac{l}{2c}$. In order to calculate the derivative of the velocity potential, the following definition is used:

$$\phi(X,\psi,\varphi,\psi_w) = \frac{1}{8\pi V_\infty}\int_0^{2\pi} m(\varphi_d)\cdot f_2(\psi,\varphi,\psi_w)\cdot f_3(X,\psi,\varphi,\psi_w)\,\mathrm{d}\varphi_d, \tag{I.2}$$

where:

$$\begin{aligned}
f_2 &= \tfrac{(\sinh(\psi+\psi_w)\cos(\varphi-\varphi_d)+\sinh(\psi-\psi_w)\cos(\varphi+\varphi_d)-\sinh 2\psi_w)}{\sinh^2\psi+\sin^2\varphi+\sinh^2\psi_w+\sin^2\varphi_d-\cosh(\psi+\psi_w)\cos(\varphi-\varphi_d)+\cosh(\psi-\psi_w)\cos(\varphi+\varphi_d)} = \tfrac{N}{D},\\
f_3 &= \tfrac{X}{\sqrt{X^2+D}} + 1,\\
N &= \sinh(\psi+\psi_w)\cos(\varphi-\varphi_d) + \sinh(\psi-\psi_w)\cos(\varphi+\varphi_d) - \sinh 2\psi_w,\\
D &= \sinh^2\psi + \sin^2\varphi + \sinh^2\psi_w + \sin^2\varphi_d - \cosh(\psi+\psi_w)\cos(\varphi-\varphi_d) +\\
&\quad + \cosh(\psi-\psi_w)\cos(\varphi+\varphi_d).
\end{aligned} \tag{I.3}$$

In the derivative of the small perturbation velocity potential, the following quantity appears:

$$\left[\frac{\partial}{\partial\psi}(f_2\cdot f_3)\right]_{\psi=\psi_w;\,X=X_0} = \left[\frac{\partial f_2}{\partial\psi}f_3 + f_2\frac{\partial f_3}{\partial\psi}\right]_{\psi=\psi_w;\,X=X_0}. \tag{I.4}$$

Now, the principal operations are shown:

$$
\begin{aligned}
&[N]_{\psi=\psi_w} = -\sinh(2\psi_w)\left(1-\cos(\varphi-\varphi_d)\right),\\
&[D]_{\psi=\psi_w} = 2\left(H_5\right)\left(1-\cos(\varphi-\varphi_d)\right),\\
&[f_2]_{\psi=\psi_w} = \tfrac{-\sinh 2\psi_w}{2(H_5)},\\
&[f_3]_{\psi=\psi_w,X=X_0} = \tfrac{X_0}{\sqrt{H_6}}+1,\\
&\left[\tfrac{\partial N}{\partial\psi}\right]_{\psi=\psi_w} = 2\left(\cosh^2\psi_w\cos(\varphi-\varphi_d)-\sin\varphi\sin\varphi_d\right),\\
&\left[\tfrac{\partial D}{\partial\psi}\right]_{\psi=\psi_w} = \sinh(2\psi_w)\left(1-\cos(\varphi-\varphi_d)\right) = -\left[N\right]_{\psi=\psi_w},\\
&\left[\tfrac{\partial f_2}{\partial\psi}\right]_{\psi=\psi_w} = \tfrac{\left(\cosh^2\psi_w\cos(\varphi-\varphi_d)-\sin\varphi\sin\varphi_d\right)}{(H_5)(1-\cos(\varphi-\varphi_d))}+\tfrac{\sinh^2\psi_w\cosh^2\psi_w}{(H_5)^2},\\
&\left[\tfrac{\partial f_3}{\partial\psi}\right]_{\psi=\psi_w,X=X_0} = -\tfrac{X_0\cosh\psi_w\sinh\psi_w(1-\cos(\varphi-\varphi_d))}{(H_6)^{\frac{3}{2}}},\\
&\left[f_2\tfrac{\partial f_3}{\partial\psi}\right]_{\psi=\psi_w,X=X_0} = \tfrac{X_0\cosh^2\psi_w\sinh^2\psi_w(1-\cos(\varphi-\varphi_d))}{(H_5)(H_6)^{\frac{3}{2}}},\\
&\left[\tfrac{\partial f_2}{\partial\psi}f_3\right]_{\psi=\psi_w,X=X_0} = \left(\tfrac{\cosh^2\psi_w\cos(\varphi-\varphi_d)-\sin\varphi\sin\varphi_d}{(H_5)(1-\cos(\varphi-\varphi_d))}+\tfrac{\sinh^2\psi_w\cosh^2\psi_w}{(H_5)^2}\right)\cdot\left(\tfrac{X_0}{\sqrt{H_6}}+1\right),\\
&H_5 = \sinh^2\psi_w+\cos^2\tfrac{\varphi+\varphi_d}{2},\\
&H_6 = X_0^2+2\left(\sinh^2\psi_w+\cos^2\tfrac{\varphi+\varphi_d}{2}\right)\left(1-\cos(\varphi-\varphi_d)\right).
\end{aligned}
\tag{I.5}
$$

Notice that the term $\left[\frac{\partial f_2}{\partial\psi}f_3\right]_{\psi=\psi_w,X=X_0}$ contains the *singular* term $\frac{X_0}{\sqrt{H_6}}$ (when $\varphi=\varphi_d$, it reaches infinity), Thus, $\left[\frac{\partial f_2}{\partial\psi}f_3\right]_{\psi=\psi_w,X=X_0}$ is rewritten in the form

$$
\left[\frac{\partial f_2}{\partial\psi}f_3\right]_{\psi=\psi_w,X=X_0} = \left(\left[\frac{\partial f_2}{\partial\psi}\right]^S f_3\right)_{\psi=\psi_w,X=X_0} + \left(\left[\frac{\partial f_2}{\partial\psi}\right]^R f_3\right)_{\psi=\psi_w,X=X_0}, \tag{I.6}
$$

where the superscripts "S" and "R" indicate "singular" and "regular", respectively.

I.2 Treatment of the Singularity

The goal of this paragraph is to isolate the singularity from the term $\left(\left[\frac{\partial f_2}{\partial \psi}\right]^S f_3\right)_{\psi=\psi_w, X=X_0}$. That term is:

$$\left(\left[\frac{\partial f_2}{\partial \psi}\right]^S f_3\right)_{\psi=\psi_w, X=X_0} = \frac{\cosh^2\psi_w \cos(\varphi-\varphi_d) - \sin\varphi \sin\varphi_d}{(H_5)(1-\cos(\varphi-\varphi_d))} \cdot \left(\frac{X_0}{\sqrt{H_6}} + 1\right). \tag{I.7}$$

In a compact form:

$$\left(\left[\frac{\partial f_2}{\partial \psi}\right]^S f_3\right)_{\psi=\psi_w, X=X_0} = \frac{\left(\cosh^2\psi_w \cos(\varphi-\varphi_d) - \sin\varphi \sin\varphi_d\right)}{(H_5)} \cdot \frac{f_3(X_0,\varphi,\psi_w,\varphi_d)}{1-\cos(\varphi-\varphi_d)}. \tag{I.8}$$

Using the following identity:

$$\frac{f_3\left(X_0,\varphi,\psi_w,\varphi_d\right)}{1-\cos\left(\varphi-\varphi_d\right)} = \frac{f_3\left(X_0,\varphi,\psi_w,\varphi_d\right) - f_3\left(X_0,\varphi,\psi_w,\varphi\right)}{1-\cos\left(\varphi-\varphi_d\right)} + \frac{f_3\left(X_0,\varphi,\psi_w,\varphi\right)}{1-\cos\left(\varphi-\varphi_d\right)}, \tag{I.9}$$

where

$$f_3\left(X_0,\varphi,\psi_w,\varphi\right) = 2, \tag{I.10}$$

$$\frac{f_3\left(X_0,\varphi,\psi_w,\varphi_d\right) - f_3\left(X_0,\varphi,\psi_w,\varphi\right)}{1-\cos\left(\varphi-\varphi_d\right)} = f_I, \tag{I.11}$$

$$f_I = \frac{-2(H_5)}{\left(X_0+\sqrt{H_6}\right)\sqrt{H_6}}, \tag{I.12}$$

thus,

$$\frac{f_3\left(X_0,\varphi,\psi_w,\varphi_d\right)}{1-\cos\left(\varphi-\varphi_d\right)} = f_I + \frac{2}{1-\cos\left(\varphi-\varphi_d\right)}. \tag{I.13}$$

Using expression (I.13), equation (I.8) becomes:

$$\begin{aligned}\left(\left[\frac{\partial f_2}{\partial \psi}\right]^S f_3\right)_{\psi=\psi_w, X=X_0} &= \frac{\left(\cosh^2\psi_w \cos(\varphi-\varphi_d) - \sin\varphi \sin\varphi_d\right)}{(H_5)} \cdot f_I + \\ &+ 2\frac{\left(\cosh^2\psi_w \cos(\varphi-\varphi_d) - \sin\varphi \sin\varphi_d\right)}{(H_5)(1-\cos(\varphi-\varphi_d))}.\end{aligned} \tag{I.14}$$

The second term which appears in equation (I.14) can be manipulated more. Considering the identities

$$2\frac{\left(\cosh^2\psi_w \cos(\varphi-\varphi_d) - \sin\varphi \sin\varphi_d\right)}{(H_5)(1-\cos(\varphi-\varphi_d))} = 2\frac{\cosh^2\psi_w \cos(\varphi-\varphi_d) - \sin\varphi \sin\varphi_d - (H_5)}{(H_5)(1-\cos(\varphi-\varphi_d))} + \frac{2}{1-\cos(\varphi-\varphi_d)}, \tag{I.15}$$

$$\cosh^2\psi_w \cos\left(\varphi-\varphi_d\right) - \sin\varphi \sin\varphi_d - (H_5) = \frac{-(\cosh(2\psi_w))(1-\cos(\varphi-\varphi_d))}{2}, \tag{I.16}$$

it can be deduced that

$$2\frac{\cosh^2\psi_w\cos\left(\varphi-\varphi_d\right)-\sin\varphi\sin\varphi_d}{\left(H_5\right)\left(1-\cos\left(\varphi-\varphi_d\right)\right)}=\frac{-\left(\cosh\left(2\psi_w\right)\right)}{\left(H_5\right)}+\frac{2}{1-\cos\left(\varphi-\varphi_d\right)}. \quad \text{(I.17)}$$

Finally, equation (I.14) is rewritten as:

$$\left(\left[\frac{\partial f_2}{\partial\psi}\right]^S f_3\right)_{\psi=\psi_w,X=X_0}=\frac{\cosh^2\psi_w\cos(\varphi-\varphi_d)-\sin\varphi\sin\varphi_d}{(H_5)}\cdot f_I-\frac{\cosh(2\psi_w)}{(H_5)}+\frac{2}{1-\cos(\varphi-\varphi_d)}. \quad \text{(I.18)}$$

Appendix J

Circular Annular Wing. Analytical Solution of the Euler-Lagrange Equation

The following system of equations has to be solved:

$$\begin{cases} \frac{1}{4R_w V_\infty^2} \oint\limits_{-1}^{+1} \frac{m_{\text{opt}}(s)}{1-\cos(\pi(t-s))}\,\mathrm{d}s - \lambda \sin(\pi t) = 0, \\ -\frac{\pi}{2lV_\infty^2} \int\limits_{-1}^{+1} m_{\text{opt}}(t) \sin(\pi t)\ \mathrm{d}t = \overline{C}_L, \end{cases} \tag{J.1}$$

under the assumption of

$$m_{\text{opt}}(t) = k \sin(\pi t) \qquad k \ \text{ real number.} \tag{J.2}$$

Using the following identities:

$$\begin{aligned} \sin a &= \tfrac{2\tan\frac{a}{2}}{1+\tan^2\frac{a}{2}}, \\ \cos a &= \tfrac{1-\tan^2\frac{a}{2}}{1+\tan^2\frac{a}{2}}, \end{aligned} \tag{J.3}$$

it can be deduced:

$$\begin{aligned} \sin(\pi t) &= \tfrac{2\tan\frac{\pi t}{2}}{1+\tan^2\frac{\pi t}{2}} = \tfrac{2u}{1+u^2}, \\ \cos(\pi t) &= \tfrac{1-u^2}{1+u^2}, \\ \sin(\pi s) &= \tfrac{2\tan\frac{\pi s}{2}}{1+\tan^2\frac{\pi s}{2}} = \tfrac{2v}{1+v^2}, \\ \cos(\pi s) &= \tfrac{1-v^2}{1+v^2}. \end{aligned} \tag{J.4}$$

where

$$\begin{aligned} u &= \tan\tfrac{\pi t}{2}, \\ v &= \tan\tfrac{\pi s}{2}. \end{aligned} \tag{J.5}$$

Observing that

$$1-\cos\left(\pi\left(t-s\right)\right) = 1-\cos\left(\pi t\right)\cos\left(\pi s\right)-\sin\left(\pi t\right)\sin\left(\pi s\right), \tag{J.6}$$

yields

$$1-\cos\left(\pi\left(t-s\right)\right) = 1-\frac{1-u^2}{1+u^2}\frac{1-v^2}{1+v^2}-\frac{2u}{1+u^2}\frac{2v}{1+v^2}. \tag{J.7}$$

Using the same method:

$$k\sin\left(\pi s\right) = k\frac{2v}{1+v^2}, \tag{J.8}$$

$$v=\tan\frac{\pi s}{2} \Rightarrow \mathrm{d}v = \frac{\pi}{2}\left(\tan^2\frac{\pi s}{2}+1\right)\mathrm{d}s. \tag{J.9}$$

Elaborating the previous expression:

$$\mathrm{d}v = \frac{\pi}{2}\left(v^2+1\right)\mathrm{d}s \Rightarrow \mathrm{d}s = \frac{2}{\pi\left(v^2+1\right)}\mathrm{d}v. \tag{J.10}$$

The integral expressed using the new variables becomes:

$$\frac{2k\left(1+u^2\right)}{\pi}\oint\limits_{-\infty}^{+\infty}\frac{v}{1+v^2}\frac{1}{\left(v-u\right)^2}\mathrm{d}v. \tag{J.11}$$

But[1]

$$\begin{aligned} \int \tfrac{v}{1+v^2}\tfrac{1}{(v-u)^2}\mathrm{d}v = \ln\frac{\left(1+v^2\right)^{\frac{u^2}{2\left(u^4+2u^2+1\right)}}}{\left(1+v^2\right)^{\frac{1}{2\left(u^4+2u^2+1\right)}}} - \tfrac{2}{u^4+2u^2+1}u\arctan v + \\ + \ln\frac{\left|(v-u)\right|^{\frac{1}{u^4+2u^2+1}}}{\left|(v-u)\right|^{\frac{u^2}{u^4+2u^2+1}}} - \tfrac{u}{(1+u^2)(v-u)}. \end{aligned} \tag{J.12}$$

Calculating the integral in the Hadamard finite-part sense:

$$\oint\limits_{-\infty}^{+\infty}\frac{v}{1+v^2}\frac{1}{\left(v-u\right)^2}\mathrm{d}v = -\frac{2\pi u}{u^4+2u^2+1}. \tag{J.13}$$

Therefore:

$$\frac{2k\left(1+u^2\right)}{\pi}\oint\limits_{-\infty}^{+\infty}\frac{v}{1+v^2}\frac{1}{\left(v-u\right)^2}\mathrm{d}v = -\frac{2\pi u}{u^4+2u^2+1}\frac{2k\left(1+u^2\right)}{\pi} = -2k\frac{2u}{1+u^2}. \tag{J.14}$$

[1]For the analytical evaluation of the integral, the website [69] has been used.

Remembering the definition of u:

$$-2k\frac{2u}{1+u^2} = -2k\sin(\pi t)\,. \tag{J.15}$$

Thus, it has been demonstrated that, under the hypothesis of $m_{\text{opt}}(s) = k\sin(\pi s)$,

$$\fint_{-1}^{+1} \frac{m_{\text{opt}}(s)}{1-\cos(\pi(t-s))}\,\mathrm{d}s = -2k\sin(\pi t). \tag{J.16}$$

Using this result, the Euler-Lagrange equation becomes

$$\frac{-2k\sin\pi t}{4R_w V_\infty^2} - \lambda\sin(\pi t) = 0. \tag{J.17}$$

But the condition of coefficient of lift assigned has to be satisfied. Hence,

$$-\frac{\pi}{2lV_\infty^2}\int_{-1}^{+1} m_{\text{opt}}(t)\sin(\pi t)\,\mathrm{d}t = \overline{C}_L, \tag{J.18}$$

which now is:

$$-\frac{\pi}{2lV_\infty^2}\int_{-1}^{+1} k\sin^2(\pi t)\,\mathrm{d}t = -\frac{1}{2}\frac{\pi}{lV_\infty^2}k = \overline{C}_L. \tag{J.19}$$

Therefore, from the previous equation, it can be deduced that

$$k = -\frac{2lV_\infty^2\overline{C}_L}{\pi}. \tag{J.20}$$

Substituting into the Euler-Lagrange equation:

$$\frac{2\frac{2lV_\infty^2\overline{C}_L}{\pi}}{4R_wV_\infty^2} - \lambda = 0. \tag{J.21}$$

Simplifying:

$$\lambda = \frac{l\overline{C}_L}{\pi R_w}. \tag{J.22}$$

Appendix K

Elliptical Annular Wing with $b_w > a_w$. Analytical Solution of the Euler-Lagrange Equation

The following system of equations has to be solved:

$$\begin{cases} \frac{1}{4b_w V_\infty^2} \oint\limits_{-1}^{+1} m_{\text{opt}}(s)\, \overline{Y}(t,s)\, \mathrm{d}s - \lambda \sin(\pi t) = 0, \\ -\frac{\pi}{2lV_\infty^2} \int\limits_{-1}^{+1} m_{\text{opt}}(t) \sin(\pi t)\, \mathrm{d}t = \overline{C}_L, \end{cases} \tag{K.1}$$

where

$$\overline{Y}(t,s) = \frac{\sinh^2\psi_w \cosh^2\psi_w}{\left(\sinh^2\psi_w + \sin^2\left(\frac{\pi(t+s)}{2}\right)\right)^2} - \frac{\frac{1}{2}\cosh(2\psi_w)}{\left(\sinh^2\psi_w + \sin^2\left(\frac{\pi(t+s)}{2}\right)\right)} + \frac{1}{(1-\cos(\pi(t-s)))}. \tag{K.2}$$

The candidate optimal doublet distribution is:

$$m_{\text{opt}}(t) = k \sin(\pi t) \qquad k \ \text{ real number.} \tag{K.3}$$

Substituting (K.3) into the first expression in equation (K.1):

$$\begin{aligned} &\frac{1}{4b_w V_\infty^2} \int\limits_{-1}^{+1} \frac{k \sin(\pi s) \sinh^2\psi_w \cosh^2\psi_w}{\left(\sinh^2\psi_w + \sin^2\left(\frac{\pi(t+s)}{2}\right)\right)^2}\, \mathrm{d}s - \frac{1}{4b_w V_\infty^2} \int\limits_{-1}^{+1} \frac{\frac{1}{2}k \sin(\pi s)\cosh(2\psi_w)}{\left(\sinh^2\psi_w + \sin^2\left(\frac{\pi(t+s)}{2}\right)\right)}\, \mathrm{d}s + \\ &+ \frac{1}{4b_w V_\infty^2} \oint\limits_{-1}^{+1} \frac{k \sin(\pi s)}{(1-\cos(\pi(t-s)))}\, \mathrm{d}s - \lambda \sin(\pi t) = 0. \end{aligned} \tag{K.4}$$

Expression (K.4) can be written in a compact form:

$$\frac{1}{4b_w V_\infty^2} I_A - \frac{1}{4b_w V_\infty^2} I_B + \frac{1}{4b_w V_\infty^2} I_C - \lambda \sin(\pi t) = 0, \tag{K.5}$$

where

$$
\begin{aligned}
I_A &= \int_{-1}^{+1} \frac{k\sin(\pi s)\sinh^2\psi_w\cosh^2\psi_w}{\left(\sinh^2\psi_w+\sin^2\left(\frac{\pi(t+s)}{2}\right)\right)^2}\,\mathrm{d}s = k\sinh^2\psi_w\cosh^2\psi_w\int_{-1}^{+1}\frac{\sin(\pi s)}{\left(\sinh^2\psi_w+\sin^2\left(\frac{\pi(t+s)}{2}\right)\right)^2}\,\mathrm{d}s,\\
I_B &= \int_{-1}^{+1} \frac{\frac{1}{2}k\sin(\pi s)\cosh(2\psi_w)}{\left(\sinh^2\psi_w+\sin^2\left(\frac{\pi(t+s)}{2}\right)\right)}\,\mathrm{d}s = \frac{k\cosh(2\psi_w)}{2}\int_{-1}^{+1}\frac{\sin(\pi s)}{\left(\sinh^2\psi_w+\sin^2\left(\frac{\pi(t+s)}{2}\right)\right)}\,\mathrm{d}s,\\
I_C &= \int_{-1}^{+1} \frac{k\sin(\pi s)}{(1-\cos(\pi(t-s)))}\,\mathrm{d}s = k\int_{-1}^{+1}\frac{\sin(\pi s)}{(1-\cos(\pi(t-s)))}\,\mathrm{d}s.
\end{aligned}
\tag{K.6}
$$

K.1 Elaboration of I_A

Using the identity

$$
\sin\left(\frac{\pi\,(t+s)}{2}\right) = \sin\frac{\pi s}{2}\cos\frac{\pi t}{2} + \sin\frac{\pi t}{2}\cos\frac{\pi s}{2},
\tag{K.7}
$$

it is possible to write:

$$
\sin^2\left(\frac{\pi\,(t+s)}{2}\right) = \sin^2\frac{\pi t}{2}\cos^2\frac{\pi s}{2} + \sin^2\frac{\pi s}{2}\cos^2\frac{\pi t}{2} + \frac{1}{2}\sin\left(\pi t\right)\sin\left(\pi s\right).
\tag{K.8}
$$

Setting

$$
\begin{aligned}
u &= \tan\tfrac{\pi t}{2},\\
v &= \tan\tfrac{\pi s}{2},
\end{aligned}
\tag{K.9}
$$

the following can be written:

$$
\begin{aligned}
\sin^2\tfrac{\pi t}{2} &= \frac{\tan^2\frac{\pi t}{2}}{\tan^2\frac{\pi t}{2}+1} = \frac{u^2}{u^2+1},\\
\cos^2\tfrac{\pi t}{2} &= \frac{1}{\tan^2\frac{\pi t}{2}+1} = \frac{1}{u^2+1},\\
\sin^2\tfrac{\pi s}{2} &= \frac{\tan^2\frac{\pi s}{2}}{\tan^2\frac{\pi s}{2}+1} = \frac{v^2}{v^2+1},\\
\cos^2\tfrac{\pi s}{2} &= \frac{1}{\tan^2\frac{\pi s}{2}+1} = \frac{1}{v^2+1},\\
\sin\left(\pi t\right) &= \frac{2\tan\frac{\pi t}{2}}{\tan^2\frac{\pi t}{2}+1} = \frac{2u}{u^2+1},\\
\sin\left(\pi s\right) &= \frac{2\tan\frac{\pi s}{2}}{\tan^2\frac{\pi s}{2}+1} = \frac{2v}{v^2+1}.
\end{aligned}
\tag{K.10}
$$

Substituting (K.10) into (K.8):

$$
\sin^2\left(\tfrac{\pi(t+s)}{2}\right) = \frac{u^2}{u^2+1}\frac{1}{v^2+1} + \frac{v^2}{v^2+1}\frac{1}{u^2+1} + \frac{1}{2}\frac{2u}{u^2+1}\frac{2v}{v^2+1} = \frac{(v+u)^2}{(u^2+1)(v^2+1)}.
\tag{K.11}
$$

The differential is:

$$v = \tan\frac{\pi s}{2} \Rightarrow \mathrm{d}v = \frac{\pi}{2}\left(1+\tan^2\frac{\pi s}{2}\right)\mathrm{d}s = \frac{\pi}{2}\left(1+v^2\right)\mathrm{d}s \Rightarrow \mathrm{d}s = \frac{2}{\pi(1+v^2)}\mathrm{d}v. \tag{K.12}$$

Thus,

$$I_A = k\sinh^2\psi_w\cosh^2\psi_w \int_{-\infty}^{+\infty} \frac{\frac{2v}{v^2+1}}{\left(\sinh^2\psi_w + \frac{(v+u)^2}{(u^2+1)(v^2+1)}\right)^2}\frac{2}{\pi\left(1+v^2\right)}\mathrm{d}v. \tag{K.13}$$

With a few algebraic manipulations:

$$I_A = \frac{4k\sinh^2\psi_w\cosh^2\psi_w\left(u^2+1\right)^2}{\pi}\int_{-\infty}^{+\infty}\frac{v}{\left((u^2+1)(v^2+1)\sinh^2\psi_w+(v+u)^2\right)^2}\mathrm{d}v. \tag{K.14}$$

The corresponding indefinite integral ($\sinh\psi_w = a$, for brevity) is:

$$\begin{aligned}\int \frac{v}{\left((u^2+1)(v^2+1)a^2+(v+u)^2\right)^2}\,\mathrm{d}v = {} & \frac{-a^2-u^2-a^2u^2-uv}{2a^2(1+a^2)(1+u^2)^2(a^2+u^2+a^2u^2+2uv+v^2+a^2v^2+a^2u^2v^2)} + \\ & - \frac{u\arctan\left(\frac{u+v+a^2v+a^2u^2v}{a\sqrt{1+a^2(1+u^2)}}\right)}{2a^3(1+a^2)^{\frac{3}{2}}(1+u^2)^3}.\end{aligned} \tag{K.15}$$

Observing that

$$\begin{aligned}&\lim_{v\to\pm\infty}\frac{-a^2-u^2-a^2u^2-uv}{2a^2(1+a^2)(1+u^2)^2(a^2+u^2+a^2u^2+2uv+v^2+a^2v^2+a^2u^2v^2)} = 0,\\ &\lim_{v\to\pm\infty} -\frac{u\arctan\left(\frac{u+v+a^2v+a^2u^2v}{a\sqrt{1+a^2(1+u^2)}}\right)}{2a^3(1+a^2)^{\frac{3}{2}}(1+u^2)^3} = \mp\frac{\pi u}{4a^3(1+a^2)^{\frac{3}{2}}(1+u^2)^3},\end{aligned} \tag{K.16}$$

the integral in equation (K.14) becomes:

$$\int_{-\infty}^{+\infty}\frac{v}{\left(\left(u^2+1\right)\left(v^2+1\right)\sinh^2\psi_w+\left(v+u\right)^2\right)^2}\,\mathrm{d}v = -\frac{\pi u}{2a^3\left(1+a^2\right)^{\frac{3}{2}}\left(1+u^2\right)^3}. \tag{K.17}$$

Returning to the original variables:

$$\int_{-\infty}^{+\infty}\frac{v}{\left(\left(u^2+1\right)\left(v^2+1\right)\sinh^2\psi_w+\left(v+u\right)^2\right)^2}\,\mathrm{d}v = -\frac{\pi u}{2\sinh^3\psi_w\cos^3\psi_w\left(1+u^2\right)^3}. \tag{K.18}$$

Therefore:

$$I_A = -\frac{4k}{\pi}\frac{\pi u}{2\sinh\psi_w\cos\psi_w\left(1+u^2\right)}. \tag{K.19}$$

But $\sin(\pi t) = \frac{2u}{u^2+1}$; hence,

$$I_A = -2k\frac{\sin(\pi t)}{\sinh 2\psi_w}. \tag{K.20}$$

K.2 Elaboration of I_B

Using the same changing of variables seen in the previous section (elaboration of I_A), it is possible to write:

$$I_B = \frac{k\cosh(2\psi_w)}{2}\int_{-\infty}^{+\infty}\frac{\frac{2v}{v^2+1}}{\left(\sinh^2\psi_w + \frac{(v+u)^2}{(u^2+1)(v^2+1)}\right)}\frac{2}{\pi(1+v^2)}\,\mathrm{d}v. \tag{K.21}$$

Simplifying:

$$I_B = \frac{2k\cosh(2\psi_w)(u^2+1)}{\pi}\int_{-\infty}^{+\infty}\frac{\frac{v}{v^2+1}}{\left((u^2+1)(v^2+1)\sinh^2\psi_w + (v+u)^2\right)}\,\mathrm{d}v. \tag{K.22}$$

The corresponding indefinite integral is:

$$\begin{aligned}
&\int \frac{\frac{v}{v^2+1}}{\left((u^2+1)(v^2+1)\sinh^2\psi_w+(v+u)^2\right)}\,\mathrm{d}v = \\
&= \frac{2u}{(u^2+1)^2}\left[\arctan v - \frac{\cosh 2\psi_w}{\sinh 2\psi_w}\arctan\left(2\frac{u+v+v\left(1+u^2\right)\sinh^2\psi_w}{\sinh 2\psi_w(u^2+1)}\right)\right] + \\
&+ \ln\left(\frac{\left(1+v^2\right)}{\left((u^2+1)(v^2+1)\sinh^2\psi_w+(v+u)^2\right)}\right)^{\frac{u^2-1}{2(u^2+1)^2}}.
\end{aligned} \tag{K.23}$$

Considering that

$$\begin{aligned}
&\lim_{v\to\pm\infty}\frac{2u}{(u^2+1)^2}\left[\arctan v - \frac{\cosh 2\psi_w}{\sinh 2\psi_w}\arctan\left(2\frac{u+v+v\sinh^2\psi_w\left(1+u^2\right)}{\sinh 2\psi_w(u^2+1)}\right)\right] = \\
&= \pm\frac{u\pi}{(u^2+1)^2}\left(1 - \frac{\cosh 2\psi_w}{\sinh 2\psi_w}\right), \\
&\lim_{v\to\pm\infty}\ln\left(\frac{\left(1+v^2\right)}{\left((u^2+1)(v^2+1)\sinh^2\psi_w+(v+u)^2\right)}\right)^{\frac{u^2-1}{2(u^2+1)^2}} = \\
&= \ln\left(\frac{1}{1+(u^2+1)\sinh^2\psi_w}\right)^{\frac{u^2-1}{2(u^2+1)^2}},
\end{aligned} \tag{K.24}$$

it can be deduced that:

$$\int_{-\infty}^{+\infty}\frac{\frac{v}{v^2+1}}{\left((u^2+1)(v^2+1)\sinh^2\psi_w+(v+u)^2\right)}\,\mathrm{d}v = \frac{2u\pi}{(u^2+1)^2}\left(1 - \frac{\cosh 2\psi_w}{\sinh 2\psi_w}\right). \tag{K.25}$$

Finally, remembering that $\sin(\pi t) = \frac{2u}{(u^2+1)^2}$:

$$I_B = 2k \sin(\pi t) \cosh(2\psi_w) \left(1 - \frac{\cosh 2\psi_w}{\sinh 2\psi_w}\right). \tag{K.26}$$

K.3 Elaboration of I_C

It has already been demonstrated that[1]:

$$\oint_{-1}^{1} \frac{\sin(\pi s)}{(1 - \cos(\pi(t-s)))} \, \mathrm{d}s = -2 \sin(\pi t). \tag{K.27}$$

Thus, it can be concluded that

$$I_C = -2k \sin(\pi t). \tag{K.28}$$

K.4 Substitution of I_A, I_B, I_C into the Euler-Lagrange Equation

Using the expressions of I_A, I_B and I_C obtained in previous sections, the Euler-Lagrange Equation becomes:

$$-\frac{k}{2b_w V_\infty^2} \frac{\sin \pi t}{\sinh 2\psi_w} - \frac{k \sin \pi t \cosh(2\psi_w)}{2b_w V_\infty^2} \left(1 - \frac{\cosh 2\psi_w}{\sinh 2\psi_w}\right) - \frac{k}{2b_w V_\infty^2} \sin(\pi t) - \lambda \sin(\pi t) = 0, \tag{K.29}$$

while the constraint is:

$$\begin{aligned} \overline{C}_L &= -\frac{\pi}{2lV_\infty^2} \int_{-1}^{+1} m(t) \sin(\pi t) \, \mathrm{d}t = -\frac{\pi}{2lV_\infty^2} \int_{-1}^{+1} k \sin^2(\pi t) \, \mathrm{d}t = -\frac{\pi}{2lV_\infty^2} k \Rightarrow \\ &\Rightarrow k = -\frac{2lV_\infty^2}{\pi} \overline{C}_L. \end{aligned} \tag{K.30}$$

Substituting the last formula into (K.29):

$$\lambda = \frac{l\overline{C}_L}{\pi b_w} (\cosh 2\psi_w - \sinh 2\psi_w + 1). \tag{K.31}$$

Remembering the relations:

$$\begin{aligned} \cosh 2\psi_w &= 2\cosh^2 \psi_w - 1 = 2\frac{b_w^2}{b_w^2 - a_w^2} - 1 = \frac{b_w^2 + a_w^2}{b_w^2 - a_w^2}, \\ \sinh 2\psi_w &= 2 \cosh \psi_w \sinh \psi_w = 2 \frac{b_w}{\sqrt{b_w^2 - a_w^2}} \frac{a_w}{\sqrt{b_w^2 - a_w^2}} = 2\frac{a_w b_w}{b_w^2 - a_w^2}, \end{aligned} \tag{K.32}$$

[1] See minimum induced drag of a circular annular wing in chapter 9.

The Lagrange multiplier is obtained:

$$\lambda = \frac{2l\overline{C}_L}{\pi\left(b_w + a_w\right)}. \tag{K.33}$$

Notice that, if $b_w \to a_w = R_w$ (circular annular wing), $\lambda = \frac{l\overline{C}_L}{\pi R_w}$, as has been found for the circular annular wing.

Appendix L

Elliptical Annular Wing with $b_w < a_w$. Analytical Solution of the Euler-Lagrange Equation

The following system of equations has to be solved:

$$\begin{cases} \frac{1}{4b_w V_\infty^2} \oint\limits_{-1}^{+1} m_{\text{opt}}(s)\, \overline{Y}(t,s)\, \mathrm{d}s - \lambda \sin(\pi t) = 0, \\ -\frac{\pi}{2lV_\infty^2} \int\limits_{-1}^{+1} m_{\text{opt}}(t) \sin(\pi t)\, \mathrm{d}t = \overline{C}_L, \end{cases} \tag{L.1}$$

where

$$\overline{Y}(t,s) = \frac{\sinh^2\psi_w \cosh^2\psi_w}{\left(\sinh^2\psi_w + \cos^2\left(\frac{\pi(t+s)}{2}\right)\right)^2} - \frac{\frac{1}{2}\cosh(2\psi_w)}{\left(\sinh^2\psi_w + \cos^2\left(\frac{\pi(t+s)}{2}\right)\right)} + \frac{1}{1-\cos(\pi(t-s))}. \tag{L.2}$$

The candidate optimal doublet distribution is:

$$m_{\text{opt}}(t) = k \sin(\pi t) \qquad k \ \text{ real number.} \tag{L.3}$$

Substituting (L.3) into the first expression in equation (L.1):

$$\begin{aligned} &\frac{1}{4b_w V_\infty^2} \int\limits_{-1}^{+1} \frac{k\sin(\pi s)\sinh^2\psi_w \cosh^2\psi_w}{\left(\sinh^2\psi_w + \cos^2\left(\frac{\pi(t+s)}{2}\right)\right)^2}\, \mathrm{d}s - \frac{1}{4b_w V_\infty^2} \int\limits_{-1}^{+1} \frac{\frac{1}{2}k\sin(\pi s)\cosh(2\psi_w)}{\left(\sinh^2\psi_w + \cos^2\left(\frac{\pi(t+s)}{2}\right)\right)}\, \mathrm{d}s + \\ &+ \frac{1}{4b_w V_\infty^2} \oint\limits_{-1}^{+1} \frac{k\sin(\pi s)}{1-\cos(\pi(t-s))}\, \mathrm{d}s - \lambda \sin(\pi t) = 0. \end{aligned} \tag{L.4}$$

Expression (L.4) can be written in a compact form:

$$\frac{1}{4b_w V_\infty^2} I_A - \frac{1}{4b_w V_\infty^2} I_B + \frac{1}{4b_w V_\infty^2} I_C - \lambda \sin(\pi t) = 0, \tag{L.5}$$

where

$$
\begin{aligned}
I_A &= \int_{-1}^{+1} \frac{k \sin(\pi s) \sinh^2 \psi_w \cosh^2 \psi_w}{\left(\sinh^2 \psi_w + \cos^2\left(\frac{\pi(t+s)}{2}\right)\right)^2} \, \mathrm{d}s = k \sinh^2 \psi_w \cosh^2 \psi_w \int_{-1}^{+1} \frac{\sin(\pi s)}{\left(\sinh^2 \psi_w + \cos^2\left(\frac{\pi(t+s)}{2}\right)\right)^2} \, \mathrm{d}s, \\
I_B &= \int_{-1}^{+1} \frac{\frac{1}{2} k \sin(\pi s) \cosh(2\psi_w)}{\left(\sinh^2 \psi_w + \cos^2\left(\frac{\pi(t+s)}{2}\right)\right)} \, \mathrm{d}s = \frac{k \cosh(2\psi_w)}{2} \int_{-1}^{+1} \frac{\sin(\pi s)}{\left(\sinh^2 \psi_w + \cos^2\left(\frac{\pi(t+s)}{2}\right)\right)} \, \mathrm{d}s, \\
I_C &= \int_{-1}^{+1} \frac{k \sin(\pi s)}{1 - \cos(\pi(t-s))} \, \mathrm{d}s = k \int_{-1}^{+1} \frac{\sin(\pi s)}{1 - \cos(\pi(t-s))} \, \mathrm{d}s.
\end{aligned}
\tag{L.6}
$$

L.1 Elaboration of I_A

Using the identity

$$
\cos\left(\frac{\pi\,(t+s)}{2}\right) = \cos\frac{\pi s}{2} \cos\frac{\pi t}{2} - \sin\frac{\pi t}{2} \sin\frac{\pi s}{2}, \tag{L.7}
$$

it is possible to write:

$$
\cos^2\left(\frac{\pi\,(t+s)}{2}\right) = \cos^2\frac{\pi s}{2} \cos^2\frac{\pi t}{2} + \sin^2\frac{\pi t}{2} \sin^2\frac{\pi s}{2} - \frac{1}{2} \sin(\pi s) \sin(\pi t)\,. \tag{L.8}
$$

Setting

$$
\begin{aligned}
u &= \tan\tfrac{\pi t}{2}, \\
v &= \tan\tfrac{\pi s}{2},
\end{aligned}
\tag{L.9}
$$

the following can be written:

$$
\begin{aligned}
\sin^2\tfrac{\pi t}{2} &= \frac{\tan^2\frac{\pi t}{2}}{\tan^2\frac{\pi t}{2}+1} = \frac{u^2}{u^2+1}, \\
\cos^2\tfrac{\pi t}{2} &= \frac{1}{\tan^2\frac{\pi t}{2}+1} = \frac{1}{u^2+1}, \\
\sin^2\tfrac{\pi s}{2} &= \frac{\tan^2\frac{\pi s}{2}}{\tan^2\frac{\pi s}{2}+1} = \frac{v^2}{v^2+1}, \\
\cos^2\tfrac{\pi s}{2} &= \frac{1}{\tan^2\frac{\pi s}{2}+1} = \frac{1}{v^2+1}, \\
\sin(\pi t) &= \frac{2\tan\frac{\pi t}{2}}{\tan^2\frac{\pi t}{2}+1} = \frac{2u}{u^2+1}, \\
\sin(\pi s) &= \frac{2\tan\frac{\pi s}{2}}{\tan^2\frac{\pi s}{2}+1} = \frac{2v}{v^2+1}.
\end{aligned}
\tag{L.10}
$$

Substituting (L.10) into (L.8):

$$
\cos^2\left(\tfrac{\pi(t+s)}{2}\right) = \frac{1}{v^2+1}\frac{1}{u^2+1} + \frac{u^2}{u^2+1}\frac{v^2}{v^2+1} - \frac{1}{2}\frac{2u}{u^2+1}\frac{2v}{v^2+1} = \frac{(uv-1)^2}{(v^2+1)(u^2+1)}. \tag{L.11}
$$

The differential is:

$$v = \tan\frac{\pi s}{2} \Rightarrow \mathrm{d}v = \frac{\pi}{2}\left(1+\tan^2\frac{\pi s}{2}\right)\mathrm{d}s = \frac{\pi}{2}\left(1+v^2\right)\mathrm{d}s \Rightarrow \mathrm{d}s = \frac{2}{\pi(1+v^2)}\mathrm{d}v. \tag{L.12}$$

Thus,

$$I_A = k\sinh^2\psi_w\cosh^2\psi_w \int_{-\infty}^{+\infty} \frac{\frac{2v}{v^2+1}}{\left(\sinh^2\psi_w + \frac{(uv-1)^2}{(v^2+1)(u^2+1)}\right)^2}\frac{2}{\pi\left(1+v^2\right)}\mathrm{d}v. \tag{L.13}$$

With a few algebraic manipulations:

$$I_A = \frac{4k\sinh^2\psi_w\cosh^2\psi_w\left(u^2+1\right)^2}{\pi}\int_{-\infty}^{+\infty}\frac{v}{\left((u^2+1)(v^2+1)\sinh^2\psi_w+(uv-1)^2\right)^2}\mathrm{d}v. \tag{L.14}$$

Using $\sinh\psi_w = a$ for brevity , yields:

$$\begin{aligned}&\int \frac{v}{\left((u^2+1)(v^2+1)a^2+(uv-1)^2\right)^2}\,\mathrm{d}v = \\ &= \frac{-1-a^2-a^2u^2+uv}{2a^2(1+a^2)(1+u^2)^2(1+a^2+a^2u^2-2uv+a^2v^2+u^2v^2+a^2u^2v^2)} + \frac{u\arctan\left(\frac{-u+a^2v+u^2v+a^2u^2v}{a\sqrt{1+a^2}(1+u^2)}\right)}{2a^3(1+a^2)^{\frac{3}{2}}(1+u^2)^3}.\end{aligned} \tag{L.15}$$

Observing that

$$\begin{aligned}&\lim_{v\to\pm\infty}\frac{-1-a^2-a^2u^2+uv}{2a^2(1+a^2)(1+u^2)^2(1+a^2+a^2u^2-2uv+a^2v^2+u^2v^2+a^2u^2v^2)} = 0,\\ &\lim_{v\to\pm\infty}\frac{u\arctan\left(\frac{-u+a^2v+u^2v+a^2u^2v}{a\sqrt{1+a^2}(1+u^2)}\right)}{2a^3(1+a^2)^{\frac{3}{2}}(1+u^2)^3} = \pm\frac{u\pi}{4a^3(1+a^2)^{\frac{3}{2}}(1+u^2)^3},\end{aligned} \tag{L.16}$$

the integral in (L.14) becomes

$$\int_{-\infty}^{+\infty}\frac{v}{\left(\left(u^2+1\right)\left(v^2+1\right)\sinh^2\psi_w+\left(uv-1\right)^2\right)^2}\,\mathrm{d}v = \frac{\pi u}{2a^3\left(1+a^2\right)^{\frac{3}{2}}\left(1+u^2\right)^3}. \tag{L.17}$$

Returning to the original variables:

$$\int_{-\infty}^{+\infty}\frac{v}{\left(\left(u^2+1\right)\left(v^2+1\right)\sinh^2\psi_w+\left(uv-1\right)^2\right)^2}\,\mathrm{d}v = \frac{\pi u}{2\sinh^3\psi_w\cos^3\psi_w\left(1+u^2\right)^3}. \tag{L.18}$$

Therefore:

$$I_A = \frac{4k}{\pi}\frac{\pi u}{2\sinh\psi_w\cos\psi_w\left(1+u^2\right)}. \tag{L.19}$$

But $\sin(\pi t) = \frac{2u}{u^2+1}$; hence,

$$I_A = 2k\frac{\sin(\pi t)}{\sinh 2\psi_w}. \tag{L.20}$$

L.2 Elaboration of I_B

Operating similar positions used for the calculation of I_A:

$$I_B = \frac{k\cosh(2\psi_w)}{2}\int_{-\infty}^{+\infty}\frac{\frac{2v}{v^2+1}}{\left(\sinh^2\psi_w+\frac{(uv-1)^2}{(v^2+1)(u^2+1)}\right)}\frac{2}{\pi\left(1+v^2\right)}\,\mathrm{d}v, \tag{L.21}$$

$$I_B = \frac{2k\cosh(2\psi_w)\left(u^2+1\right)}{\pi}\int_{-\infty}^{+\infty}\frac{\frac{v}{v^2+1}}{\left(\left(u^2+1\right)\left(v^2+1\right)\sinh^2\psi_w+\left(uv-1\right)^2\right)}\,\mathrm{d}v. \tag{L.22}$$

But

$$\begin{aligned}
&\int\frac{\frac{v}{v^2+1}}{\left(\left(u^2+1\right)\left(v^2+1\right)\sinh^2\psi_w+\left(uv-1\right)^2\right)}\,\mathrm{d}v = \\
&= \frac{2u}{\left(u^2+1\right)^2}\left[-\arctan v+\frac{\cosh 2\psi_w}{\sinh 2\psi_w}\arctan\left(\frac{-u+v\sinh^2\psi_w+u^2v+u^2v\sinh^2\psi_w}{\sinh\psi_w\cosh\psi_w\left(u^2+1\right)}\right)\right]+ \\
&+\ln\left|\frac{\left(1+\sinh^2\psi_w+u^2\sinh^2\psi_w-2uv+v^2\sinh^2\psi_w+u^2v^2+u^2v^2\sinh^2\psi_w\right)}{\left(1+v^2\right)}\right|^{\frac{\left(u^2-1\right)}{2\left(1+u^2\right)^2}}.
\end{aligned} \tag{L.23}$$

Considering

$$\begin{aligned}
&\lim_{v\to\pm\infty}\frac{2u}{\left(u^2+1\right)^2}\left[-\arctan v+\frac{\cosh 2\psi_w}{\sinh 2\psi_w}\arctan\left(\frac{-u+v\sinh^2\psi_w+u^2v+u^2v\sinh^2\psi_w}{\sinh\psi_w\cosh\psi_w\left(u^2+1\right)}\right)\right] = \\
&\qquad = \pm\frac{u\pi}{\left(u^2+1\right)^2}\left(-1+\frac{\cosh 2\psi_w}{\sinh 2\psi_w}\right), \\
&\lim_{v\to\pm\infty}\ln\left|\frac{\left(1+\sinh^2\psi_w+u^2\sinh^2\psi_w-2uv+v^2\sinh^2\psi_w+u^2v^2+u^2v^2\sinh^2\psi_w\right)}{\left(1+v^2\right)}\right|^{\frac{\left(u^2-1\right)}{2\left(1+u^2\right)^2}} = \\
&\qquad = \ln\left(\left(1+u^2\right)\sinh^2\psi_w+u^2\right)^{\frac{\left(u^2-1\right)}{2\left(1+u^2\right)^2}},
\end{aligned} \tag{L.24}$$

it can be deduced that

$$\int_{-\infty}^{+\infty}\frac{\frac{v}{v^2+1}}{\left(\left(u^2+1\right)\left(v^2+1\right)\sinh^2\psi_w+\left(uv-1\right)^2\right)}\,\mathrm{d}v = \frac{2u\pi}{\left(u^2+1\right)^2}\left(-1+\frac{\cosh 2\psi_w}{\sinh 2\psi_w}\right). \tag{L.25}$$

Finally, remembering that $\sin(\pi t) = \frac{2u}{\left(u^2+1\right)^2}$:

$$I_B = -2k\sin(\pi t)\cosh(2\psi_w)\left(1-\frac{\cosh 2\psi_w}{\sinh 2\psi_w}\right). \tag{L.26}$$

L.3 Elaboration of I_C

It has already been demonstrated that (see minimum induced drag of a circular annular wing):

$$\oint_{-1}^{1} \frac{\sin(\pi s)}{(1-\cos(\pi(t-s)))}\,\mathrm{d}s = -2\sin(\pi t)\,. \tag{L.27}$$

It can be concluded that

$$I_C = -2k\sin(\pi t)\,. \tag{L.28}$$

L.4 Substitution of I_A, I_B, I_C into the Euler-Lagrange Equation

The Euler-Lagrange Equation is:

$$\frac{k}{2b_w V_\infty^2}\frac{\sin\pi t}{\sinh 2\psi_w} + \frac{k\sin\pi t\cosh(2\psi_w)}{2b_w V_\infty^2}\left(1-\frac{\cosh 2\psi_w}{\sinh 2\psi_w}\right) - \frac{k}{2b_w V_\infty^2}\sin(\pi t) - \lambda\sin(\pi t) = 0, \tag{L.29}$$

while the constraint is:

$$\overline{C}_L = -\frac{\pi}{2lV_\infty^2}\int_{-1}^{+1} m(t)\sin(\pi t)\,\mathrm{d}t = -\frac{\pi}{2lV_\infty^2}\int_{-1}^{+1} k\sin^2(\pi t)\,\mathrm{d}t = -\frac{\pi}{2lV_\infty^2}k \Rightarrow k = -\frac{2lV_\infty^2}{\pi}\overline{C}_L. \tag{L.30}$$

Substituting the last formula into (L.29):

$$\lambda = -\frac{l\overline{C}_L}{\pi b_w}(\cosh 2\psi_w - \sinh 2\psi_w - 1)\,. \tag{L.31}$$

Remembering the relations:

$$\begin{aligned}\cosh 2\psi_w &= 2\cosh^2\psi_w - 1 = 2\frac{a_w^2}{a_w^2-b_w^2} - 1 = \frac{b_w^2+a_w^2}{a_w^2-b_w^2},\\ \sinh 2\psi_w &= 2\cosh\psi_w\sinh\psi_w = 2\frac{a_w}{\sqrt{a_w^2-b_w^2}}\frac{b_w}{\sqrt{a_w^2-b_w^2}} = 2\frac{a_w b_w}{a_w^2-b_w^2},\end{aligned} \tag{L.32}$$

the following result is obtained:

$$\lambda = \frac{2l\overline{C}_L}{\pi(b_w+a_w)}. \tag{L.33}$$

Notice that, if $b_w \to a_w = R_w$ (circular annular wing), $\lambda = \frac{l\overline{C}_L}{\pi R_w}$, as has been found for the circular annular wing.

Appendix M

Elliptical Annular Wing with $b_w > a_w$. Integrals I'_A, I'_B for a Constant Doublet Distribution

The goal of this appendix is to find the following integrals:

$$\begin{aligned} I'_A &= \sinh^2\psi_w \cosh^2\psi_w \int_{-1}^{+1} \frac{1}{\left(\sinh^2\psi_w + \sin^2\left(\frac{\pi(t+s)}{2}\right)\right)^2}\,\mathrm{d}s, \\ I'_B &= \tfrac{1}{2}\cosh(2\psi_w) \int_{-1}^{+1} \frac{1}{\left(\sinh^2\psi_w + \sin^2\left(\frac{\pi(t+s)}{2}\right)\right)}\,\mathrm{d}s. \end{aligned} \tag{M.1}$$

M.1 Elaboration of I'_A

With the transformation

$$\begin{aligned} u &= \tan\tfrac{\pi t}{2}, \\ v &= \tan\tfrac{\pi s}{2}, \end{aligned} \tag{M.2}$$

integral I'_A becomes:

$$I'_A = (u^2+1)^2 \tfrac{2}{\pi} \sinh^2\psi_w \cosh^2\psi_w \int_{-\infty}^{+\infty} \frac{\left(v^2+1\right)}{\left((u^2+1)(v^2+1)\sinh^2\psi_w + (v+u)^2\right)^2}\,\mathrm{d}v. \tag{M.3}$$

Setting $a = \sinh^2\psi_w$, the corresponding indefinite integral is:

$$\begin{aligned} \int \frac{\left(v^2+1\right)}{\left((u^2+1)(v^2+1)a^2 + (v+u)^2\right)^2}\,\mathrm{d}v = \frac{u+2a^2u+v+a^2v-a^2u^2v}{2a^2(1+a^2)(1+u^2)(1+a^2+a^2u^2)(a^2+u^2+a^2u^2+2uv+v^2+a^2v^2+a^2u^2v^2)} + \\ + \frac{\left(1+2a^2\right)\arctan\left[\frac{u+v+a^2v+a^2u^2v}{a\sqrt{1+a^2}(1+u^2)}\right]}{2a^3(1+a^2)^{\frac{3}{2}}(1+u^2)^2}. \end{aligned} \tag{M.4}$$

Observing that

$$\begin{aligned}
&\lim_{v\to\pm\infty} \frac{u+2a^2u+v+a^2v-a^2u^2v}{2a^2(1+a^2)(1+u^2)(1+a^2+a^2u^2)(a^2+u^2+a^2u^2+2uv+v^2+a^2v^2+a^2u^2v^2)} = 0,\\
&\lim_{v\to\pm\infty} \frac{\left(1+2a^2\right)\arctan\left[\frac{u+v+a^2v+a^2u^2v}{a\sqrt{1+a^2}(1+u^2)}\right]}{2a^3(1+a^2)^{\frac{3}{2}}(1+u^2)^2} = \frac{\left(1+2a^2\right)}{2a^3(1+a^2)^{\frac{3}{2}}(1+u^2)^2}\left(\pm\frac{\pi}{2}\right),
\end{aligned} \tag{M.5}$$

it can be deduced that

$$\int_{-\infty}^{+\infty} \frac{\left(v^2+1\right)}{\left((u^2+1)(v^2+1)\sinh^2\psi_w+(v+u)^2\right)^2}dv = \frac{\left(1+2\sinh^2\psi_w\right)\pi}{2\sinh^3\psi_w\left(1+\sinh^2\psi_w\right)^{\frac{3}{2}}(1+u^2)^2}. \tag{M.6}$$

Therefore, the integral I'_A is:

$$I'_A = \frac{\cosh 2\psi_w}{\sinh\psi_w\cosh\psi_w}. \tag{M.7}$$

M.2 Elaboration of I'_B

Using the transformation adopted for I'_A, I'_B can be written as

$$I'_B = \frac{2}{\pi}\frac{(u^2+1)\cosh(2\psi_w)}{2}\int_{-\infty}^{+\infty}\frac{1}{\left((u^2+1)(v^2+1)\sinh^2\psi_w+(v+u)^2\right)}\,\mathrm{d}v. \tag{M.8}$$

The corresponding indefinite integral is:

$$\int\frac{1}{\left((u^2+1)(v^2+1)a^2+(v+u)^2\right)}\,\mathrm{d}v = \frac{\arctan\left[\frac{u+v+a^2v+a^2u^2v}{a\sqrt{1+a^2}(1+u^2)}\right]}{a\sqrt{1+a^2}(1+u^2)}. \tag{M.9}$$

Thus,

$$\int_{-\infty}^{+\infty}\frac{1}{\left((u^2+1)(v^2+1)a^2+(v+u)^2\right)}\,\mathrm{d}v = \frac{\pi}{a\sqrt{1+a^2}(1+u^2)}. \tag{M.10}$$

Finally, integral I'_B can be written as

$$I'_B = \frac{2}{\pi}\frac{\left(u^2+1\right)\cosh(2\psi_w)}{2}\frac{\pi}{a\sqrt{1+a^2}(1+u^2)} = \frac{\cosh(2\psi_w)}{a\sqrt{1+a^2}} = \frac{\cosh(2\psi_w)}{\sinh\psi_w\cosh\psi_w}. \tag{M.11}$$

Appendix N

Details About the Nonlinear Matrices

This appendix expressly shows one of the terms of the $\boldsymbol{K}_{nl\,nl}$ matrix. That matrix can be written as

$$\boldsymbol{K}_{nl\,nl} = \boldsymbol{K}^{1}_{nl\,nl} + \boldsymbol{K}^{2}_{nl\,nl} + \boldsymbol{K}^{3}_{nl\,nl} + \boldsymbol{K}^{4}_{nl\,nl} + \boldsymbol{K}^{5}_{nl\,nl} + \boldsymbol{K}^{6}_{nl\,nl} + \boldsymbol{K}^{7}_{nl\,nl} + \boldsymbol{K}^{8}_{nl\,nl} + \boldsymbol{K}^{9}_{nl\,nl}. \tag{N.1}$$

The term $\boldsymbol{K}^{9}_{nl\,nl}$ is:

$$\boldsymbol{K}^{9}_{nl\,nl} = \frac{A_{66}}{2} \begin{bmatrix} \mathbf{0}^{u}\mathbf{0}^{u\,T} & \mathbf{0}^{u}\mathbf{0}^{v\,T} & \mathbf{0}^{u}\mathbf{0}^{w\,T} \\ \mathbf{0}^{v}\mathbf{0}^{u\,T} & \mathbf{0}^{v}\mathbf{0}^{v\,T} & \mathbf{0}^{v}\mathbf{0}^{w\,T} \\ \mathbf{0}^{w}\mathbf{0}^{u\,T} & \mathbf{0}^{w}\mathbf{0}^{v\,T} & \int\limits_{x,y} \left[\boldsymbol{F}^{w}_{,y}\boldsymbol{F}^{w\,T}_{,x} + \boldsymbol{F}^{w}_{,x}\boldsymbol{F}^{w\,T}_{,y}\right] \boldsymbol{q}_{w}\boldsymbol{q}^{T}_{w} \left[\boldsymbol{F}^{w}_{,x}\boldsymbol{F}^{w\,T}_{,y} + \boldsymbol{F}^{w}_{,y}\boldsymbol{F}^{w\,T}_{,x}\right] \mathrm{d}\,x \mathrm{d}\,y \end{bmatrix}. \tag{N.2}$$

Appendix O

Transformation of the Integrals to Perform their Analytical Computation

The integrals that appear in the nonlinear stiffness matrices have to be transformed in order to perform the analytical calculation. This operation is required because the table of integrals calculated once is preferred. To illustrate the method, one of the integrals in the first term $\boldsymbol{K}^1_{nl\,nl}$ is analyzed:

$$\int\limits_{x,y} \boldsymbol{F}^w_{,x} \boldsymbol{F}^{w\,T}_{,x} \boldsymbol{q}_w \boldsymbol{q}^T_w \boldsymbol{F}^w_{,x} \boldsymbol{F}^{w\,T}_{,x}\, \mathrm{d}x\, \mathrm{d}y. \tag{O.1}$$

It is easy to see that the terms

$$\begin{aligned} &\boldsymbol{F}^{w\,T}_{,x} \boldsymbol{q}_w, \\ &\boldsymbol{q}^T_w \boldsymbol{F}^w_{,x}, \end{aligned} \tag{O.2}$$

are *scalar* quantities. For this reason, they can be written as:

$$\begin{aligned} \boldsymbol{F}^{w\,T}_{,x} \boldsymbol{q}_w &= \boldsymbol{q}^T_w \boldsymbol{F}^w_{,x}, \\ \boldsymbol{q}^{T_w} \boldsymbol{F}^w_{,x} &= \boldsymbol{F}^{w\,T}_{,x} \boldsymbol{q}_w. \end{aligned} \tag{O.3}$$

By using the previous expressions, the integrals become:

$$\begin{aligned} &\int\limits_{x,y} \boldsymbol{F}^w_{,x} \boldsymbol{F}^{w\,T}_{,x} \boldsymbol{q}_w \boldsymbol{q}^T_w \boldsymbol{F}^w_{,x} \boldsymbol{F}^{w\,T}_{,x} \mathrm{d}x\, \mathrm{d}y = \int\limits_{x,y} \boldsymbol{F}^w_{,x} \left[\boldsymbol{F}^{w\,T}_{,x} \boldsymbol{q}_w\right] \left[\boldsymbol{q}^T_w \boldsymbol{F}^w_{,x}\right] \boldsymbol{F}^{w\,T}_{,x} \mathrm{d}x\, \mathrm{d}y = \\ &\int\limits_{x,y} \left[\boldsymbol{F}^{w\,T}_{,x} \boldsymbol{q}_w\right] \boldsymbol{F}^w_{,x} \boldsymbol{F}^{w\,T}_{,x} \left[\boldsymbol{q}^T_w \boldsymbol{F}^w_{,x}\right] \mathrm{d}x\, \mathrm{d}y = \int\limits_{x,y} \left[\boldsymbol{q}^T_w \boldsymbol{F}^w_{,x}\right] \boldsymbol{F}^w_{,x} \boldsymbol{F}^{w\,T}_{,x} \left[\boldsymbol{F}^{w\,T}_{,x} \boldsymbol{q}_w\right] \mathrm{d}x\, \mathrm{d}y = \\ &\int\limits_{x,y} \left[q_{w\,k_w} F^w_{,x\,k_w}\right] F^w_{,x\,i_w} F^w_{,x\,j_w} \left[F^w_{,x\,l_w} q_{w\,l_w}\right] \mathrm{d}x\, \mathrm{d}y = \int\limits_{x,y} q_{w\,k_w} F^w_{,x\,k_w} F^w_{,x\,i_w} F^w_{,x\,j_w} F^w_{,x\,l_w} q_{w\,l_w} \mathrm{d}x\, \mathrm{d}y = \\ &q_{w\,k_w} q_{w\,l_w} \int\limits_{x,y} F^w_{,x\,k_w} F^w_{,x\,i_w} F^w_{,x\,j_w} F^w_{,x\,l_w} \mathrm{d}x\, \mathrm{d}y \qquad k_w, l_w, i_w, j_w = 1,\ldots,N_w. \end{aligned} \tag{O.4}$$

This expression is useful because the integrals contain only Ritz functions, and, because the polynomials $x^s y^r$ were used, it is possible to use the analytical integration, as seen in chapter 11.